LONDON'S GLOBAL UNIVERSITY

A neuroprotective strategy to reduce acute and chronic disability, and slowly progressive central nervous system atrophy in a new model of multiple sclerosis

Erika Antuanette Aguzzi

UCL Institute of Neurology

A thesis submitted for the degree of

Doctor of Philosophy (Ph.D.)

DECLARATION

I, Erika Antuanette Aguzzi confirm that the work presented in this thesis is my own. Where information has been derived from other sources, I confirm that this has been indicated in the thesis.

Pimonidazole injections, perfusion of animals and embedding of ventral horn lesions were carried out in collaboration with Dr Roshni Desai, Ph.D.

MRI processing was carried out by Dr Bernard Siow, Ph.D.

ACKNOWLEDGEMENTS

First, I would like to express my sincerest gratitude to my principal supervisor Professor Kenneth J. Smith for the continuous support of my Ph.D. study and related research. I am thankful for his immense knowledge and motivation. His mentoring helped me throughout my research study and especially during the writing of this thesis. I would also like to express gratitude to Professor Smith for allowing me to be a member of his esteemed research group, and for trusting me with this project. It has been an invaluable experience.

I would like to thank my other supervisors, Dr. Declan Chard for his research and career advice, and Dr. Roshni Desai, to whom I am extremely thankful for, in particular, her insurmountable encouragement, support, training, and friendship. All of her guidance, and generosity of time, contributed immensely to the development of this project, and to my growth as a scientist.

I extend a warm thanks to Dr. Bernard Siow for his contribution to this study.

I would also like to thank my colleagues in the Smith lab and my friends for making this experience more enjoyable and memorable.

I would like to thank my beloved father for transcendentally believing in me and guarding me. Thank you for teaching me to be perseverant. I thank my mother, and role model, for her unwavering support, and advice, but also for the extraordinary life she has given me. A special thanks to Mansour, whom I consider a member of my family, for his friendship, encouragement, support, and absolute faith in me. Finally, I am thankful to Ralph and Alfred for being my pride and joy.

ABSTRACT

Multiple sclerosis (MS) is a neuroinflammatory demyelinating disease of the central nervous system that causes severe neurological deficits, starting in young adulthood. Early in the course of disease the deficits usually manifest as temporary 'attacks', or relapses, but later in the disease they manifest as a slowly progressive, irreversible worsening. Relapses are primarily due to impaired neuro/axonal function in the short term, whereas the progressive deficits are principally due to the slow accumulation of neuro/axonal degeneration and tissue atrophy. Regarding therapy, current evidence suggests that the acute neurological deficit can arise from inflammation, even in the absence of demyelination, although the mechanism(s) remain uncertain. Equally uncertain, is the cause of the slowly progressive degeneration and atrophy. Current disease-modifying treatments for MS can reduce the frequency of relapses, but, when they occur, they can still be severe. Steroids can shorten the duration of relapses, but any benefit regarding disability in the long-term is negligible. There are no very effective therapies to prevent progressive disease, and developing a therapy is hampered by the lack of an accepted animal model. Here, we introduce a new animal model of MS which causes severe neurological deficits with a time course similar to that in MS. Thus, acute deficits arise in young adulthood from CNS inflammation in the absence of demyelination, and chronic, progressive deficits accumulate throughout life due to neurodegeneration and atrophy. In MS, damage to the grey matter, particularly that of the spinal cord, correlates more precisely with the progression of disability than damage to the white matter, and here we describe a new animal model that leads to post-inflammatory, slowly progressive disability resulting from damage to the spinal grey matter. We aim to use the model to explore the mechanisms responsible for both acute and chronic deficit, and to identify a rational and effective strategy for neuroprotection.

The lesion is induced in the rat spinal cord by the unilateral, intraspinal injection of pro-inflammatory lipopolysaccharide (LPS, or saline control) into the ventral horn at the 13th thoracic vertebra. The lesion consists of a period of acute inflammation, characterized by oedema and local tissue hypoxia, which peaks at 48 hours post-injection, subsiding within 4 days. The inflammatory lesion is accompanied by the expression of a neurological deficit, namely hind limb and tail weakness, both of which subside within 4 days. Interestingly, the acute inflammatory lesion is gradually replaced over the lifetime by a slowly progressive degeneration of the previously inflamed grey matter, resembling the slow and progressive grey

matter degeneration in MS. The progressive degeneration is accompanied by the return of the neurological deficit which gradually worsens over the following months, surpassing the disability observed in the acute stage of the disease, and modelling the slow, relentless accumulation of disability seen in progressive MS.

We have used the histological characteristics of the acute inflammatory lesion, including the evidence of hypoxia, to devise a potential therapeutic strategy based on maintaining adequate tissue oxygenation. Two therapies have been explored, namely increasing respiratory oxygen, and use of the vasodilating agent nimodipine. The therapies have been applied acutely, just during the initial period of inflammatory hypoxia. Both therapies were effective in reducing the acute disability, indicating a potential therapy for relapses in MS. Remarkably, both therapies were also effective in reducing both the slowly progressive accumulation of permanent disability and the accompanying atrophy, indicating a therapeutic opportunity to avoid the severity of progressive MS. These observations illuminate the important question in MS of whether the degeneration and atrophy that accompany progressive disease are due to contemporaneous events, or whether they are the delayed consequences of events occurring long before, in the acute inflammatory lesion.

In summary, we introduce a new animal model of MS that illuminates the mechanisms contributing to both acute and chronic disability and use the model to identify therapies effective in reducing both acute and chronic disability, and the underlying pathology. The therapies are safe and inexpensive, and are suitable for testing in clinical trial in MS.

IMPACT STATEMENT

This project introduces a new model of progressive MS, characterised by slowly progressive atrophy of the spinal cord grey matter, which is driven by innate immune and hypoxic mechanisms and is later accompanied by chronic and progressive disability and atrophy. We believe this model closely mirrors the acute inflammatory events seen in MS patients. Therefore, this new model presents a unique opportunity to study the mechanisms responsible for the acute and chronic slow-burning degeneration that often characterizes the aetiology observed in patients suffering from secondary progressive MS and other neurodegenerative diseases. At present, there is a keen interest in the study of neurodegeneration within the academic community. Our novel model of slowly progressive neurodegeneration can be used to advance understanding of the inflammatory and hypoxic events that lead to degeneration, as well form a 'test bed' for the development of future therapeutic avenues. We anticipate that our model and findings will also be of interest to clinical neurologists, the pharmaceutical industry and ultimately the patients.

This research provides compelling evidence that therapies targeting tissue oxygenation can confer neuroprotective effects, diminishing the devastating degeneration that results from the progressive phase of the disease. As such, this study guides future research into the potential repurposing of therapies that may already be safely used in other conditions. This new therapeutic approach has the potential to improve the quality of life not only for patients with MS, but also patients with other neurological conditions where hypoxia plays a role.

HYPOTHESES

1. An acute inflammatory event in the spinal grey matter will have chronic consequences that persist, resulting in a slow, neurodegenerative pathology.
2. Treatment to restore tissue oxygenation, either by increasing the concentration of inspired oxygen or by improving blood flow, during the acute hypoxic window, will protect from acute disability, and the accumulation of progressive disability and atrophy.

TABLE OF CONTENTS

LIST OF FIGURES

Page

Chapter 1

Chapter 2

Chapter 3

Chapter 4

LIST OF TABLES

Page

ABBREVIATIOS

ANOVA	Analysis of Variance
APCs	Antigen Presenting Cells
aSAH	Aneurysmal Subarachnoid Hemorrhage
ATP	Adenosine Triphosphate
Aβ	Amyloid-β
BBB	Blood Brain Barrier
C3d	Coupling Compound 3
CBF	Cerebral Blood Flow
CD8	Cluster of Differentiation 8
CIS	Clinically Isolated Syndrome
CNS	Central Nervous System
COX	Cytochrome *c* oxidase
COX 1	Cytochrome *c* oxidase 1
COX 2	Cytochrome *c* oxidase 2
CV	Cresyl Violet
DA	Dark Agouti
DAB	Diaminobenzidine
DCI	Delayed Cerebral Ischaemia
DIS	Dissemination in Space
DTH	Delayed-Type Hypersensitivity
EAE	Experimental Autoimmune Encephalomyelitis
eNOS	Endothelial Nitric Oxide Synthase
ET-1	Endothelil-1
FIH	Asparagine-Hydroxylase Factor-Inhibiting HIF
GFAP	Glial Fibrillary Acidic Protein
GM	Grey Matter
GT	Glucuronyl Transferase
H&E	Haematoxylin & Eosin
H_2O_2	Hydrogen Peroxide
HIF-1	Hypoxia Inducible Factor-1
HIF-1α	Hypoxia Inducible Factor-1α
HRE	Hypoxic-Response Element
IF	Immunofluorescence
IFN-γ	Interferon-γ
IFNs	Interferons
IgG	Immunoglobulin G

IHC	Immunohistochemistry
IL-1	Interleukin-1
IL-10	Interleukin-10
IL-6	Interleukin-6
iNOS	Nitric Oxide Synthase
IP	Intraperitoneal Injection
LDF-5	Lactate Dehydrogenase-5
LF	Lipofuscin
LFB	Luxol Fast Blue
LPS	Lipopolysaccharide
MAG	Myelin-Associated Glycoprotein
MBP	Myelin Basic Protein
MHC	Major Histocompatibility
MHC-II$^+$	Major Histocompatibility Class II Complex
MOG	Myelin-Oligodendrocyte Glycoprotein
MOG-AD	MOG-Antibody Disease
MRI	Magnetic Resonance Imaging
MS	Multiple Sclerosis
NAWM	Normal Appearing White Matter
NF-kB	Nuclear Factor Kappa-Light- Chain-Enhancer of Activated B Cells
NGS	Normal Goat Serum
NADH	Nicotinamide Adenine Dinucleotide
NADPH	Nicotinamide Adenine Dinucleotide Phosphate
NHS	Normal Horse Serum
NMO	Neuromyelitis Optica
NO	Nitric Oxide
Nrf2	Nuclear Factor Erythroid 2-Related Factor-2
OCT	Optimal Cutting Temperature
PBS	Phosphate Buffered Saline
PEG	Polyethylene Glycol
PFA	Paraformaldehyde
PHD	Prolyl-Hydroxylases Domain Proteins
PIMO	Pimonidazole
PLP	Proteolipid Protein
PO_2	Partial Pressure of Oxygen
PPMS	Primary Progressive MS

RECA-1	Rat Endothelial Cell Antigen-1
RIS	Radiologically Isolated Syndrome
RNS	Reactive Nitrogen Species
ROS	Reactive Oxygen Species
RRMS	Relapsing-Remitting MS
RT	Room Temperature
S.D.	Standard Deviation
S.E.M	Standard Error of Mean
SD	Sprague Dawley
SOD	Superoxide Dismutase
SPMS	Secondary Progressive MS
SPT	Spinothalamic Tract
ST	Sulfotransferase
TBI	Traumatic Brain Injury
TMEV	Theiler's Murine Encephalomyelitis Virus
TNF- α	Tumor Necrosis Factor-α
TV	Theiler's Virus
VEGF	Vascular Endothelial Growth Factor
VHL	von Hippel-Lindau
WM	White Matter

Chapter 1 Introduction

1.1 Multiple Sclerosis

In 1868, Jean-Martin Charcot described *sclérose en plaques*, now known as multiple sclerosis (MS), during a series of lectures based on his clinical and anatomo-pathology observations at La Salpêtrière hospital in Paris (Zalc, 2018). Although the disease was identified more than 150 years ago, it remains largely enigmatic to this day. Typically thought of as an inflammatory disorder of the central nervous system (CNS), MS is characterized by focal lesions in the white matter (WM) and grey matter (GM), leading to damage of myelin and axons alike (Compston *et al.*, 2008). Genetic susceptibilities as well as environmental factors contribute to the occurrence and progression of MS. The disorder typically follows a pattern that begins with the relapsing of symptoms but ultimately develops into a progressive form of the disease (Compston & Coles, 2008). Notably, the age of the patient also interplays with the course of the disease. The majority of young adult patients present with an acute episode, accompanied by white matter abnormalities at one or several sites, as shown on magnetic resonance imaging (MRI) scans. These components are consistent with the diagnostic criteria for relapsing-remitting MS (RRMS) (Castellazzi *et al.*, 2018). With time, more episodes are likely to continue to occur, and over time adult patients may never fully recover, leading to continuous disease progression and symptom accumulation. This phase is known as secondary progressive MS (SPMS), and it accounts for approximately 65% of the patients. A small number of patients do not show any relapses, but rather a progression of the disease from onset, and this is known as primary progressive MS (PPMS) (Compston & Coles, 2008). Figure 1-1shows a schematic representation of the different disease stages.

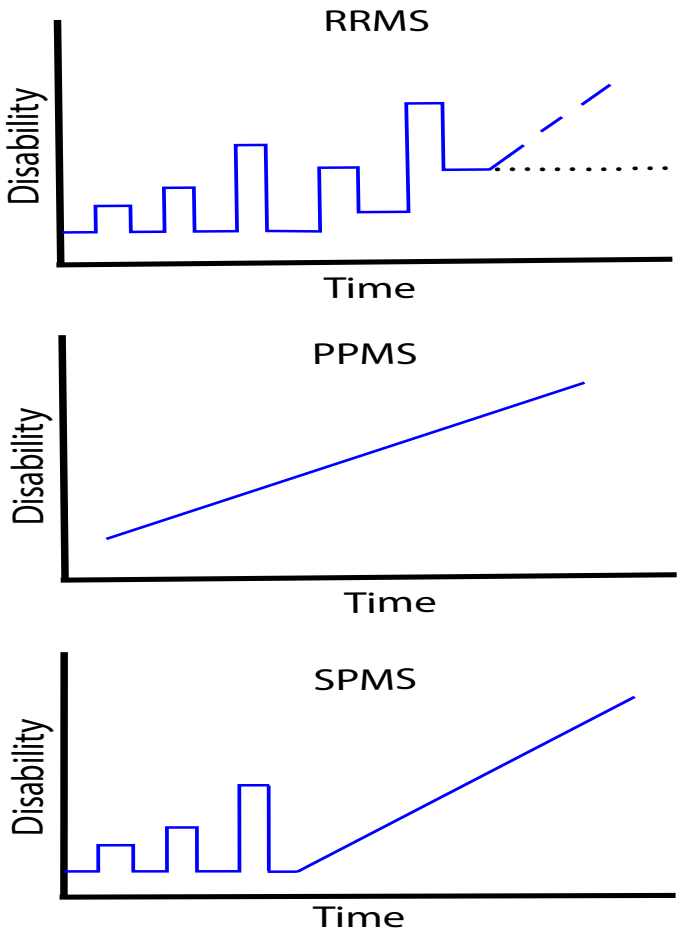

Figure 1-1 Schematic representation of the progressive disability seen in MS patients

RRMS: Relapsing remitting multiple sclerosis, PPMS: Primary progressive multiple sclerosis, SPMS: Secondary progressive multiple sclerosis.

In terms of pathology, MRI images and clinical data suggest that inflammation and focal white matter lesions occur abruptly in the RRMS phase of the disease (Coles *et al.*, 2006). However, in the progressive phases, changes in the normal-appearing white matter (NAWM) become persistent, and the pre-existing focal lesions slowly and progressively appear and result in atrophy of both the grey matter and white matter (Lassmann *et al.*, 2007).

In the early stages of RRMS, inflammation is the driving force. Anti-inflammatory and immunosuppressive therapies could potentially affect the very early course of the disease; however, this phase is often missed in clinical settings (Lassmann *et al.*, 2007). During this, and the progressive phases of MS, both PPMS and SPMS, the pathology is defined by

demyelination and neurodegeneration, which seem to develop partly independently from inflammation (Lassmann *et al.*, 2007; Zamvil *et al.*, 2003). Attention has primarily been focused on the degeneration present in the white matter. Grey matter atrophy, on the other hand, appears to be more changing during the course of the disease, and particularly prominent during the SPMS stage (Chard *et al.*, 2003; Fisniku *et al.*, 2008).

1.2 Aetiology of MS

Conventionally, MS has been regarded as an autoimmune disease. Published literature has highlighted the T-cell-mediated immune response that occurs in MS, associated with the activation of macrophages and microglia, ultimately resulting in the destruction of myelin (Lassmann, 1999). Immunological activation has been shown to occur during the first stages of active myelin destruction, beginning with macrophage and microglial activation (Barrett *et al.*, 2004; Newcombe *et al.*, 1994), followed by pro and anti-inflammatory cytokines and chemokines. T-cells activation has also been shown early in the course of the disease (Bonetti *et al.*, 1997; Newcombe *et al.*, 1994). However, what leads to the initiation of inflammation remains unclear. The immunological reaction briefly described above is not specific to MS, in fact it is common in other nervous system diseases, notably diseases arising from a viral infection to the CNS (Lassmann, 1999). As a result, it is believed that the immune activation and inflammation appearing in MS patients early in the disease has similarities with other immune system responses within the CNS, and instead, the key to identifying the cause of the disease may lie in the pathology of the tissue affected by the presence of demyelination and degeneration (Lassmann, 1999; Lassmann *et al.*, 2001).

1.3 Relapsing Remitting MS

The majority of MS patients initially follow a relapsing-remitting disease course (RRMS), that is characterised by alternating periods of disability, with full or partial recovery. Studies and MRI data have suggested that white matter lesions predominate the pathology in

RRMS (Coles *et al.*, 2006; Lassmann *et al.*, 2007), with evidence of blood brain barrier (BBB) breakdown, oedema (Dutta *et al.*, 2014), oligodendrocyte death and demyelination. Together, these factors contribute to the transient disability observed in RRMS (Calabrese *et al.*, 2007; Dutta & Trapp, 2011). Following acute demyelination, sodium channels are re-distributed along the denuded axolemma, in order to maintain action potential conduction. Such a mechanism is thought to be related to the transient recovery of neurological function observed in RRMS (Dutta & Trapp, 2011).

The severity and duration of the RRMS phase can determine the transition to progressive disease, however, they have no impact on the rate of progression once SMPS begins. Furthermore, therapies that focus on the modulating the early inflammatory response have shown a higher rate of efficacy during the RRMS phase, than the progressive phase (La Mantia *et al.*, 2016). Therefore, it has been suggested that, during the early stages of MS, inflammation is the driving mechanism that ultimately leads to SPMS and long-term atrophy (Lassmann *et al.*, 2007). Understanding the cellular and molecular cascade of events that give rise to the early inflammation, demyelination and axonal transection observed during the acute phase of MS is imperative for the understanding of progressive MS and the development of neuroprotective therapies (Dutta & Trapp, 2011; Lassmann *et al.*, 2001).

1.4 Inflammation in SPMS

The pathology of MS includes the formation of plaques that form within the CNS along with the presence of inflammation, demyelination, pronounced axonal injury and a reduction in axonal density (Bitsch *et al.*, 2000; Bø *et al.*, 2000; Lassmann, 1999). In general, patients with MS initially suffer from a relapsing-remitting disease course, followed by a progressive phase years later (Compston & Coles, 2008). It is believed that during the early stages of the relapsing remitting course of MS, the pathology is marked by focal inflammatory plaques and oedema, accompanied by a reduction in oligodendrocytes, astrocyte proliferation and

infiltration of lymphocytes and macrophages (Lassmann *et al.*, 2001). Typically, this early inflammatory phase of the disease is thought to be mediated mostly by T-cells, most predominantly $CD8^+$ T-cells, as well as activated microglia and macrophages (Traugott *et al.*, 1983). Other inflammatory mediators, such as $CD4^+$ T lymphocytes, TNF-α, interferon-γ (IFN-γ) and other cytokines are also likely to be present in acute MS lesions (Lassmann *et al.*, 2007). A remission of symptoms seen in MS patients is attributed to the conclusion of inflammatory cascades of events, resolution of oedema and partial remyelination (Noseworthy *et al.*, 2000). In the past, it was hypothesised that reducing acute attacks of the disease would be sufficient to reduce the severity of progression, but unfortunately most patients seem to continue to suffer relapses and progression of the disease despite anti-inflammatory therapy (Krapf *et al.*, 1999). These observations have seemed to require a revision of the hypothesis, because they superficially appear to focus attention on the possibility that progression may be due to events occurring later in the disease course.

There are other ways in which inflammation and oedema may be manipulating features of the pathology of MS. For instance, ongoing damage seen in SPMS patients occurs in conjunction with mitochondrial dysfunction, which may ultimately contribute to axonal death (Mahad *et al.*, 2009; Mahad *et al.*, 2008; Nikić *et al.*, 2011; Sadeghian *et al.*, 2016). Pro-inflammatory cytokines, such as TNF-α, promote the formation of the inducible form of nitric oxide synthase (iNOS) and the consequent release of nitric oxide (NO). NO mediates mitochondrial dysfunction by competing with the binding of oxygen to complex IV, and thereby inhibiting adenosine triphosphate (ATP) synthesis. Ultimately, proton pumping is disrupted, disrupting homeostasis and eventually leading to mitochondrial dysfunction (Plantone *et al.*, 2016), which in turn causes vulnerable cells like oligodendrocytes and neurons to die (Aboul-Enein *et al.*, 2003). Due, at least in part, to these findings, inflammation is increasingly recognised to play an important role in the pathogenesis of MS.

1.5 Clinico-Pathology of MS

MS is a disease that affects the human CNS by the appearance of multifocal demyelinating lesions, inflammation and degeneration (Lassmann, 1999). MS lesions occur throughout the CNS, however, there seems to be a preference for lesion formation in certain sites of the CNS, such as the optic nerve, brainstem, spinal cord and subcortical areas (Noseworthy *et al.*, 2000). The plethora of neurological deficits experienced by MS patients include blindness, paralysation, fatigue, numbness, tingling and pain. These symptoms are primarily due to the loss of conduction in the appropriate pathways, possibly due to demyelination (Smith *et al.*, 2005; Smith *et al.*, 1999). Contrary to what may be expected, the correlation between lesions and deficit is not imperative, however, it is often observed. This is well illustrated in the optic nerve, where pathways can be anatomically circumscribed and monitored using MRI techniques (Smith *et al.*, 2005). Optic neuritis, for instance, is an inflammatory and demyelinating disorder of the optic nerve, and it is often associated with MS, particularly during the RRMS phase. Typical symptoms of MS-associated optic neuritis correlate with the symptomatic nerve, as well as disseminated white matter brain lesions (Kupersmith *et al.*, 2002; Smith *et al.*, 2005; Toosy *et al.*, 2014).

MS lesions have also been found in the cerebral cortex and other grey matter regions (Bø *et al.*, 2000). These lesions largely contribute to the motor and sensory impairment, as well as the cognitive dysfunction present in more than 50% of MS patients (Rao *et al.*, 1991). Regardless of the exact location of the lesion within the CNS, it has proven to be increasingly difficult to decipher the molecular cascade of events that give rise to lesion formation as it has been found that significant tissue damage occurs in the very early stages of the disease, largely going unnoticed. As a consequence, the cause of the disease remains enigmatic to this day (McDonald *et al.*, 1992).

1.5.1 Heterogeneity of Lesions

As previously described, most MS patients' disease begins with a T-cell and macrophage inflammatory reaction, however, the pattern of demyelinating lesions is heterogenous, as shown in biopsy cases, yet when multiple active lesions are present, they show a homogeneity within the same patient. The heterogeneity of plaques in different MS patients is an important consideration in the understanding of MS and future therapeutic therapies (Lucchinetti *et al.*, 2000). Four different types of lesion (Patterns I-IV) have been identified based on pathological profiles, such as the sequence of myelin protein loss, the patterns of oligodendrocyte destruction and the morphology of the plaques (Lassmann *et al.*, 2001; Lucchinetti *et al.*, 2000). Patterns I and II are often discussed together because they share similar characteristics, for instance the distributions of lesions are typically perivenular, and the active demyelination is due to a T-lymphocyte- and macrophage-mediated inflammation (Lassmann *et al.*, 2001). Pattern I demyelination is often associated with macrophage-mediated demyelination, conversely, pattern II demyelination is mediated by antibody binding and complement activation. The main feature that sets these two lesions apart is the deposition of immunoglobulin G (IgG) at active sites of myelin damage, which is not unique to pattern II lesions, but it is accentuated in comparison with the other patterns (Lucchinetti *et al.*, 2000). Pattern III demyelination also involves an inflammatory response composed of macrophages and activated microglia, together with some T-lymphocytes, although the abundance of these latter cells is questioned by different authors (Barnett *et al.*, 2004). However, a notable feature of Pattern III lesions is that they are not centred on veins and venules, unlike patterns I and II. The main characteristic of pattern III lesions is the degeneration of the most distal regions of oligodendrocytes, which are the inner tongues of their myelin sheaths, followed by apoptosis and demyelination (Lassmann *et al.*, 2001). Pattern IV lesions also involve inflammatory infiltrates mostly made up of T lymphocytes and macrophages, however, demyelination

associated with oligodendrocytes occurs in small regions restricted to the periplaque white matter, bordering the zone of active myelin destruction (Lucchinetti *et al.*, 2000).

Patterns I and II demyelination have in common a perivascular inflammation, leading to larger demyelinating plaques due to the initial T-cell and macrophage activation (Lassmann, 1999). However, it has become apparent that even in these similar patterns the mechanism of demyelination varies, indicating that therapeutic strategies need a specific understanding of lesion formation in order to target the different mechanisms (Lucchinetti *et al.*, 2000).

1.5.2 White Matter Lesions

The hallmark of MS is the demyelination of focal WM plaques which typically results in the relapsing-remitting pattern of MS that patients often show in the early stages of the disease, as illustrated in a study performed on 52 autopsies from MS patients (Lassmann *et al.*, 2011). A system to classify different types of white matter lesions has been designed by Bø and Trapp, which categorizes lesions between preactive lesions, active lesions, chronic active lesions and inactive lesions (Prins *et al.*, 2015; Trapp *et al.*, 1998).

Preactive lesions can appear normal on MRI scans, as they show no apparent loss of myelin and no presence demyelination. From a histological perspective, the white matter is characterized by clusters of major histocompatibility (MHC) class II molecule-positive (MHC-II^+) microglia, which are associated with inflammatory cells, in conjunction with cytokines, specifically tumour necrosis factor-α (TNF- α) and interleukin-10 (IL-10) (Neumann *et al.*, 1997; Prins *et al.*, 2015; van Horssen *et al.*, 2012). There is also a strong expression of macrophages, microglia, leucocytes and MHC-II^+ antigens in close proximity to micro-vessels of the white matter, along with a certain degree of oedema on the otherwise NAWM (De Groot *et al.*, 2001). Preactive lesions have been shown to be present in a vast majority of MS samples in a study conducted in post-mortem brain tissue. Given the frequent occurrence of preactive lesions in the samples, researchers concluded that not all preactive lesions will progress to

become demyelinating lesions (van Horssen *et al.*, 2012). A determining factor for the development of preactive lesions is proposed to be a link between pro-inflammatory mediators and anti-inflammatory signals, which, given the right combination, may result in preactive lesions spontaneously resolving, ultimately bypassing an active demyelinating stage (van Horssen *et al.*, 2012).

Active lesions are described as being hypercellular lesions that retain, to a certain extent, axonal density. These lesions are characterized by the early stages of demyelination, as shown by the presence of macrophages with luxol fast blue (LFB) histological protocols (Prins *et al.*, 2015; Van Der Valk *et al.*, 2000). Later and more specific staging systems further categorize active lesions as early active and late active lesions, such as the staging system introduced by Lassmann and Brück (Brück *et al.*, 1995). Generally, early active lesions include macrophages containing myelin proteins, and lipids such as myelin oligodendrocyte glycoprotein (MOG) -positive fragments and myelin-associated glycoprotein (MAG) -positive fragments (Brück *et al.*, 1995; Van Der Valk & De Groot, 2000). Active lesions have shown that in the early stages of myelin breakdown, there is a preferential sequence of molecular events in which the myelin proteins are degraded. For instance, MOG and MAG have been shown to break down at the acute stages of the disease (Brück *et al.*, 1995; Van Der Valk & De Groot, 2000).

In common with acutely active lesions, chronic active lesions retain, to a certain extent, axonal density, however, the hypercellularity appears towards the edge of the lesion, rather than at its centre. These lesions have active demyelination present. Late active lesions involve macrophages that have already engulfed myelin debris, and they contain myelin basic protein (MBP) and proteolipid protein (PLP), which are degraded more slowly than the previously mentioned MOG and MAG (Brück *et al.*, 1995; Van Der Valk & De Groot, 2000).

As previously discussed, myelin proteins and lipids are substantially reduced in MS active lesions due to the significant myelin loss (Möller *et al.*, 1987). Intraspinal injection of LPS has shown that MAG, in particular, is lost before other myelin proteins, and this loss seems to occur prior to the initiation of frank demyelination (Felts *et al.*, 2005). This preferential loss of MAG also occurs in pattern III demyelinating lesions (Aboul-Enein *et al.*, 2003; Kornek *et al.*, 2003; Lucchinetti *et al.*, 2000), and is a characteristic of such lesions. Both intraspinal injection of LPS and pattern III MS lesions have shown that demyelination occurs alongside microglial activation and prominent expression of iNOS (Felts *et al.*, 2005). MOG, on the other hand, is a key CNS-specific antigen and it is thought to be one of the antigens responsible for the initiation of primary autoimmune-mediated demyelination in MS (Rosbo *et al.*, 1990). However, MOG-specific antibody presence is associated with MOG-antibody disease (MOG-AD), therefore, to avoid misdiagnosis, MRI characteristics should be implemented to differentiate MOG-AD from other neuro-inflammatory disorders, such as MS and neuromyelitis optica (NMO) (Wynford-Thomas *et al.*, 2018). Nonetheless, studies have shown that MOG can intrinsically aid in generating both an encephalitogenic T-cell response and an antibody response in animal models such as experimental autoimmune encephalomyelitis (EAE) in Lewis and Dark Agouti (DA) rats (Bernard *et al.*, 1997). MOG is externally located on oligodendrocyte surfaces, at the outermost lamellae of myelin sheaths. MOG location, therefore, makes it directly accessible to an immune response and it is one of the reasons it is thought to be a primary target antigen for autoimmune responses in MS (Bernard *et al.*, 1997; Johns *et al.*, 1995). The pathology of active demyelinating MS lesions is diverse, and as previously described is made up of 4 different patterns of demyelination. Pattern III is particularly susceptible to the loss of MAG, and it is often associated with fragmentation of oligodendrocytes. To describe the extent of MAG destruction, a “loss index” system was introduced by Aboul-Enein and Lassmann (Aboul-Enein *et al.*, 2003). A detailed

immunohistochemical analysis of acute white matter lesions showed that while MAG was either completely lost or in the early process of degeneration, MOG (and other dominant myelin proteins) was relatively preserved (Aboul-Enein *et al.*, 2003).

Inactive lesions are hypocellular lesions that are characterized by a significant loss of oligodendrocytes and axons, accompanied by an increase in astrogliosis, including an abnormal increase in astrocyte number, probably as a result of neuronal death (Prins *et al.*, 2015). Inactive lesions show minor infiltration of macrophages and microglia, indicating that the immune response has diminished. The limited levels of macrophages present in inactive lesions no longer contain myelin breakdown products such as MOG, MAG, MBP and PLP (Prins *et al.*, 2015; Van Der Valk & De Groot, 2000).

1.6 Grey matter lesions

Cerebral white matter MS lesions have been thoroughly researched in past years, however, pathology has also been found in deep cerebral nuclei, the cerebral cortex and the spinal cord (Calabrese *et al.*, 2013; Fisniku *et al.*, 2008; Lassmann *et al.*, 2007; Schmierer *et al.*, 2018). Cross-sectional studies show clinical disability is critically linked to grey matter atrophy, more so than white matter lesions. Indeed, most MS patients present symptoms consistent with grey matter damage, such as a progressive paraparesis, cognitive and sensory disturbances, suggesting that atrophy to the grey matter of the cortex and the spinal cord is crucial for determining disease progression (Pirko *et al.*, 2007; Schmierer *et al.*, 2018).

Similar to the white matter, grey matter lesions are defined as sharply demarcated areas (Kutzelnigg *et al.*, 2005). As previously mentioned, grey matter lesions are found in various regions, such as the thalamus (Gilmore *et al.*, 2009), as well as the hippocampus (Geurts *et al.*, 2007), the cerebellum (Kutzelnigg *et al.*, 2007) and the grey matter of the spinal cord (Gilmore *et al.*, 2009; Katz Sand, 2015). In fact, “dissemination in space” (DIS) is a clinical term used

in MS diagnostic criteria, and it refers to the requirement that lesions affect at least two areas of the CNS in MS patients (Katz Sand, 2015). Although the mechanisms responsible for grey matter atrophy are poorly understood, studies have indicated that grey matter lesions may form due to inflammation, mitochondrial injury (Lassmann *et al.*, 2012), and secondary degeneration or Wallerian-like degeneration (Calabrese *et al.*, 2015).

1.6.1 Cortical Demyelination

Cortical demyelination is rare in MS patients in the early acute and relapsing stages of the disease (Peterson *et al.*, 2001). Patients that have suffered from MS over a longer period of time show widespread demyelination in the cerebral cortex and grey matter (Confavreux *et al.*, 2006). These patients often display symptoms, such as impaired memory, that are closely associated with the hippocampus, parahippocampal complex and amygdala (Benedict *et al.*, 2009; Hulst *et al.*, 2012; Peterson *et al.*, 2001). Advancements in MRI technology have allowed for the increase of possible research on grey matter involvement in MS disease progress. Previously, MRI techniques had less accurate results, as the contrast resolution between NAWM and grey matter areas was poor, due, in part, to grey matter lesions having longer relaxation times (Kidd *et al.*, 1999). Furthermore, in studies of SPMS patients, some changes within the grey matter, such as the ones responsible for deficits, occur at the molecular level in axonal membranes, and are therefore indistinguishable whilst using MRI techniques (Smith *et al.*). As white matter lesions are indicative of an acute and relapsing state of the disease in MS patients, cortical lesions have been shown to be a characteristic feature in SPMS or PPMS, where the cortical brain was shown to be affected in MS autopsies, along with cortical demyelination (Kutzelnigg *et al.*, 2005). Pathological differences between patients with acute and relapsing disease in comparison with patients with a progressive form of the disease need to be highlighted in order to understand the evolution of MS over time.

Cortical demyelination can be extensive in progressive stages of MS, the damage can reach averages of affected areas between 38.7% up to an extreme 92% of the total cortical area, as shown by the analysis of double hemispheres in post mortem tissue (Kutzelnigg *et al.*, 2007; Kutzelnigg *et al.*, 2005). These lesions can be extensive in progressive MS, they have been described as being proportionately and significantly larger than lesions in the subcortical white matter (Bø, Vedeler*, et al.*, 2003a). A site of propensity to cortical demyelination is the cerebellum, even more intensely than other affected cortical regions in the forebrain. Four main cortical lesions have been described that relate to both cerebellum and forebrain lesions. Intracortical lesions, leukocortical lesions, subpial lesions and lesions in both the grey and white matter (Bø *et al.*, 2000; Kutzelnigg *et al.*, 2007). Leukocortical lesions (type 1) normally do not extend to the surface of the brain and are located in the interface of the white matter and the cortex, whilst the centre of the lesion is typically located in the white matter (Bø *et al.*, 2000). Leukocortical lesions are the largest in lesion area, therefore they have the highest detection rate. Studies have highlighted the clinical importance of these lesions, as their presence has correlated with lower cognitive scores (Forslin *et al.*, 2018). Intracortical lesions (type 2) have no contact with the white matter, as these lesions have the lowest mean lesion area they are difficult to detect in MS patients (Bø *et al.*, 2000). Subpial lesions (type 3) are by far the most common cortical lesions. The localization of subpial lesions is thought to be superficial and it is believed that by-products of early inflammation in acute stages of the disease, such as myelin-toxic substances, may contribute to the formation of these lesions (Kooi *et al.*, 2012). Meningeal inflammation may be one of the inflammatory sites to release these myelin-toxins (Kooi *et al.*, 2009). Another type of intracortical lesion (type 4) has been described: the main difference between type 2 lesions and type 4 lesions is that the latter does not extend as far as having any contact with white matter (Bø, Vedeler*, et al.*, 2003b).

1.6.2 Inflammation in Grey Matter Lesions

A paucity of inflammation is commonly reported in post-mortem cortical MS tissue. In contrast to white matter lesions, the activation of immune cells that infiltrate the grey matter is barely present, as seen by the paucity of infiltrating T-lymphocytes and complement deposition (Brink *et al.*, 2005; Prins *et al.*, 2015). The lack of lymphocyte activity raises the question of the importance of the acquired immune system in grey matter lesion formation, which remains to be answered: this thesis illuminates this issue. Likewise, activated microglia and hypertrophic astrocytes are present to a lesser extent in grey matter lesions, in comparison with white matter lesions, as shown on MS tissue (Peterson *et al.*, 2001; Petzold *et al.*, 2002; Prins *et al.*, 2015). Microglia are the primary immune cells that respond to the loss of homeostasis in the CNS (Lawson *et al.*, 1992). Astrocytes have a variety of roles within the CNS, such as providing metabolic support for neurons, supporting synaptic activity and controlling neurotransmitter release as well as maintaining the BBB functionality (Eddleston *et al.*, 1993). The effect of microglia and astrocytes' action in MS plaques depends on the time of activation, and the consequent production of anti-inflammatory components. The time at which the cells are activated can be the decisive factor between demyelination or remyelination, and averting the loss of myelin, oligodendrocytes and axons alike (Prins *et al.*, 2015).

In the areas surrounding the grey matter, there is a diminishing presence of microglia, astrocytes, and oligodendrocytes, in comparison with the white matter. However, in contrast to white matter, grey matter areas have a high density of neurons (Kutzelnigg *et al.*, 2007). Neurons have immunosuppressive properties, as shown by their ability to block the proliferation of T- lymphocytes (Michel-Monigadon *et al.*, 2011). Neurons may diminish the inflammation as a quick survival response, inhibiting an immune response, by expressing

membrane-bound molecules and releasing chemokines and neurotransmitters (Biber *et al.*, 2007; Prins *et al.*, 2015). One of the molecules expressed by neurons is chemokine CX3CL1 (Harrison *et al.*, 1998), which in turn interacts with microglial receptors and T-cells (Smolders *et al.*, 2013), leading to the suppression of pro-inflammatory cytokines, nitric oxide (NO) and, therefore, limiting the cell death caused by microglial activation (Mizuno *et al.*, 2003; Prins *et al.*, 2015).

Combined, these observations suggest that grey matter lesions may indeed have a detrimental effect on disease severity. Grey matter lesions may, partly, occur separately from white matter lesions. Another factor to consider is the reduced inflammation in demyelinating grey matter lesions. Altogether, these factors imply that demyelination within grey matter lesions may have a different underlying causal mechanism.

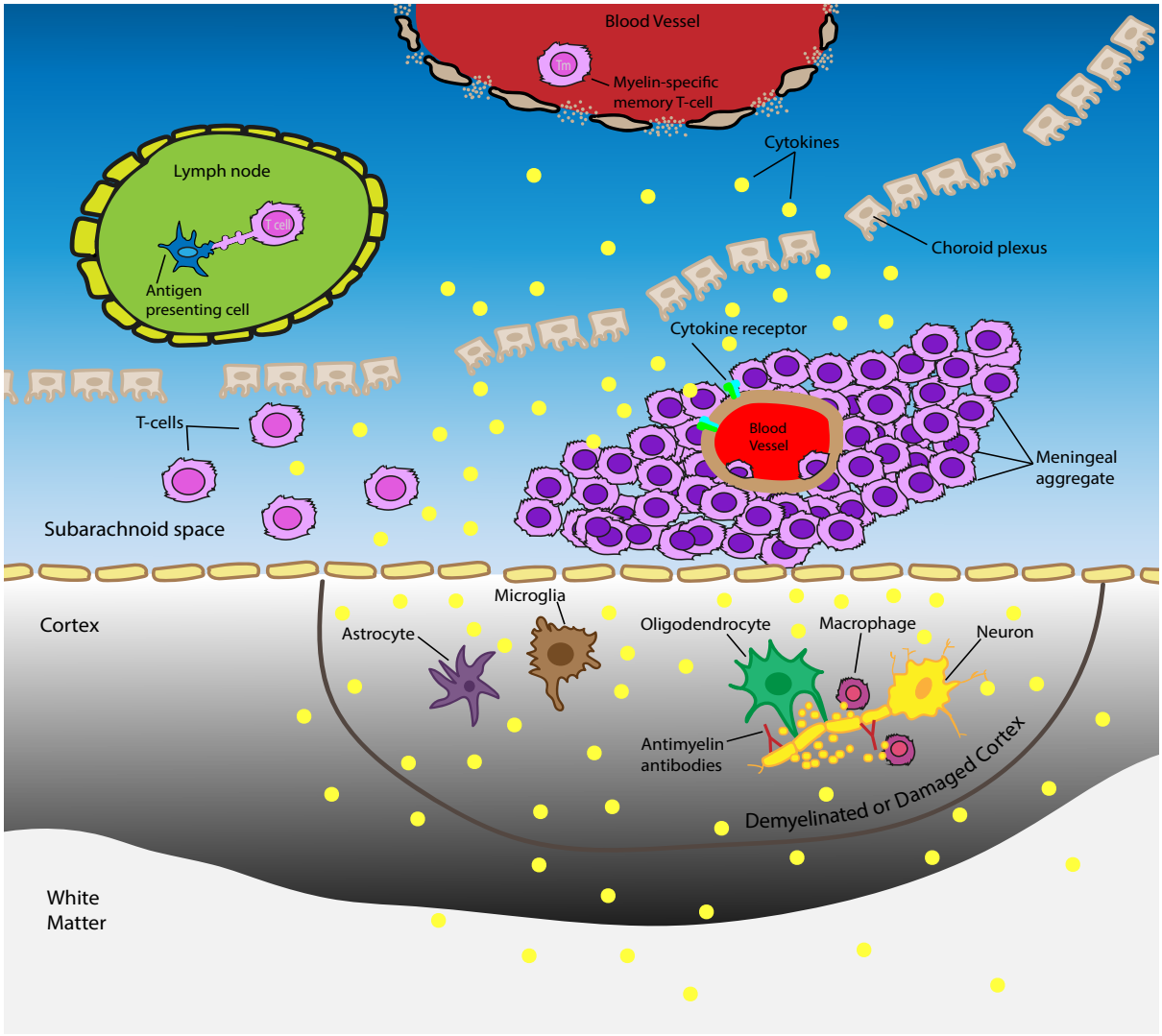

Figure 1-2 Schematic representation of meningeal infiltrates on cortical reasons

Schematic representation of the cellular events of meningeal infiltrates and immune processes involved in cortical lesion formation (adapted from: Kooi *et al*, 2009).

1.7 Gliosis

Astrocytes are a key feature of structural lesions, as they are imperative to the support of neurons, and, reactive astrogliosis is a reliable marker for injured CNS tissue (Sofroniew *et al.*, 2009). Throughout the CNS there are few, if any, regions devoid of astrocytes. Heavily branched *protoplasmic* astrocytes are quite evenly distributed throughout the grey matter, but, in contrast, *fibrous* astrocytes are found throughout the white matter and exhibit long fibrous processes (Miller *et al.*, 1984; Sofroniew & Vinters, 2009).

Astrocytic activation occurs as a cellular response following CNS insult. Astrogliosis is defined as the fibrinoid scar tissue that surfaces as a result of lost tissue (Compston & Coles, 2008; Eng *et al.*, 1994; Petzold *et al.*, 2002). In active MS lesions, reactive astrocytes are prominent and may produce a variety of pro- and anti-inflammatory responses (Sofroniew & Vinters, 2009). In EAE models of MS, reactive astrocytes have been shown to form scar tissue as a "barrier" around the perivascular cuff of inflammatory cells, thereby restricting the inflammatory cells, such as leukocytes, from migrating into neighbouring healthy tissue (Sofroniew, 2016). These observations highlight the potent ability of astrocytes to exert suppressive mechanisms on inflammatory responses. These properties may help to limit the inflammatory response during the acute stages of disease (Voskuhl *et al.*, 2009).

Glial fibrillary acidic protein (GFAP) has become a useful prototypical marker for the immunohistochemical identification of astrocytes. GFAP was isolated as a protein highly concentrated in demyelinated MS plaques, and its expression is regarded as being highly specific and reliable to particular reactive astrocytes that are responding to CNS injuries (Prineas *et al.*, 2001; Sofroniew & Vinters, 2009). Subsequently, GFAP was found in normal astrocytes as well (Eng & Ghirnikar, 1994; Lucas *et al.*, 1980; Petzold *et al.*, 2002). However, protoplasmic astrocytes in normal grey matter has been shown to have a low content of GFAP (Eng & Ghirnikar, 1994). Transgenic mice studies have indicated that expression and accumulation of GFAP is one of the prominent features in reactive astrogliosis and glial scar formation (Sofroniew & Vinters, 2009). Inhibition or delay in GFAP synthesis in damaged and reactive astrocytes might affect astrogliosis and delay scar formation (Eng & Ghirnikar, 1994; Lucas *et al.*, 1980; Yu *et al.*, 1993). Furthermore, GFAP has been shown to correlate with disability scales of MS patients and may be considered a marker for irreversible damage, and a non-specific biomarker of CNS tissue injury (Petzold *et al.*, 2002).

1.8 Slowly expanding demyelinating lesion

Active lesions, previously described as affecting the white matter during early stages of myelin breakdown, are present at acute stages of MS (Lassmann *et al.*, 2012). On the other hand, slowly expanding lesions continue to affect the white matter, however they are seen during the chronic stages of the disease. Unlike active lesions, slowly expanding lesions of progressive MS lack the abundant presence of macrophages at the site of the lesion, instead there are some intermingled macrophages around the lesion rim (Lassmann *et al.*, 2007; Lassmann *et al.*, 2012). Slowly expanding demyelinating lesions also show the presence of activated microglia at the edge of the lesion (Lassmann *et al.*, 2007). T-cells are rarely present in these slowly expanding lesions, however a moderate number of T-cells can be found in perivascular spaces and in the parenchyma, as shown by CD45RO, a marker of activated T-cells (Prineas *et al.*, 2001).

An important immunological characteristic in the demyelination of chronic and slowly expanding lesions involves coupling compound 3 (C3d), a protein of the innate immune system (Ingram *et al.*, 2014; Prineas *et al.*, 2001). It has been shown that C3d is potent in increasing the immunogenicity of other potential antigens which, in this instance, leads to the ongoing yet slow destruction of myelin. C3d is thought to play an important role in the interaction between microglia and myelin. In theory, C3d is targeted specifically by microglia, in a process closely resembling phagocytosis. A cascade of immune events ultimately leads to myelin fragments attaching to the surface of microglia/macrophages, with little phagocytosis of the myelin, unlike the process described in acute lesions, where microglia/macrophages completely engulf the fresh myelin debris, at times forming microglial nodules (Prineas *et al.*, 2001). That said, a substantial number of the microglial nodules hardly contain any myelin degradation product, suggesting a lack of demyelination (Lassmann *et al.*, 2007). The poor internalization of myelin

by microglia/macrophages, as well as the slow ongoing demyelination on the white matter border, are interpreted overall as signs of downregulation of the inflammatory response, in comparison with the immunological response that occurs during the acute phase of the disease (Lassmann *et al.*, 2007; Prineas *et al.*, 2001).

The BBB is comprised of specialized endothelial cells that regulate the delicate homeostasis of ions, nutrients and other molecules required for the health and proper CNS function. Normally in infectious or inflammatory diseases the pathology of endothelial cells that make up tight junctions is disrupted, making them prone to leakiness (Leech *et al.*, 2007). In slowly expanding chronic lesions these highly specialized endothelial cells have been studied to assess their permeability range, which if present would disrupt the balance of ions and serum proteins within the CNS (Pache *et al.*, 2003). Dysferlin, a muscle protein involved in cell membrane repair has been shown to be an appropriate marker for "leaky" endothelial cells in MS tissue. Slowly expanding chronic lesions showed little expression of leaky endothelial cells in comparison with those of active lesions, particularly pattern II lesions (Hochmeister *et al.*, 2006).

The proportion of slowly expanding lesions present in chronic MS patients is surprising. These lesions are characterized by a significant diminishment of macrophage and microglial activation in comparison with active white matter plaques (Lassmann *et al.*, 2007; Lassmann *et al.*, 2012). These slow or progressive expanding plaques continue to show demyelination long after they have been established, whilst in the absence of obvious signs of inflammation (Prineas *et al.*, 2001). In view of these important observations, a plausible speculation is that inflammation alone may be sufficient to cause significant damage in the beginning of the disease, ultimately leading to a slow and progressive demyelination in more chronic stages.

1.9 The Spinal Cord Functional Anatomy

The CNS consists of the brain and the spinal cord. Unlike the rest of the CNS, the spinal cord preserves its long and tubular-like embryonic appearance. The spinal cord is composed of the highly myelinated white matter, which contains the motor and sensory axons, as well as the grey matter, which contains the neuronal cell bodies. This structure extends from the medulla oblongata in the brainstem, all the way to the lumbar region in the vertebral column. Its most important function is to serve as a bridge of communication between the brain and the peripheral nervous system (PNS) (Diaz *et al.*, 2016). In MS, the symptoms and disability of patients correlates most with spinal cord atrophy, specifically the damage to the grey matter in the spinal cord, rather than atrophy in the brain (Lassmann, 2015; Schmierer *et al.*, 2018; Tsagkas *et al.*, 2018, 2019). For instance, a progressive paraparesis, a partial paralysis of the lower limbs, rather than sensory disturbances, is a common disability seen in SPMS patients (Thompson *et al.*, 1997; Tsagkas *et al.*, 2019). This seemingly irreversible atrophy to the spinal cord has become a focal point of research, however the mechanisms responsible for this grey matter damage remain poorly understood. The causes of the atrophy are illuminated by the findings of this thesis.

1.9.1 White Matter of the Spinal Cord

The spinal cord has three main propriospinal pathways, the descending tracts are known as corticospinal, whereas the ascending tracts are known as the cuneatus fasciculi and spinothalamic tracts (Diaz & Morales, 2016). These ascending and descending tracts are fundamental projections that connect the brain to spinal cord areas that ultimately control motor, sensory and proprioceptive functions.

1.9.2 Descending spinal tracts

The cerebral cortex is made of six distinct layers. Descending tracts originate from the fifth internal pyramidal layer of the cortex. The internal pyramidal layer is made up of pyramidal cells, which send direct outputs to neurons in the descending motor pathways (Patestas, 2006). The descending white matter tracts are located ventrolaterally in the spinal cord. These pathways are mostly responsible for transmitting motor functions. The descending motor system is divided into the pyramidal or corticospinal tracts and the extrapyramidal tracts. The pyramidal/corticospinal tracts are very important in mammals, as they are involved in the control of skilled motor movements, whereas the extrapyramidal tracts are involved in the control of complex behaviours such as body posture and locomotion (Guertin, 2013).

1.9.3 Ascending spinal tracts

The ascending white matter tracts are located dorsally and laterally within the spinal cord. These tracts are responsible for conveying all type of somatosensory information, such as temperature, touch, vibration, pressure and pain. Most transmission occurs along the dorsal columns, which convey proprioceptive and tactile information from the ipsilateral side of the body, using highly myelinated mechanosensory pathways, known as the dorsal-column medial lemniscus, to propagate this information towards the contralateral medulla before continuing towards the thalamus and eventually reaching the sensory cortex (Diaz & Morales, 2016; Guertin, 2013).

1.9.4 Grey matter of the spinal cord

In the spinal cord, the grey matter is divided into the ventral, and dorsal horns, with a small lateral horn only present from the T1 to L2 spinal cord segments. The ventral horn is responsible for processing information about motor movements, whereas the dorsal horn is responsible for processing sensory information. The middle grey area between the two processes autonomic functions for the sympathetic and parasympathetic nervous systems. The

grey matter, which contains the nerve cell bodies, has been subdivided into 9 layers. The ninth layer is not a true lamina, but rather a set of columns embedded on layers 7 and 8, which has been extrapolated only for humans. Table 1 contains information pertaining to each layer and their anatomical function (Diaz and Morales, 2016).

Grey Matter Laminae	Anatomical Function
1	Processes pain and temperature. Axons cross the midline and relay information via the contralateral lateral spinothalamic tract (SPT).
2	Processes pain and temperature. Axons cross the midline and relay information via the contralateral lateral SPT.
3	Processes vibration and pressure touch stimuli.
4	Processes vibration and pressure touch stimuli.
5	Involved in processing sensory afferent stimuli from cutaneous, muscle, and joint mechanical nociceptors as well as visceral nociceptors.
6	Involved in the flexion reflex, that is, withdrawal from painful stimulus.
7	Important component of the intermediate grey zone. The lateral grey horn only exists from T1-L2. Rostrally and caudally the lamina extends into the anterior grey horn. Contains several prominent nuclei.
8	Contains interneurons and proprioceptive neurons.
9	Not a true lamina. Contains the large majority of the spinal cord motor neurons and can be further subdivided by medial, central, and lateral nuclear columns.

Table 1 Anatomical Function of Grey Matter Laminae

Table summarizing the information pertaining to each layer and anatomical function of the nine grey matter laminae.

1.10 Tissue damage contributors

1.10.1 Hypoxia and reactive species

Hypoxia is here defined as a reduction in the concentration of oxygen from normal, more explicitly measured by the reduction of the partial pressure of oxygen (PO_2) (LaManna, 2007). The brain is considered one of the highest consumers of oxygen within the human body, utterly reliant on oxygen and using up to 20% of inspired oxygen. For the most part, the brain and the spinal cord are thought of as having a rich vasculature. However, there are areas of vascular watersheds that render the CNS especially susceptible to hypo-perfusion (Backes *et al.*, 2014; Moody *et al.*, 1990). Reduction of blood flow reduces oxygen availability and can result in prompt unconsciousness, causing deleterious effects, including neurodegeneration (LaManna, 2007). There are thus, complex adaptive mechanisms in place that aim to sustain the brain when oxygen levels are not ideal (Acker, 2005). These physiological regulatory processes compensate for mild hypoxia, and it usually does not lead to tissue damage. Chronic hypoxia leads to structural and functional adaptations of the brain, such as a decrease in inter-capillary distances (LaManna *et al.*, 2004), and changes in volume density of neuronal mitochondria, amongst others (Chávez *et al.*, 1995; LaManna *et al.*, 2004). A key regulator of hypoxic angiogenesis is hypoxia-inducible factor (HIF)-1, a transcription factor that activates many downstream genes when oxygen levels are low (Sharp *et al.*, 2004). HIF-1 activated downstream genes have a hypoxic-response element (HRE) in their promoter regions, signalling molecular mechanisms that regulate angiogenesis until it is restored. One of the molecules up-regulated by HIF-1 is vascular endothelial growth factor (VEGF), which initiates capillary angiogenesis (LaManna, 2007).

1.10.2 Oxidative damage and Reactive Oxygen Species

The CNS, especially neurons, is highly sensitive to high or low oxygen levels, as reactive oxygen species (ROS) can be toxic (Cornet *et al.*, 2013; Dore-Duffy *et al.*, 2007; Rossignol *et al.*, 2007). ROS are capable of oxidizing macromolecules crucial for physiological endurance, such as lipids, proteins, and nucleic acids (Di Meo *et al.*, 2016).

Reactive oxygen and nitrogen species (ROS; RNS) are important components of inflammatory lesions. ROS are the most important free radicals produced during metabolic reactions and both ROS and RNS can be subclassified into two groups of compounds, namely radicals and non-radicals (Adamczyk *et al.*, 2016). A free radical is an atom or molecule which contains one or more unpaired electrons in its valency shell, and they are produced as a natural by-product of cellular metabolism. Due to their chemical composition, free radicals are unstable, short lived and highly reactive (Phaniendra *et al.*, 2015). In neurodegenerative disorders, some of the most important ROS are superoxide and the hydroxyl radical, and for RNS, NO has been shown to be one of the most prominent damage-inducing molecules in neurodegeneration (Correale *et al.*, 2019; Hamby *et al.*, 2006). Furthermore, recent studies suggest a strong relationship between glutamate receptor stimulation, and increased NO synthase activity, as well as the increased formation of ROS. Elevated levels of extracellular glutamate can be toxic to white matter oligodendrocytes and myelin, as well as axons and neurons (Correale *et al.*, 2019; Matute *et al.*, 1997).

Observations in different studies have confirmed that oxidative stress is an important component associated with the development of demyelination in MS patients (Gonsette, 2008; Miller *et al.*, 2012). As previously mentioned, it is not fully understood how demyelination and degeneration take place in MS, however, it has been stated that mitochondrial dysfunction results in an increased production of ROS, which, in turn, is detrimental to the survival of neurons and glia (Beckman *et al.*, 1996; Correale *et al.*, 2019). Oxidative stress damages the

mitochondria, which therefore disrupts the production of ATP within axons, and consequently leads to blocking of axonal conduction and neurodegeneration (Mahad *et al.*, 2009; Qi *et al.*, 2006; Redford *et al.*, 1997). It has been observed that the CNS, but in particular brain tissue, is sensitive to the action of free radicals, mostly because of its high dependency on adequate oxygen levels due to significant presence of mitochondria and consequently massive oxygen metabolic processes, as well its vulnerability to oxidants (Phaniendra *et al.*, 2015). A build-up of free radicals, ROS and RNS, can adversely disrupt important processes that maintain homeostasis, leading to the damage of important biological molecules, such as nucleic acids, lipids and proteins, thereby altering the normal redox balance and effectively increasing oxidative stress (Adamczyk & Adamczyk-Sowa, 2016; Phaniendra *et al.*, 2015). Depending on the location of the cell, ROS may cause mutations in mitochondrial DNA, and perhaps mitochondrial permeability, which in turn lead to mitochondrial oxidative phosphorylation dysfunction, increasing ROS production even further, thereby possibly triggering a vicious cycle that ultimately leads to neuronal death (Correale, 2014). Altogether, these observations further highlight the importance of adequate oxygen levels to the proper function of the CNS.

Imaging studies in MS patients have shown that microglial cell activation occurs in acute stages of the disease and appears to be directly linked to disability and atrophy (Versijpt *et al.*, 2005). In SPMS patients the activation of microglia is a mechanism behind the activation of astrocytosis (Correale *et al.*, 2019). Astrocytes are able to survive the oxidative stress that comes about as a result of inflammation and the build-up of ROS/RNS (Correale *et al.*, 2019). However, there are signs of post oxidative damage in astrocytes, mainly reflected on their cell morphology and molecular expression. It has been shown that astrocyte dysfunction precedes demyelination in experimental models of inflammatory demyelination (Sharma *et al.*, 2010).

Some immunomodulatory therapies used to treat MS patients, particularly during RRMS stages, have a direct action of reducing oxidative damage. Dimethyl fumarate (DMF), marketed as Tecfidera, activates anti-inflammatory and antioxidative pathways to upregulate expression of transcription factor nuclear factor erythroid 2-related factor-2 (Nrf2), which stimulates endogenous antioxidant defence mechanisms. Target genes of Nrf2 include NAD(P)H oxidoreductase-1, which results in cytoprotective effects against oxidative injury, thereby protecting oligodendrocytes from damage (Adamczyk & Adamczyk-Sowa, 2016; Correale *et al.*, 2016). Overall, Tecfidera is believed to work by attenuating the overproduction of ROS and by inducing the Nrf2 pathway, as shown on EAE models, however, it may be ineffective and even counterproductive in advanced MS cases, where extensive oxidative injury has already taken place, astrocyte dysfunction is severe and demyelination has already begun (Schuh *et al.*, 2014).

1.10.3 Mitochondrial dysfunction

In MS, inflammation is often associated with active lesions and the production of highly toxic radical species that lead to neuronal and oligodendrocyte damage, ultimately leading to disease progression (Negre-Salvayre *et al.*, 2008). An important consequence of oxidative stress is a change to the function and transport of mitochondria to synaptic regions, which leads to a decrease in synaptic function, and it is hypothesised that this, in turn, results in neurodegeneration, as shown in EAE studies (Nikić *et al.*, 2011). Mitochondria are the most efficient producers of ATP, and they play an important role in the generation and balance of ROS, as well as buffering calcium (Dimauro *et al.*, 2003). The mitochondrial respiratory chain is composed of four complexes, and complex IV, or cytochrome *c* oxidase (COX), is where 90% of oxygen is converted into water. It has been noted that complex IV can be targeted and irreversibly compromised by NO, as is believed to occur within MS lesions (Mahad *et al.*, 2009; Redford *et al.*, 1997; Smith *et al.*, 2002).

Mitochondrial damage is increasingly recognised as a crucial mediator of both acute and chronic MS lesions (Mahad *et al.*, 2009; Mahad *et al.*, 2008). Due to mitochondrial damage, energy production is impaired, which leads to an accumulation of intra-axonal Ca^{2+}. This imbalance appears to be involved in the degeneration of axons, following ischaemia and oedema, resulting in atrophy (Mahad *et al.*, 2009; Waxman, 1982, 2001). In MS active lesions, the first signs of mitochondrial injury are reflected by a dominant loss of immunoreactivity to cytochrome C oxidase-1 (COX-1), and loss of the respective complex IV activity of the mitochondrial respiratory chain, particularly in Pattern III MS lesions (Mahad *et al.*, 2008). On the other hand, mitochondrial complex I activity is considerably reduced in chronic active MS lesions, whilst complex I and III activity are substantially decreased in non-lesion areas within the cortex of MS patients. In contrast, chronic inactive MS lesions show an increase in the activity and numbers of mitochondria, suggesting the higher energy demand of demyelinating lesions in comparison with myelinated axons (Lassmann & Van Horssen, 2011; Mahad *et al.*, 2009; Mahad *et al.*, 2008). These findings highlight the importance of deciphering the exact mechanisms of mitochondrial damage and energy failure in MS patients, particularly during the different stages of the disease.

1.11 Hypoxia Detection

1.11.1 Pimonidazole

Pimonidazole is a 2-nitroimidazole chemical compound sometimes used for the detection of hypoxia *in vivo.* In hypoxic cells, pimonidazole gets reduced and binds to macromolecules at areas of low oxygen concentration, hence why it is used as a hypoxic marker. In past years, pimonidazole was often used for the detection of hypoxia in tumour and cancer studies (Arteel *et al.*, 1998; Raleigh *et al.*, 1998; van Laarhoven *et al.*, 2006), however it still remains one of the best ways to detect cellular hypoxia. The process by which pimonidazole measures hypoxia begins when insufficient oxygen becomes the limiting

reactant in a series of steps in which pimonidazole would normally be oxidized. In the presence of adequate oxygen concentration, pimonidazole is either oxidized into pimonidazole *N*- oxide or conjugated via glucuronyl transferase (GT) or sulfotransferase (ST). Nitroreductases, such as nicotinamide adenine dinucleotide (NADH) or nicotinamide adenine dinucleotide phosphate (NADPH), then transfer electrons to the parent compound via reductive metabolism leading to the re-oxidation of oxygen into nitro radical anion, therefore blocking any further reduction of the parent compound. This chemical reaction relies on oxygen to be the rate limiting factor that competes for the transfer of electrons to pimonidazole, thereby preventing the reduction of pimonidazole by nitroreductases. In the absence of adequate oxygen, pimonidazole is reduced and is able to bind to -SH containing molecules such as proteins, and these can accumulate in live tissue (Arteel *et al.*, 1995; Rademakers *et al.*, 2011).

As previously mentioned, the effects of hypoxia and its metabolic markers have been studied on malignant tumour cells (Arteel *et al.*, 1998; Raleigh *et al.*, 1998; van Laarhoven *et al.*, 2006). Under chronic hypoxic conditions, cells use anaerobic glycolysis as their primary energy source, however, tumour cells continue to use aerobic glycolysis even in the presence of adequate amounts of oxygen (Arteel *et al.*, 1995; Arteel *et al.*, 1998). This is due to a modification of the metabolism of these cells, which ultimately leads to extremely high levels of glucose consumption. These cellular environments have been described as an optimal condition for carcinomas to proliferate. Pimonidazole has been identified as having a special affinity to lactate dehydrogenase-5 (LDH-5) in tumour tissue. LDH-5 is one of the target enzymes of hypoxia-inducible factor-1 α (HIF-1α), another endogenous hypoxia marker (Rademakers *et al.*, 2011). This suggests that pimonidazole can be colocalized with other metabolic markers of hypoxia and therefore it can simultaneous be used as a way of labelling and confirming hypoxia in the CNS.

1.11.2 Hypoxia Inducible Factor- α

HIF-1 is a heterodimer found in mammalian cells and it consists of two subunits: a constitutively expressed stable β- subunit and an oxygen-sensitive rate limiting α-subunit (Wang *et al.*, 1995). HIF-1 has many roles, such as inducing inflammation, initiating apoptosis and inhibiting cell death, however, its most important role is as a hypoxia regulator by orchestrating the genetic responses to hypoxia and inflammatory conditions (Greijer *et al.*, 2004; Guan *et al.*, 2017; Saravani *et al.*, 2019). As a transcription factor, HIF-1α can bind to hypoxia-responsive elements in DNA and activate the transcription factors of genes involved in processes such as angiogenesis, glycolysis and differentiation (Semenza, 2002, 2003, 2010). In addition, studies have shown that the HIF-1 signalling pathway and hypoxia are present in active MS lesions, and therefore HIF-1α has been postulated as a suitable therapeutic target for MS disease management (Guan *et al.*, 2017; Saravani *et al.*, 2019).

Under normoxic conditions, HIF-1 expression is tightly regulated in an oxygen-dependant manner and it is able to bind to the von Hippel-Lindau (VHL) protein (Guan *et al.*, 2017). This process begins when HIF-1α protein is hydroxylated, a process facilitated by two proline residues. These prolines are members of a family of prolyl hydroxylase domain proteins, (PHD 1, 2 and 3), which require oxygen for their function (Tao *et al.*, 2015). The hydroxylation of either of these prolines results in the VHL tumour suppressor protein to target HIF-1α rapidly for proteasomal degradation. Subsequent polyubiquitination of HIF-1α by ubiquitin E3 and the VHL complex leads to the degradation of the HIF-1α molecule (Guan *et al.*, 2017; Semenza, 2010; Tao *et al.*, 2015).

Under hypoxic conditions, HIF-1 α degradation is inhibited due to its inability to be hydroxylated by any of the PHD proteins. Therefore, the protein accumulates, dimerises with HIF-1β, then binds to cis-acting hypoxia response elements that target genes and ultimately

leads to increased transcription (Semenza, 2007). It has been noted that the complete HIF-1 transcriptome is likely to include thousands of genes and *in vitro* studies have shown than many of these genes appear to be completely dependent on HIF-1α (Elvidge *et al.*, 2006; Semenza, 2007). Some of the target genes of HIF-1 play key roles in critical development and physiological processes that include angiogenesis, iron transport, cell proliferation/survival and energy metabolism (Semenza, 2003, 2007, 2010). HIF-1 is also able to promote the delivery of oxygen to hypoxic areas by the upregulation of vascular endothelial growth factor (VEGF) (Semenza, 2002). These findings further highlight the importance pathways mediated by HIF-1α in directing the global transcriptional response to hypoxia.

1.12 Hypoxia and MS lesions

Evidence has shown signs of damage caused by hypoxia-like metabolic injury in MS tissue, that closely resembles lesions produced in the white matter as a result of strokes (Aboul-Enein *et al.*, 2003). In such injuries, oligodendrocytes degenerate and are eventually destroyed due to apoptosis (Lassmann, 2016). ROS and RNS, such as NO, superoxide and peroxynitrite, become by-products of inflammatory responses and hypoxia. Increased production of these reactive species is a feature of MS (Martinez Sosa *et al.*, 2017). The presence of ROS and RNS induces mitochondrial injury, which, amongst many effects, also leads to oligodendrocyte damage and ultimately neurodegeneration (Lassmann *et al.*, 2012). Oligodendrocytes have been shown to survive insufficient oxidative phosphorylation and lack of ATP production due to hypoxia. Therefore, it has been postulated that oxidative damage due to ROS presence, more than lack of aerobic respiration, is the lethal determinant factor for apoptosis of oligodendrocytes (Martinez Sosa & Smith, 2017). Grey matter pathophysiology has shown high levels of hypoxia after induction of autoimmunity, as seen in the cerebellum and cortex of mice with the EAE model of MS (Johnson *et al.*, 2016). Genuine hypoxia is present in inflammatory demyelinating lesions, as seen in a study by Desai et al. (2016). Normobaric

oxygen treatments (80%) prevent or diminish active demyelination and neurodegeneration when administered during the early acute stages of lesion formation and severe hypoxia (Desai *et al.*, 2016). Therefore, alleviating transient hypoxia may become a neuroprotective strategy for the adverse effects of low oxygen levels present in the brain and spinal cord of MS lesions.

1.13 Hypoperfusion and MS

From a physiological perspective, the brain has a dense vasculature to serve its high metabolic needs, particularly in comparison with the other human organs (Mink *et al.*, 1981). Two main pairs of arteries supply blood to the brain: the vertebral arteries and the internal carotid arteries. The vertebral arteries converge near the base of the pons to form the unpaired basilar artery (Moody *et al.*, 1990). This artery, in turn, splits into two left and right cerebral arteries that reach the superior and posterior cerebral arteries. These major arteries then continue to bifurcate and branch to form a connection of arteries at the base of the brain, altogether conforming a ring called the circle of Willis (Bear, 2001). However, because of variations in the diameter and lengths of these vessels, their ability to provide a luxuriant blood supply to all parts of the brain is limited. As a result, certain regions of the brain, including parts of the cortex and the thalamus are rendered vulnerable to hypoperfusion (Moody *et al.*, 1990). Furthermore, areas supplied by the end branches of two or more arteries, known as vascular watershed zones, are also particularly vulnerable to poor perfusion (Duschek *et al.*, 2007; Martinez Sosa & Smith, 2017; Mayer *et al.*, 1991).

A number of findings from epidemiological studies in MS patients have found that cerebral blood flow (CBF) is impaired in particular areas of the brain, including the cortex, thalamus and the basal ganglia, all of which have a single supply of blood through a penetrating artery (D'Haeseleer *et al.*, 2011; D'Haeseleer *et al.*, 2015; D'Haeseleer *et al.*, 2013; Holland *et al.*, 2012; Moody *et al.*, 1990). The underlying mechanism of reduced CBF in MS remains unknown, however, two distinct observations have been made. First, imaging studies in

patients with MS have revealed that hypoperfusion affects widespread areas including the NAWM, as well as the grey matter. Second, MS has been directly associated with a reduced venous blood drainage in the CNS (D'Haeseleer *et al.*, 2011). It is also reported that cerebral hypoperfusion in MS might occur secondarily to axonal degeneration, which in turn may lead to a further decrease in axonal survival (D'Haeseleer *et al.*, 2015). Furthermore, in a study comparing gene expression in the NAWM of patients with SPMS with that of healthy controls, it was found that one of the most consistent differences was the upregulated expression of HIF-1α in patients with MS, as well as the enhanced expression of HIF-1α target genes, such as vascular endothelial growth factor (VEGF) receptor-1. These findings are of particular importance because, as previously stated, upregulation of HIF-1α has a direct effect in increasing oxidative stress and triggering long-term ischaemic preconditioning (Graumann *et al.*, 2006).

In addition, the spinal cord is also vulnerable to hypoperfusion and hypoxia, due to its vascular architecture. The supply of blood flow to the spinal cord arises from the aorta and it supplies the cord partly by major arteries, such as the great artery of Adamkiewicz, and by division into a series of radicular arteries that gain access to the spinal cord along the spinal roots (Martirosyan *et al.*, 2011). These trunks continue onto the midline of the ventral cord surface, and there they connect to the ventral spinal artery, which has an ascending and descending branch (Novy *et al.*, 2006). Due to these opposing blood flow directions, as well as the narrow diameter of these arteries, watershed regions form, rendering the spinal cord highly susceptible to hypoperfusion (Backes & Nijenhuis, 2014). Within the spinal cord, the network of capillary density is far higher in the grey matter in comparison with the white matter, however, even within the grey matter, the artery density can vary, and it often depends on the metabolic demand of the region within the spinal cord. For instance, the dorsal horns have been identified as receiving less blood flow (Novy *et al.*, 2006). Motor neurons are

situated in the ventral horn of the spinal cord and are particularly vulnerable compared with other cells to any reductions in blood supply and consequent hypoxia (Hernandez-Gerez *et al.*, 2019; Zhang *et al.*, 1997). In MS, most patients present with symptoms associated with spinal cord lesions, particularly in the grey matter, rather than the brain (Thompson *et al.*, 1997; Tsagkas *et al.*, 2019). Indeed, MS lesions have a predilection to form in the watershed areas of the spinal cord, notably in regions with lower perfusion than NAWM (Martinez Sosa & Smith, 2017). *In vivo* models of early MS demyelinating lesions have shown that spinal cord tissue hypoxia is associated with profound hypoperfusion, which can be significantly reduced by treatment with a CNS selective vasodilator, further indicating the importance of appropriate vascular supply to the CNS (Davies *et al.*, 2013; Desai *et al.*, 2020).

1.13.1 Nimodipine

As MS lesions form, mitochondrial dysfunction occurs on a background of inflammation and hypoxia (Lassmann, 2016; Mahad *et al.*, 2015; Martinez Sosa & Smith, 2017). As a consequence of hypoxia, there is an increase in astrocytic calcium levels (Angelova *et al.*, 2015), which can promote the excessive production of free radicals and excitotoxic acids, such as glutamate, and possibly pathologic apoptosis, all which contribute to neuronal damage (Dolga *et al.*, 2011; Haile *et al.*, 2009). Calcium channel antagonists are widely used in the therapy of hypertension and cardiac arrhythmias. In neurons, L-type calcium channel blockers contribute to neuronal survival, help prevent from ischaemic-induced axonal injury, and aid in preventing membrane depolarization following energy failure. L-type channels are known to display a particularly high sensitivity to hypoxia (Gleichmann *et al.*, 2011; Lipscombe *et al.*, 2004). In the past, evidence has shown that some L-type calcium channel blockers have a direct neuronal effect and may be used for the treatment of many CNS disorders (LeVere *et al.*, 1989; Pisani *et al.*, 1998; Scriabine *et al.*, 1989).

Nimodipine is one such calcium channel blocker, with potent and selective CNS-vasodilatory and anti-ischaemic effects, that binds to rat and human CNS membranes with high affinity, and is able to pass through the BBB (Haws *et al.*, 1983; Scriabine *et al.*, 1989). In animals with middle cerebral artery occlusion, nimodipine has been found to reduce neurological deficits without a significant increase in intracranial pressure (Bork *et al.*, 2015; Haile *et al.*, 2009; Horn *et al.*, 2001; LeVere *et al.*, 1989; Levy *et al.*, 1991). During acute CNS hypoxia, calcium channel blocking, via nimodipine administration, has also been shown to reduce cytotoxic oedema and attenuate cognitive dysfunction (Rowland *et al.*, 2019). In addition, nimodipine protects against demyelination in EAE models, and against the Pattern III type of demyelination observed in early MS lesions, by promptly increasing perfusion and thereby diminishing the effects of focal tissue hypoxia (Davies *et al.*, 2013; Desai *et al.*, 2020). Moreover, during neuroinflammatory reactions, activated microglia can have a negative effect on the nervous system, such as promoting the production of proinflammatory factors, such as iNOS and COX. These factors have been implicated in neuronal damage and various neurodegenerative diseases (Huang *et al.*, 2014; Johnson *et al.*, 2016; Lin *et al.*, 2012; Loihl *et al.*, 1998). Previous studies have reported on the efficacy of nimodipine, which leads to the accumulation and release of IL-1β, and protects microglial cells against amyloid-β (Aβ) peptide-mediated damage, thereby inducing anti-inflammatory effects on microglia (Sanz *et al.*, 2012).

1.14 Animal models of MS

Many different models of MS have been developed, each proving to be useful in a specific aspect that defines the disease, such as demyelination, remyelination, inflammation and degeneration, however, none of these models are able to cover the entire pathological, clinical and inflammatory hallmarks of the disease. Nevertheless, significant understanding of MS pathology has arisen from these models (Lassmann *et al.*, 2017). A relevant model of MS

is EAE, which has proven helpful in understanding some aspects of the acute pathogenesis of the disease. EAE mainly focuses on inflammation, however, a significant number of therapies that were successful in EAE studies have failed to pass clinical trials, such as studies designed to target TNF-α blockers (Lassmann & Van Horssen, 2011).

Acute models of MS have focused mostly on the inflammatory response that some believe is a result of a viral infection. Models that comprise dominant features of chronic and progressive MS are not as abundant, as they must account not only for the initial inflammation, remission, but also for the relapse, chronic neurodegeneration and atrophy (Lassmann & Bradl, 2017). In this thesis we will introduce a new model of slow-burning neurodegeneration, which we believe encompasses these features. This model is characterised by slowly progressive atrophy of the spinal grey matter, which is driven by an innate immune mechanism, followed by a remission of symptoms and later accompanied by chronic and progressive disability and atrophy.

1.14.1 Theiler's virus induces chronic demyelinating encephalomyelitis

Theiler's virus (TV) belongs to the *Cardiovirus* genus of the family *Picornaviridae* (Tsunoda *et al.*, 2010). The DA strain of the virus is used to create an encephalomyelitis model known as Theiler's murine encephalomyelitis virus (TMEV). This strain initiates a biphasic disease by causing a mild encephalomyelitis followed by a chronic inflammatory demyelinating process. The DA strain of TV is often used as a model of MS because its pathology and immune response have similarities with those seen in MS patients (Stavrou *et al.*, 2010). In this model of disease, the virus is isolated from the CNS of mice and later injected into DA mice to produce a viral infection that causes a chronic demyelinating disease, via an immune pathogenesis to attack myelin-supporting cells (Dal Canto, 1982). During the acute phase of the disease, which generally occurs 1 week after injection, TMEV causes encephalomyelitis which is followed by neuronal death in the grey matter. In the chronic phase

of the disease, which generally occurs 1 month after initial infection, the virus attacks macrophages, and ultimately induces an inflammatory response that leads to demyelination, apoptosis of oligodendrocytes and degeneration of the white matter on the spinal cord (Tsunoda & Fujinami, 2010).

In contrast to EAE models, which mostly follow a monophasic disease course, closely mirroring RRMS, the DA-induced TMEV serves as a good model of PPMS and SPMS because of the biphasic disease that correlates with the acute and chronic stages of MS (Tsunoda & Fujinami, 2010). During the acute phase of DA-induced TMEV infection, there is already a significant number of viral antigen-positive neurons and apoptotic neurons present. Parenchymal, perivascular and subarachnoid inflammatory cell infiltrates are present in the grey matter of the brain (Tsunoda & Fujinami, 2010; Tsunoda *et al.*, 2007). During the early viral infection that occurs after injection of DA induced TMEV, cytokines produced by antigen presenting cells (APCs) trigger the activation of T-cells, including but not limited to $CD3^+$ T-cells, therefore stimulating an innate immune response. The extent of initial viral infection is a determining factor for the severity of the acute phase of the disease, and subsequently the chronic level of demyelination that will ultimately occur in the mice (Jin *et al.*, 2015).

During the chronic phase of the DA-induced TMEV infection, the initially acute inflammation in the grey matter has ceased. Chronic persistence of the viral infection leads to the susceptibility of the CNS and the development of long-term demyelinating disease. In this later phase, the demyelinating lesions are well-demarcated and visible in the ventral horn of the spinal cord, although the dorsal area is reported to be relatively preserved (Tsunoda & Fujinami, 2010; Tsunoda *et al.*, 2007). Studies have shown that the level of activation of innate immune cytokines, such as interleukin-6 (IL-6) and type I interferons (IFNs), is a determining factor in the degree of demyelination. It has been suggested that the response from such cytokines can lead to the immune system being unresponsive to T-cell mechanisms, rendering

the mice less protected and more susceptible to pathogenic pathways (Dal Canto *et al.*, 1996; Jin *et al.*, 2015; Tsunoda & Fujinami, 2010). The determining factor as to how the host immune response will take place, and the degree of susceptibility to long term demyelination, are genes in and out of the histocompatibility complex, rather than the actual viral cytopathic mechanism. If the TMEV is able to successfully bind to a cell-mediated delayed-type hypersensitivity (DTH) response, involving macrophages, monocytes and T-cells, then it is likely that the disease will be induced. Generally speaking, the number of activated macrophages and other pro-inflammatory molecules is directly correlated with the size and severity of the chronic demyelinating lesion (Dal Canto *et al.*, 1996).

1.14.2 LPS Dorsal column model of the MS Pattern III lesion

Substantial demyelination can be achieved by the injection of LPS into the Sprague Dawley (SD) dorsal column white matter (Desai *et al.*, 2016; Felts *et al.*, 2005; Sharma *et al.*, 2010). This demyelination is a direct result of a focal inflammatory lesion, caused by the injection of the bacterium endotoxin, exhibiting characteristics closely resembling human Pattern III lesions. LPS is microinjected intraspinally under anaesthesia at the T12 vertebral level. Soon after the injection, neutrophils and monocytes are present at the site of injection, and within 24 hours post LPS injection, the focal inflammatory response consists of polymorphonuclear cells and inducible nitric oxide synthase (iNOS)-positive macrophages and microglia (Felts *et al.*, 2005). At this stage there is also a clear presence of hypoxia and some astrocytic activity post injection of LPS (Desai *et al.*, 2016). The inflammatory response is significantly reduced by 1-week post injection (Felts *et al.*, 2005). Following this stage, and without the presence of inflammation, a large demyelinating lesion develops, lasting between 9 to 14 days, and often expanding to a substantial 50% of the affected area, around the site of injection. Repair by remyelination commences by the 14th day, and by 28 days after injection remyelination is well advanced and large numbers of remyelinated axons are present; most

remyelination is done by Schwann cells. Overall, this LPS-induced lesion tends to be located preferentially to involve the grey-white matter border (Felts *et al.*, 2005).

The relatively slow formation of lesions in this model can mirror MRI studies of MS patients, in which the pathology has shown that an inflammatory response and early changes in the NAWM may arise weeks before a demyelinating plaque is seen in some patients (Wuerfel *et al.*, 2004). Furthermore, microglial activation in this model may resemble focal areas of microglial activation in MS patients, that may precede the formation of demyelinating plaques that exhibit hypoxia-like conditions seen in pattern III demyelinating lesions (Felts *et al.*, 2005; Marik *et al.*, 2007). The demyelination that occurs in this model after the LPS injection is primary, and there is relatively little Wallerian degeneration rostral or caudal to the injection site (Felts *et al.*, 2005). Oligodendrocyte numbers appear to be reduced in the region of demyelination post LPS injection (Desai *et al.*, 2016; Felts *et al.*, 2005). It has been suggested that LPS may have a detrimental effect on the survival of oligodendrocytes, as shown by its toxicity to oligodendrocyte progenitors in *in vitro* experiments (Molina-Holgado *et al.*, 2001).

In this model of disease, there is a selective vulnerability of white matter to hypoxia, suggesting that LPS is indeed especially toxic towards oligodendrocytes, in comparison with neurons, resulting in demyelination rather than degeneration. This preferential vulnerability is most probably due to the location of oligodendrocytes at regions remote from blood vessels (Desai *et al.*, 2016). In addition, MAG immunoreactivity is seen in LPS lesions at 3 days after LPS injection, but it is significantly reduced by day 5, and even more so by day 7, particularly in the deep dorsal funiculus, compared with the immunoreactivity present more superficially in the dorsal column. MAG reduction seems to occur before any other myelin protein, and indeed before the initiation of demyelination (Felts *et al.*, 2005). This preferential loss of MAG mirrors that of pattern III demyelination in MS patients, which is not reproduced by the usual

experimental model of MS, namely EAE (Aboul-Enein *et al.*, 2003; Lucchinetti *et al.*, 2000). Furthermore, the LPS injection into the dorsal column and MS both show an unusual pattern of demyelination, which occurs in conjunction with microglial activation, prominent expression of iNOS, as well as hypoxia, NO and superoxide. These factors can ultimately promote energy deficiency through mitochondrial dysfunction and further aid in the progression of the demyelination (Desai *et al.*, 2016; Felts *et al.*, 2005). These findings suggest that the LPS-induced model of MS can be useful in studying the events that precede lesion formation in Pattern III MS patients, as well as in increasing our understanding of the mechanism of demyelination and potential therapeutic targets.

Chapter 2 Model of post-inflammatory slow-burning neurodegeneration

2.1. Introduction

The mechanisms by which slow neurodegeneration occurs in neurological diseases, such as MS, remain unclear. The symptoms and neurological deficit observed in MS patients are associated with inflammation, demyelination and degeneration within the CNS (Dutta & Trapp, 2011; Frischer *et al.*, 2009; Lassmann, 2016; Lassmann & Van Horssen, 2011; Trapp *et al.*, 2009). The assumption is that most of the degeneration occurs purely within the white matter, particularly involving the periventricular white matter, however, a number of histopathological and MRI studies have demonstrated that grey matter and cortical atrophy are more frequent than previously perceived (Bø, Vedeler, Nyland, Trapp, & Mork, 2003; Fischer *et al.*, 2013; Kidd *et al.*, 1999; Kooi *et al.*, 2012; Lucchinetti *et al.*, 2011). Grey matter damage and atrophy seem to be more closely related to symptoms of progression and disability of MS than white matter atrophy and damage (Fisniku *et al.*, 2008). The degeneration occurring in the cortical area explains some of the symptoms, however, the atrophy to the grey matter in the spinal cord is more consistently associated with the advancing disability, such as progressive paraparesis, a partial paralysis of the lower limbs, a common disability seen in SPMS patients (Thompson *et al.*, 1997; Tsagkas *et al.*, 2019).

Typically, in slow forming lesions, demyelination occurs in the most acute stage of the disease, followed by axonal degeneration in the more chronic phase. The most chronic phase of disease, and perhaps the most severe, can occur many years after the first manifestation of disability and relapse, suggesting the process of degeneration is slow and detrimental to the course of lesion formation (Correale *et al.*, 2019; Lassmann, 1999; Lassmann *et al.*, 2012). Much research has been dedicated to early demyelination, in particular the different processes

that have been postulated to have an effect on the severity of disease, some of which include demyelination, due to inflammation, along with a combination of hypoxic-ischaemic neuronal environment (Desai *et al.*, 2016; Lucchinetti *et al.*, 2000; Lucchinetti *et al.*, 2011; Sharma *et al.*, 2010). These early developments are the prelude to the chronic active phase which includes axonal death and irreversible neurological damage (Lovas *et al.*, 2000; Love, 2006).

Studies have shown that grey matter lesions may form due to inflammation, mitochondrial injury, hypoxia (Lassmann *et al.*, 2012), and due to secondary degeneration or Wallerian-like degeneration (Cifelli *et al.*, 2002). The degree of degeneration is directly correlated with the abundance of white matter plaques, which harbour macrophage-rich lesions during the ongoing demyelinating acute process, indicating the importance of early inflammation for lesion formation (Bitsch *et al.*, 2000). In order to understand the underlying mechanisms that cause inflammation, which, ultimately, may lead to the overall neurological degeneration seen in slow lesions, particularly within the grey matter, we have examined a novel neuroinflammatory model of disease that is mediated by the intraspinal injection of LPS, and which results in degeneration in the grey matter. This new model of MS is characterised by slowly progressive atrophy of the spinal grey matter, which is driven by an innate immune mechanism and later accompanied by chronic and progressive disability and atrophy. This model presents an opportunity to study the mechanisms responsible for the acute and chronic slow-burning degeneration seen in MS patients.

2.1.1 Hypothesis

We hypothesise that an acute inflammatory event in the spinal grey matter will have chronic consequences that persist throughout the lifetime, resulting in slowly-progressive neurodegeneration.

2.1.2 Aims

1. To develop a new model of slow-burning neurodegeneration in the spinal grey matter that mimics disease progression in MS.
2. To study the progression of the pathophysiological and pathological sequelae of an acute inflammatory lesion in the spinal grey matter.

2.2 Materials and Methods

2.2.1 Introduction to the ventral horn LPS injection

Male adult SD rats (313g ± 28, mean ± SD) were anaesthetized with isoflurane (2% in room air), and a laminectomy performed between T13 and L1 vertebral segments, where the motor neuron pool controlling hind limb function is located. Intraspinal injections were made by inserting a glass micropipette into the right ventral horn, using a micromanipulator, approximately 750µm away from the midline, via a small hole made in the dura. The site of injection was marked on the dura with sterile charcoal. Animals (n=3 rats per time point) were injected with 0.5µl of LPS (*Salmonella enterica*, serotype typhimurium, Sigma-Aldrich) (100ng/µl saline) at depths of 1300µm and 1100µm. Control animals were similarly injected, but with saline alone (n=2 per time point). Animals were randomised into groups prior to surgery.

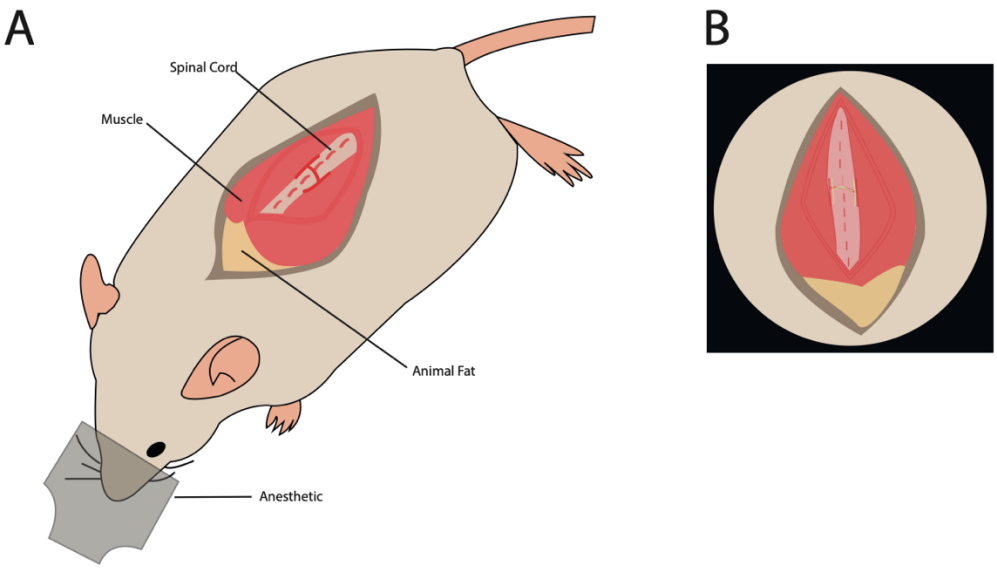

Figure 2-1 Schematic representation of the site of laminectomy.

2.2.2 Behavioural assessment

2.2.2.1 Ladder test

Walking and coordination of the animals was assessed by observing hind foot placement whilst walking along uneven rungs, the positions of which were randomised daily. The test assesses not only skill in walking, but also forelimb and hindlimb placing, and coordination (Metz *et al.*, 2002). The animals were recorded on video, with subsequent manual study, frame by frame, to determine whether the hind feet missed accurate placement on any rungs. Animals were trained the week prior to surgery, and baseline recordings obtained. Following surgery, animals were assessed using the rung ladder hind limb test for 4 days. A description of the scoring system used is outlined below in Table 2.

Category	Type of foot misplacement	Characteristics
1	Deep slip	Deep fall after limb slipped off the rung
2	Slight slip	Slight fall after limb slipped off the rung
3	Replacement	Limb replaced from one rung to another
4	Correction	Limb aimed for one rung but was placed on another
5	Partial placement	Limb placed on rung with either digits/toes or wrist/heel
6	Correct placement	Mid-portion of limb placed on rung

Table 2 Scoring scale used on the horizontal rung ladder-walking test for data analysis.
(Metz and Whishaw, 2002).

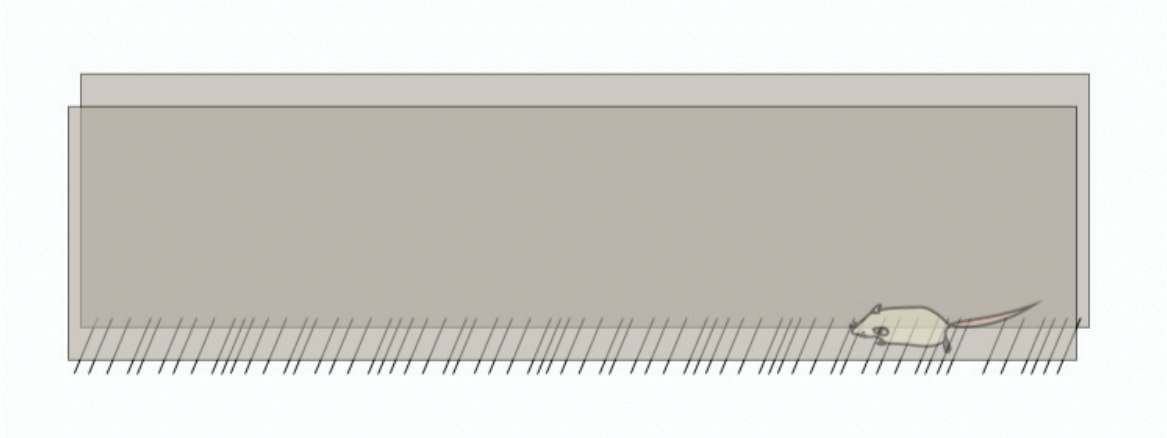

Figure 2-2 Depiction of the test apparatus to assess ladder walking.

2.2.2.2 Horizontal walking test-tail analysis

Tail deficits were determined by observing animals whilst they walked on a flat surface, for the same 1m distance as the ladder test. Rats normally walk with their tails in the air, and so tail weakness was assessed by how many times it touched the ground, in addition to the proportion of the tail that touched the surface. To create a scoring system, the tail of the rats was visually divided into sections. Depending on the section that was touching the surface, and for how long, the tail would be given a score, as shown in Figure 2-3. If the tip of the tail touched the surface it was given a score of 0.1 per touch, but if the tip of the tail touched the ground throughout the entirety of the walk, it was given a score of 1. When half of the tail was touching the flat surface throughout, it would be given a score of 2. In the case that more than half of the tail, or its entirety, was touching the flat surface, the scoring would increase to 2.5 or 3. As described above, animals were trained the week prior to surgery to obtain baseline recordings. Following surgery, animals were assessed daily for 4 days.

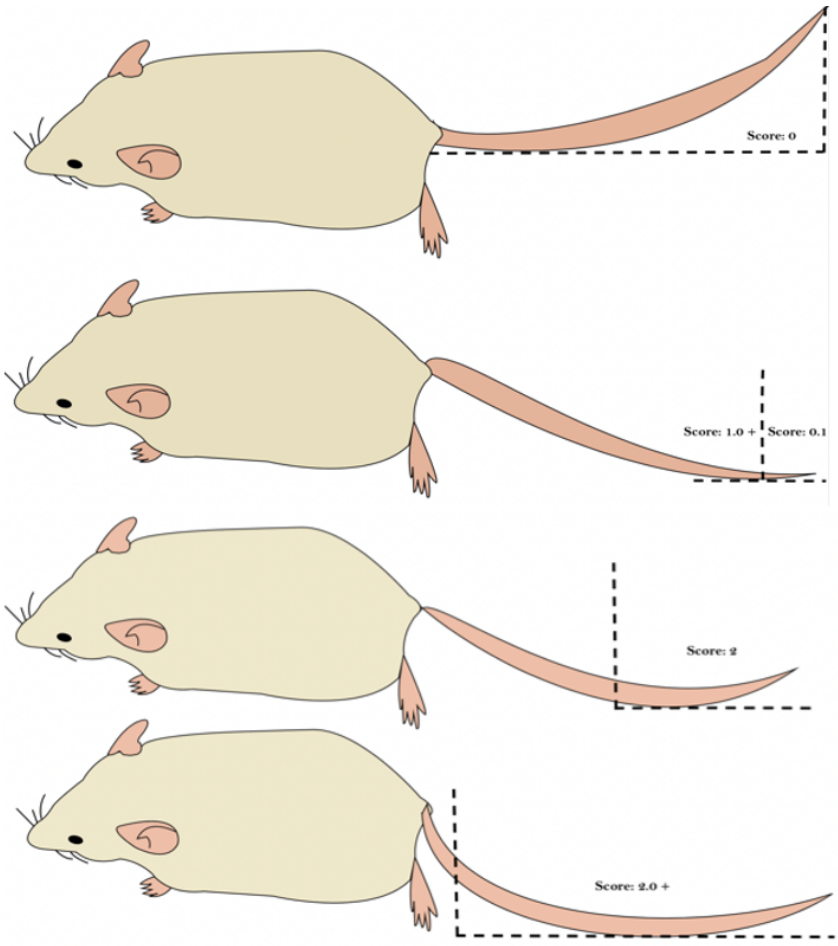

Figure 2-3 Scoring System for tail disability

Representation of the scoring system created to measure disability of the tail on the horizontal walking test.

2.2.2.3 Treadmill test-running speed

"TreadScan" apparatus and "DigiGait" imaging software were used to perform an assessment of any deficits in gait. The treadmill is made up of a Plexiglas compartment and a transparent belt that makes up the moving "treadmill". To record videos and perform analysis, an angled mirror is placed below the transparent belt. Video recording sessions lasted 1 minute, at a walking speed of 20 cm/s. This speed was chosen for a variety of reasons:

I. Animals did not perform a full 1-minute walk at higher speeds

II. This speed was optimal for post-surgery animals

III. Speed was within the recommended range by TreadScan advisory

The videos were taken with TreadScan software (ClearSys), which enables the analysis of each individual paw within each frame. The system also outlines the paws and calculates stance time, speed and gait angle. These are useful tools to measure deficit after surgery. Training sessions were used to create a background for the software to differentiate pixel and paw placement.

Animals were trained the week prior to surgery by increasing the treadmill speed each day and allowing animals to acclimatize to the process. Animals were also assessed daily, for 4 consecutive days and 1 month following lesion induction. Animals grew too large to perform the task at subsequent ages.

2.2.3 Histological preparation

Pimonidazole (PIMO) (HPI Inc, Burlington, MA; 60mg/kg body weight) was administered intravenously via the saphenous vein, under light anaesthesia (1.5% isoflurane in room air), 4 hours prior to perfusion. Animals were anaesthetized (2% isoflurane in room air) and trans-cardially perfused using heparinized saline, followed by 4% paraformaldehyde (PFA; Sigma) in 0.4M phosphate buffer (PBS; Sigma- Aldrich, USA). Spinal cords were harvested and post-fixed in PFA overnight, followed by cryoprotection in 30% sucrose (Sigma- Aldrich, USA). Spinal cords were cut at the site of the injection (as determined by the charcoal mark), and rostral and caudal portions embedded in optimal cutting temperature (OCT) compound, using isopentane pre-cooled in liquid nitrogen. Tissue blocks were stored at -80°C, until use. A cryostat (Leica Microsystems, Germany) was used to cut transverse sections 12 μm thick, which were thaw-mounted on glass slides. Sections were frozen at -20°C until required for immunohistology.

2.2.4 Histology

2.2.4.1 H&E staining

Transverse sections of the spinal cord were chosen 5 slides apart to be stained with haematoxylin and eosin (H&E), as follows. Following, 5 min PBS washes (Sigma- Aldrich, USA), the slides were incubated in haematoxylin for 2 minutes and washed again under running tap water. Slides were incubated for 30 to 60 seconds in 1% acid alcohol solution. Again, slides were washed for up to 10 minutes under running tap water. Slides were immersed for 2 minutes consecutively in 70%, 90% and 95% ethanol, followed by 1-minute incubation in 0.25% eosin. Slides were then dehydrated by immersing in fresh 90% ethanol twice for 2 minutes, and once in 100% (VWR) for 2 minutes. Finally, slides were immersed in xylene for 2 minutes, twice. The sections were cover slipped using DPX (VWR) and were left to dry at room temperature overnight, and imaged using light microscopy.

2.2.4.2 Luxol Fast Blue staining

Transverse sections of the spinal cord containing key lesion areas, as observed via H&E staining, were left to air-dry overnight. Sections were stained with luxol fast blue (LFB)/periodic acid- Schiff (VWR), and Harris haematoxylin to assess demyelination. Sections were taken to 100% ethanol (VWR) by gentle shaking with intervals of 70% ethanol for 5 minutes, followed by 90% ethanol for 5 minutes. The sections were incubated overnight at 50 °C with LFB solution: 0.1% LFB (BDH) in acidified 95% ethanol (1.0g LFB, 1000 ml 95% ethanol, 0.5ml glacial acetic acid). The next day, the sections were washed well in running tap water for about 5 minutes, or until the water ran clear. Afterwards, the sections were differentiated by cycling through saturated lithium carbonate (Merck, Germany) for 30 seconds, and continue to differentiate with 70% ethanol for 30 seconds, washing with running tap water in between each step. These two last steps were repeated as necessary to remove

LFB from white matter. Following these steps, the sections were oxidized in 1% periodic acid (VWR) for 20 minutes at room temperature (RT). Once more, the sections were washed under running tap water for at least 5 minutes. Sections were then incubated in neat Schiff's reagent (VWR) for 20 minutes at RT, washing in running tap again after this step for 5 minutes. The sections were counterstained in neat Harris haematoxylin (VWR) for 2 minutes, washed again for 5 minutes under running tap water, differentiated again until clear in 1% acid alcohol, and then washed for another 5 minutes under running tap water. Slides were then dehydrated by immersing in fresh 90% ethanol twice for 2 minutes, and once in 100% ethanol (VWR) for 2 minutes. Finally, slides were immersed in xylene for 2 minutes, twice. The sections were cover slipped using DPX (VWR) left to dry at room temperature overnight, and imaged using light microscopy.

2.2.4.3 Cresyl Violet staining

Three transverse sections of the spinal cord were chosen 5 slides apart from the epicentre of the lesion. Sections were left to air-dry overnight. The sections were rehydrated with PBS (Sigma- Aldrich, USA) for a minimum of 5 minutes, three different times. The sections were then incubated in preheated cresyl violet (CV) for 5 minutes, followed by immersion in distilled water 2 times, for 5 minutes each. Slides were then dehydrated by immersing in fresh 70%, followed by 90% ethanol for 2 minutes each, and once in 100% ethanol (VWR) for 2 minutes. Finally, slides were immersed in xylene for 2 minutes, twice. Stained sections were then mounted in DPX mounting medium (VWR), left to dry at room temperature overnight, and imaged using light microscopy.

2.2.5 Immunohistochemistry

Transverse sections of the spinal cord sections were left to air-dry overnight. Sections were rehydrated with PBS (Sigma- Aldrich, USA) for a minimum of 5 minutes, prior to incubation in 0.3% hydrogen peroxide (H_2O_2; Sigma-Aldrich, USA) in neat methanol (BDH International, UK) for 15 minutes with gentle agitation in to block endogenous peroxidase. All sections were incubated with 5% horse serum (Sigma) in PBS containing 0.1% Triton X-100 (Thermo Fischer Scientific) blocking buffer for a minimum of 30 minutes in order to minimize non-specific antibody binding. Next, sections were incubated overnight at 4 °C with primary monoclonal antibody (Table 3) diluted in the same blocking buffer previously described. The next day, all sections were washed with PBS three times, followed by incubation with biotinylated anti-mouse secondary antibody, diluted to 1/200 in the appropriate blocking buffer, for at least an hour at room temperature, see Table 3. Next, the sections were washed with PBS prior to incubation with the avidin-peroxidase complex (Vectastain Elite: Vector Laboratories Ltd, USA), for a minimum of 1 hour at room temperature, followed by another three PBS washes. Finally, the sections were exposed to a 3'-diaminobenzidine (DAB) reaction mixture (Vector DAB kit; Vector Laboratories Ltd, USA). When the developing brown colour appeared optimal, about 4 minutes later, the sections were immersed in tap water to stop the reaction, and then rinsed for an additional 10 minutes in running tap water. Slides were then dehydrated by immersing in graded alcohols (70%, 90 %, 100% x2) followed by two changes of xylene for 2 minutes. Stained sections were then mounted in DPX mounting medium (VWR), left to dry at room temperature overnight, and imaged using light microscopy.

Antibody	Target	Isotype	Blocking Buffer	Dilution	Source
Mouse Anti- GFAP	Astrocytes	Mouse IgG	5% normal horse serum (Sigma) in 0.01% PBS- triton-x	1:200	Sigma
Mouse Hydroxyprobe-1-anti- pimonidazole	Pimonidazole adducts	Mouse IgG	0.25% casein (VWR International, UK), in 0.01% PBS-triton-x	1:500	HPI Inc
Mouse Anti-rat ED1	Activated macrophages/ microglia	Mouse IgG1	5% normal horse serum (Sigma) in 0.01% PBS- triton-x	1:200	Abcam
Mouse anti- rat endothelial cell antigen-1 (RECA-1)	Endothelial cells	Mouse IgG1	5% normal horse serum (Sigma) in 0.01% PBS- triton-x	1:200	Abcam
Rabbit anti-IBA	Macrophages /Microglia	Rabbit IgG	5% normal goat serum (Sigma) in 0.01% PBS-triton-x	1:500	WAKO
Rabbit Anti- HIF-1α	Hypoxia inducible factor-1α	Rabbit IgG	5% normal goat serum (Sigma) in 0.01% PBS-triton-x	1:200	Abcam

Table 3 Antibody details for immunohistochemistry (IHC).

2.2.6 Immunofluorescence

Spinal cord sections were air dried overnight. The sections were rehydrated with PBS (Sigma- Aldrich, USA), prior to incubation in neat methanol, with three subsequent PBS washes. Sections were blocked in normal goat serum (NGS) for 30 minutes, prior to incubation in primary antibody overnight at 4^{o}C. The following day, the sections were washed with PBS. Sections were then separately incubated with polyclonal goat anti-rabbit (1:200, Invitrogen) and goat anti-rabbit Cy3 (1:200, Invitrogen) secondary antibodies for 60 minutes each at room temperature (Table 4). PBS washes were carried out between each step. Slides were mounted with Vectashield mounting medium (Vector) and stored at 4°C in the dark, prior to examination with confocal microscopy (Zeiss 710).

Antibody	Target	Isotype	Blocking Buffer	Dilution	Source
Rabbit Anti- GFAP	Astrocytes	Rabbit IgG	5% NGS in 0.01% PBS-triton	1:500	DAKO
Rabbit Anti-IBA	Microglia/ macrophages	Rabbit IgG	5% NGS in 0.01% PBS-triton	1:200	Abcam

Table 4 Antibody details for immunofluorescence (IF).

2.2.7 Microscopy

2.2.7.1 Light microscopy and quantification

Tissue sections were viewed using an Axiophot light microscope (Zeiss, Germany), and micrographs taken using a Nikon D300 camera (Nikon, USA). The illumination was kept constant throughout image acquisition, under the same magnification. Analysis of the grey matter atrophy was carried out by tracing around the grey matter spinal cord sections lesion side, and its corresponding counterpart, as well as all grey matter. Quantification was carried out using the "analyse measurement" tool on Image J (National institute of health, USA). Analysis of the intensity of the labelling with pimonidazole was carried out by tracing around the spinal cord sections (white and grey matter, and grey matter alone, irrespectively), and measuring the pixel intensity using Image J. Quantification of all other markers was carried out using the 'analyse particles' tool, on thresholded images, to determine the number, of positively labelled cells. The same settings were used for each image, and area measurements were carried out concurrently.

2.2.7.2 Confocal microscopy

Confocal fluorescent images were obtained using a Zeiss 710 confocal microscope, with a 40X water immersion objective. Excitation wavelengths of 488 nm and 543 nm were provided by argon and helium-neon gas lasers.

2.2.8 Statistical analysis

2.2.8.1 Behavioral analysis

All data were tested for normality using the D'Agostino & Pearson test. Data that were not normally distributed were evaluated using non-parametric statistics as indicated. P-values of 0.05 (*), 0.01 (**), 0.001 (***) and 0.0001(****), were considered as statistically significant. All statistical analyses were carried out GraphPad Prism version 8.

A two-way analysis of variance (ANOVA) test was performed on time course scoring experiments, to compare the significance between different time points and between the two treatment groups, those being saline and LPS. When treatment groups were compared at a single time point, t- tests were performed to assess significance.

2.2.8.2 Neuronal counts

Large neurons with visible nucleus present were counted as motor neurons using Image J (National institute of health, USA). All data were tested for normality using the Shapiro-Wilk test. A two-way ANOVA test was performed on neuronal counts to assess the significance between different time points and between the two treatment groups, those being saline and LPS. P- values of 0.05 (*), 0.01 (**), 0.001 (***) and 0.0001(****), were considered as statistically significant. All statistical analyses were carried out using GraphPad Prism version 8.

2.2.8.3 Statistical analysis of PIMO labelling

The pixel intensity of the pimonidazole labelling was normally distributed in all spinal cord sections examined. Therefore, the percentage of pixels labelled with an intensity greater than the mean of the corresponding controls plus one standard deviation was counted and compared to the appropriate vertebral segment-matched control using a Wilcoxon test; the

saline-injected group served as controls in each of the respective experiments, for each individual animal. All statistical analyses were carried out using GraphPad Prism version 8.

2.2.8.4 Statistical analysis of RECA-1

The data obtained from sections labelled with RECA-1 followed a normal distribution, therefore, the independent t-test was used to compare the RECA-1 cell density, at each spinal cord segment, between the two groups (saline and LPS). A repeated measures Two-Way ANOVA was used to compare the cumulative RECA-1 cell density. All statistical analyses were carried out using GraphPad Prism version 8.

2.3 Results

2.3.1 Acute disability

2.3.1.1 LPS injection on the ventral horn causes acute disability

Animals were assessed for functional disability following the intraspinal injection of LPS. LPS injected animals exhibited transient tail weakness following lesion induction (Figure 2-4), with disability particularly significant at 48 hours (Figure 2-5), however by 72 hours (Figure 2-6), function began to recover and was similar to baseline levels by 96 hours. No such changes were evident in saline injected control animals at any of the time points examined. As the deficit observed in LPS injected animals subsided by 96 hours post-injection, subsequent acute studies have focused on this time window.

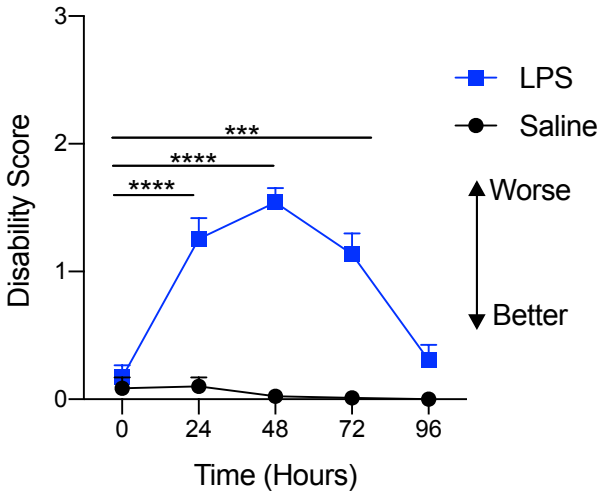

Figure 2-4 Acute tail disability

Tail disability scores while walking horizontally for animals injected with saline (n=10) or LPS (n=19). Animals were trained from one day before surgery (baseline) up to four days after surgery. Values are means ± SEM. Statistical analysis was performed with a *Two-way ANOVA* test (****: $P<0.0001$), (***: $P<0.001$).

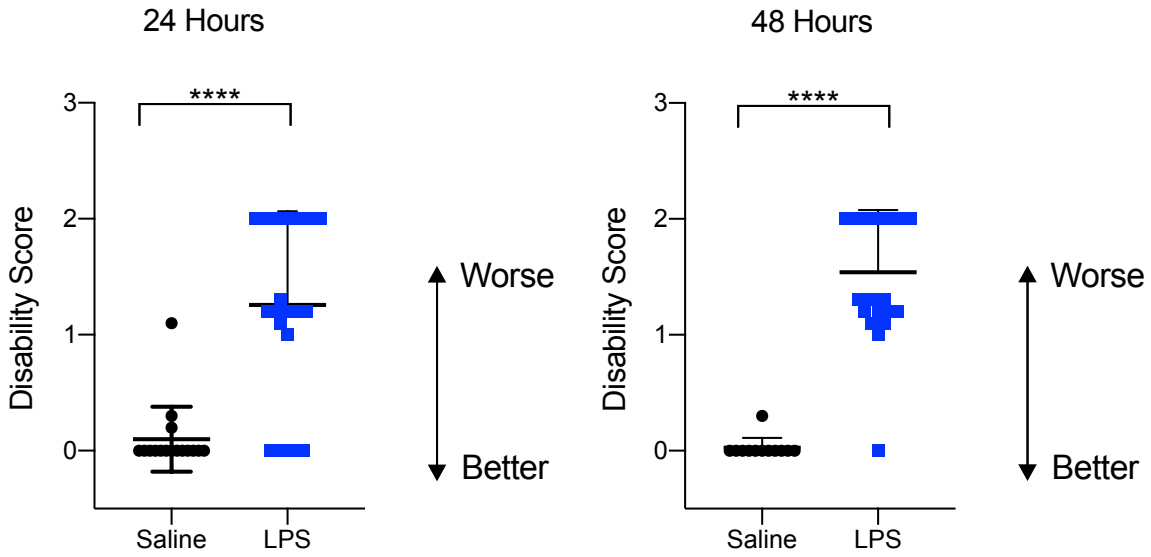

Figure 2-5 24 and 48 Hours tail deficit

Tail deficit scores while walking on a horizontal surface for animals injected with saline (n=16) or LPS (n=25) after 24 hours (A) and after 48 hours (B), saline (n=12) or LPS (n=22). Statistical analysis was performed with a Welch's Test (****: P=<0.0001).

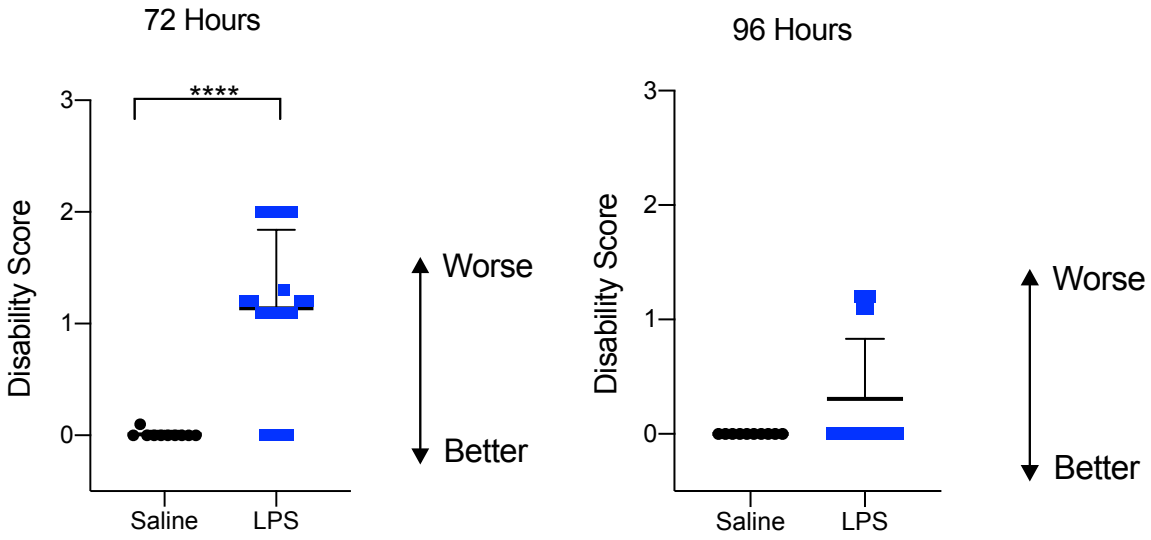

Figure 2-6 72 and 96 Hours tail deficit

Tail deficit scores while walking on a horizontal surface for animals injected with saline (n=10) or LPS (n=19) after 72 hours (A) and after 96 hours (B), with Saline (n=10) or LPS (n=19). Statistical analysis was performed with a Welch's Test (****: P<0.0001).

2.3.1.2 LPS injection causes hindlimb acute motor deficit on horizontal ladder

Animals were assessed for hindlimb functional disability while walking on the horizontal ladder with unevenly spaced rungs. When different errors occurred, the worst of the scores was recorded, as advised by the foot fault scoring system previously published (Metz and Whishaw, 2002).

Saline controls showed a decrease in the ability to walk smoothly along the horizontal ladder at the 24-, 48- and 96-hour periods, compared with baseline, in particular at the 24, 48 and 96 time points *(*P=<0.05).* LPS groups showed a worse ability to walk along the horizontal ladder, most significantly at 24 hours post injection (***P*<0.01), compared with baseline scores. Disability for LPS group was also seen after 48 hours, 72 hours and 96 hours compared with baseline, however, it was less significant (**P*<0.05). All data are presented as mean ± standard error.

Both saline and LPS groups showed a similar trend of hindlimb disability (Figure 2-7). However, LPS group scoring averages were lower, categorizing animal group as being acutely less able to anticipate rung location with accuracy.

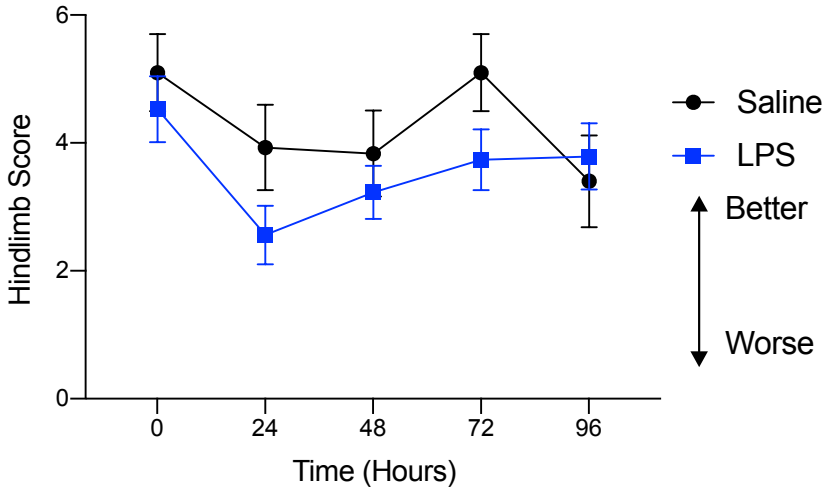

Figure 2-7 Acute hindlimb score

Hindlimb scores while walking on horizontal ladder of animals injected with saline (Controls) and LPS. Graph shows combined means of control saline-injected animals (n=14) and -LPS injected animals (n=25) ± SEM. *Two-way ANOVA.*

2.3.1.3 LPS injections have an effect on the running speed of SD rats

Animals were subject to running on the TreadScan treadmill for 1 minute at every time point (baseline, 24-, 48-, 72-, 96 hours and 1- month post-surgery). After 24 hours post-surgery, running speed of animals injected with saline continuously increased at all points, in comparison with baseline, however, at no time were the results statistically significant. Similar to control animals, the speed of LPS animals dropped slightly at 24 hours post-surgery, however, it continued to drop at 48 hours. There was then a significant increase in speed of the LPS group at 72 hours post-surgery, in comparison with 24 hours ($P^* < 0.05$) and 48 hours ($P^{**} < 0.01$). The speed at 96 hours and 1-month post-surgery recovered close to around 65 mm/s, namely similar to 72 hours.

The change in scores was similar between the groups, except at 48 hours post-surgery. At this time the average speed for the saline group was near 50 mm/s, however, for the LPS group the average speed was closer to 13 mm/s. The difference between the two groups was statistically significant ($P^* < 0.05$) at 48 hours.

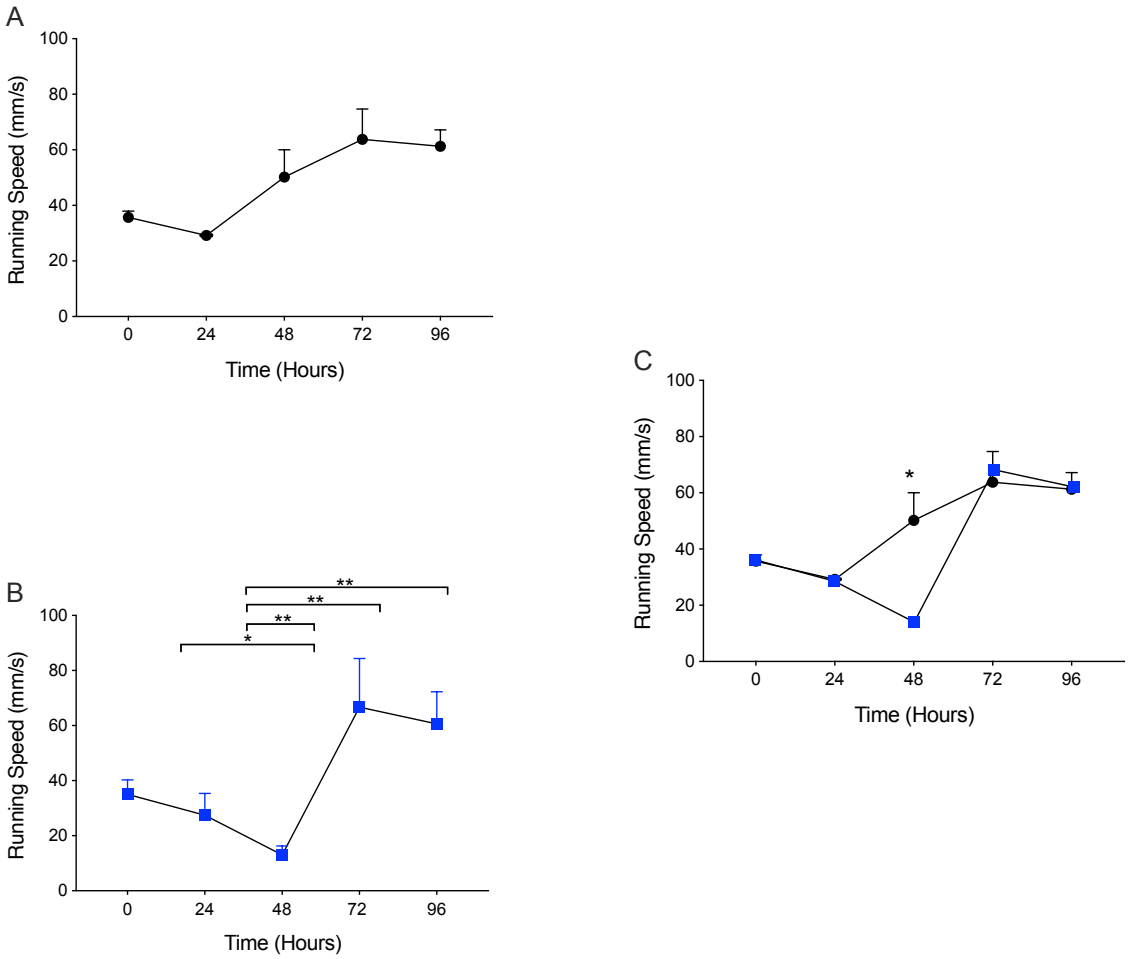

Figure 2-8 Saline and LPS hindlimb Score

A. Running speed while placed on treadmill at speed 20cm/s of animals injected with saline (n=5) as controls. **B.** Overall average running speed while walking on the treadmill at speed 20cm/s of animals injected with LPS (n=5). **C).** Overall average running speed of animals injected with saline (Controls) and LPS. Graph shows combined means of control saline-injected animals (n=5) and -LPS injected animals (n=5). Results were subject to *Two-way ANOVA*, ($P^* < 0.05$), ($P^{**} < 0.01$).

2.3.2 Acute histology

2.3.2.1 H&E staining on sections from acute animal

Structural changes, post injection, were assessed by looking at sections stained with H&E. Acute tissue was collected at four different time points: 24 hours, 48 hours, 72 hours and 96 hours post-surgery. No statistical analysis has been conducted on the tissue, as the number of animals per group was insufficient for this purpose. Sections from saline-injected animals did not show inflammation, or a difference in motor neuron numbers at any of the acute stages shown below. At 24, 48- and 72-hours post injection, the spinal cords of animals injected with LPS showed oedema and inflammation near the ventral horn, particularly at 48 hours, coinciding with the expression of acute behavioural deficits. A conundrum arose regarding the number of motor neurons present at the site of injection. In H&E sections, the number of motor neurons counted in the injected side of LPS animals was reduced at 24 and 48 hours, but was less so at 72 and 96 hours. Of course, the observations are necessarily made in different animals, rather than longitudinally. An additional complication is that the animals studied at 24 and 48 hours were injected on a different day to the ones studied at 72 and 96 hours, which introduces the possibility of an unintended difference in injection between the different occasions. To obtain a different perspective on motor neuron survival, a different stain was employed, namely cresyl violet (CV), but this stain provided the same conundrum as observed with the H&E, as shown in Figure 2-10. The conundrum is discussed further in the Discussion. LFB staining was also done on the acute time point saline and LPS sections, to look for early signs of demyelination, as shown in Figure 2-11. The LFB staining of the myelin was not intense in this staining ‘run’, but there was no suggestion of demyelination, and since other experiments have not shown any demyelination at this time, the staining was not repeated.

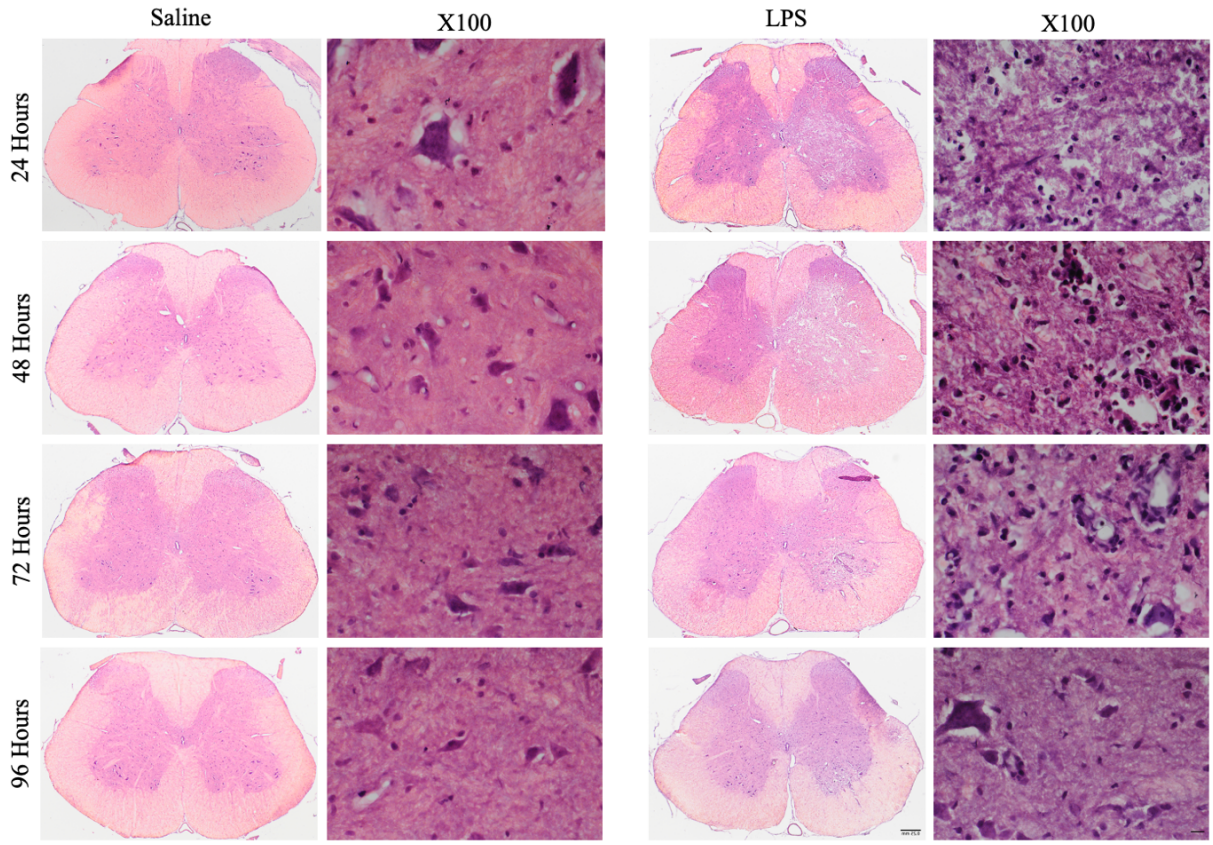

Figure 2-9 H&E of acutely lesioned spinal cords

Transverse sections showing acute lesions in spinal cords stained with H&E, comparing the ipsilateral and contralateral ventral horn 24-, 48-, 72- and 96 hours post-surgery. Left column shows control tissue injected with saline, whereas the right column shows spinal cords injected with LPS, each with its corresponding lesioned sides. Scale bars are 250µm (low magnification) and 25µm (higher magnification).

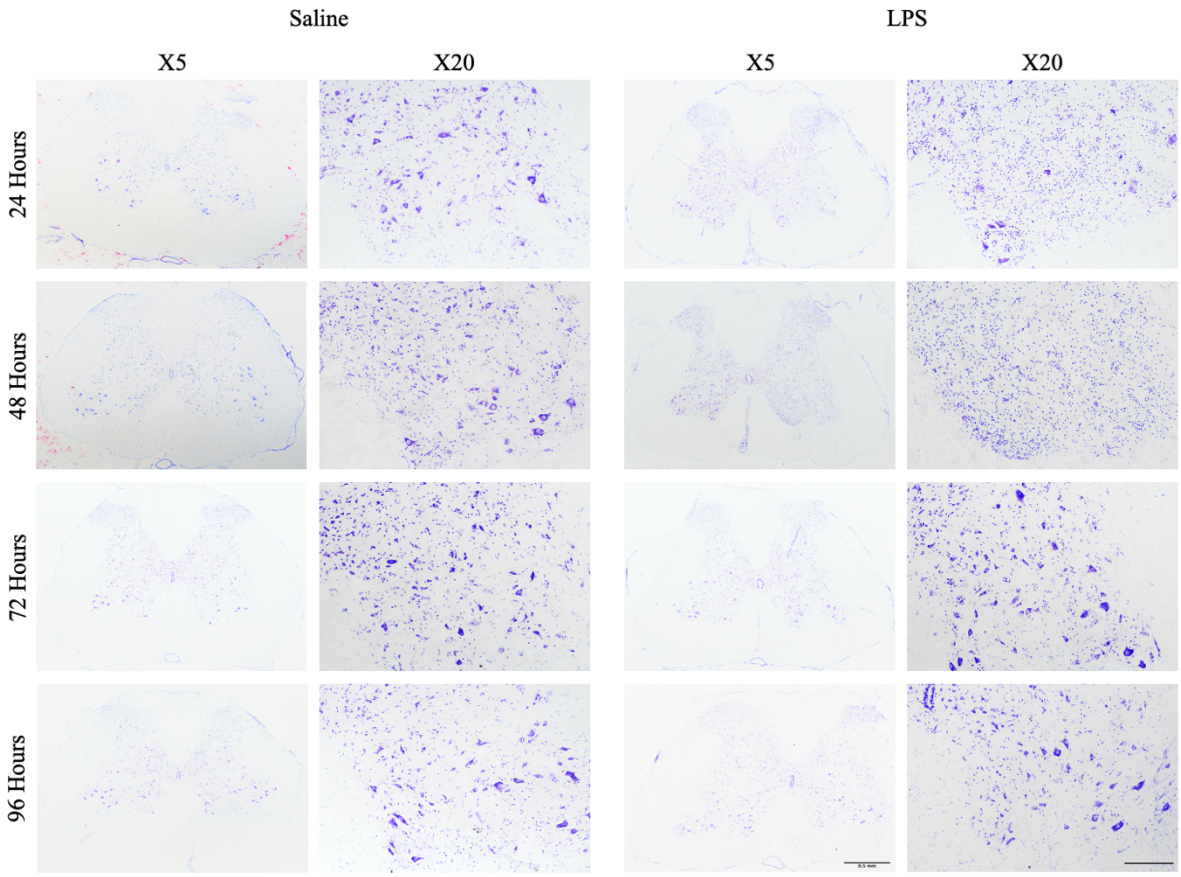

Figure 2-10 CV of acutely lesioned spinal cords

Transverse sections showing acute lesions in spinal cords stained with CV, comparing the ipsilateral and contralateral ventral horn 24-, 48-, 72- and 96 hours post-surgery. Left column shows control tissue injected with saline, whereas the right column shows spinal cords injected with LPS, each with its corresponding lesioned sides. Scale bars are 500µm (low magnification) and 200µm (higher magnification).

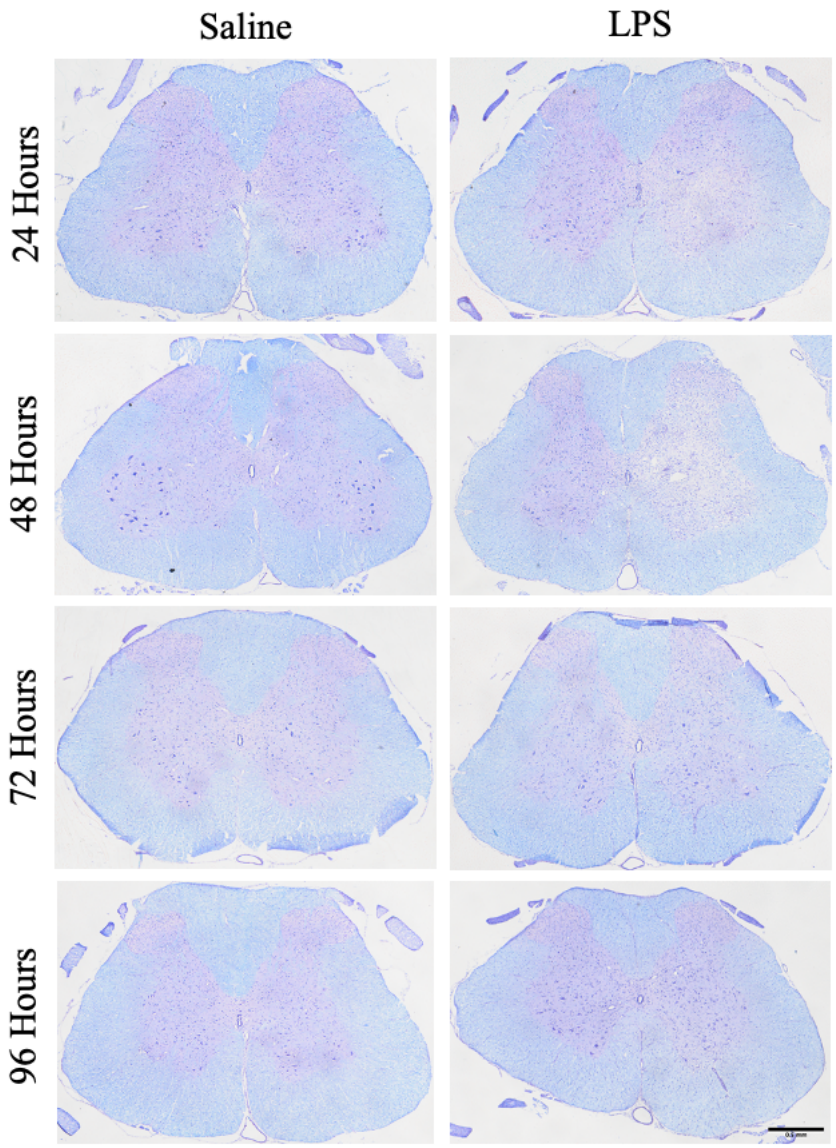

Figure 2-11 LFB of acutely lesioned spinal cords

Transverse sections showing acute lesions in spinal cords stained with LFB (myelin), comparing the ipsilateral and contralateral ventral horn 24-, 48-, 72- and 96 hours post-surgery. Left column shows control tissue injected with saline, whereas the right column shows spinal cords injected with LPS. Scale bar is 500µm.

2.3.3 Acute immunohistochemistry

2.3.3.1 LPS injection induces inflammation acute stages of lesion development

2.3.3.1.1 ED1 Labelling

ED1 primary antibody was used to mark activated microglia/macrophages in the acute LPS- and saline-injection experiments. We anticipated that animals injected with LPS would have an increased macrophage activation. Anti-ED1 antibody revealed that microglia in the spinal cord of animals injected with saline at 24 hours, 48 hours, 72 hours and 96 hours post injection did not express ED1 antigen. In contrast, there was clear expression of ED1 antigen at 24 hours, and 48 hours, with significant diminishment at 72 hours post injection in the LPS experiments. The ED1 expression was especially apparent at 48 hours post LPS injection, particularly near the injection area, as expected. Figure 2-12 shows images of transverse spinal cord sections labelled for ED1. The labelling is unambiguous, but no statistical analysis has been conducted due to the small sample size.

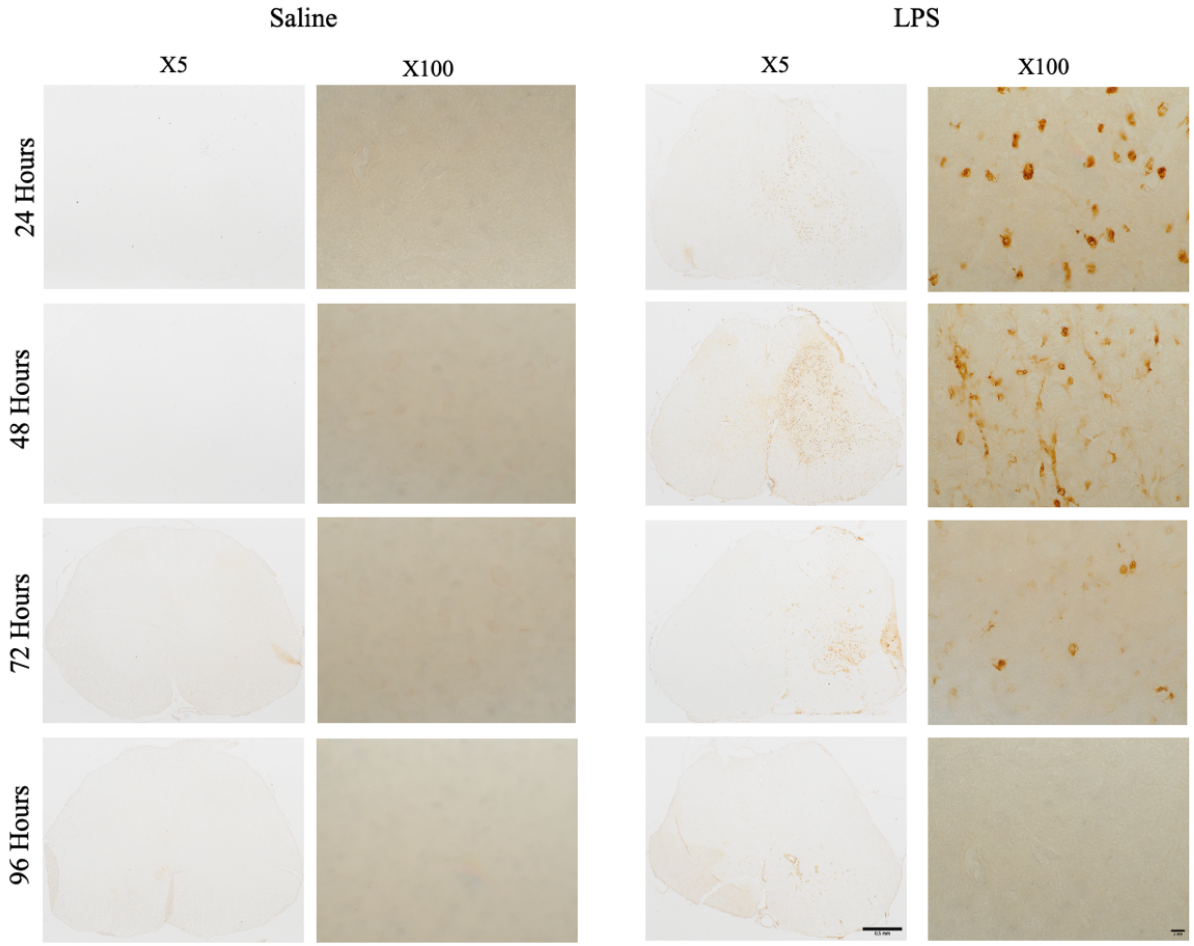

Figure 2-12 ED1 labelling of acutely lesioned tissue

Spinal cords from acutely lesioned animals labelled with ED1, comparing the ipsilateral and contralateral ventral horn 24-, 48-, 72- and 96 hours post-surgery. Left column shows control tissue injected with saline, whereas the right column shows spinal cords injected with LPS, each with its corresponding lesion side magnification images. Scale bars are 500 μm (low magnification) and 2000μm (higher magnification).

2.3.3.1.2 IBA Labelling

IBA primary antibody was used to mark activated macrophages and microglia in the acute LPS- and saline-injection experiments (Figure 2-13 A). Anti-IBA labelling revealed no microglia/macrophages activation in the spinal cord of animals injected with saline at any of the acute timepoints. In contrast, there was clear expression of IBA labelling at 24-, 48-, and 72 hours with significant diminishment at 96 hours post injection in the LPS experiments. The IBA labelling was especially apparent at 48 hours post LPS injection, particularly near the injection area, as expected and in correlation with the ED1 labelling results. Overall, the difference in IBA labelling on the grey matter between the saline controls and LPS groups is significant (***: P=<0.001) on all acute time points.

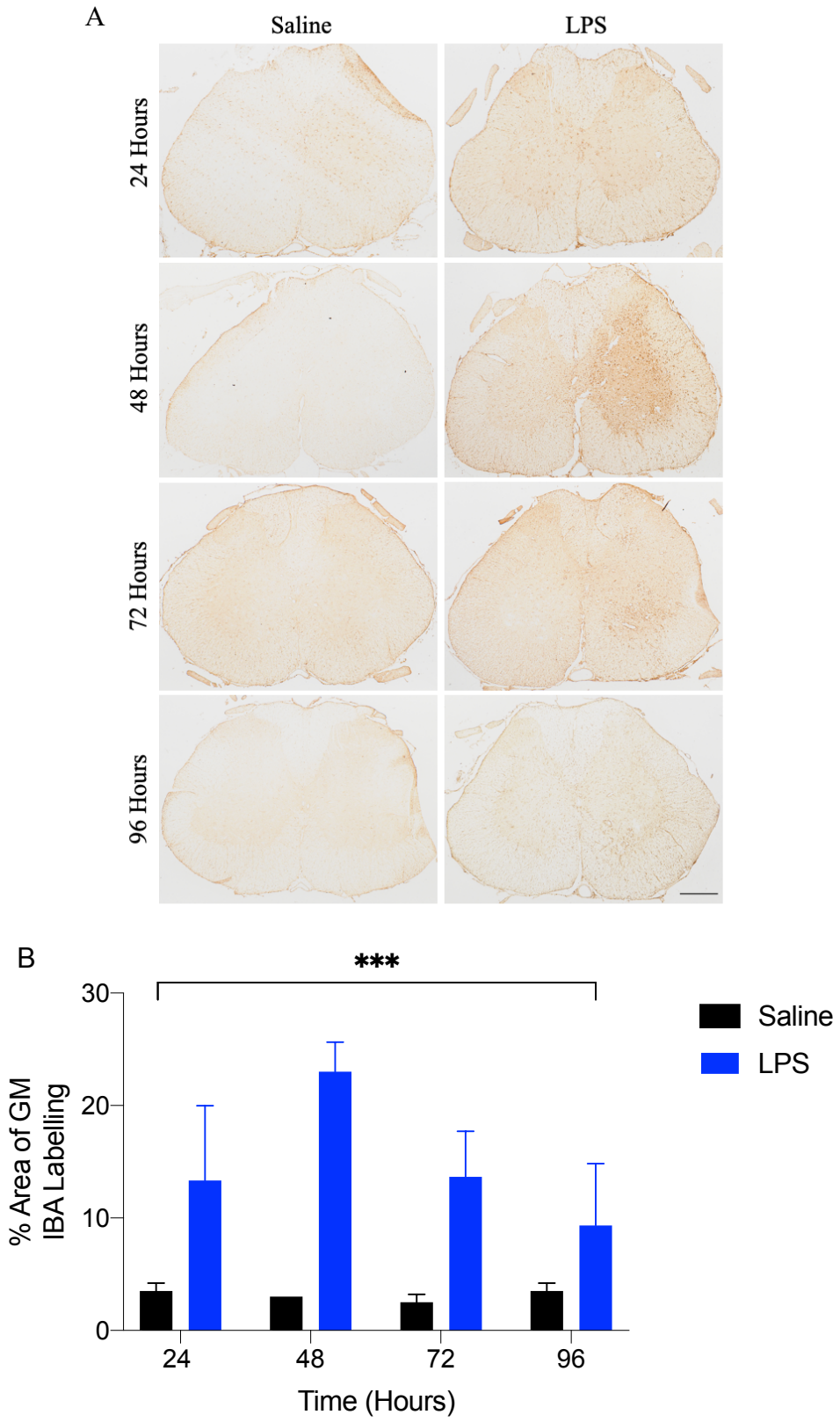

Figure 2-13 IBA Labelling of acutely lesioned spinal cords

A. Spinal cords from acutely lesioned animals labelled with IBA, comparing the ipsilateral and contralateral ventral horn 24-, 48-, 72- and 96 hours post-surgery, scale bar 500 µm. Left column shows

control tissue injected with saline, whereas the right column shows spinal cords injected with LPS. **B.** Graph showing the magnitude of IBA percentage labelling of the grey matter spinal cord of animals injected with saline (Controls)(n=2) and LPS (n=3) ± S.D. *Two-way ANOVA* (***: P=<0.001).

2.3.3.2 GFAP labelling shows acute signs of astrocyte activity

GFAP primary antibody was used to mark the presence of astrocytes, and possible gliosis. Overall, saline control groups showed little to no abnormal immunoreactivity at any acute time point. However, LPS-injected groups showed a significant and unambiguous increase in GFAP labelling, particularly at 24-hours, 48-hours and 72-hours post LPS injection, in comparison with the non-injected contralateral side (Figure 2-14). At the 48-hour post LPS injection time point the GFAP labelling was its most intense, correlating to the other histological markers previously described, as well as the peak of disability.

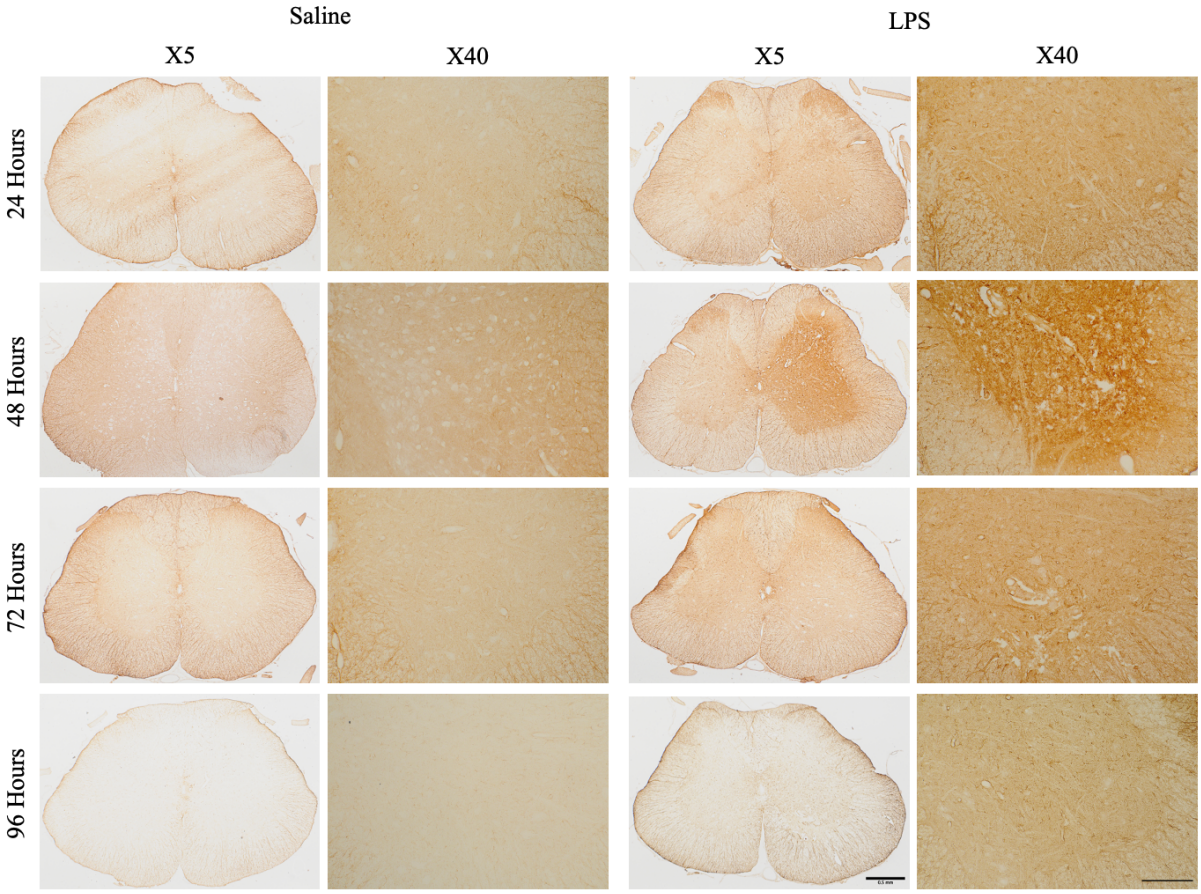

Figure 2-14 GFAP Labelling of acutely lesioned spinal cords

Spinal cords from acutely lesioned animals labelled with GFAP, comparing the ipsilateral and contralateral ventral horn 24-, 48-, 72- and 96 hours post-surgery. Left column shows control tissue injected with saline, whereas the right column shows spinal cords injected with LPS, each with its corresponding lesion side magnification images. Scale bars are 500µm (low magnification) and 100µm (higher magnification).

2.3.3.3 PIMO Labelling shows acute evidence of hypoxia

PIMO was used to investigate a role for hypoxia in the motor disability. As shown in Figure 2-15, there is no visible PIMO labelling present in any of the acute saline spinal cord sections. At 24 hours post injection, there is some PIMO labelling present in the LPS spinal cord section, which incremented in intensity after 48 hours. After 72 hours post injection, PIMO labelling appeared to be reduced and it finally disappeared by 96 hours post injection. The difference in PIMO labelling on the grey matter between the saline controls and LPS groups is significant (*: P=<0.05) on all acute time points.

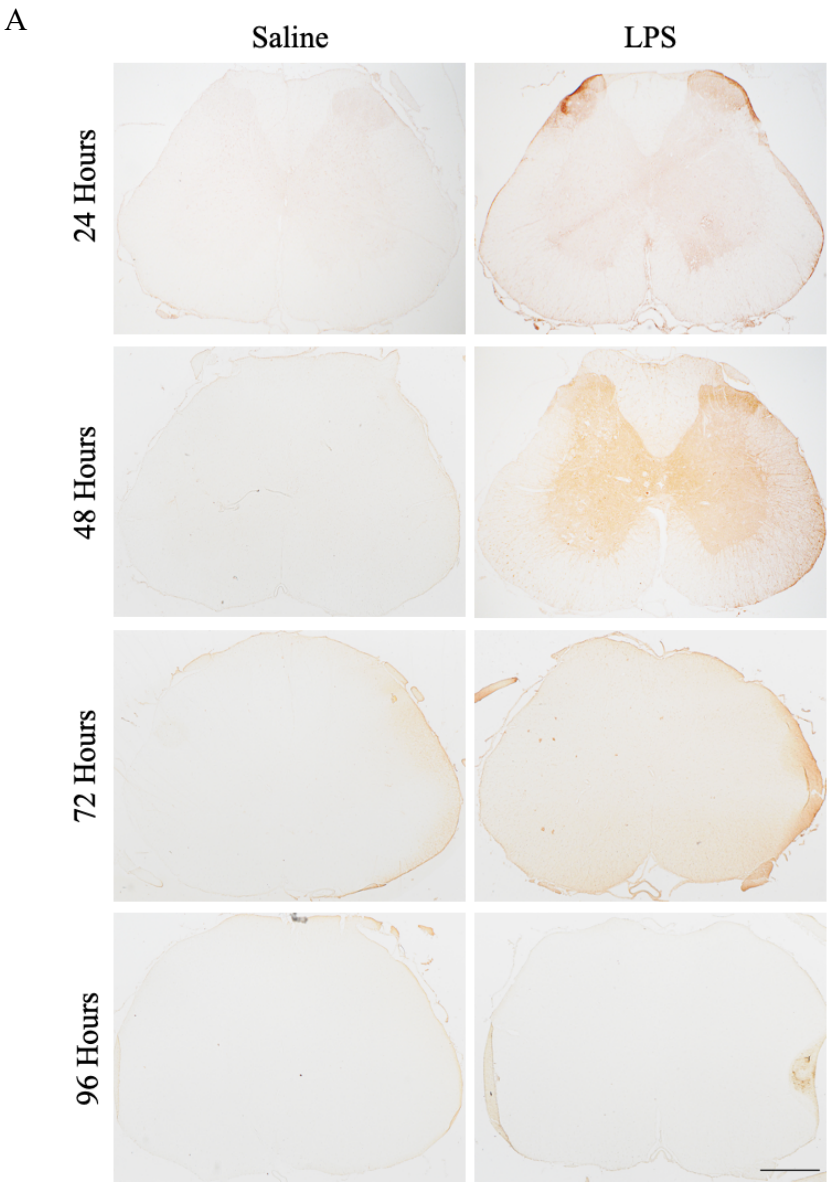

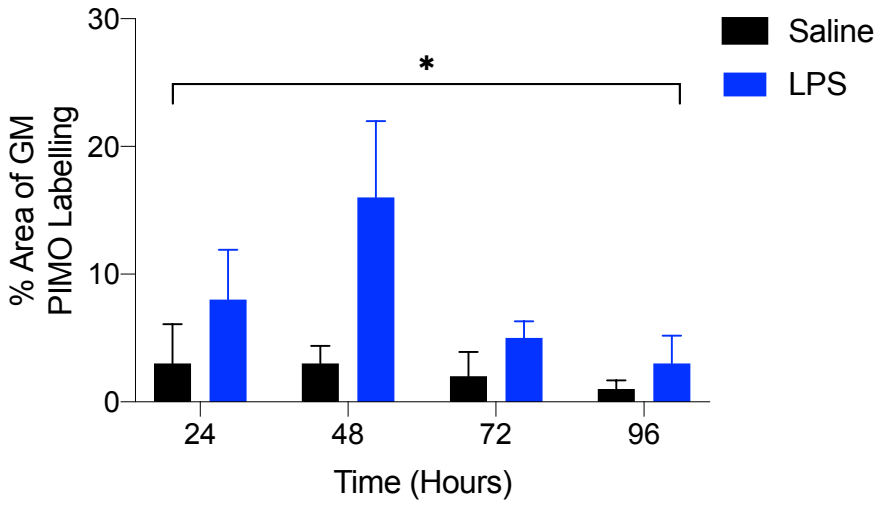

Figure 2-15 PIMO Labelling of acutely lesioned spinal cords

A. Transverse sections showing acute lesions in spinal cords labelling with PIMO, comparing the ipsilateral and contralateral ventral horn 24 hours, 48 hours, 72 hours and 96 hours post-surgery. Left column shows control tissue injected with saline, whereas the right column shows spinal cords injected with LPS, each with its corresponding non-lesion and lesioned sides. Scale bar is 500 µm. **B.** Graph showing the acute PIMO labelling percentage area of the GM of animals injected with saline (Controls) and LPS, injected side only. Graph shows combined means of control saline-injected animals (n=2) and -LPS injected animals (n=4) ± SEM. *Two-way ANOVA* (*: *P*=<0.05).

2.3.3.4 HIF-1α Labelling shows acute evidence of hypoxia

HIF-1α was used to investigate, and further confirm, the presence of hypoxia in the motor disability. As shown in Figure 2-16, there is no visible HIF-1α labelling present in any of the acute saline spinal cord sections. At 24-and 48 hours post injection, there is some HIF-1α labelling present in the LPS spinal cord section. HIF-1α labelling was reduced by 72 hours and completely disappeared by 96 hours post. These results are in agreement with the immunohistochemical PIMO labelling mentioned earlier (Figure 2-15), as well as motor deficit at these time points. Overall, the difference in HIF-1α labelling on the grey matter between the saline controls and LPS groups is significant (****: P=<0.001) on all acute time points.

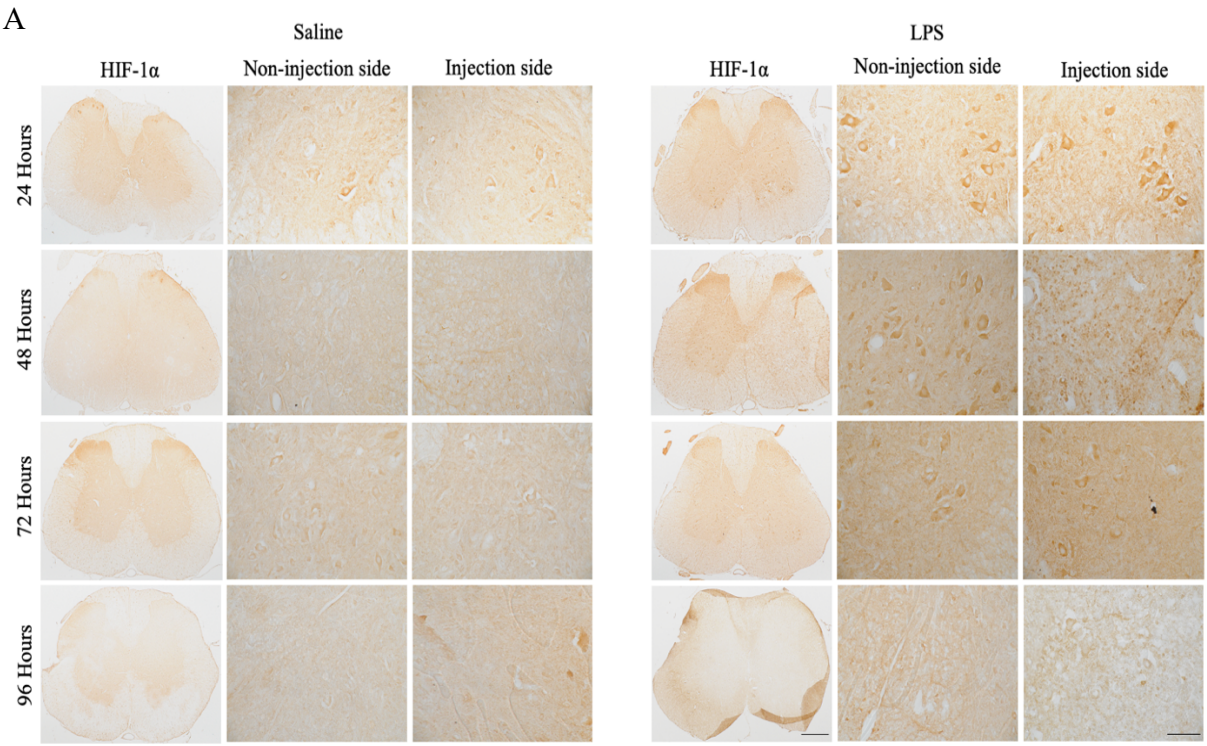

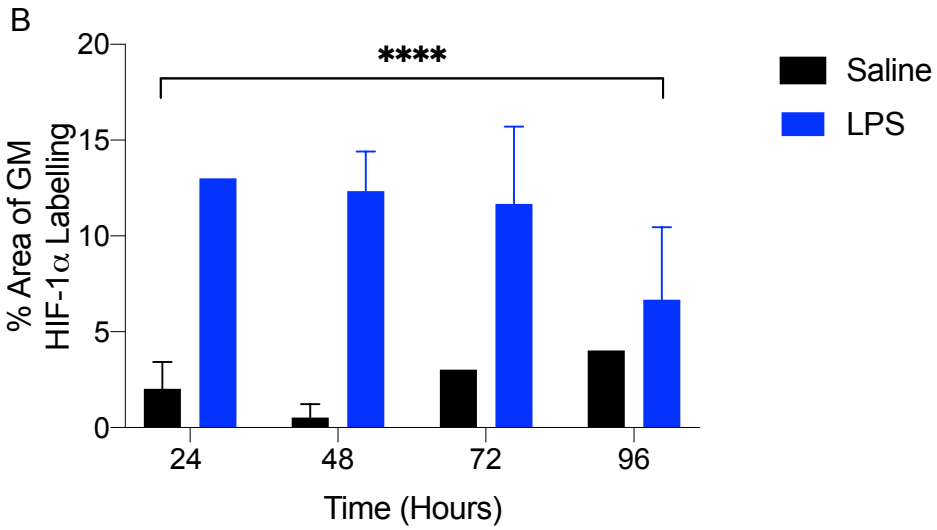

Figure 2-16 HIF-1α Labelling of acutely lesioned tissue

A. Transverse sections showing acute lesions in spinal cords labelled with HIF-1α, comparing the ipsilateral and contralateral ventral horn 24-, 48-, 72- and 96 hours post-surgery. Left column shows control tissue injected with saline, whereas the right column shows spinal cords injected with LPS, each with its corresponding non-lesion and lesion side magnification images. Scale bars are 500µm (low magnification) and 100µm (higher magnification). **B.** Graph showing the acute HIF-1α labelling percentage area of the spinal cord of animals injected with saline (Controls) and LPS. Graph shows combined means of control saline-injected animals (n=2) and LPS-injected animals (n=3) ± S.D. *Two-way ANOVA* (****: *P*=<0.0001).

2.3.3.5 RECA-1 Labelling and acute variation in vascular density

RECA-1 primary antibody was used to determine vessel size and volume. As shown in Figure 2-17 A, there is no visible difference in RECA-1 presence in any of the acute saline spinal cord sections, on both the non-lesion and lesion sides. At 24-, 48- and 72- hours post injection, there is some decrease in RECA-1 labelling present in the injected of the LPS injected spinal cord section, in comparison with the non-injected side. At 96 hours post injection of LPS, the RECA-1 labelling appeared to be more equal between the non-injected side and the injected side. The results were not statistically significant (Figure 2-17 B).

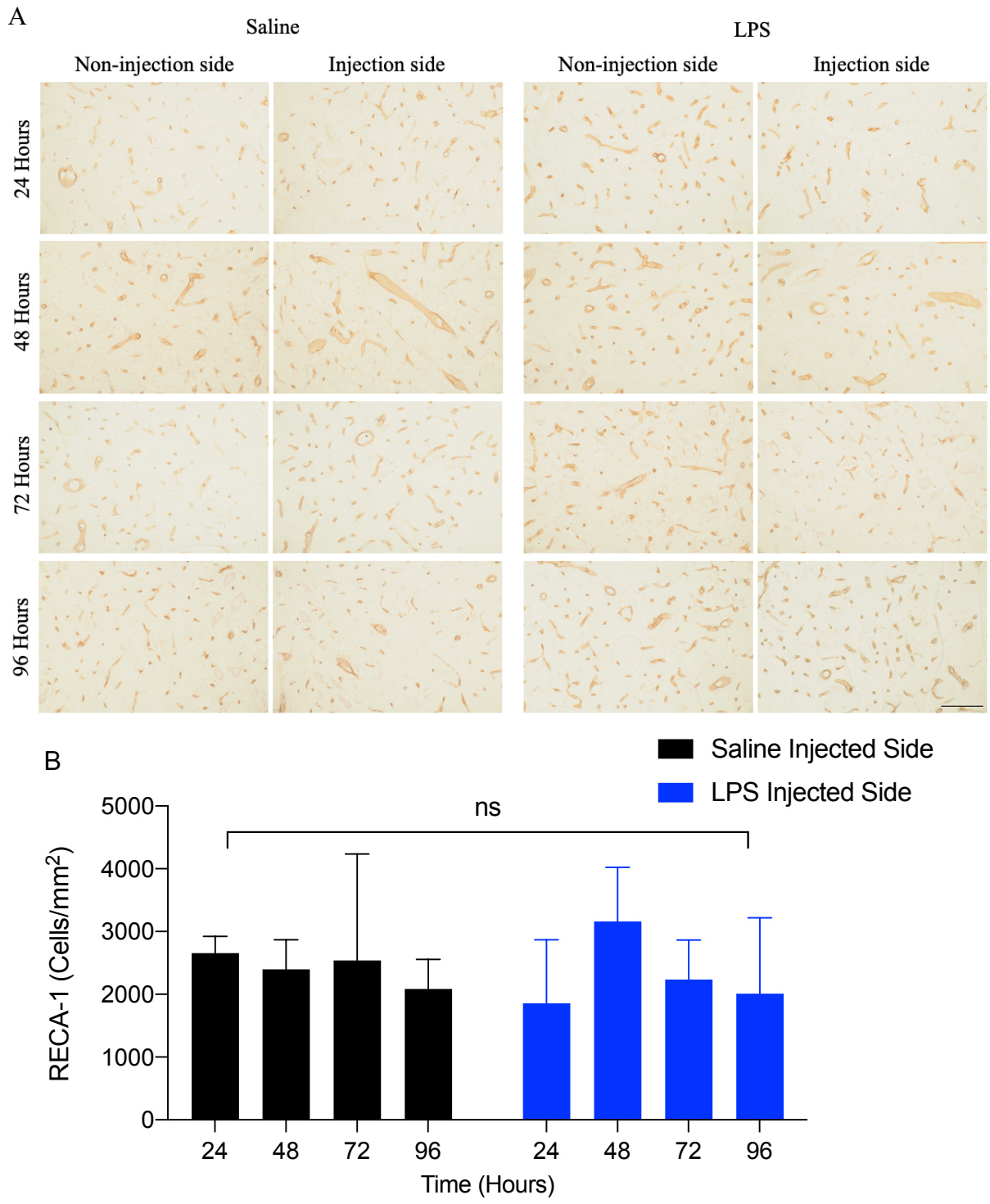

Figure 2-17 RECA-1 Labelling of acutely lesioned tissue

A. Transverse sections showing acute lesions in spinal cords labelled with RECA-1, comparing the ipsilateral and contralateral ventral horn 24-, 48-, 72- and 96 hours post-surgery. Left column shows control tissue injected with saline, whereas the right column shows spinal cords injected with LPS. Scale bar is 100µm. **B.** Graph showing the acute RECA-1 cell density of the spinal cord of animals injected with saline (Controls) and LPS. Graph shows combined means of control saline-injected animals (n=2) and LPS-injected animals (n=3) ± S.D. *Two-way ANOVA.*

2.3.4 Chronic disability

2.3.4.1 LPS injection causes hindlimb deficit in SD rats

Animals were assessed for chronic hindlimb disability while walking on the horizontal ladder with unevenly spaced rungs. Saline and LPS animals did not show any significant change from baseline in ladder scores throughout the 12 months of recording sessions. However, a clear trend towards a difference between the groups developed over time. From months 2 to 4 post-surgery, both control and LPS groups slightly improved their performance, however, as control groups continued to do well, LPS animals clearly declined in their ability to walk. At month 7, there was a significant difference between saline and LPS groups (*: $P<0.5$).

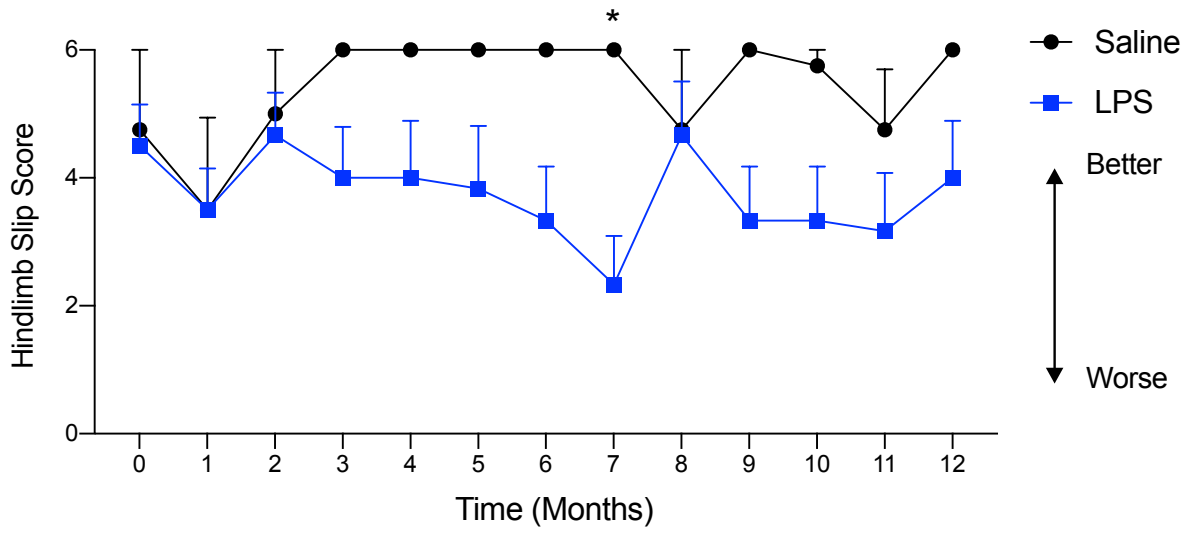

Figure 2-18 Chronic hindlimb disability

Tail disability scores of controls (n=4) and LPS groups (n=10). Animals were trained from one day before surgery, and every month after that. Month 0 corresponds to baseline value recorded before surgery. Results were subject to *Two*-way ANOVA; $P^* < 0.05$. Values are means ± SEM.

2.3.4.2 LPS injection causes chronic tail deficit in SD rats

Disability was assessed for functional deficit following the intraspinal injection of LPS, as described earlier (Figure 2-3), once every month after surgery. Animals injected with saline showed no significant difference between baseline and subsequent months. As mentioned earlier, LPS injection caused acute tail weakness, which recovered close to baseline after 96 hours post-surgery (Figure 2-6). Tail disability worsened again, particularly after 1-month post LPS injection (****: $P<0.0001$). Tail weakness does not significantly recover in LPS-injected animals post 1 month after surgery; on the contrary, as animals start to age, tail strength continued to decrease, such that a very significant (****: $P<0.0001$) decrease in disability was maintained compared to baseline. Figure 2-19 shows a month- by-month comparison of LPS-injected animals compared to saline controls.

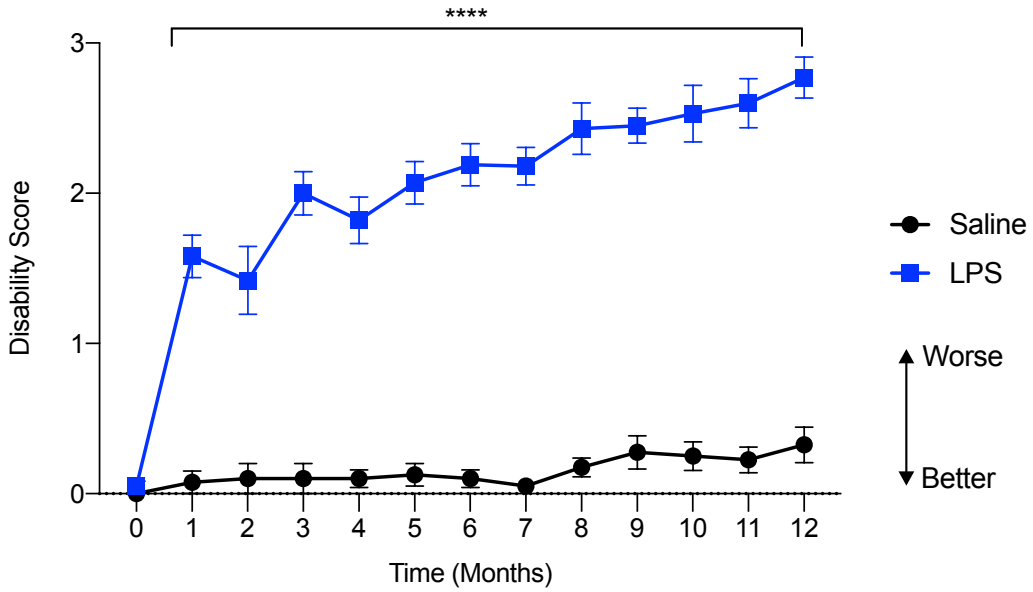

Figure 2-19 Chronic tail disability

Tail disability scores while walking on a horizontal surface for 1 metre, for animals injected with saline (n=4), or LPS (n=10). Animals were trained from one day before surgery, and every month after that. Month 0 corresponds to baseline value recorded before surgery. Results were subject to *Two-way ANOVA* (****: $P<0.0001$). Values are means ± SEM.

Figure 2-20 describes the acute and chronic response to the saline (controls) and LPS injection, which causes an early and significant (****: $P<0.0001$) tail weakness in LPS groups, as described earlier (Figure 2-4). Acute tail weakness diminishes after 96 hours post LPS injection, however, a delayed chronic response arises at 1-month post LPS injection, one that equals that of the peak disability at 48 hours post LPS injection. Hereafter, the LPS injected group tail disability continues to increase, reaching a new chronic peak of the disease at the end of the one-year experiment. Saline control animals, however, do not show any significant change in the tail strength experiment in both acute and chronic time points, ruling out that age is a major contributing factor in this behavioural test.

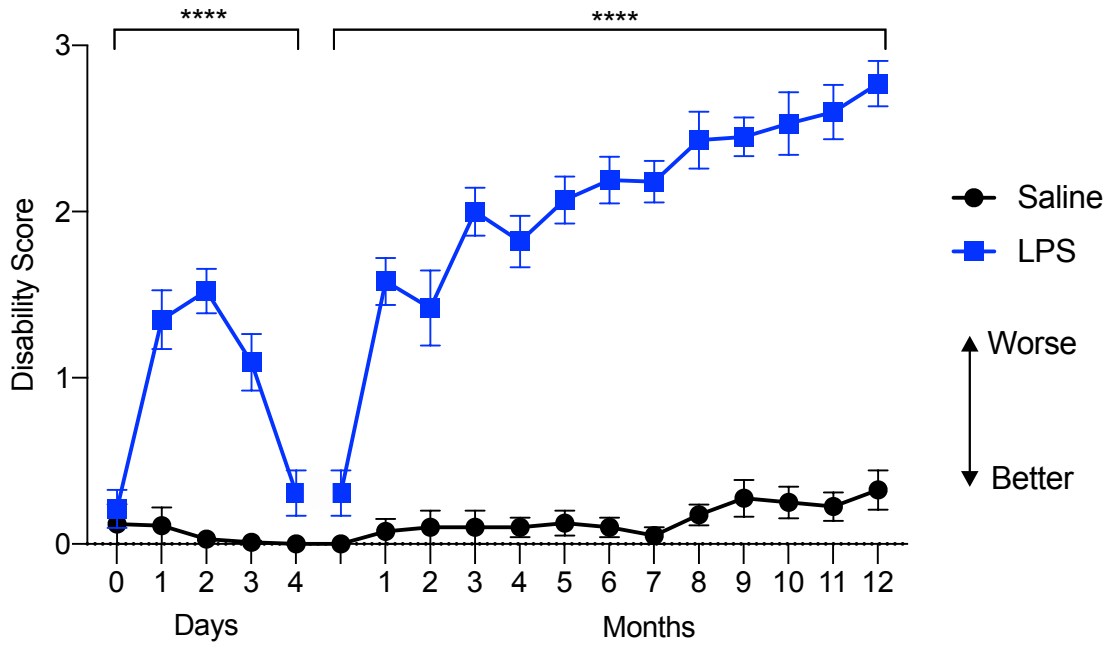

Figure 2-20 Acute and chronic tail disability represented on the same graph

Tail disability scores while walking on a horizontal surface for 1 metre, for animals injected with saline (n=4), or LPS (n=10). Animals were trained from one day before surgery, 4 consecutive days after injection and every month after that. Results were subject to *Two*-way *ANOVA* (****: $P<0.0001$). Values are means ± SEM.

2.3.5 Chronic histology

2.3.5.1 Structural changes to chronically lesioned spinal cords post LPS injection

Chronic sections were collected at 1 month, 3 months, 6 months and 12 months post injection. H&E staining shows clear signs of chronic inflammation around the site of injection, particularly at 1- and 3- months post LPS injection, in comparison with saline controls, as shown in Figure 2-21. Sections at 6 months and 12 months injection showed a decrease in grey matter area in LPS-injected groups, particularly at 12-months post LPS injection (*: $P<0.05$) (Figure 2-22). H&E staining showed a trend in the decrease of motor neuron numbers at the site of injection in LPS groups. This was later confirmed with CV staining techniques, as shown in Figure 2-23. There is a significant decrease in the number of stained motor neurons on the injected ventral horn site, at 1 month (*: $P<0.05$), 3 months (****: $P<0.0001$) in comparison with its ipsilateral counterpart. At the 6 months and 12 months time points, the difference in neuronal count on the injected side, in comparison with its ipsilateral counterpart, between saline control and LPS is unambiguous, but no statistical analysis has been conducted due to the small sample size (Figure 2-24). Saline controls did not show any decrease in grey matter area or motor neuron density at any time point.

Possible demyelination in chronic time points was assessed using LFB staining techniques, as shown in Figure 2-25. There seems to be some demyelination present on the LPS injected sections of 6 months and 12 months groups. Demyelination is noticeable near the site of LPS injection only, and closer to the midline, as expected.

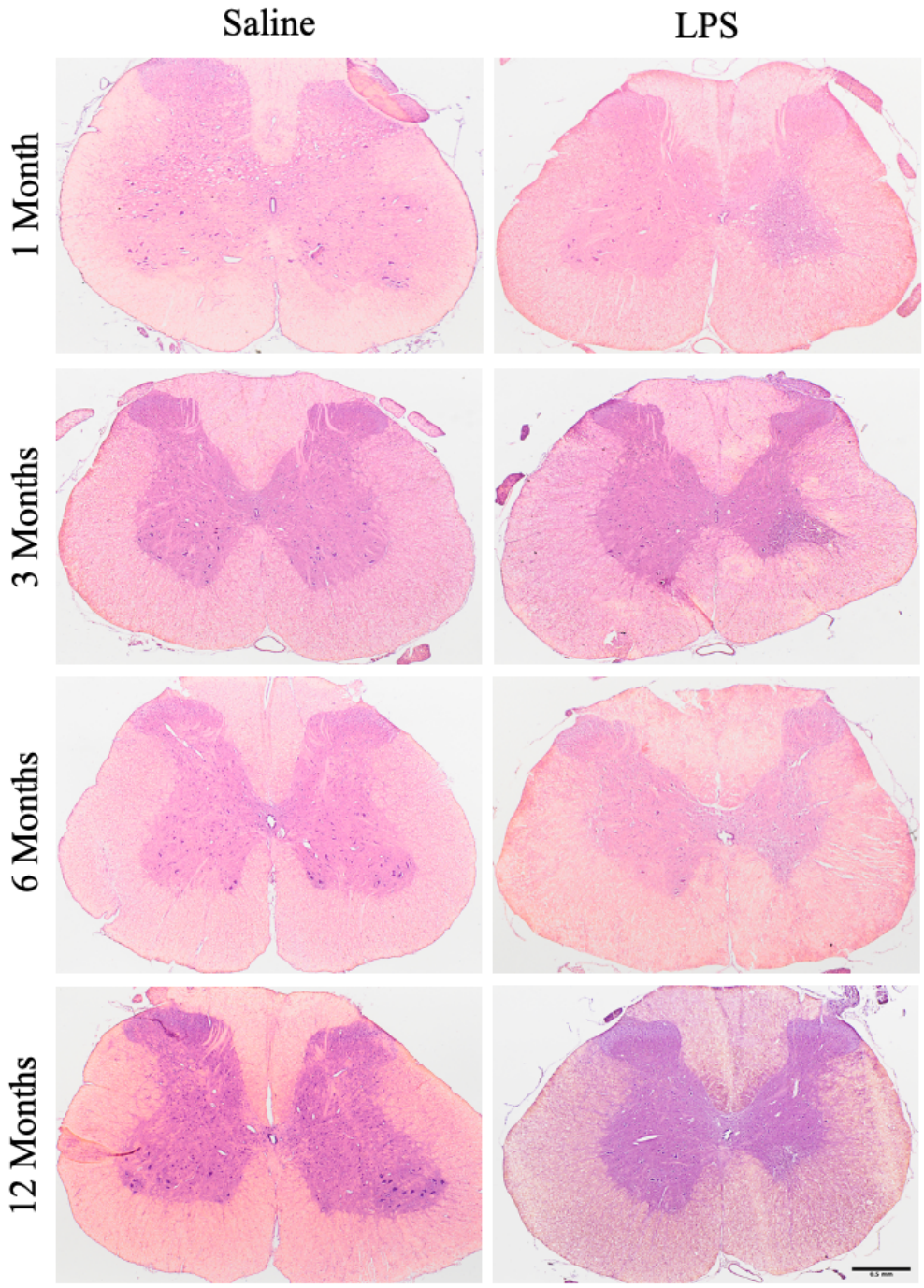

Figure 2-21 H&E Staining of chronically lesioned animals

Transverse sections from chronically lesioned spinal cords stained with H&E comparing the ipsilateral and contralateral ventral horn 1-, 3-, 6- and 12 months post-surgery. Left column shows control tissue injected with saline, whereas the right column shows spinal cords injected with LPS. Scale bar is 500 μm.

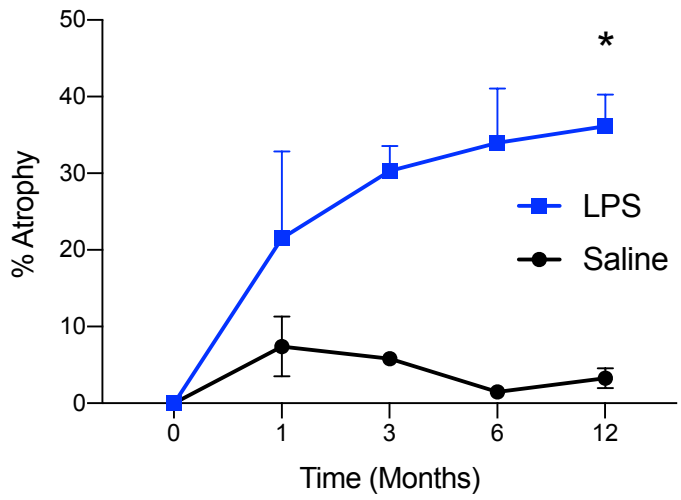

Figure 2-22 Chronic Atrophy Graph

Graphs showing the average percentage atrophy at the lesion site of induced with saline (n=2) and LPS at the preceding times shown ± S.D. Injection of LPS causes clear atrophy of the grey matter ipsilateral to the lesion, at 1 month (n=3), 3 months (n=3), 6 months (n=4) and 12-months (n=12) post-surgery (*: $P<0.05$).

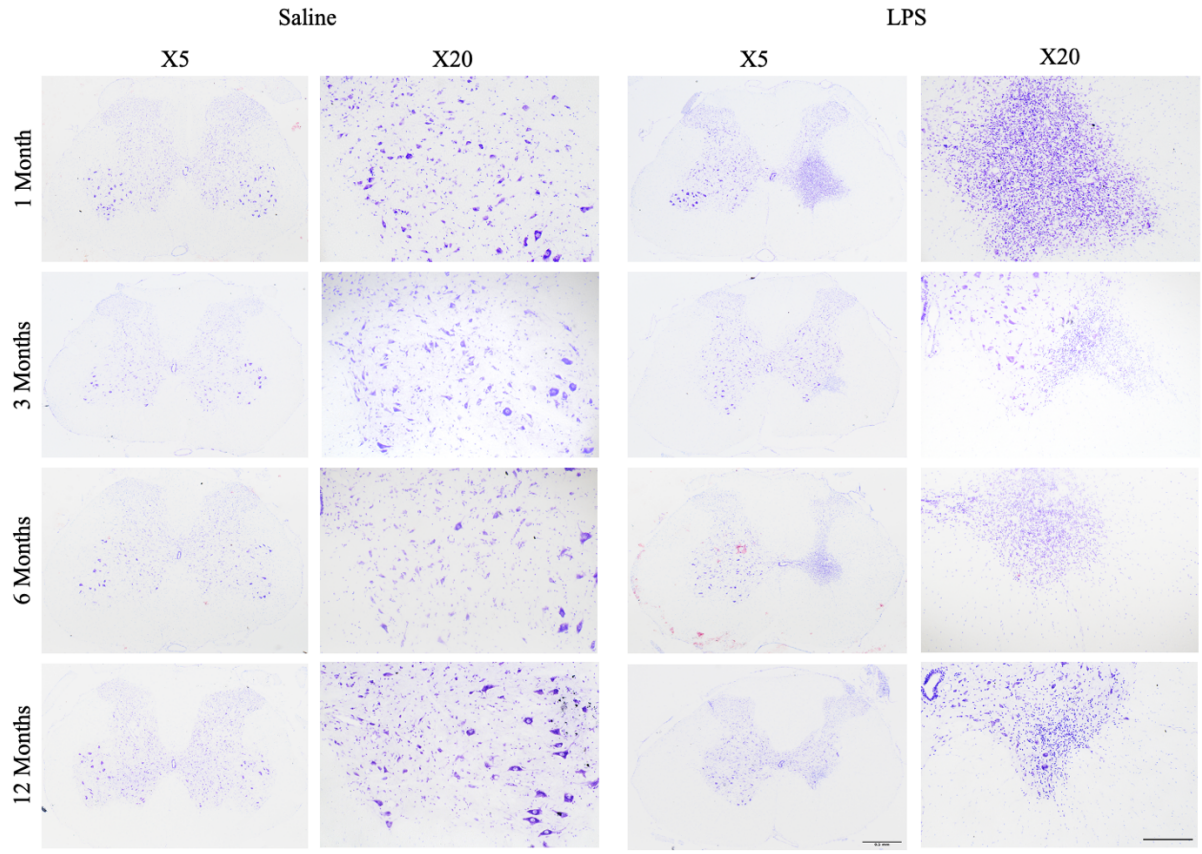

Figure 2-23 CV Staining of chronically lesioned animals

Transverse sections from chronically lesioned spinal cords stained with CV, comparing the ipsilateral and contralateral ventral horn 1-, 3-, 6- and 12 months post-surgery. Left columns show control tissue

injected with saline, whereas the right columns show spinal cords injected with LPS, each with its corresponding lesioned side magnification images. Scale bars are 500 µm (low magnification) and 200 µm (higher magnification).

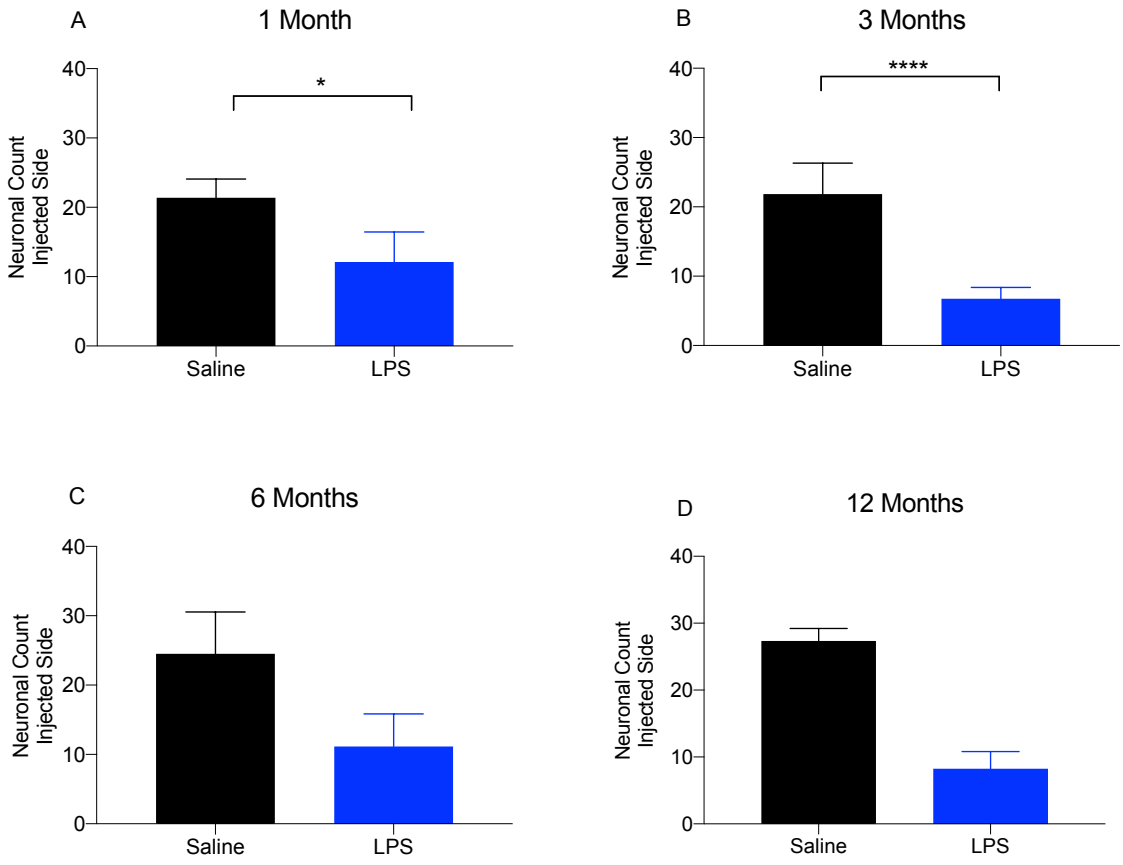

Figure 2-24 Chronic neuronal count graph

Graphs showing the reduction in motor neurons counted at the site of lesions induced at the preceding times shown. Injection of LPS causes a significant decrease in the number of stained motor neurons ipsilateral to the lesion, at 1 month (A), 3 months (B), 6 months (C) and 12 months (D) post-surgery, saline controls (n=2) and LPS groups (n=3). Results were subject to *Two*-way *ANOVA* (*: $P<0.05$), (****: $P<0.0001$); Values are means ± S.D.

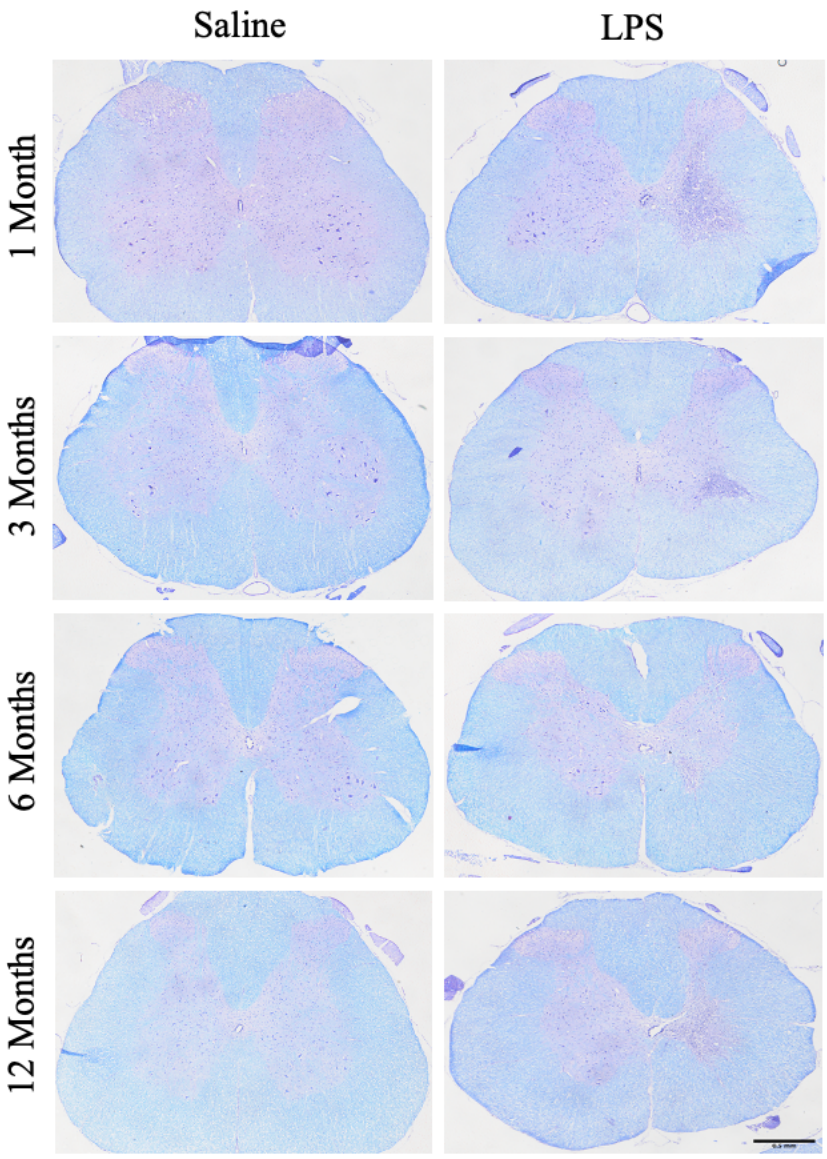

Figure 2-25 LFB Staining of chronically lesioned animals

Transverse sections showing from chronically lesioned spinal cords stained with LFB (myelin), comparing the ipsilateral and contralateral ventral horn 1-, 3-, 6- and 12 months post-surgery. Left column shows control tissue injected with saline, whereas the right column shows spinal cords injected with LPS. Scale bar is 500 µm.

2.3.6 Chronic immunohistochemistry

2.3.6.1 LPS injection induces inflammation at chronic stages of lesion development

2.3.6.1.1 ED1 Labelling

Immunohistochemistry for ED1 revealed the presence of inflammation in the spinal cord of animals injected with LPS at 1 month and 3 months post injection, with significant diminishment at 6 months and 12 months (Figure 2-26). Chronic saline-injected control groups did not show any signs of ED1 staining or inflammation. The ED1 expression was substantially diminished at 6 months, the point at which degeneration began to become apparent, as shown earlier in Figure 2-21. No statistical analysis has been conducted on the tissue, due to the small sample size.

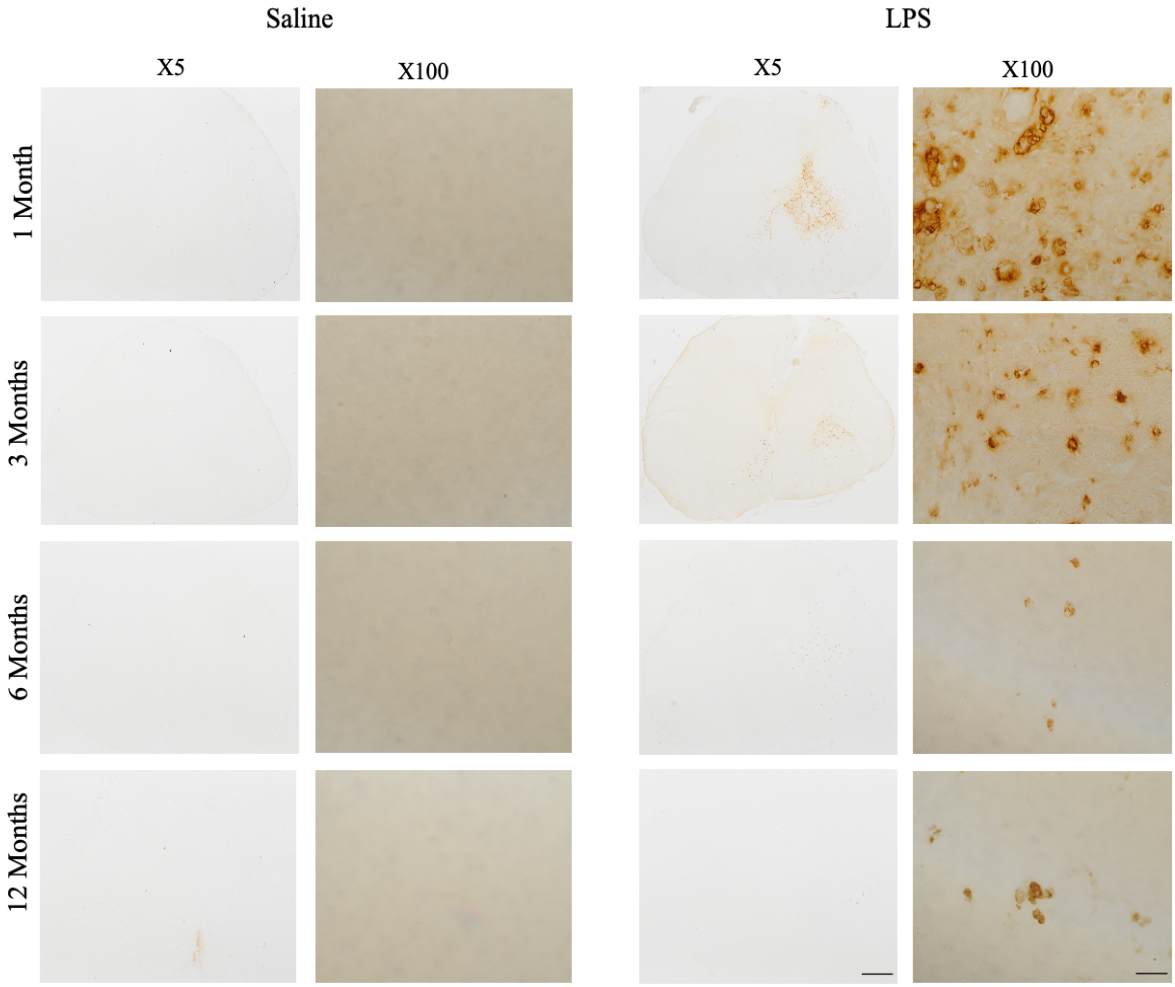

Figure 2-26 ED1 Labelling of chronically lesioned spinal cords

Spinal cords from chronically lesioned animals labelled with ED1, comparing the ipsilateral and contralateral ventral horn 1-, 3-, 6- and 12 months post-surgery. Left column shows control tissue injected with saline, whereas the right column shows spinal cords injected with LPS, each with its corresponding lesion side magnification images. Scale bars are 500 µm (low magnification) and 50 µm (higher magnification).

2.3.6.1.2 IBA Labelling

IBA primary antibody was used to mark activated macrophages and microglia in the acute LPS- and saline-injection experiments. Immunohistochemistry with anti-IBA antibody revealed that microglia in the spinal cord of animals injected with saline did not express IBA antigen at any of the chronic time points. In contrast, there was clear expression of IBA antigen at 1-, 3-, 6- and 12 months post injection in the LPS experiments (Figure 2-27). The IBA expression was especially apparent at the ventral horn, the area near the injection site, as expected and in correlation with the ED1 labelling results.

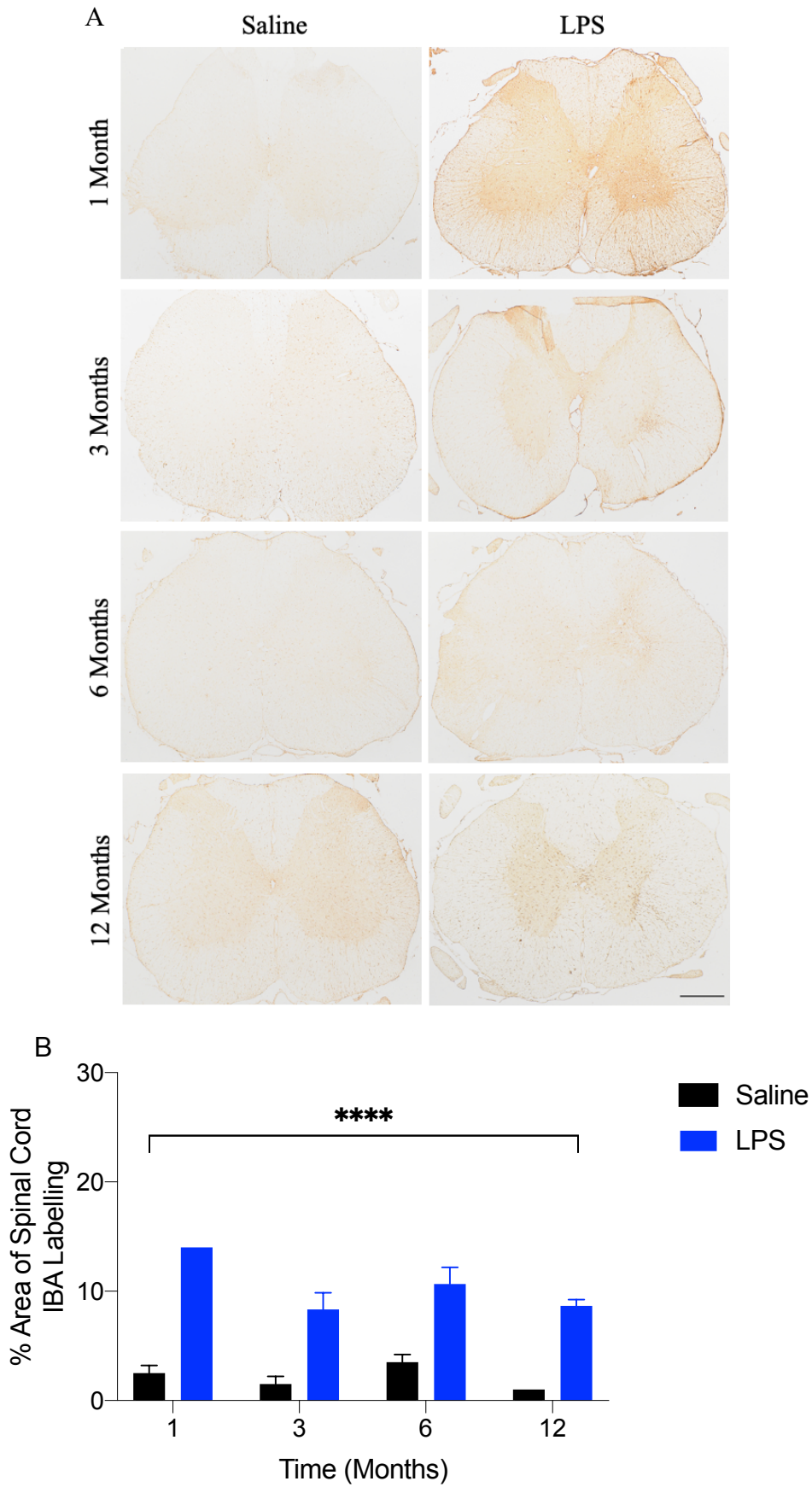

Figure 2-27 IBA Labelling of chronically lesioned spinal cords

A. Transverse sections showing chronic lesions in spinal cords labelled with IBA, comparing the ipsilateral and contralateral ventral horn 1-, 3-, 6- and 12 months post-surgery. Left column shows control tissue injected with saline, whereas the right column shows spinal cords injected with LPS. Scale bar is 500 μm. **B.** Graph showing the chronic IBA percentage area of the spinal cord of animals injected with saline (Controls)(n=2) and LPS-injected animals (n=3). Values are means and S.D. *Two-way ANOVA* (****: P=<0.0001).

2.3.6.2 GFAP labelling shows chronic signs of astrocytic activity

2.3.6.2.1 GFAP/DAB

GFAP primary antibody was used to mark the presence of astrocytes, and possible gliosis at all chronic time points. Overall, saline control groups showed little to no abnormal immunoreactivity at any chronic time point. However, LPS-injected groups showed a significant and unambiguous increase in GFAP labelling at 1-, 3-, 6- and 12 months post LPS injection, in comparison with the non-injected contralateral side (Figure 2-28). As previously discussed, at the 96-hour post LPS injection time point the GFAP labelling had diminished (Figure 2-14), however it is clear that by 1 month after LPS injection, gliosis had begun at the lesion site, only worsening with time.

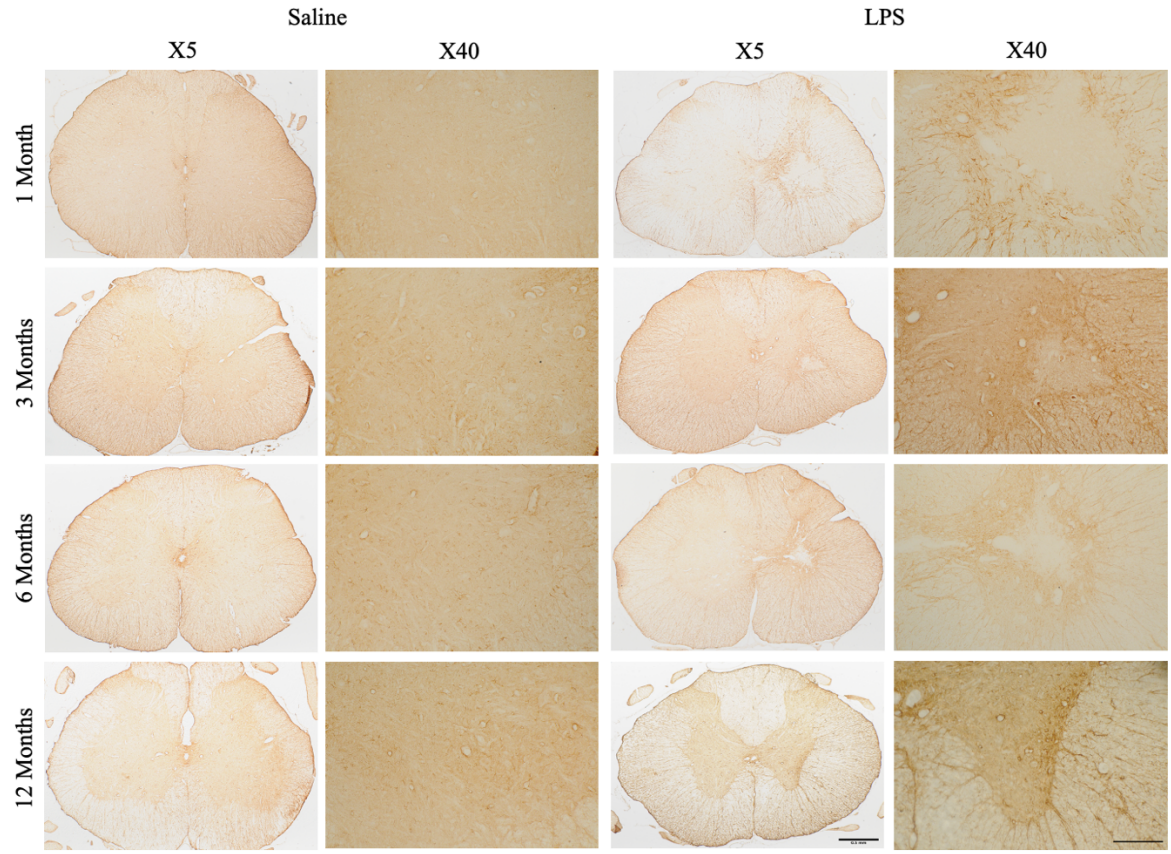

Figure 2-28 GFAP/DAB Labelling of chronically lesioned spinal cords

Spinal cords from chronically lesioned animals labelled with GFAP, comparing the ipsilateral and contralateral ventral horn 1-, 3-. 6- and 12 months post-surgery. Left column shows control tissue

injected with saline, whereas the right column shows spinal cords injected with LPS, each with its corresponding lesion side magnification images. Scale bars are 500μm (low magnification) and 100μm (higher magnification).

2.3.6.2.2 IBA/GFAP

To confirm the presence of inflammation at different chronic time points, confocal imaging was performed on transverse spinal cord sections, labelling for rabbit anti-IBA. To determine the activity level of astrocytes, and possible gliosis, double-label immunofluorescence was conducted using GFAP and DAPI. Saline and LPS transverse sections were imaged and the site of injection (Figure 2-29). Overall, saline control groups showed little to no abnormal immunoreactivity at any chronic time point, with the exception of some IBA labelling at the 1-month time point on the lesion site, in comparison with the contralateral side. However, LPS-injected groups showed a significant increase in IBA labelling, particularly at 1-month, 3-months and 12-months post LPS injection, in comparison with the non-injected contralateral side. Similar to the results shown by ED1 labelling, the 6-month chronic LPS injection site showed little presence of IBA labelling. GFAP labelling results show a statistically significant difference between saline controls and LPS injected animals at every chronic time point (*: P=<0.05) (Figure 2-29 B).

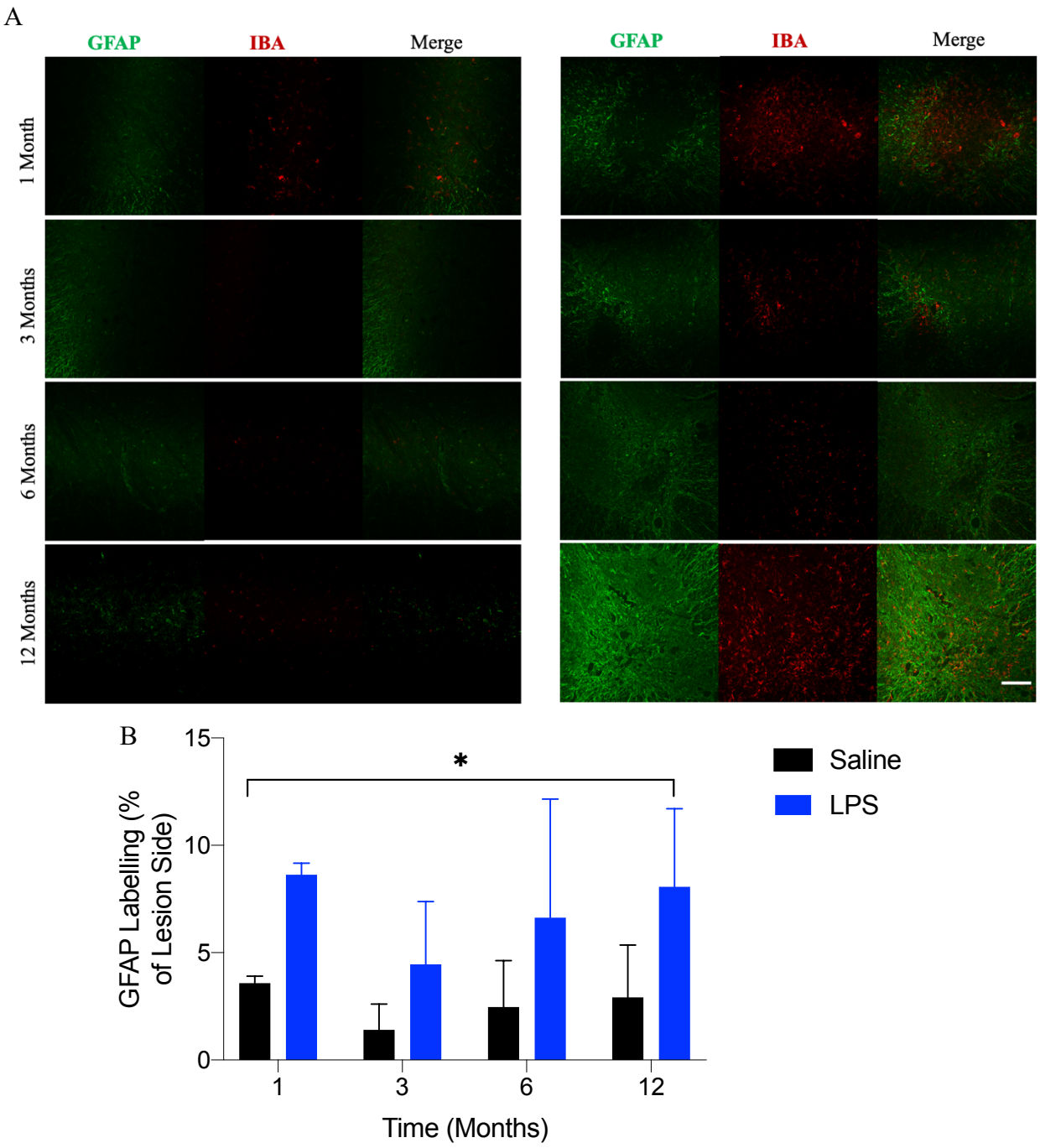

Figure 2-29 GFAP/IBA Labelling of chronically lesioned spinal cords

A. Chronic spinal cords shown at different stages of disease progression in the lesion side of the ventral horn 1-, 3-, 6- and 12 months post-surgery. Confocal laser microscopy of transverse chronic spinal cord sections labelled with anti-IBA (microglia) and anti-GFAP (astrocytes) antibodies. All micrographs are representative. Left column shows tissue treated with saline. Right column corresponds to LPS-injected tissue. Scale bar is 100 µm. **B.** Graph showing the chronic GFAP labelling percentage on the GM injected side of animals injected with saline (Controls) (n=2) and LPS-injected animals (n=3) ± S.D. *Two-way ANOVA* (*: P=<0.05).

2.3.6.3 Immunohistochemical labelling of chronic tissue hypoxia

2.3.6.3.1 PIMO labelling does not show evidence of chronic hypoxia

PIMO was used to investigate a role for hypoxia in the motor disability. Spinal cord transverse sections of animals at chronic disease time points labelled with PIMO at 1-, 3-, 6-, and 12 months post saline and LPS injections (Figure 2-30) showed no visible PIMO labelling upon DAB immunohistology, and no statistical significance (Figure 2-30 B).

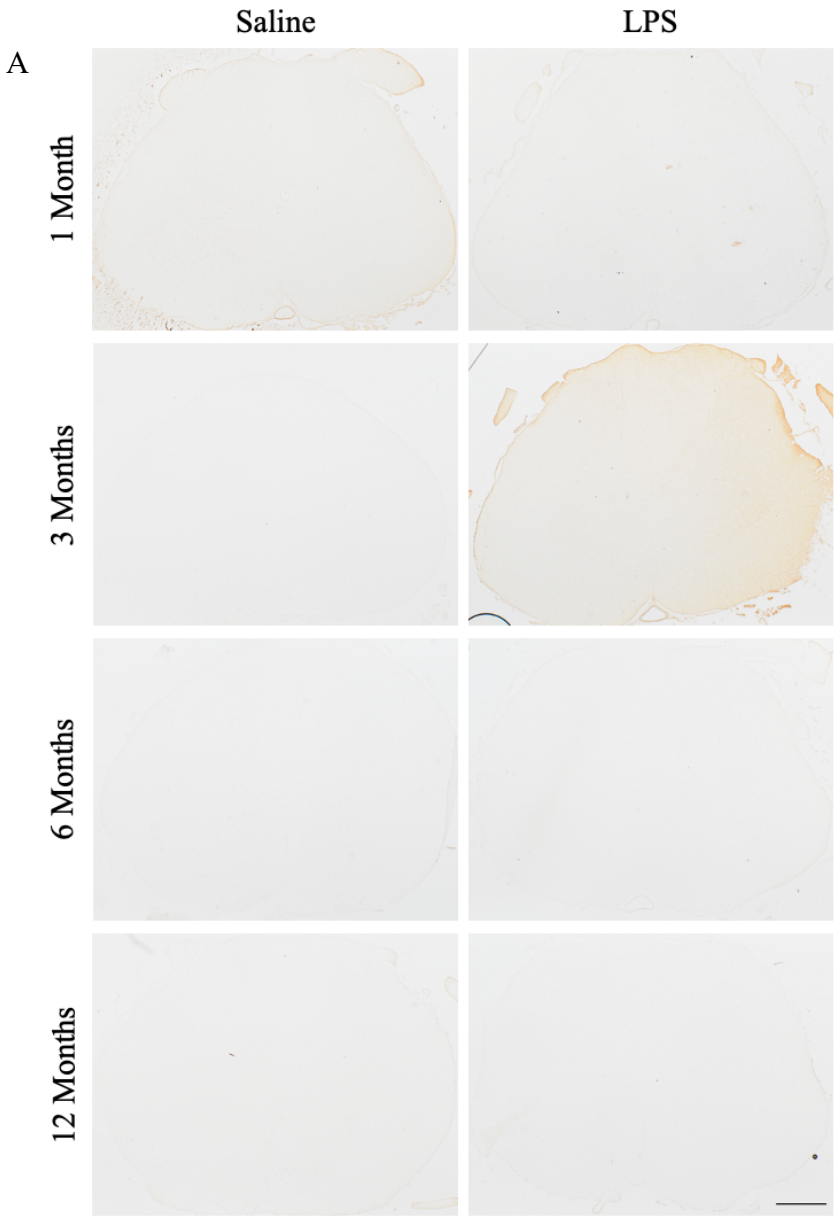

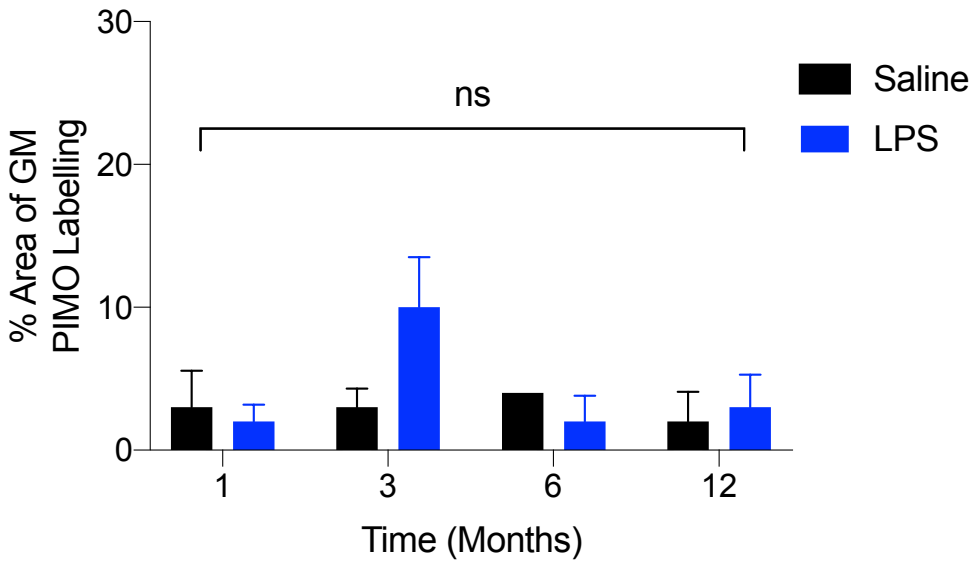

Figure 2-30 PIMO Labelling of chronically lesioned spinal cords

A. Spinal cords from chronically lesioned animals labelled with PIMO at 1-, 3-, 6- and 12 months post-surgery. The column on the left shows tissue injected with saline, whereas the column on the right corresponds with LPS-injected tissue. Scale bar is 500µm. **B.** Graph showing the magnitude of PIMO labelling of the spinal cord of animals injected with saline (Controls) and LPS. Graph shows combined means of control saline-injected animals (n=2) and LPS-injected animals (n=3) ± S.D. *Wilcoxon test* (*n.s*).

2.3.6.3.2 HIF-1 α labelling does not show evidence of chronic hypoxia

HIF-1α was used further to corroborate the presence of hypoxia as a potential cause of the chronic motor disability. Spinal cord transverse sections of animals injected with LPS showed some HIF-1α positive labelling at 1-, 3-, 6- and 12 months post LPS injection (Figure 2-31 A), as well as all saline time points. These results are similar to the PIMO revealed by DAB labelling, as the HIF-1α labelling is not significant in the grey matter, or in the grey matter motor neurons, as shown by Figure 2-31 B-C.

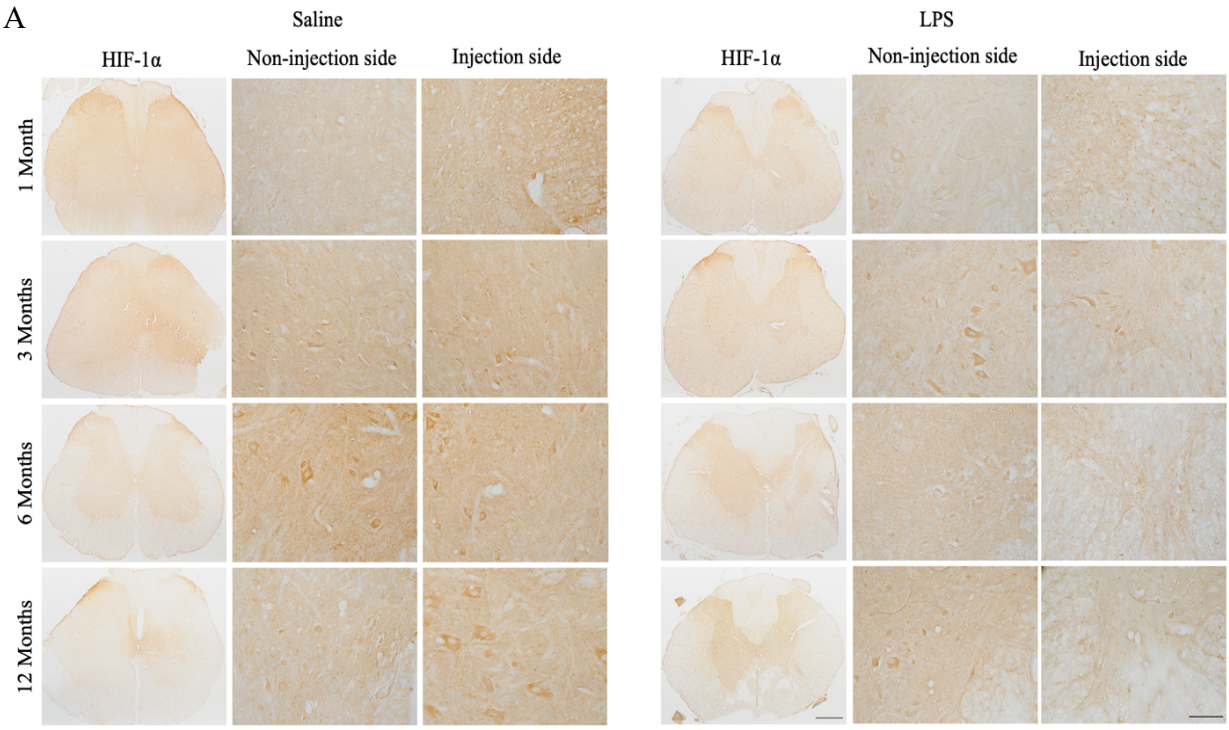

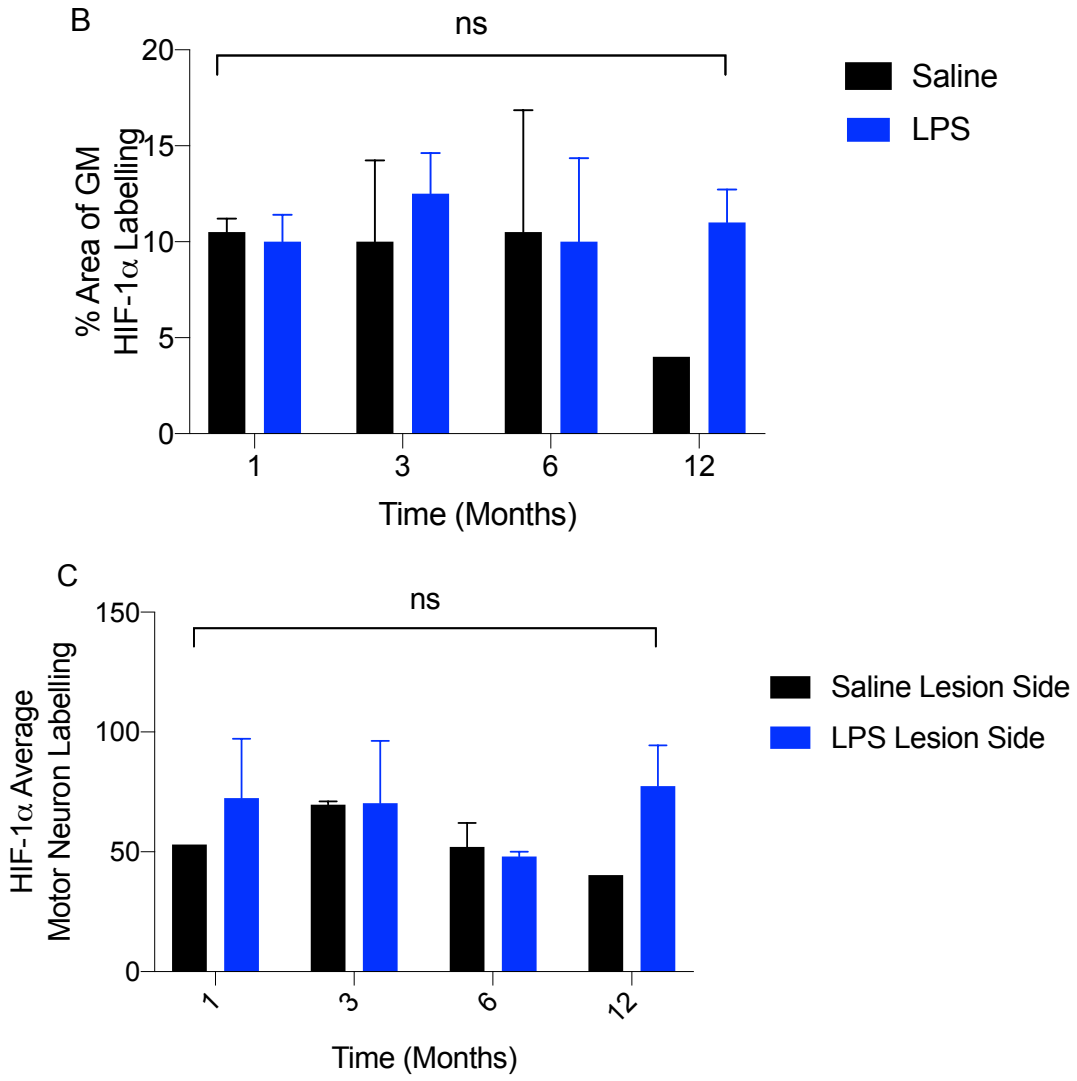

Figure 2-31 HIF-1α Labelling of chronically lesioned spinal cords

A. Transverse sections showing chronic lesions in spinal cords labelled with HIF-1α, comparing the ipsilateral and contralateral ventral horn 1 month, 3 months, 6 months and 12 months post-surgery. Left column shows control tissue injected with saline, whereas the right column shows spinal cords injected with LPS, each with its corresponding non-lesion and lesion side magnification images. Note the atrophy of the grey matter which is faintly discernible in the injected ventral horns. Scale bars are 500µm (low magnification) and 100µm (higher magnification). **B.** Graph showing the chronic HIF-1α labelling percentage area of the spinal cord grey matter of animals injected with saline (controls) and LPS. Graph shows combined means of control saline-injected animals (n=2) and LPS-injected animals (n=3) ± S.D. *Two-way ANOVA* (*n.s*). **C.** Graph showing the average chronic HIF-1α labelling of the spinal cord grey matter motor neurons of animals injected with saline (controls) and LPS, on the injected side only. Graph shows combined means of control saline-injected animals (n=2) and LPS-injected animals (n=3) ± S.D. *Two-way ANOVA* (*n.s*).

2.3.6.4 RECA-1 labelling shows chronic variation in vascular density

RECA-1 antibody was used to determine vessel size. Spinal cord cross sections were labelled with RECA-1 at 1-, 3-, 6- and 12 months post saline and LPS injections. As shown in Figure 2-32 A, saline control groups showed no obvious or significant decrease in density of vessel at any of the chronic time points when comparing the density of blood vessels in the non-lesioned side to the contralateral side, as expected. At all chronic time points, there is some evident decrease in RECA-1 labelling present in the injected side of LPS cords, in comparison with the non-injected side, and the injected side of saline controls. Figure 2-32 B illustrates the decrease of vessel density per mm^2 of LPS injected sides in comparison with the saline counterparts (n.s).

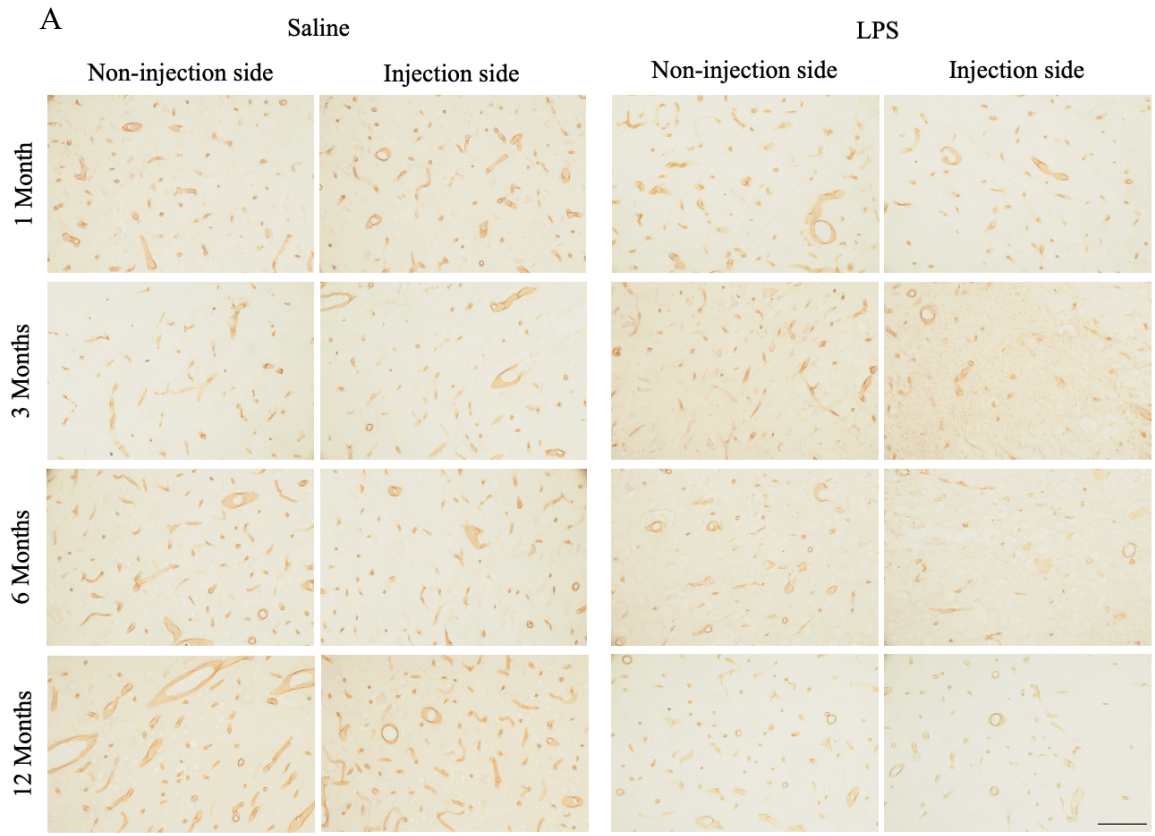

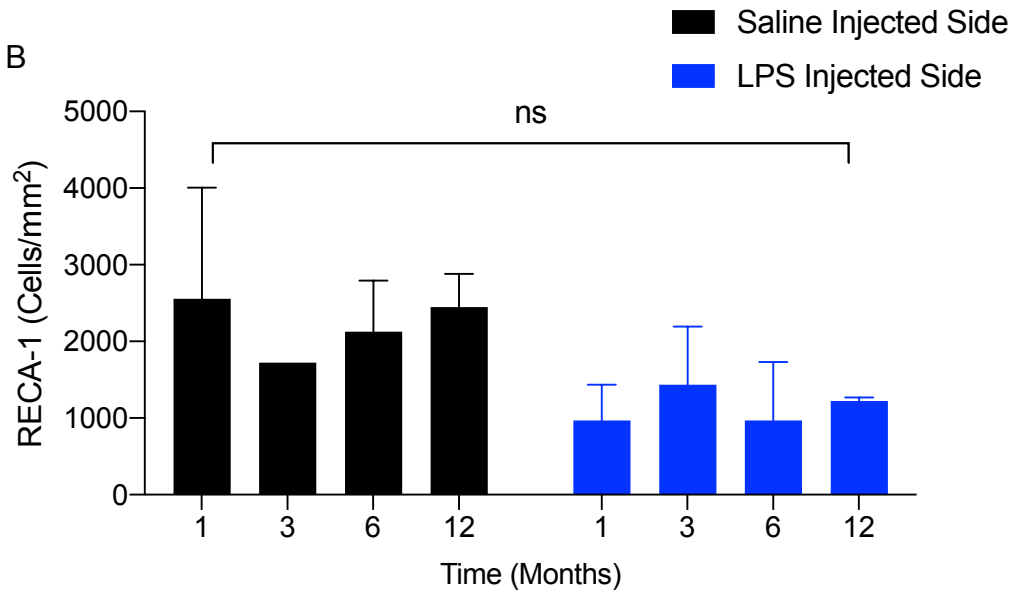

Figure 2-32 RECA-1 Labelling of chronically lesioned spinal cords

A. Transverse sections showing chronic lesions in spinal cords labelled with RECA-1, comparing the ipsilateral and contralateral ventral horn 1-, 3-, 6- and 12 months post-surgery. Left columns show control tissue injected with saline, whereas the right columns show spinal cords injected with LPS, each with its corresponding non-lesion and lesioned sides. Scale bar is 100µm. **B.** Graph showing the RECA-1 cell density of animals injected with saline (Controls) and LPS, injected side only. Graph shows combined means of control saline-injected animals (n=2) and LPS-injected animals (n=3). *Two-way ANOVA* (*n.s*).

2.4 Discussion

The present study shows that the injection of LPS into the spinal grey matter causes an acute disability characterised by inflammation and hypoxia, which resolves after 4 days. However, the disability is present a month later and slowly progresses over the following 11 months, associated with significant neuronal loss and atrophy of the grey matter.

2.4.1 Acute disability

The current study presents evidence that the intraspinal injection of LPS results in an acute disability characterised by tail and hind limb weakness. Importantly, this loss in function is most prominent 48 hours following lesion induction, which is precisely the time point at which hypoxic inflammation is most prominent. Thus, it seems reasonable to suggest that the hypoxia represents an important mediator of disability in this model.

Tail movements in rats have been shown to be controlled within the low sacral spinal level (S2) of the spinal cord (Bennett *et al.*, 1999), which is located beneath the L1 vertebra. Interneurons close to the S2 spinal level are responsible for muscle afferents that give rise to a variety of reflex pathways controlling motor neurons, including those responsible for tail movement (Cavallari *et al.*, 1989). We found that tail function was particularly affected in animals injected with LPS, compared with those injected with saline. The intraspinal injections were made at the T13/L1 vertebral junction, close to the spinal control of tail movement, which would predictably be involved because the lesions expand caudally (and rostrally) from the site of the injection, and so likely affect neurons controlling tail movement.

2.4.1.1 Oedema

Severe neurological deficits in inflammatory demyelinating diseases such as MS are usually attributed to various factors, such as the early oedema, inflammation, demyelination and axonal death, but in this study the timing of the deficits and the plausible demyelination

and axonal death are temporally separated (Lassmann, 2005; Lassmann *et al.*, 2007). In fact, the peak of acute disability occurs in conjunction with prominent oedema and inflammation, as was also observed in a related model where LPS was injected into the dorsal column (Felts *et al.*, 2005). The timing of the demyelination was carefully mapped in the LPS dorsal column lesion and found to be delayed until around 10-14 days post injection (Felts *et al.*, 2005). The behavioural deficits seen in this study as early as 2-3 days cannot therefore easily be attributed to demyelination, suggesting that inflammation itself is sufficient to cause significant motor deficits, in the absence of demyelination, and a similar finding has been made in a biopsy study in MS (Bitsch *et al.*, 2000). The precise mechanism by which the inflammation affects locomotion might be driven by cytokine activity, hypoxia, ROS and RNS, all of which have been advanced by different authors as contributing to the level of disability, e.g. raised concentration of RNS, such as NO, can impair mitochondrial metabolism and block axonal conduction (see Introduction) (Qi *et al.*, 2006; Redford *et al.*, 1997; Smith *et al.*, 2001; Smith & Lassmann, 2002). More recently, the onset of neurological deficit has been directly linked to an exacerbation of mitochondrial dysfunction and axonal depolarisation, resulting in a deficit of ATP (Sadeghian *et al.*, 2016), but the cause of the mitochondrial dysfunction has been ambiguous, although hypoperfusion and hypoxia have been implicated in related models in our laboratory (Davies *et al.*, 2013; Desai *et al.*, 2020; Desai *et al.*, 2016).

2.4.1.2 Inflammation

A conundrum arose regarding the number of motor neurons present at the 24-, 48- and 72 time points, specifically at the site of LPS injection. The decrease in the visibility of the motor neurons within the ventral horn occurred in concert with an increasing severity of disability, and this combination is unsurprising, but the motor neurons were largely present at later time points. Assuming that they were not recreated *de novo,* they were presumably present at the early time points, but not recognised as motor neurons. We have noticed previously that

hypoxic neurons can lose their histological markers, presumably because they decrease protein synthesis as a survival mechanism (Smith *et al.*, 2016), and this may explain their temporary disappearance. Alternatively, the prominent oedema may have been so severe that it obscured the histological appearance at the injection site, giving the impression of motor neuron loss. As oedema resolved, more of the motor neurons became visible again. These observations highlight that inflammation, as a direct result from the LPS injection, is the cause of the early disability, as it is highly unlikely that the motor neurons died and regenerated in this mammalian tissue (Reimer *et al.*, 2008). How inflammation causes neurological deficits is explored below.

LPS injection induced an acute inflammatory response during the beginning stages of the disease, coinciding with the acute peak of disability in both the tail and the hindlimbs. The inflammation subsided after 96 hours, only to reappear by 1-month post LPS injection, and endure for the remainder of the chronic experiment, notably correlating with the worsening atrophy. Animals injected with LPS exhibited extensive inflammation as evident by immunoreactivity for ED1 and IBA, which are markers of microglia/ macrophages. ED1 is a marker of phagocytic capacity (Damoiseaux *et al.*, 1994), and its presence at the site of LPS injection indicates the presence of activated microglia/macrophages. Furthermore, IBA, is a pan- microglial/macrophage marker (Mikkelsen *et al.*, 2017), but the increased labelling in animals injected with LPS compared with saline-injected controls is suggestive of enhanced expression due to active inflammation.

Acute inflammation can have a deleterious effect on the CNS, affecting levels of NO and inducing hypoxia, both of which can compromise mitochondrial function and eventually diminish ATP production in the CNS (Michiels, 2004). NO has been shown to block axonal conduction in rats, and demyelinated axons are especially vulnerable (Smith *et al.*, 2001). Additionally, energy failure due to mitochondrial damage as a result of inflammation can lead

to functional impairment and structural damage of axons, as seen in MS patients (Mahad *et al.*, 2009).

2.4.1.3 Hypoxia

The current study provides evidence that tissue hypoxia is precisely correlated with the acute disability observed following the injection of LPS into the spinal grey matter. The data are consistent with previous findings that established hypoxia as an important mediator of neurological dysfunction in EAE (Davies *et al.*, 2013), the most widely used animal model of MS. The authors found hypoxia to be quantitatively, temporally and spatially associated with the expression of neurological deficits in EAE. Furthermore, they found that raising the inspired oxygen concentration rapidly reversed the tissue hypoxia, as well as promptly diminishing the disability. These data suggest that the neurological deficit in the LPS lesion is, at least partly, dependant on tissue hypoxia, and as a result driven by metabolic deficit (Davies *et al.*, 2013).

As in the Davies paper, pimonidazole was used in the present study for the detection of hypoxia. Although pimonidazole is routinely used to detect tissue hypoxia in various diseases and tissues, it has its caveats. False positive labelling is possible, particularly in instances where the BBB is disrupted, as in MS and the present lesion. Furthermore, extravascular haem-iron complexes can amplify the hypoxia-dependent chemical mechanism that allows the detection of hypoxia in immunohistochemistry to take place (Walton *et al.*, 1985). However, we used HIF-1α labelling as a second marker to confirm the pimonidazole findings. HIF-1α has many roles, such as inducing inflammation, initiating apoptosis and inhibiting cell death, however, its most important role is as a hypoxia regulator by orchestrating the genetic responses to hypoxia and inflammatory conditions (Greijer & van Der Wall, 2004; Guan *et al.*, 2017; Saravani *et al.*, 2019). As a transcription factor, HIF-1 can bind to hypoxia-responsive elements in DNA and activate the transcription factors of genes involved in processes such as

angiogenesis, glycolysis and differentiation (Semenza, 2003, 2007, 2010). HIF-1 is also able to promote the delivery of oxygen to hypoxic areas by the upregulation of VEGF (Semenza, 2002). In this study, HIF-1α labelling is evident during the peak of disability, near the location of the injection in the ventral horn. These results correlate with our pimonidazole labelling, suggesting that LPS injection into the ventral horn renders the spinal cord acutely hypoxic for at least the first 72 hours following injection.

The hypoxia labelling in this study is present throughout the spinal cord sections, affecting all cell types, however the grey matter is labelled in a particularly obvious manner. It has been observed that the grey matter requires greater vascular perfusion and oxygen availability than the white matter (Leenders *et al.*, 1990), therefore the seemingly increased levels of hypoxia in the grey matter of the spinal cord tissue, as illustrated by PIMO labelling, do not seem surprising, particularly as they further emphasize the results from the neurological disability. In addition, in this study, neurons in the grey matter in the spinal cord sections labelled more intensely for hypoxia, in contrast to the white matter, as cellular adducts of PIMO labelling do not label myelin and therefore the white matter tends to appear unlabelled at first glance, even if it is hypoxic (Arteel *et al.*, 1995; Desai *et al.*, 2016). The hypoxia labelling in the grey matter neurons also correlates with the disability observations, which is not unexpected because the grey matter ventral horn is comprised of motor neurons that innervate the tail and hindlimbs (Grossman *et al.*, 1982; Stifani, 2014).

Furthermore, an intracellular hypoxic environment may result in the upregulation of HIF-1α, which in turn can cause the activation of immune system modulator 'nuclear factor kappa-light- chain-enhancer of activated B cells' (NF-kB). NF-kB is an important regulator of inflammatory responses, controlling the expression of many pro-inflammatory cytokines such as TNF-α, and IL-1β, and enzymes such as iNOS (Johnson *et al.*, 2016). Additionally, NO, as well as TNF-α, a cytokine involved in inflammatory responses and activation of macrophages,

further increment HIF-1α, creating a chain reaction between CNS injury, hypoxia and inflammation (Johnson *et al.*, 2016; Lucchinetti *et al.*, 2000). Moreover, strong histological evidence has been previously presented on the involvement of stress-induced endoplasmic reticulum and hypoxia in the development of demyelination in MS, specifically in grey matter pathology, which show an increased level of HIF-1α, together with its downstream signalling molecules, including VEGF (McMahon *et al.*, 2012).

Hypoxia and inflammation share an "interdependent" relationship. Hydroxylases seem to play a crucial role in linking hypoxia to inflammation, in particular PHD 1-, 2- and 3-, along with asparagine-hydroxylase factor-inhibiting HIF (FIH), all of which have been shown to be implicated in the post-translational regulation of hypoxia-inflammatory signalling pathways (Karsten *et al.*, 2013; Taylor, 2008). These enzymes work as cofactors of hydroxylation in an oxygen-dependant manner. Thereby they are responsible for stabilising the α subunit of HIF and play an important role as oxygen sensors. During hypoxic conditions, hydroxylation is blocked, leading to HIF activation (Karsten *et al.*, 2013). Furthermore, the process of phagocytosis is known to consume substantial amounts of oxygen, indeed, it has been shown that over expression of HIF-1 α and hypoxia correlate with striking increases in particle internalisation (Anand *et al.*, 2007), and therefore the extensive labelling for ED1, as seen in the present study, may indicate a mechanism through which hypoxia is induced.

Thus, the presence of hypoxia in grey matter tissue may come as a direct result of inflammation, which as previously discussed, is an important characteristic of the ventral horn lesion post LPS injection. There is a clear interaction between hypoxia and inflammation in MS lesions (Hernandez-Gerez *et al.*, 2019; Martinez Sosa & Smith, 2017), which for this model of disease is particularly relevant as we have found both inflammation and hypoxia to be driving forces in the acute stages of lesion formation.

Inflammation can cause hypoxia via different mechanisms, as explained above. Two central transcription factors are involved in the cascades of events that promote the relation between inflammation and hypoxia, mainly HIF and NF-kB, both of which display different degrees of sensitivity to hypoxic environments (Taylor, 2008). The likely scenarios in which acutely inflamed tissue drives hypoxia are twofold. Firstly, inflamed tissue shows an increase in metabolic demand, due to infiltrating inflammatory cells, resulting in an elevated oxygen demand. Moreover, multiple mitochondrial studies have shown that hypoxia directly impairs mitochondrial respiration, via leakage of protons, thereby inhibiting the respiratory chain reaction and further deteriorating metabolic activity (Michiels, 2004). Secondly, lasting inflammation often leads to a vasculopathy, and therefore poor perfusion, which subsequently promotes hypoxia (Martirosyan *et al.*, 2011; Taylor, 2008). We believe the model of disease we have presented will be valuable in understanding the inflammatory mechanisms driving hypoxia.

2.4.2 Long term atrophy and chronic disability

Animals injected with LPS recover from the acute disability by 4 days post-lesion induction, however, the disability returns a month later and progresses over the subsequent months, but in particular within the first 3 months following LPS injection. The progression of disability can be described to comprise three phases, namely: acute, early chronic and chronic progressive. The acute phase can be attributed to the acute inflammation, and therefore hypoxia. The early chronic phase that occurs during the first three months is accompanied by the re-emergence of inflammation and the beginning stages of motor neuron loss and atrophy. Finally, the chronic phase of the disease is associated with progressive atrophy of the grey matter, and a progressive loss of motor neurons, in the absence of overt inflammation. Thus, the acute inflammatory period in the first few days following lesion induction appears to initiate a cascade of events that cause the same tissue to atrophy weeks and months later.

Understanding the relation between acute inflammation and slow burning neurodegeneration is key. The pathological mechanisms that drive chronic neurodegeneration in both the experimental lesion and in MS are poorly understood, however, neurodegeneration has been regarded as a direct result of inflammatory responses, due mainly to peripheral immune system activation, also commonly known as the 'outside-in hypothesis' (Pérez-Cerdá *et al.*, 2016). MS progression may come as a result of early inflammatory processes that trigger a cascade of events, mainly microglial/macrophage activation, chronic oxidative injury, mitochondrial damage and axonal death (Lassmann *et al.*, 2012; Mahad *et al.*, 2008). In all stages of MS, neurodegeneration is accompanied by the invariable presence of inflammation, mediated by T-cells, B cells, macrophages and microglia. The patterns of localization of these cells can be used as an indicator for disease progression and tissue damage (Frischer *et al.*, 2009). In active lesions, during the prephagocytic stage of lesion formation, there are low numbers of T-cells present at the site of atrophy. This initial inflammatory response, is mainly mediated by $CD8^+$ T-cells, followed by a secondary recruitment of microglia and macrophages, as a response to myelin degeneration (Prineas *et al.*, 2001). In these early inflammatory stages, various products are released, such as cytotoxic cytokines, excitotoxins, ROS and RNS, which in turn contribute to the accumulation of tissue damage and degeneration over time, by promoting hypoxia-like tissue injury (Pattern III lesions) and axonal injury, for instance (Martinez Sosa & Smith, 2017; Prineas *et al.*, 2001; Smith *et al.*, 2001; Smith & Lassmann, 2002). The profound and cumulative damage caused by the initial inflammation further stimulate the return of inflammatory cells, as seen in more chronic stages of MS, such as SPMS, where large aggregates of inflammatory cells such as T cells and B cells infiltrate into the CNS (Lassmann *et al.*, 2012).

As previously mentioned, the inflammation and disability that arises due to the LPS injection reappears after 1-month post injection. Thereafter, the disability continues to increase

as the lesion progresses, much as in SPMS patients (Lassmann *et al.*, 2007). These results suggest the presence of another determining factor affecting disability that is not acute inflammation. We postulate that the profound hypoxia seen at early stages of lesion development seems to be overwhelming, and ultimately may result in progressive and chronic atrophy and degeneration.

It is widely recognised that in MS, the progression of the disease is highly reliant on the accumulation over time of white matter demyelination, along with grey matter degeneration and demyelination, particularly within the subpial area (Lassmann, 1999). Grey matter demyelination is significantly lower than that of the white matter, as myelin is not its main constituent, but also its remyelination capacity is extremely limited, and often accompanied by the loss of nerve cell bodies (Pérez-Cerdá *et al.*, 2016), possibly explaining the lack of major long term demyelination present in our model of disease. This model closely mirrors the neurological deficit in SPMS patients, but is in contrast to most MS models, such as EAE, in which an early neurological deficit tends to reach a plateau that may or may not progress. Often, the worsening condition of EAE animals requires their euthanasia before progressive additional worsening takes place, if such worsening might otherwise occur (Robinson *et al.*, 2014).

2.4.2.1 Chronic gliosis

The severity of astrogliosis in MS is defined as a gradated and complicated process (Sofroniew & Vinters, 2009). Our results highlight that severe diffuse gliosis is occurring around the inflammation during the progressive atrophy. In diffuse gliosis, there is a pronounced up-regulation of GFAP expression, together with increased hypertrophy of cell bodies (Eng & Ghirnikar, 1994; Ingram *et al.*, 2014; Lucas *et al.*, 1980). As a result, there is substantial overlapping of neighbouring astrocytic processes, which lead to chronic changes in the tissue architecture, and, in time, may diffuse extensively over the compact barriers formed

earlier by glial scars and necrotic tissue. Severe diffuse reactive astrogliosis is generally found in areas surrounding severe focal lesions, inflammation and in response to chronic neurodegeneration (Sofroniew & Vinters, 2009). Furthermore, reactive astrocytes have been shown to form scar tissue as a "barrier" around the perivascular cluster surrounding the inflammatory response, thereby compartmentalizing the inflammation, and preventing inflammatory cells such as leukocytes, from migrating into neighbouring healthy tissue during an inflammatory response (Nataf *et al.*, 2019).

2.4.3 The slow lesion as a new model of slowly progressive degeneration

Studies have shown that grey matter MS lesions may form due to inflammation, mitochondrial injury and hypoxia (Lassmann *et al.*, 2012). To understand the underlying mechanisms that may lead to chronic neurological degeneration seen in slow lesions, particularly within the grey matter, we have examined a novel neuroinflammatory model of disease developed in our lab. This model is mediated by an initial innate immune response, due to LPS, which results in acute disability due to inflammation and hypoxia. However, this initial response is transient, and dissipates shortly after it is induced, only to reappear a month later and slowly progress over the following year. The data presented in this chapter stresses particular mechanisms, mainly hypoxia, by which an acute inflammatory response may drive acute disability, and perhaps chronic and significant grey matter atrophy and neuronal loss.

This model presents an opportunity to study the mechanisms responsible for the acute and chronic slow-burning degeneration seen in MS patients, as it mirrors some key mechanisms that drive SPMS disease progression (Bendfeldt *et al.*, 2009; Calabrese *et al.*, 2013; Lassmann *et al.*, 2007; Lassmann *et al.*, 2012; Plantone *et al.*, 2016). For instance, throughout the CNS there are areas of vascular watersheds that render it especially susceptible to a hypoxic-ischaemic neuronal environment. MS patients are particularly vulnerable to such conditions (Lassmann, 2016; Martinez Sosa & Smith, 2017). In our model, the acute hypoxia, developed

as a result of the induced inflammation, may have profoundly overwhelmed the physiological mechanisms that maintain spinal cord homeostasis, initiating a cascade of events that would later contribute to degeneration, demyelination, gliosis and changes in the healthy vasculature, as demonstrated by the data presented in this thesis.

2.4.4 Conclusion

In conclusion, the findings of this study have started to explore the consequences of neuroinflammatory lesions induced by LPS in the grey matter of the spinal cord. The results show that severe neurological deficits can be acutely attributed to inflammation-induced hypoxia, and chronically attributed to atrophy and motor neuron loss, as a consequence of the acute inflammatory event. The findings raise the possibility of the use of this novel lesion as a model of slowly burning degeneration as observed in MS, and opens up the potential for an early neuroprotective window to exist as a new avenue for neuroprotection in the disease.

Chapter 3 Oxygen as a therapy to protect from acute inflammation and chronic degeneration and atrophy

Studies have shown that MS grey matter lesions may form due to inflammation, mitochondrial injury and hypoxia (Lassmann *et al.*, 2012; Mahad *et al.*, 2015; Martinez Sosa & Smith, 2017). Typically, in acute MS lesions, the most influential inflammatory events occur during the early stages of lesion development, when symptoms are starting to become apparent (Lassmann *et al.*, 2001). Furthermore, studies emphasize that even during the chronic stages of disease, including active and inactive lesions, inflammation continues to play a big role in atrophy, via a slow-burning process (Lassmann, 1999). The acute inflammation induces a hypoxic-ischaemic milieu, which contributes to the presentation of neurological deficits. These early developments are the prelude to the progressive phase, which includes degeneration, axonal death and irreversible neurological damage (Felts *et al.*, 2005; Lovas *et al.*, 2000; Love, 2006).

Increasing evidence points to the role of inflammatory hypoxia in the CNS of MS patients in inducing the pathological hallmarks of MS (Aboul-Enein *et al.*, 2003; Desai *et al.*, 2016), but whether inflammatory hypoxia also drives atrophy and neuro/axonal degeneration remains unknown. In this thesis, we have described a model of SPMS, characterised by slowly progressive atrophy of the spinal grey matter. Our previous results have indicated a potential role for inflammatory hypoxia in driving disability and long-term atrophy, therefore we wanted to examine the value of oxygen therapy as a neuroprotective strategy.

3.1.1 Hypothesis

We hypothesise that oxygen therapy during the acute hypoxic window will reduce the extent of progressive atrophy and neuronal loss in our new model of progressive MS.

3.1.2 Aims

1. To examine the therapeutic potential of oxygen treatment in ameliorating the acute disability resulting from grey matter inflammation.
2. To study the long-term effect of hyperoxia as an acute therapy to reduce progression of the pathophysiological and pathological sequelae of an acute inflammatory lesion in the spinal grey matter.
3. To compare the efficacy of two oxygen concentrations in their ability to decrease chronic atrophy.

3.2 Materials and Methods

3.2.1 Ventral horn LPS injection

Lesions of the progressive model of MS were induced in male adult SD rats (313g ± 28, mean ± SD) as previously described in section 2.2.1.

3.2.2 Acute oxygen therapy after ventral LPS injection

Following surgery, animals were blindly randomised into three groups: room air controls (n=10), 50% normobaric hyperoxia (n=11), or 80% normobaric hyperoxia (n=10). Where appropriate, animals were placed in a purpose-built chamber (BioSpherix, USA), for hyperoxic therapy for the first 96 hours following lesion induction. Temperature, oxygen concentration, and CO_2 levels were monitored and controlled throughout the experiment.

3.2.3 Behavioural assessment

3.2.3.1 Ladder test

Functional hindlimb deficit was assessed as previously described in section 2.2.2.1.

3.2.3.2 Horizontal walking test-tail deficit

Functional tail deficit was assessed as previously described in section 2.2.2.2.

3.2.3.3 Treadmill test-gait

The treadmill and gait analysis were performed as described in section 2.2.2.3.

3.2.4 Tissue perfusion

PIMO (HPI Inc, Burlington, MA; 60mg/kg body weight) was administered to animals intravenously, via the saphenous vein, under light anaesthesia (1% isoflurane in room air). After 4 hours post PIMO injection, animals were terminally anaesthetized and trans-cardially perfused, as described previously. Spinal cord tissue was post-fixed in 4% PFA, and then transferred to PBS-azide solution until imaging with MRI.

3.2.5 MRI protocol

Fixed spinal cords were arranged into a custom-built container immersed in PBS-azide solution. The container was placed in a horizontal 9.4T 20 cm preclinical bore MRI scanner (Brucker Biospec) equipped with a 40mm-diameter birdcage volume coil (Bruker Biospec). Images were taken using 3D fast low angle shot (FLASH) imaging sequence, with a spatial resolution of 30µm x 30µm x 300µm, flip angle 52.0°, matrix size 750 x 750 x 133, repetition time 100ms, time to echo 12ms and number of averages 4.

3.2.6 Tissue processing

Post MRI processing, spinal cords were cryoprotected in 30% sucrose solution (Sigma-Aldrich, USA), and processed for cryosectioning as described previously in section 2.2.3.

3.2.7 Histology

3.2.7.1 H&E staining

Transverse sections of the spinal cord block were used for H&E staining as previously described in section 2.2.4.1.

3.2.7.2 Luxol Fast Blue staining

Transverse sections at the site of the lesion were used for LFB staining as previously described in section 2.2.4.2.

3.2.7.3 Cresyl Violet staining

Transverse sections at the site of the lesion were used for CV staining as previously described in section 2.2.4.3.

3.2.8 Immunofluorescence

Spinal cord sections were air dried overnight. The sections were rehydrated with PBS (Sigma- Aldrich, USA), prior to incubation in neat methanol, with subsequent PBS washes. Sections were blocked in NGS for 30 minutes, prior to incubation in primary antibody overnight at 4^{o}C. The following day, the sections were washed with PBS. Sections were then separately incubated with polyclonal goat anti-rabbit (1:200, Invitrogen) and goat anti-rabbit Cy3 (1:200, Invitrogen) secondary antibodies for 60 minutes each at room temperature (Table 5). PBS washes were carried out between each step. Slides were mounted with Vectashield mounting medium (Vector) and stored at 4°C in the dark, prior to imaging with confocal microscopy (Zeiss 710).

Antibody	Target	Isotype	Blocking Buffer	Dilution	Source
Rabbit Anti- GFAP	Astrocytes	Rabbit IgG	5% NGS in 0.01% PBS-triton	1:500	DAKO
Rabbit Anti-IBA	Microglia/ macrophages	Rabbit IgG	5% NGS in 0.01% PBS-triton	1:200	Abcam

Table 5 Antibody details for IF.

3.2.9 Microscopy

3.2.9.1 Light microscopy and quantification

Tissue sections were viewed using an Axiophot light microscope (Zeiss, Germany), and micrographs taken using a Nikon D300 camera (Nikon, USA). The illumination was kept constant throughout image acquisition, under the same magnification. H&E grey matter quantification was carried out using the selection tool (ImageJ) to determine the average size of atrophy on the lesion side by comparing with the contralateral side.

3.2.9.2 Confocal microscopy

Confocal fluorescent images were obtained using a Zeiss 710 confocal microscope, with a 40X water immersion objective. Excitation wavelengths of 488 nm and 543 nm were provided by argon and helium-neon gas lasers.

3.2.10 Statistical analysis

3.2.10.1 Behavioral analysis

All data were tested for normality using the D'Agostino & Pearson test. Data that were not normally distributed were evaluated using non-parametric statistics as indicated. P-values of 0.05 (*), 0.01 (**), 0.001 (***) and 0.0001(****), were considered as statistically significant. All statistical analyses were carried out using GraphPad Prism version 8.

A two-way ANOVA test was performed on time course scoring experiments, to compare the significance between different time points and between the two treatment groups, those being room air and oxygen therapy. When treatment groups were compared at a single time point, t- tests were performed to assess significance.

3.2.10.2 Neuronal counts

Large neurons with visible nucleus present were counted as motor neurons using Image J (National institute of health, USA). All data were tested for normality using the Shapiro-Wilk test. Data that were not normally distributed were evaluated using non-parametric statistics as indicated. P- values of 0.05 (*), 0.01 (**), 0.001 (***) and 0.0001(****), were considered as statistically significant. Normally distributed data were evaluated using a one-way ANOVA. All statistical analyses were carried out using GraphPad Prism version 8.

3.2.10.3 Atrophy volume

The grey matter lesion cross sectional area was measured using the selection tool on Image J on each MRI slice where the lesion was visibly present. Subsequently, volume measurements were calculated using the slice thickness and cross-sectional values, where the lesion was present. A one-way ANOVA test was performed on atrophy volume results to compare the significance between different treatment groups and controls. When treatment groups were compared at a single time point, t- tests were performed to assess significance.

3.2.10.4 Grey matter percentage decrease

A one-way ANOVA test was performed on the percentage decrease of grey matter area results to compare the significance between different treatment groups and controls. P-values of 0.05 (*), 0.01 (**) and 0.001 (***), were considered as statistically significant. All statistical analyses were carried out using GraphPad Prism version 8.

3.3 Results

3.3.1 Acute disability

3.3.1.1 Oxygen therapy decreases tail disability after LPS injection on the ventral horn

Animals were assessed for functional disability following lesion induction to evaluate the efficacy of 96 hours of therapy with normobaric hyperoxia. Room air control animals exhibited transient tail weakness following lesion induction (Figure 3-1), with disability being particularly significant at 24-, 48- and 72 hours post injection. Animals exposed to 80% oxygen therapy showed little to no disability 24 hours after surgery, which was significantly lower than the control group ($P^{**} < 0.01$). Some amelioration of the disability was also observed during the first 48- and 72- hours following treatment with 80% oxygen, however this was not statistically significant. Interestingly, animals in the 50% oxygen treatment group did not show improvement in tail function after 24 hours post-surgery, however a similar level of improvement in function to that of the 80% oxygen group was observed at 48- and 96-hours post-lesion induction. All groups, including room air controls, fully recovered by 96 hours post LPS injection, as expected. The present results show that 80% oxygen is more effective treatment in decreasing tail disability compared with 50% oxygen treatment.

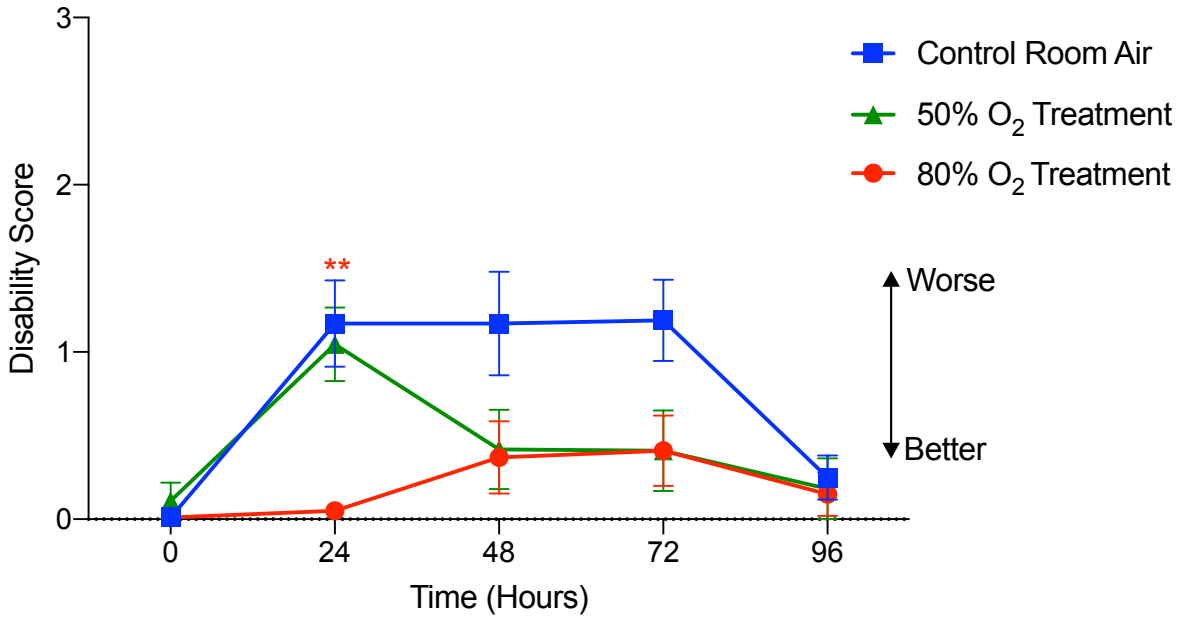

Figure 3-1 Oxygen therapy acute tail disability

Tail disability scores while walking on a horizontal surface for control animals (blue) injected with LPS and placed in room air (n=10), or animals injected with LPS and kept in normobaric hyperoxia (50%, green) (n=11) and hyperoxia (90%, red) (n=10). Animals were trained from one day before surgery (baseline) up to four days after surgery. Values are means ± SEM. Statistical analysis was performed with a *Two-way ANOVA* test (**: $P<0.01$).

3.3.1.2 The effects of oxygen therapy on hindlimb function

3.3.1.2.1 Horizontal ladder

Hind limb function, particularly the right (lesioned side), was impaired in all animals. Animals exposed to room air and 80% oxygen exhibited similar levels of impairment in the ability to walk smoothly along the horizontal ladder at 24- 72 hours post-lesion induction, compared with baseline, in particular in the right hindlimb (Figure 3-2). Interestingly, animals exposed to 50% oxygen exhibited a worse trend in hind limb disability of the left hindlimb compared with the other groups, whereas the right hindlimb showed a similar trend as all others.

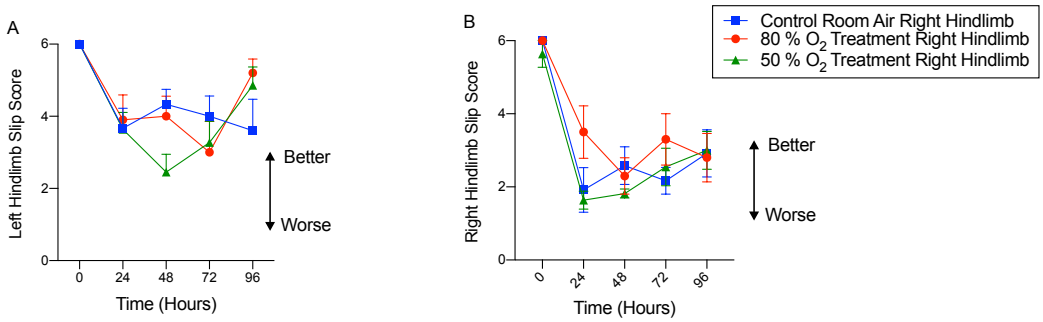

Figure 3-2 Oxygen therapy acute hindlimb disability

Hindlimb disability scores while walking on a horizontal ladder for animals injected with LPS and placed in room air (n=10, blue) or animals injected with LPS and kept in normobaric hyperoxia (50%, green) (n=11) and hyperoxia (80%, red) (n=10). Animals were trained from one day before surgery (baseline) up to four days after surgery. **A.** Shows left hindlimb acute results. **B.** Shows right hindlimb acute results. Values are means ± SEM. Statistical analysis was performed with a *Two-way ANOVA* test.

3.3.1.2.2 Hindlimb gait

Animals were subjected to running on the TreadScan treadmill for 1 minute at every time point (baseline, 24-, 48-, 72-, and 96 hours) to observe the gait. As expected, the right hindlimb exhibited a greater gait disability than the left hindlimb in all animals, irrespective of the treatment (Figure 3-3). Overall, the left hindlimb scores for all groups followed a fairly similar trend, with room air controls having a larger deficit during the first 24 hours post injection (Figure 3-3 A). On the other hand, the right hindlimbs showed more variability of gait angle scores amongst control and treatment groups. Animals in the room air and 50% oxygen treatment groups showed similar gait angle averages at all time points, with 50% oxygen treatments exhibiting worse scores at 48- and 96- hours post injection. The gait angles for animals in the 80% oxygen treatment group showed some protection from disability on the right hindlimb throughout the acute phase, however, these results were not statistically significant (Figure 3-3 B).

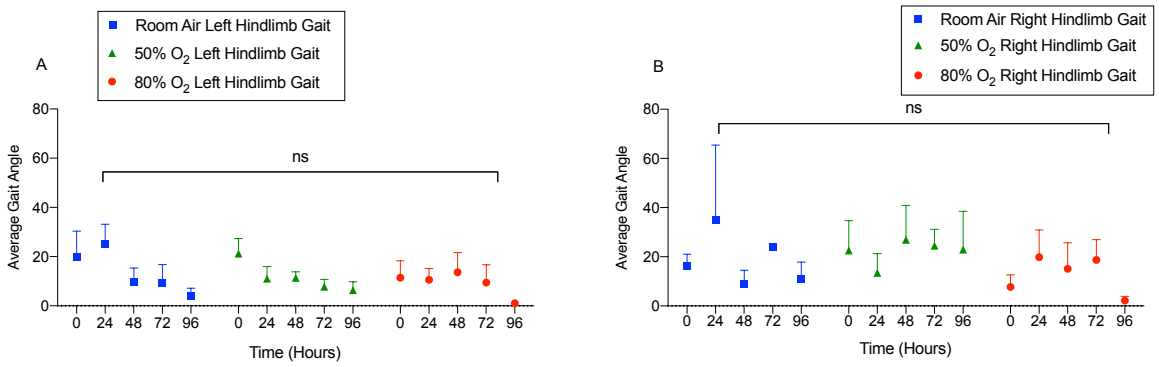

Figure 3-3 Oxygen treatment acute gait angles

Gait angle scores while running on a treadmill at speed 20 cm/s for control animals injected with LPS and placed in room air (n=6, blue) or animals injected with LPS and kept in normobaric hyperoxia (~50%, green) (n=6) and hyperoxia (80%, red) (n=5). Animals were trained from one day before surgery (baseline) up to four days after surgery. **A.** Shows left hindlimb gait acute results. **B.** Shows right hindlimb gait acute results. Values are means ± SEM

3.3.1.2.3 Hindlimb speed

All animal groups showed a similar trend in running speeds at all acute time points. However, the speed of the animals in the room air group was worse at each of the time points, in comparison to those treated with oxygen. In particular, animals treated with 80% oxygen showed statistically significant improvement of the running speed at 48 hours post-lesion induction, the peak of disability ($P^* < 0.05$), as well as at 96 hours post injection ($P^* < 0.05$), compared with room air treated controls (Figure 3-4). These results show that acute oxygen therapy, particularly at 80% hyperoxia, is able to protect against a decline in running speed at all acute time points.

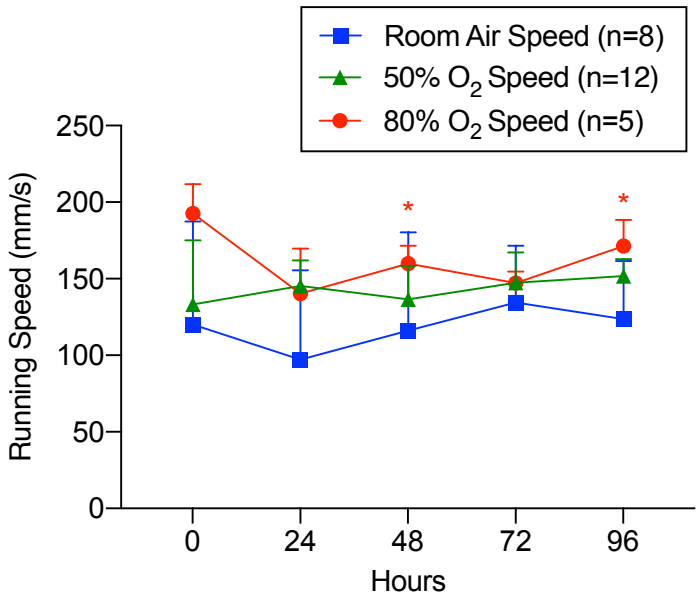

Figure 3-4 Oxygen treatment running speeds of acutely lesioned animals

Graph showing the combined averages of running speeds at speed 20cm/s of room air control (n=8) animals and 50% (n=5) and 80% (n=12) O_2 treatment groups. Values are means ± S.D. *Two-way ANOVA*, ($P^* < 0.05$).

3.3.2 Chronic disability

3.3.2.1 Acute oxygen treatment protects against chronic hindlimb neurological disability

3.3.2.1.1 Horizontal ladder

Hind limb function was assessed in animals treated for 4 days with room air or normobaric hyperoxia. Disability of the hindlimbs was similar across all treatment groups at all the time points examined (Figure 3-5). As previously noted, the left hind limb was less affected than right across all treatment groups, however the results were not statistically significant.

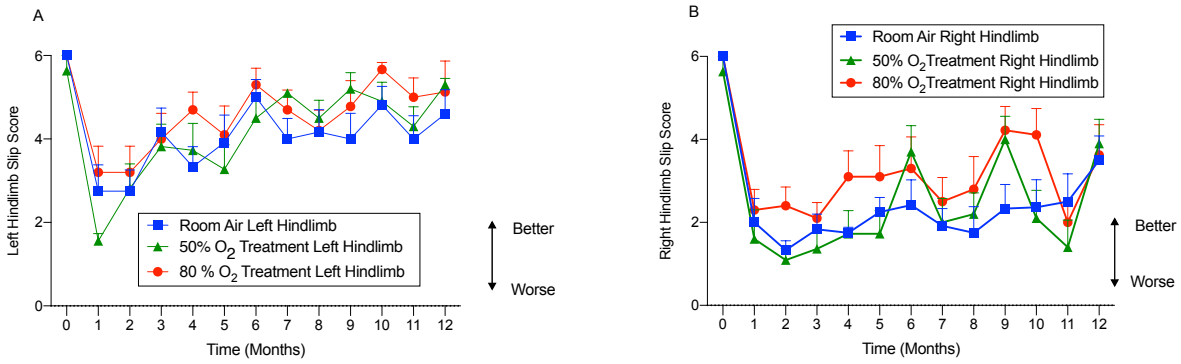

Figure 3-5 Oxygen treatment chronic hindlimb disability

Hindlimb disability scores while walking on a horizontal ladder for animals injected with LPS and breathing room air (n=10), or animals injected with LPS and kept in normobaric hyperoxia (80%) (n=10) and hyperoxia (50%) (n=11). Animals were scored every month after initial LPS surgery. **A.** Shows left hindlimb chronic results. **B.** Shows right hindlimb chronic results. Values are means ± SEM. Statistical analysis was performed with a *Two-way ANOVA* test.

3.3.2.1.2 Hindlimb speed

All animal groups showed a similar trend in running speeds after 1- and 2 months post LPS injection and treatment. However, the speed of the animals in the room air group was worse at each of the time points, in comparison with those treated with oxygen, particularly the 80% oxygen treatment group (Figure 3-6). The 50% oxygen treatment group is missing the second month measurements due to the malfunctioning of the treadmill scan equipment.

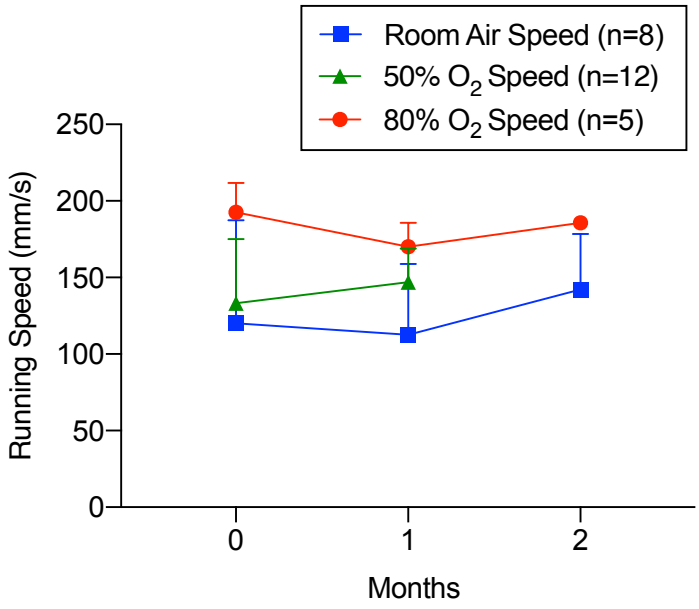

Figure 3-6 Oxygen treatment running speeds of chronically lesioned animals

Graph showing the combined averages of running speeds at speed 20cm/s of room air control (blue) (n=8) animals and 50% (green) (n=5) and 80% (red) (n=12) O_2 treatment groups. Values are means ± S.D. *Two-way ANOVA*.

3.3.2.2 Acute oxygen treatment protects against chronic tail deficit post LPS injection

Animals treated with room air exhibited significant chronic disability over the 12-month study, as expected. The disability was particularly significant at 1 month (**: $P<0.01$), 3 months (*: $P<0.05$), 7 and 9 months (**: $P<0.01$) and at 10, 11 and 12 months (****: $P<0.0001$) compared to baseline recorded pre-surgery (Figure 3-7 A). Animals treated with 50% oxygen exhibited a significantly lower tail deficit at one (*: $P<0.05$) and 12 months (**: $P<0.01$) compared with those animals treated with either room air or 80% oxygen (Figure 3-7 B). In comparison, animals treated with 80% oxygen, showed a similar level of tail weakness as those treated with room air at 1 month, however, the disability was significantly ameliorated at 10 (**: $P<0.01$) and 12 months (*: $P<0.05$) (Figure 3-7 C). Overall, disability was evidently reduced in groups of animals treated with oxygen, compared with room air-treated controls (Figure 3-7 D).

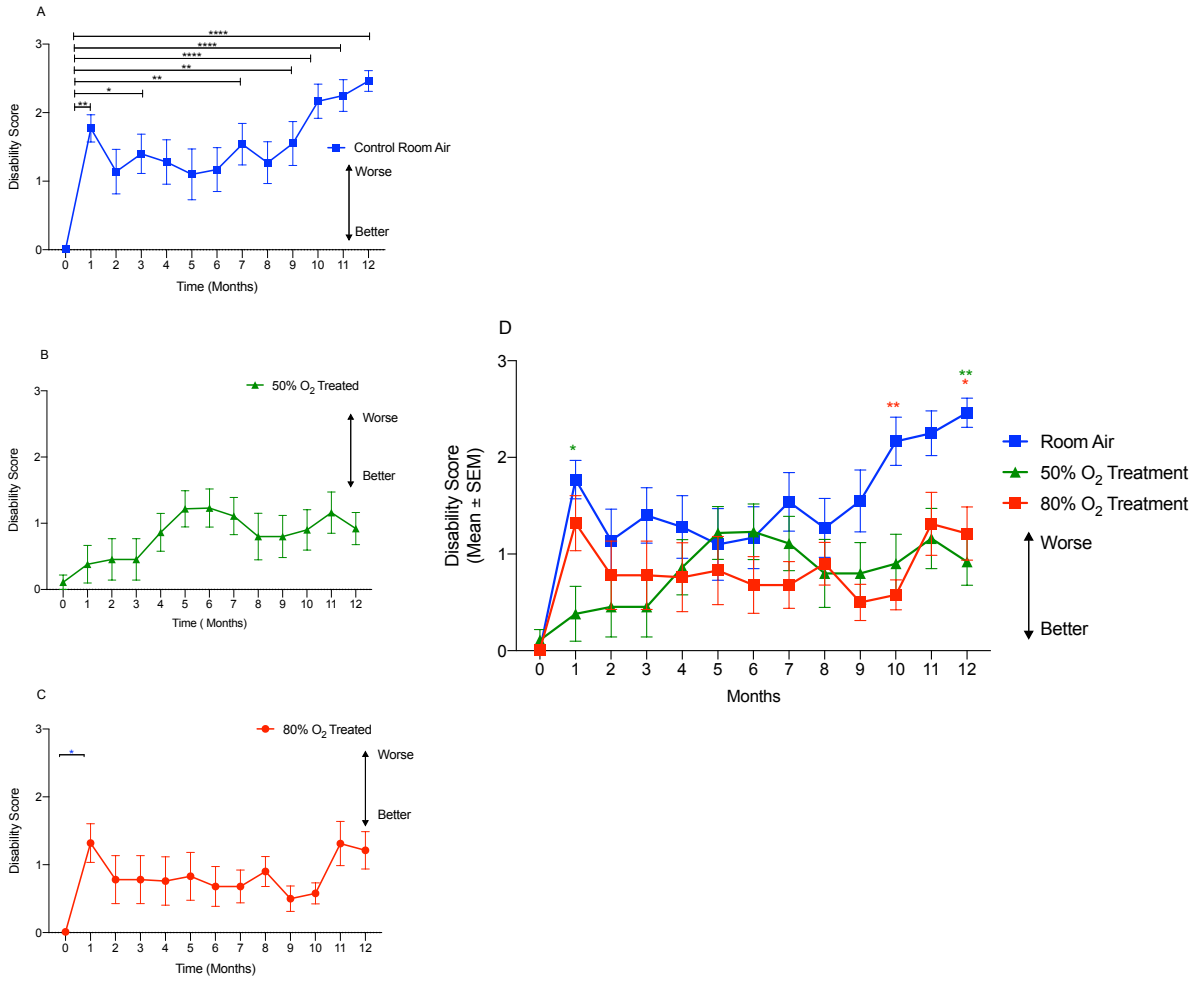

Figure 3-7 Oxygen treatment chronic tail disability

Tail disability scores while walking on a horizontal surface for animals injected with LPS and placed in a room air environment (n=10) as controls (blue) **(A)**, 50% hyperoxia treatment (n=11) (green) **(B)**, and 80% hyperoxia treatment (n=10) (red) **(C)**. **D.** Graph showing the combined relative tail disability scores of room air control animals and 50% and 80% O_2 treatment groups. Results were subject to *Two-way ANOVA*; (*: $P<0.05$) and (**: $P<0.01$), (***: $P<0.001$) and (****: $P<0.0001$). Month 0 corresponds to baseline value recorded before surgery. Values are means ± SEM.

These data sets suggest that acute exposure to hyperoxia of 80% or 50% oxygen, after LPS injection in the spinal cord, protects from neurological disability acutely and it is able to conserve protection in the long-term as well (Figure 3-8).

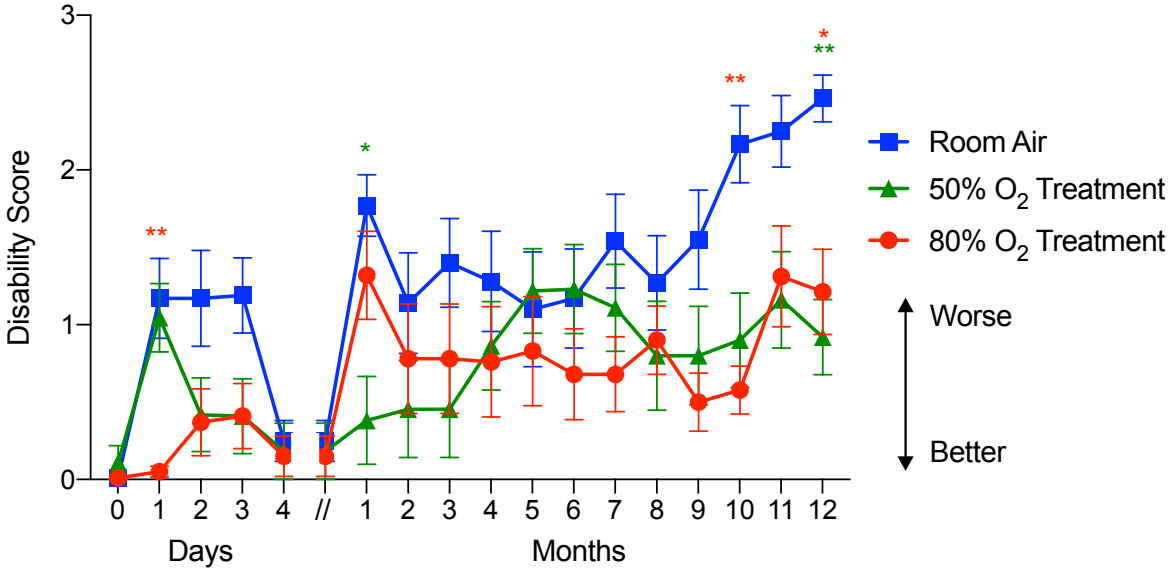

Figure 3-8 Oxygen treatment acute and chronic tail disability represented on the same graph

Tail disability scores while walking on a horizontal surface for control animals (blue) injected with LPS and placed in room air (n=10), or animals injected with LPS and kept in normobaric hyperoxia (80%, red) (n=10) and hyperoxia (50%, green) (n=11). Values are means ± SEM. Statistical analysis was performed with a *Two-way* ANOVA test (*: $P<0.05$), (**: $P<0.01$).

3.3.3 MRI Volume

Excised spinal cords were scanned using MRI to locate the lesions. A total of 133, 300 µm-thick slices per animal were taken, scanning 3.99 cm of each spinal cord centred on the injection site. Grey matter atrophy was measured to determine the lesion cross-sectional area for each scan. Subsequently, volume measurements were calculated using the slice thickness and cross-sectional values. Extensive atrophy of the injected ventral grey matter was evident in animals treated with room air. Importantly, animals treated with oxygen had reduced atrophy, in particular those treated with 80% oxygen (*: $P<0.05$), compared with room air treated controls (Figure 3-10).

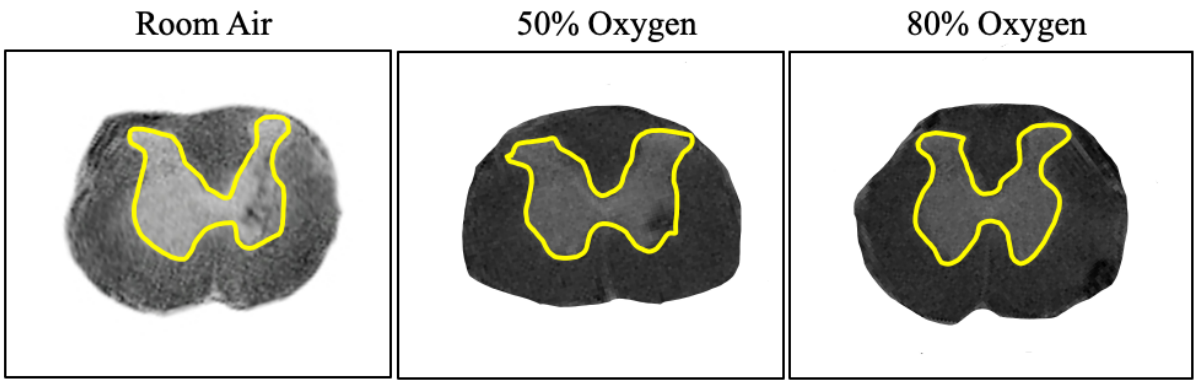

Figure 3-9 MRI of chronically lesioned spinal cords, comparing room air-treated control and after 50% and 80% O_2 treatment

Ex-vivo magnetic resonance images of sections from the lesion's epicentre of LPS-injected animals exposed to either room air (control) and 50% oxygen/ 80% oxygen (treatments), showing that treatment with oxygen decreases the size of demyelinating lesions.

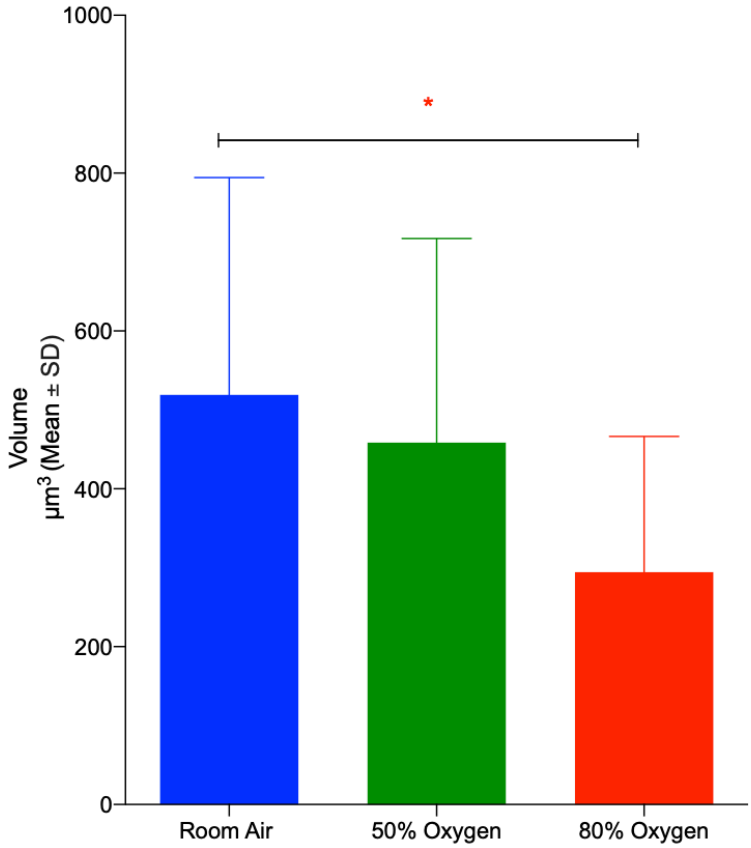

Figure 3-10 Volume after O_2 treatment

Graph showing the average atrophy volume of room air controls (n=9) and 50% (n=10) / 80% (n=7) O_2 treatments. Results were subject to *a one-way ANOVA*; (*: $P<0.05$). Values are means ± S.D.

3.3.4 Histology

3.3.4.1 Histological changes associated with oxygen therapy

The MRI findings were corroborated by histological evaluation of spinal cord sections at the lesion epicentre with H&E staining. Significant atrophy was evident in the grey matter of lesioned animals treated with room air, compared with 50% and 80% treatment groups (Figure 3-11 A). Not only was the percentage of grey matter protection provided by 80% oxygen treatment statistically significant (*: $P<0.05$; Figure 3-10 B), but a significant preservation of motor neuron numbers was also observed (*: $P<0.05$) (Figure 3-12 A,B), in comparison with its contralateral grey matter.

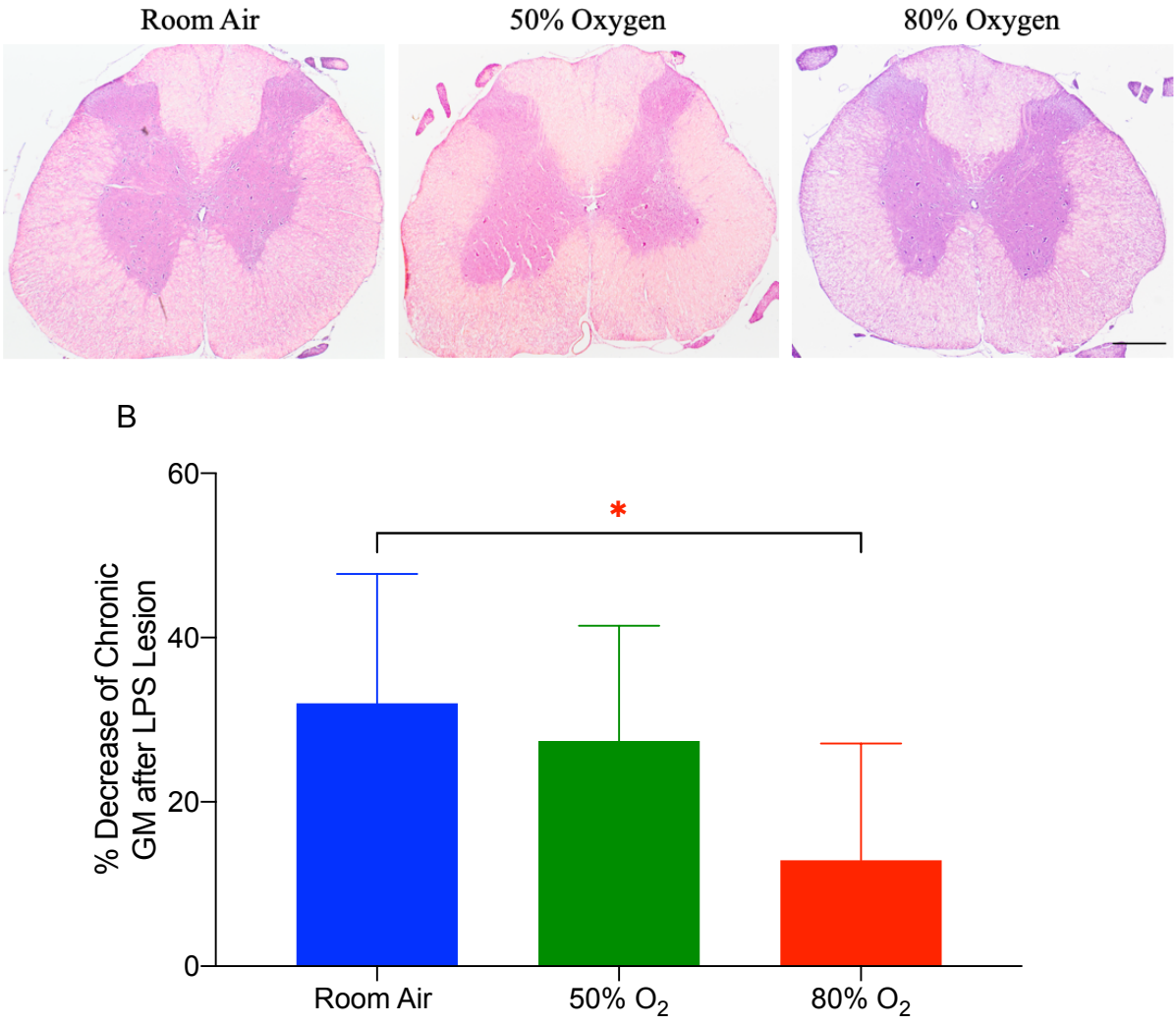

Figure 3-11 H&E Staining of chronically lesioned spinal cords after O_2 treatment

A. Transverse sections of chronically lesioned spinal cords stained with H&E of LPS- injected animals exposed to room air (control) and 50% O_2 and 80% O_2 (treatments). Scale bar is 500μm. **B.** Graph showing the percentage decrease of grey matter of chronically lesioned spinal cords. Room air (controls) (n=11) and 50% O_2 (n=7) and 80% O_2 (n=10) treatments. *One-way ANOVA*; (*: $P<0.05$). Values are means ± S.D.

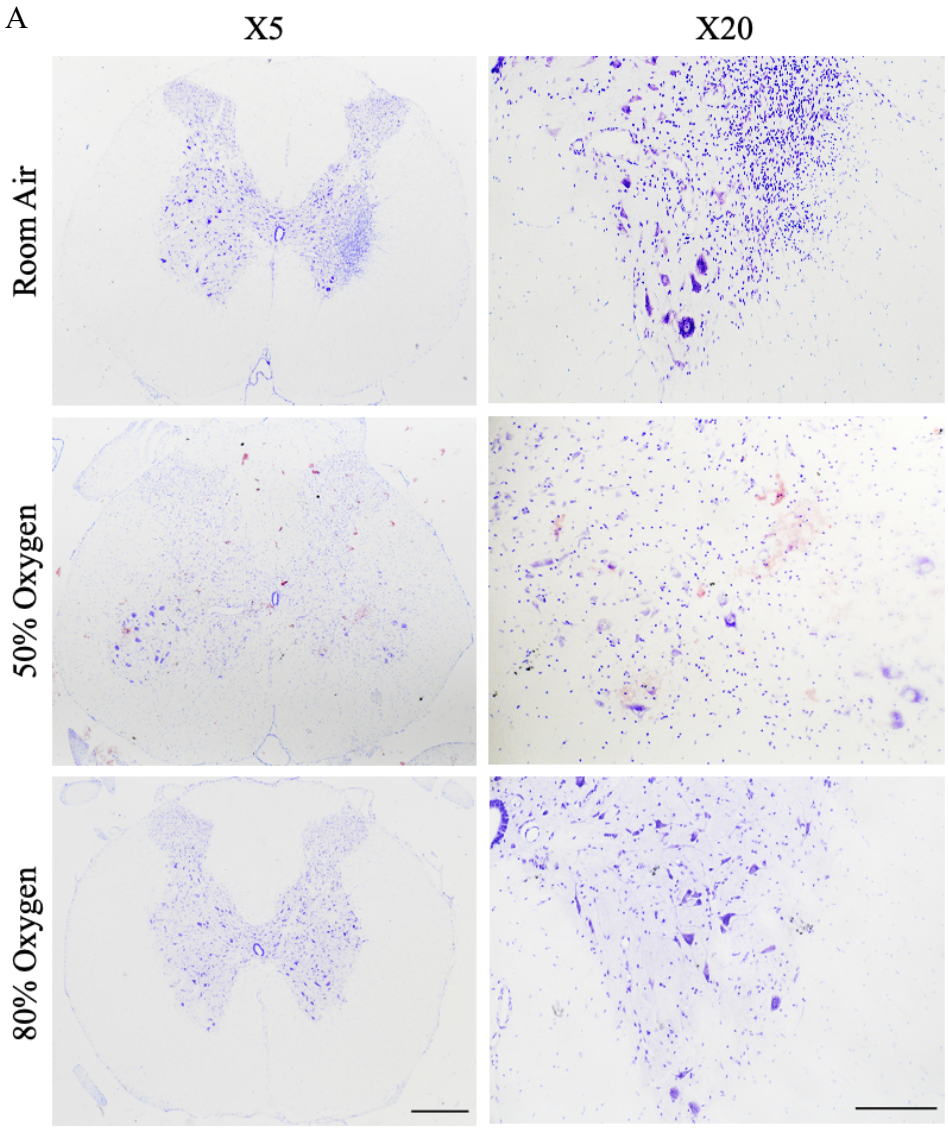
A
X5
X20
Room Air
50% Oxygen
80% Oxygen

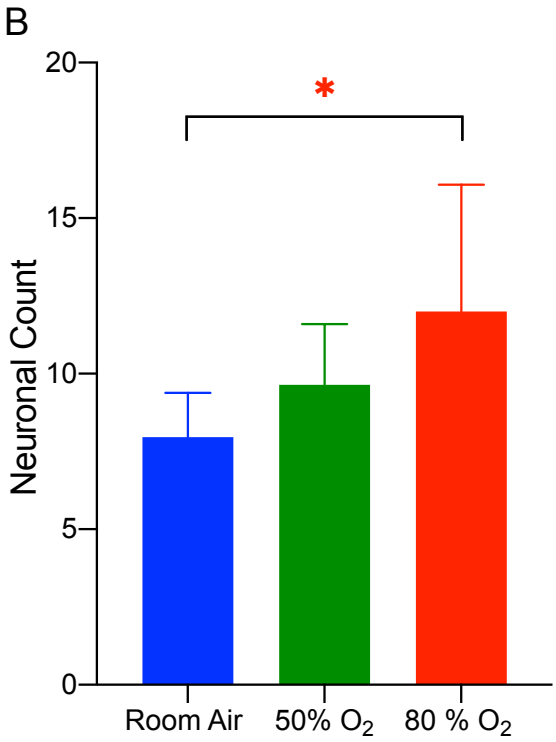

Figure 3-12 CV Staining of chronically lesioned spinal cords after O_2 treatment

A. Transverse sections of chronically lesioned spinal cords stained with CV of LPS-injected animals exposed to room air (controls) or 50% oxygen and 80% oxygen treatment, each with its corresponding lesion side. Scale bar is 500µm (low magnification) and 200µm (higher magnification). **B.** Motor neuron count of animals injected with LPS and exposed to room air (n=8) and animals exposed to normobaric chamber with 50% O_2 (n=6) and 80% O_2 (n=8) as treatment groups. *One-way ANOVA* (*: $P<0.05$); Values are means ± S.D.

Evidence of demyelination was assessed using LFB staining techniques. There appears to be some slight myelin pallor in the grey matter on the injected side but nothing overtly clear or significant, irrespective of the treatment (Figure 3-13).

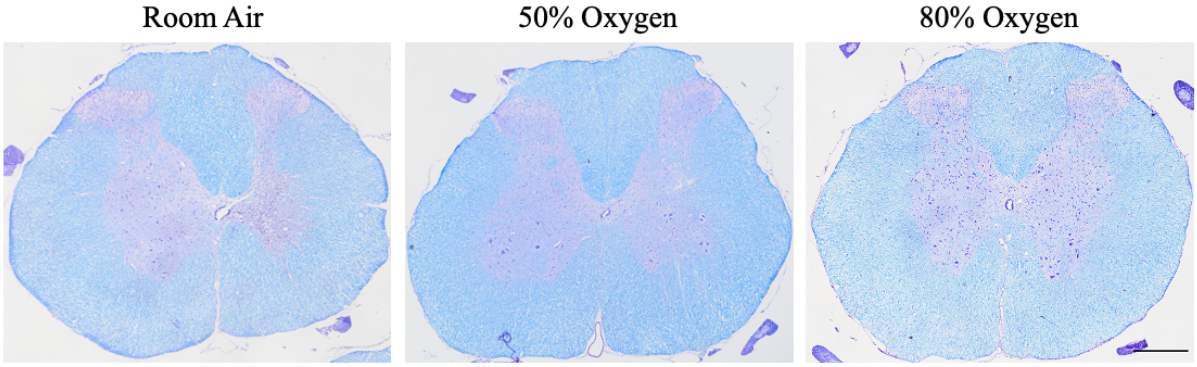

Figure 3-13 LFB Staining of chronically lesioned spinal cords after O_2 treatment

Transverse sections of chronically lesioned spinal cords stained with LFB (myelin) of LPS-injected animals exposed to room air (control) and 50% oxygen and 80% oxygen (treatments). There are no obvious changes in LFB staining between the images. Scale bar is 500µm.

3.3.4.2 Gliosis

To determine whether oxygen therapy could affect inflammation or gliosis, spinal cord sections at the lesion epicentre were double-labelled for macrophages/microglia (IBA) and astrocytes (GFAP) (Figure 3-14 A). Sections from animals treated with room air showed a substantial level of immunoreactivity for IBA and GFAP in the injected grey matter, compared with the contralateral side. Although animals treated with oxygen showed a decrease in both IBA and GFAP labelling, particularly after the 80% oxygen treatment, the difference between room air and oxygen was not statistically significant when assessed by fluorescence intensity in ImageJ (Figure 3-14 B).

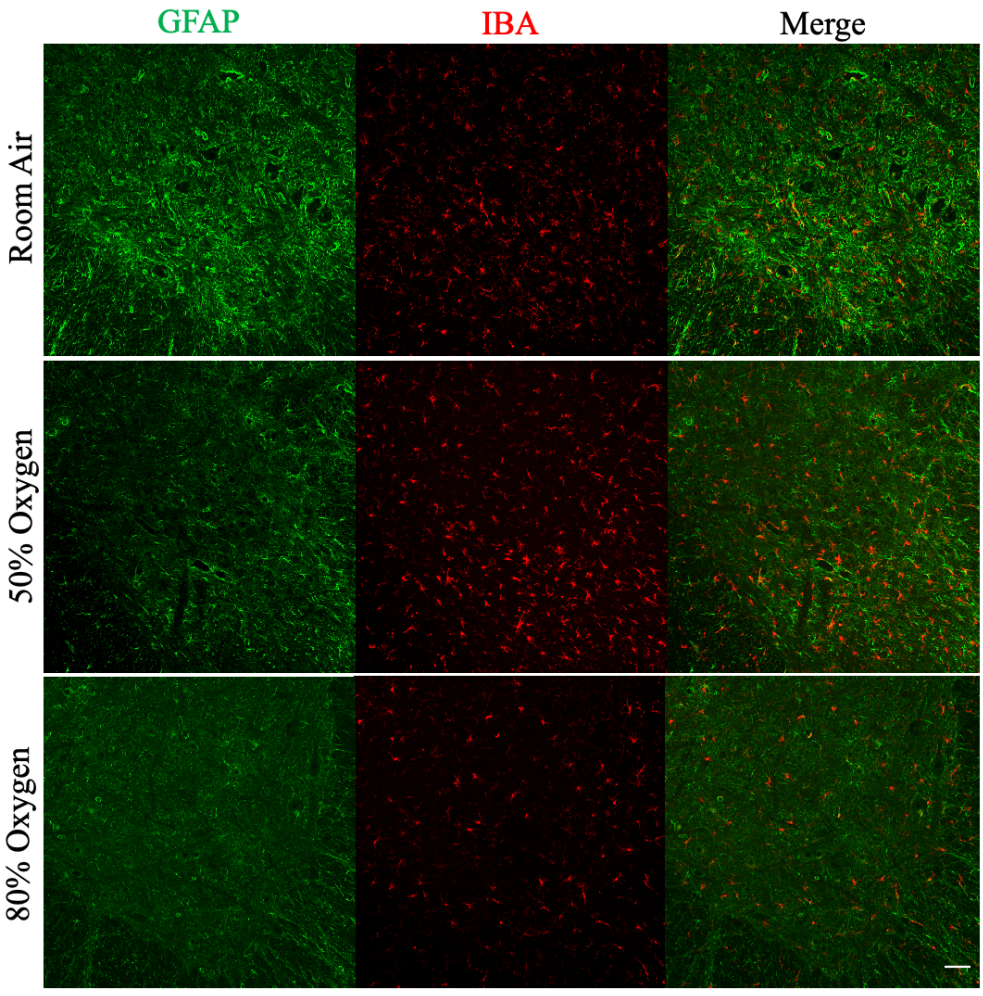

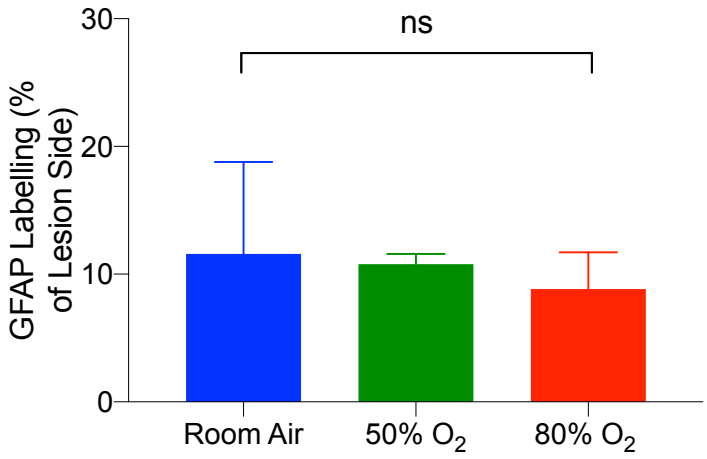

Figure 3-14 IBA/GFAP Immunohistochemistry

A. Transverse sections of chronically lesioned spinal cords labelled with anti-GFAP (astrocytes) and anti-IBA (microglia) antibodies. All micrographs are injection side only, scale bar is 100 µm. **B.** Graph showing the percentage of GFAP labelling on the injected side of the GM of animals injected with LPS. Graph shows combined means of control room air animals (n=7) and 50% oxygen treatment (n=2) and 80% oxygen treatment (n=6). *One-way ANOVA* (n.s).

3.4 Discussion

The present study shows that early, acute oxygen therapy, during key stages after injection of LPS into the spinal grey matter, significantly protects from acute and chronic disability, motor neuron loss and long-term atrophy. These findings highlight the crucial role played by hypoxia during the early inflammatory response, that lead to grey matter lesion formation.

3.4.1 Oxygen therapy reduces disability

The current study presents evidence that early treatment with normobaric hyperoxia, during the acute inflammatory-hypoxic period that follows intraspinal injection of LPS, results not only in acute, but also in long-term protection against disability, even after discontinuation of therapy. Although both 50% and 80% concentrations provided functional benefit throughout the time course of the study, the protection provided by 80% oxygen was more significant for both chronic disability and atrophy. Oxygen therapy has been shown to inhibit inflammation by downregulating TNF-α, IL-1, IL-6 and cytochrome *c* oxidase-2 (COX-2) (Duan *et al.*, 2015; Rosenberg *et al.*, 2015; Zhang *et al.*, 2005) and enhancing superoxide dismutase (SOD) activity in the ischaemic brain (Parabucki *et al.*, 2012). SOD is located in the mitochondrial matrix, and it is a critical antioxidant enzyme that catalyses the dismutation of superoxide, to oxygen and hydrogen peroxide, and it has also been linked in helping normal CNS function during early neurodegeneration and disability (Bidmon *et al.*, 1998; Kim *et al.*, 2002; Parabucki *et al.*, 2012). The mechanisms described above may be probative to the decrease in disability observed after oxygen therapy in this model of progressive MS.

Hyperbaric oxygen therapy, a related therapy to the one used in this study, was initially introduced in the belief that oxygen is immunosuppressive, but more recently its use may be based on the premise that injured or vulnerable neurons would benefit from increased oxygen

delivery and air pressure, which would act to metabolically reactivate cells (Zhang *et al.*, 2005). The findings in this study have some similarity with previous observations that show that hyperbaric oxygen therapy, used in ischaemia due to traumatic brain injury (TBI) patients, has improved neurological, neurophysiological and cognitive variables (Barrett *et al.*, 2004). Studies have shown that increasing cerebral blood flow, associated with both dissolved oxygen and elevated pressure, can be the physiological 'push' needed by non-electrically active "idling" neurons (Hadanny *et al.*, 2015; Neubauer *et al.*, 1990). In addition, clinical studies have shown that oxygen therapy can improve cognitive function and decrease neuronal cell death during a very narrow therapeutic window, preferably hours after the trauma, as executed in this study (Baratz-Goldstein *et al.*, 2017; Ciarlone *et al.*, 2019).

Animal models have outlined the multiple mechanisms by which hyperbaric oxygen therapy may reduce inflammatory and apoptotic signalling pathways (Baratz-Goldstein *et al.*, 2017; Zhang *et al.*, 2005). For instance, hyperbaric oxygen therapy can achieve neuroprotection by tackling the deficit in energy metabolism resulting from inflammation, by replenishing ATP production due to readily available oxygen, glutamate, glucose and pyruvate, and by promoting homeostasis of cytosolic calcium overload and membrane polarization (Chen *et al.*, 2020; Zhang *et al.*, 2005).

3.4.2 Oxygen therapy provides protection from neuropathology

The aetiology of MS remains unclear. However, it is widely recognised that inflammation, hypoxia and demyelination play an important role in the course of the early disease (Lassmann, 2016; Lassmann *et al.*, 2007; Lucchinetti *et al.*, 2000). As the disease advances, atrophy and neuro-axonal loss become the driving force in disease progression (Bitsch *et al.*, 2000; Correale *et al.*, 2019; Ferguson *et al.*, 1997; Kutzelnigg *et al.*, 2005; Lassmann *et al.*, 2001; Lovas *et al.*, 2000; Pirko *et al.*, 2007). Previous research in a related experimental model to the one used in this present study, have shown that during the acute

stages of lesion formation and intense CNS inflammation, oxygenation is attenuated, however oxygen therapy can significantly reduce demyelination, that would otherwise occur (Davies *et al.*, 2013; Desai *et al.*, 2016). It is speculated that, during the early phase of lesion formation, perivascular inflammatory infiltrates are partly responsible for an elevated consumption of oxygen in the already vulnerable areas known as watershed areas (Martinez Sosa & Smith, 2017).

Oxidative stress is present in MS aetiology, particularly during later stages of neurodegeneration (de Vries *et al.*, 2008; Hernandez-Gerez *et al.*, 2019). Furthermore, inflamed tissue is made even more vulnerable to oxidative stress by microenvironments within the CNS (Martinez Sosa & Smith, 2017). Together, oxidative stress and poor CNS perfusion leads to mitochondrial dysfunction, which generates ROS and RNS, such as NO (Dave *et al.*, 2003; Smith & Lassmann, 2002). NO-mediated toxicity has been shown to contribute to mitochondrial impairment, oxidative stress and DNA damage, as well as affecting microglia, axons, astrocytes, and in particular oligodendrocytes (Desai *et al.*, 2016; Lucchinetti *et al.*, 2000; Smith & Lassmann, 2002). Oxygen treatment has been shown to improve mitochondrial dysfunction by decreasing levels of TNF-α that cause lower complex IV activity, as seen in mitochondria isolated from motor cortex and spinal cord motor neurons (Dave *et al.*, 2003). Thus, in MS, mitochondrial dysfunction appears concomitant to inflammation, which significantly impairs energy production in neurons (Mahad *et al.*, 2015). Collectively, these factors conspire to exacerbate energy deficiency within the CNS, particularly within watershed areas (Aboul-Enein *et al.*, 2005; Fischer *et al.*, 2012).

Overall, oxygen administration can enhance the oxygen content in ischaemic CNS regions, and as a result help prevent from secondary injury, as shown in long term clinical studies (Meng *et al.*, 2015). However, it has been determined that the optimal therapeutic

window to implement oxygen therapy is within several hours, or days, from the onset of neurological trauma, in order to have a significant neuroprotective effect (Baratz-Goldstein *et al.*, 2017). Though we recognize that, in MS, the hypoxic and inflammatory period may occur before diagnosis, our progressive model of MS shows that tackling hypoxia early in the disease can protect from long-term neurodegeneration and disability, highlighting the imperative role played by hypoxia in driving long-term atrophy. Moreover, these results do show a potential role for oxygen therapy in the treatment of acute, forming MS lesions, in attenuating degeneration.

3.4.3 Hypoxia induces astrocytic activation

During neurological disease, astrocytes undergo complex phenotypic changes, referred to as reactive gliosis (Sofroniew & Vinters, 2009). Astrogliosis occurs in a graded mechanism, where astrocyte morphology, size and secretory profile changes from a quiescent astrocyte, to its reactive gliotic phase (Nash *et al.*, 2011). The prevailing view is that reactive gliosis reduces neuronal survival following brain injury, by secreting pro-inflammatory cytokines, and molecules with cytotoxic potential, such as ROS and NO, via the formation of a glial scar, thereby demarcating and surrounding the damaged tissue (Aviles-Reyes *et al.*, 2010; Shi *et al.*, 2016; Sofroniew, 2016). Importantly, the pro-inflammatory cytokine IL-1 has been suggested to activate astrocytes in the early stages of lesion formation (Ridet *et al.*, 1997). Consequently, HIF-1 and its downstream target VEGF-A are induced within astrocytes, which act on endothelial cells impairing BBB integrity, via a process mediated largely by endothelial nitric oxide synthase (eNOS) (Correale *et al.*, 2019).

In MS, much as in our model, acute inflammatory lesions are surrounded by astrocyte reactivity. As the lesion progresses, hypertrophic astrocytes begin to develop bundles of glial filaments, thereby increasing GFAP immunoreactivity, as oedema ceases (Correale *et al.*, 2019). Astrocytes are extremely sensitive to physiological changes in oxygen levels (Marina

et al., 2017). The hypoxia sensor in astrocytes resides within the mitochondria, where oxygen is consumed (Chandel *et al.*, 1998a). Astroglial mitochondrial respiration is inhibited in response to hypoxia, leading to mitochondrial depolarization, production of free radicals and release of calcium from intracellular compartments. Moreover, hypoxia induces an increase in calcium levels, inhibiting astrocytic signaling, due to an overexpression of ATP degrading enzymes (Angelova *et al.*, 2015). In our study, there was some decrease in astrocytic activity and gliosis, after acute normobaric oxygen therapy. This apparent decrease in chronic gliosis could potentially come as a result of the diminished astrocyte reactivity in the beginning of the disease, as a result of the oxygen therapy.

3.4.4 Oxygen treatment as a therapy for MS

Presently, there are multiple anti-inflammatory or immunosuppressive therapies targeting MS patients, some of which are of benefit to RRMS patients, yet not effective in patients with SPMS (González-Andrade *et al.*, 2010). The question arises as to why these anti-inflammatory therapies are ineffective when targeting the more progressive phases of the disease. One explanation could be that, during the progressive stages of MS, inflammation becomes "trapped" behind an intact BBB, in which case one of the requirements for a viable treatment strategy may be that a drug would have ready access across the BBB (Mahad *et al.*, 2015). An additional explanation could be that, inflammation is only the initial driving force that influences other mechanisms, such as hypoxia, and the damage caused by the latter accumulates before anti-inflammatory therapies are either introduced or effective.

The current study provides evidence that oxygen therapy can decrease disability and progressive atrophy when administered early during the inflammatory phase of the disease, indicating a key role for hypoxia in driving progressive pathology. Normobaric oxygen therapy can be easily implemented as a therapeutic treatment, and is thoroughly supported by literature as being safe (if delivered at appropriate concentrations), convenient and inexpensive (Desai

et al., 2016; Ding *et al.*, 2019). One of the consequences of elevating the pO_2 is raising intracranial blood pressure as well as downregulating zinc levels, which may contribute to the neuroprotective results provided by normobaric oxygen therapy (Ding *et al.*, 2019; Dong *et al.*, 2015). However, other studies have reported that breathing high concentrations of oxygen can result in vasoconstriction of the carotid and downstream cerebral arteries, although it was noted that those results could be unrelated to the oxygen treatment (Cornet *et al.*, 2013).

3.4.5 Conclusion

In conclusion, we have produced evidence that oxygen therapy represents a therapeutic approach for neuroprotection in MS. Further, the findings highlight important mechanisms of progressive disease, namely that the acute inflammatory hypoxia is a key driver of chronic disability and pathology.

Chapter 4 CNS-Selective vasodilator can protect from acute inflammation and chronic degeneration and atrophy

4.1 Introduction

The central nervous system comprises 2% of the total body weight in humans, but it receives approximately 20-25% of the net cardiac input (Mink *et al.*, 1981). In spite of this, there are 'vascular watershed' areas that inherently render regions of the CNS especially vulnerable to hypoxia-ischaemia-induced damage (Moody *et al.*, 1990). Studies have highlighted the important role played by the CNS vasculature in influencing the fate of MS lesions, as well as the pattern and persistence of the lesion formation (Desai *et al.*, 2020; Holland *et al.*, 2012; Martinez Sosa & Smith, 2017). Blood vessel damage and a significant reduction in their density is often seen in MS lesions (D'Haeseleer *et al.*, 2011; Lassmann, 1999), and it has been observed that the wall of cerebral veins in MS is subject to chronic inflammatory damage, promoting haemorrhage and increased permeability of endothelial cells, leading to vasculitis and blood vessel damage (Adams, 1988; Beckman & Koppenol, 1996). Moreover, inflammatory cells can reduce microvascular flow by impairing vascular regulation, through the manipulation of ROS that directly damage the vascular endothelium (Adams, 1988; Johnson *et al.*, 2016). Inflammation, as well as oxidative stress, has been shown to be highly involved in endothelial dysfunction in MS (Koch *et al.*, 2005; Sitia *et al.*, 2010). Collectively, these mechanisms render MS patients more susceptible to ischaemic strokes (D'Haeseleer *et al.*, 2013; Koch-Henriksen *et al.*, 1998).

The widespread decrease in the white and grey matter perfusion in MS may not occur secondarily to axonal degeneration, but rather as a result of diminished axonal activity, reduced energy metabolism, particularly in astrocytes, and increased levels of ET-1 (D'Haeseleer *et al.*, 2013). Endothelial cells release high levels of ET-1 in the blood in patients with MS, which

contribute to vasoconstriction and reduction of blood flow (Pache *et al.*, 2003). In addition, ET-1 may function as an important modulator of inflammation, by regulating the expression of intercellular adhesion molecules, or directly enhancing neutrophil adhesion (Pache *et al.*, 2003; Xu *et al.*, 1998; Zouki *et al.*, 1999). These observations suggest that, perhaps, as a result of inflammation, reactive astrocytes induce arteriolar vasoconstriction by the release of ET-1, thereby impairing blood flow, increasing hypoxia and disability (Castellazzi *et al.*, 2019; Chen *et al.*, 2017; D'Haeseleer *et al.*, 2015). We believe that by re-establishing tissue perfusion, particularly at vulnerable watershed areas in the CNS, we can help prevent and or reverse the damaging corollary generated by the innate immune response, and hypoxia, during acute stages of the disease. Thus, we proffer that nimodipine, a CNS-selective vasodilator, administered during the acute hypoxic phase of the disease, will work as a potential perfusion regulator, and protect against progressive disability and atrophy.

4.1.1 Hypothesis

We hypothesise that acutely improving blood flow during the hypoxic window, will attenuate disability and protect from atrophy and neuronal loss in our new model of progressive MS.

4.1.2 Aims

1. To determine whether impaired blood flow represents a mechanism through which disability, atrophy and neuronal loss develop in our model of progressive MS.
2. To determine whether increasing oxygenation, by improving blood flow, can reduce disability and protect from progressive disability, atrophy and neuronal loss.

4.2 Materials and Methods

4.2.1 Nimodipine therapy to improve blood flow and oxygenation

Nimodipine (Sigma Aldrich, UK), a CNS-selective vasodilator, or vehicle (1:4; ethanol: polyethylene glycol (PEG)), was administered by oral gavage (30mg/kg), or intraperitoneal (IP) injection, depending on the stage of the experiment.

4.2.2 Nimodipine therapy after ventral LPS injection

Animals were randomised into treatment groups (nimodipine: n=24; vehicle: n=15) prior to surgery. Lesions were induced as described previously in section 2.2.1. The first dose of nimodipine or vehicle was administered by IP injection immediately after surgery. Subsequent doses were administered by oral gavage every 12 hours for the first 96 hours following surgery. Animals underwent behavioural assessment (as below) prior to surgery for baseline measurements, and then daily for the duration of the treatment, and then monthly for one year.

4.2.3 Behavioural assessment

4.2.3.1 Ladder test

Functional hindlimb deficit was assessed as previously described in section 2.2.2.1.

4.2.3.2 Horizontal walking test-tail

Functional tail deficit was assessed as previously described in section 2.2.2.2.

4.2.3.3 Upside down grip hindlimb test

Hind limb grip strength was assessed by placing the animals on a wire grid, which was then inverted so that the animal was hanging upside down, as shown in Figure 4-1. The length

of time the animal was able to hold on to the rungs whilst upside down was recorded for each hindlimb in seconds. Animals were not trained previously as it was noticed that some animals have a natural ability to hold their bodies upside down for prolonged periods.

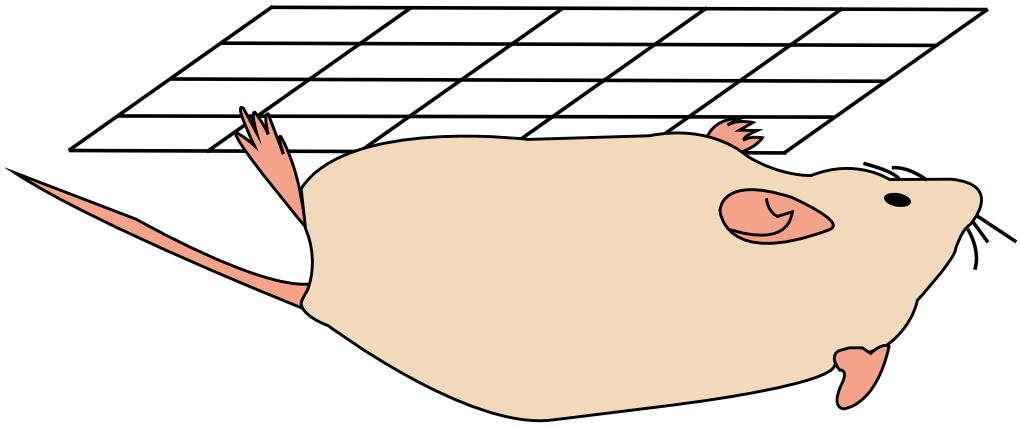

Figure 4-1 Hindlimb grip test

Representation of the behavioural test created to measure the duration of grip of hindlimbs.

4.2.4 Tissue perfusion

Animals were anaesthetized with isoflurane and a trans-cardial perfusion was performed as described previously in section 2.2.6.

4.2.5 MRI protocol

MRI was conducted on excised spinal cords as previously described in section 3.2.5.

4.2.6 Tissue processing

Post-MRI processing was performed as previously described in section 3.2.6.

4.2.7 Histology

4.2.7.1 H&E staining

Transverse sections of the spinal cord were used for H&E staining as previously described in section 2.2.4.1.

4.2.7.2 Luxol Fast Blue staining

Transverse spinal cord sections were used for LFB staining as previously described in section 2.2.4.2.

4.2.7.3 Cresyl Violet staining

Transverse spinal cord sections were used for CV staining as previously described in section 2.2.4.3.

4.2.8 Microscopy

4.2.8.1 Light microscopy and quantification

Tissue sections were viewed using an Axiophot light microscope (Zeiss, Germany), and micrographs taken using a Nikon D300 camera (Nikon, USA). The illumination was kept constant throughout image acquisition, under the same magnification. H&E grey matter quantification was carried out using the selection tool (ImageJ) to determine the average size of atrophy on the lesion side by comparing with the contralateral side.

4.2.8.2 Confocal microscopy

Confocal fluorescent images were obtained using a Zeiss 710 confocal microscope, with a 40X water immersion objective. Excitation wavelengths of 488 nm and 543 nm were provided by argon and helium-neon gas lasers.

4.2.9 Statistical analysis

4.2.9.1 Behavioral analysis

All data were tested for normality using the D'Agostino & Pearson test. Data that were not normally distributed were evaluated using non-parametric statistics, such as a paired t-test. P-values of 0.05 (*), 0.01 (**), 0.001 (***) and 0.0001(****), were considered as statistically significant. All statistical analyses were carried out GraphPad Prism version 8.

A two-way ANOVA test was performed on time course scoring experiments, to compare the significance between different time points and between the two treatment groups, those being nimodipine and vehicle. When treatment groups were compared at a single time point, t- tests were performed to assess significance.

4.2.9.2 Neuronal counts

Large neurons with visible nucleus present were counted as motor neurons using Image J (National institute of health, USA). All data were tested for normality using the Shapiro-Wilk test. Data that were not normally distributed were evaluated using non-parametric statistics as indicated. P- values of 0.05 (*), 0.01 (**), 0.001 (***) and 0.0001(****), were considered as statistically significant. Normally distributed data were evaluated using a one-way ANOVA. All statistical analyses were carried out using GraphPad Prism version 8.

4.2.9.3 Atrophy volume and length

The grey matter lesion cross sectional area was measured using the selection tool on Image J on each MRI slice where the lesion was visibly present. Subsequently, volume measurements were calculated using the slice thickness and cross-sectional values, where the lesion was present. All data were tested for normality using the D'Agostino & Pearson test. Data that were not normally distributed were evaluated using non-parametric statistics as

indicated. P-values of 0.05 (*), 0.01 (**), 0.001 (***) and 0.0001(****), were considered as statistically significant. All statistical analyses were carried out GraphPad Prism version 8.

A t- test was performed on atrophy volume results to compare the significance between different treatment groups and controls.

4.2.9.4 Grey matter area

All data were tested for normality using the D'Agostino & Pearson test or the Shapiro-Wilk test, depending on n numbers. P-values of 0.05 (*), 0.01 (**) and 0.001 (***), were considered as statistically significant. All statistical analyses were carried out using GraphPad Prism version 8.

4.3 Results

4.3.1 Acute disability

4.3.1.1 Nimodipine treatment protects against acute tail disability

Animals treated with vehicle exhibited tail weakness within the first 24 hours, which continued throughout the proceeding 72 hours. By 96 hours, the disability in vehicle-treated animals began to subside (Figure 4-2). In contrast, animals treated with nimodipine showed significant protection against tail disability at 24 hours (P^{**} <0.01), 48 hours (P^{*} <0.05), and 72 hours (P^{*} <0.05) post-injection, compared with those treated with vehicle (Figure 4-2). By 96 hours post injection, the tail disability score of animals treated with nimodipine was similar to baseline.

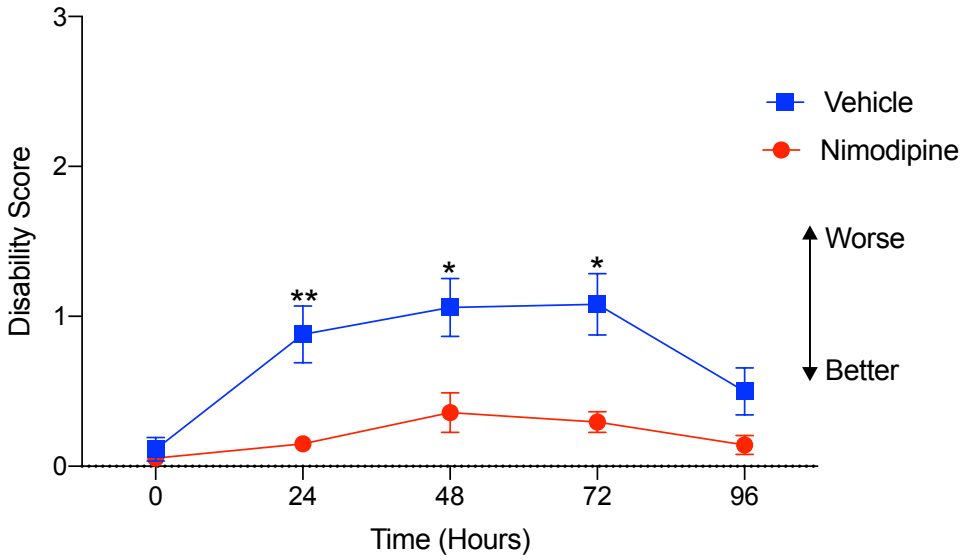

Figure 4-2 Nimodipine acute tail disability

Tail disability scores while walking on a horizontal surface for control animals (blue) following treatment with vehicle (n=15), or animals treated with nimodipine (red) (n=24). Animals were trained from one day before surgery (baseline) up to four days after surgery. Values are means ± SEM. Statistical analysis was performed with a *Two-way ANOVA* test (*: P<0.05), (**: P<0.01).

4.3.1.2 Nimodipine treatment protects against acute hindlimb neurological disability

As previously described, animals exhibited a more pronounced deficit in the right (ipsilateral to the injection) hind limb, compared with the left, although the left hindlimb also showed a neurological deficit. Significant disability was evident in the right hind limb of animals treated with vehicle, at all the acute time points (Figure 4-3 A-B), but in particular at 24 and 48 hours (***: $P<0.001$) post-injection. By 96 hours post-injection, the hind limb disability had resolved. Animals treated with nimodipine however, had a significantly lower disability score at 48 hours in the left hind limb (*: $P<0.05$), and at 24 hours in the right (***: $P<0.001$), compared with the vehicle-treated counterparts, and the left hindlimb at 48 hours post injection when comparing the scores to vehicle-treated controls (Figure 4-3A-B).

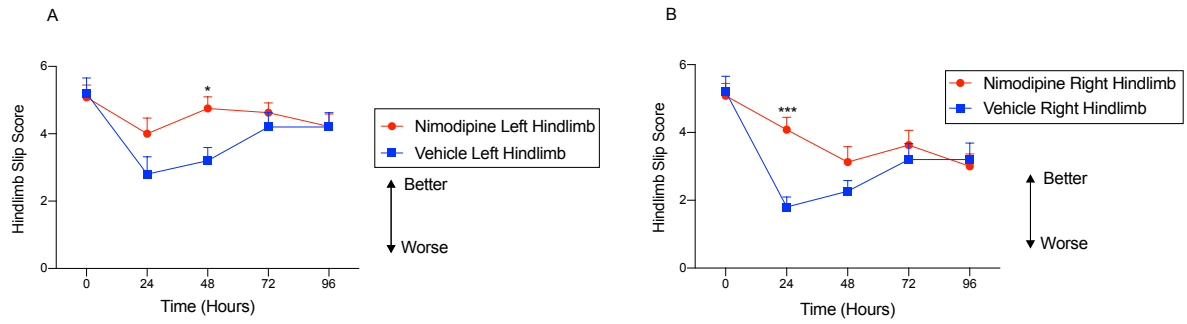

Figure 4-3 Nimodipine acute hindlimb disability

Hindlimb disability scores while walking on a horizontal ladder for animals injected with LPS, followed by treatment with vehicle (n=15) as controls, and nimodipine treatment (n=24). **A).** Left hindlimb scores for control and treatment groups. **B.** Right hindlimb scores for control and treatment groups. Results were subject to *Two-way ANOVA* (*: $P<0.05$), (***: $P<0.001$). Animals were trained from one day before surgery (baseline) up to four days after surgery. Values are means ± SEM.

4.3.1.3 Nimodipine treatment protects against hindlimb grip neurological disability

To further assess protection of hind limb disability by nimodipine, the time the right and left hind limbs were able to grip an inverted grid was measured. The left hindlimbs did not show a deficit, and so are not reported here. The time animals treated with vehicle were able to grip the inverted grid, without falling, remained stable across all the acute time points examined. However, animals treated with nimodipine showed an increase in the time they were able to grip without falling, particularly at 48 hours post-injection (*: $P<0.05$) (Figure 4-4).

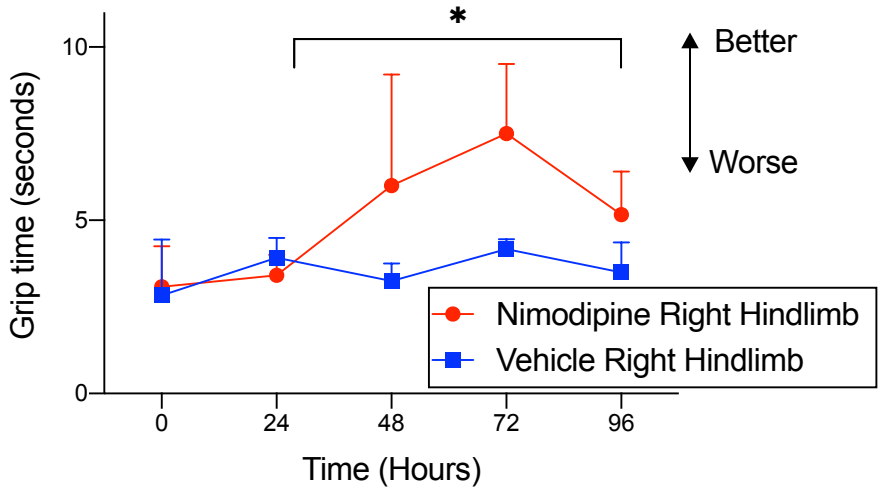

Figure 4-4 Nimodipine acute right hindlimb grip time

Relative right hindlimb grip time (seconds) while gripping upside down, for control animals following treatment with vehicle (n=7) or animals following treatment with nimodipine (n=12). Animals were examined from one day before surgery (baseline, time 0) up to four days after surgery. Values are means ± S.D. Statistical analysis was performed with a t-test (*: $P<0.05$).

4.3.2 Chronic disability

4.3.2.1 Acute nimodipine therapy protects against chronic hindlimb disability

Given the protection of acute hind limb disability observed with nimodipine, we next explored whether the protection of hind limb disability would persist in the long term. Overall, no statistical difference was evident between animals treated with vehicle and those treated with nimodipine, but there was a trend towards protection by nimodipine (Figure 4-5).

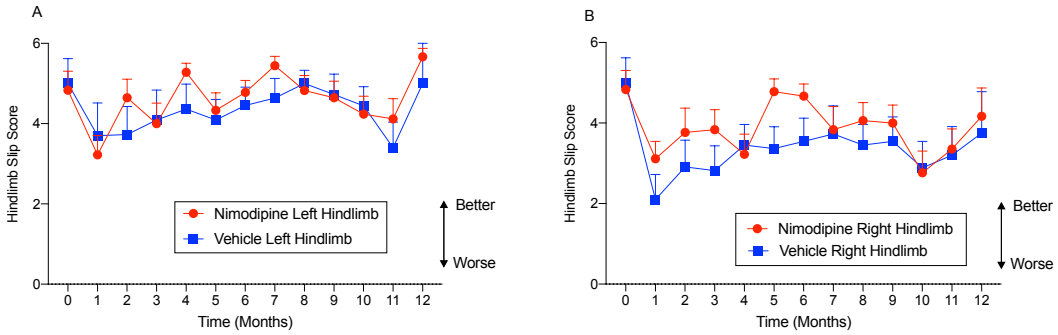

Figure 4-5 Nimodipine chronic hindlimb disability

Hindlimb disability scores while walking on a horizontal ladder of animals injected with LPS, followed by treatment with vehicle (n=11) as controls, and nimodipine treatment (n=18). **A.** Left hindlimb scores for control and treatment groups. **B.** Right hindlimb scores for control and treatment groups. Results were subject to *Two-way* ANOVA (n.s). Values are means ± SEM.

4.3.2.2 Acute nimodipine therapy and chronic hindlimb grip neurological disability

Assessment of the grip time for the right hind limb revealed a similar trend between vehicle treated and nimodipine treated animals, with no significant difference at any of the time points examined (Figure 4-6).

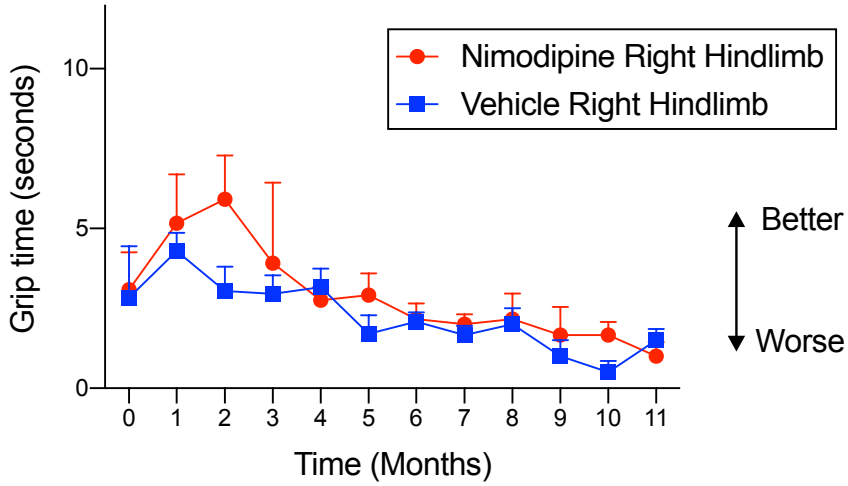

Figure 4-6 Nimodipine chronic right hindlimb grip time

Relative chronic right hindlimb grip time (seconds) while gripping upside down for control animals following treatment with vehicle (n=7), or animals following treatment with nimodipine (n=12). Values are means ± S.D.

Interestingly, as the lesion progressed, a deterioration in the ability of animals to grip for long periods was observed, irrespective of the treatment, probably related to increasing body weight.

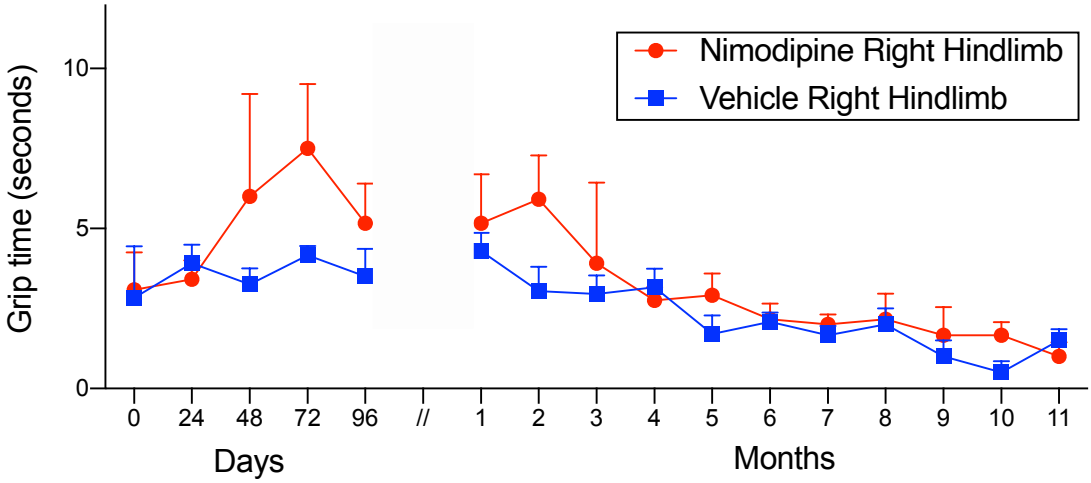

Figure 4-7 Acute and chronic right hindlimb grip time represented on the same graph

Relative acute and chronic right hindlimb grip time (seconds) while gripping upside down for control animals following treatment with vehicle (n=7) or animals following treatment with nimodipine (n=12). Animals were trained from one day before surgery (baseline) and every month after surgery. Values are means ± S.D.

4.3.2.3 Acute nimodipine therapy protects against chronic neurological disability of the tail

Animals treated with vehicle exhibited a progressive accumulation of tail disability over the course of the experiment (Figure 4-8A). In contrast, animals treated with nimodipine showed an attenuation in the progression of tail disability over the course of the experiment, with significant increases in disability only evident after 7 months post LPS injection, in comparison with baseline (Figure 4-8 B). Further the tail disability was significantly lower in the nimodipine-treated group, compared with the vehicle-treated group at all the time points examined from 2 months post-injection (Figure 4-8 C).

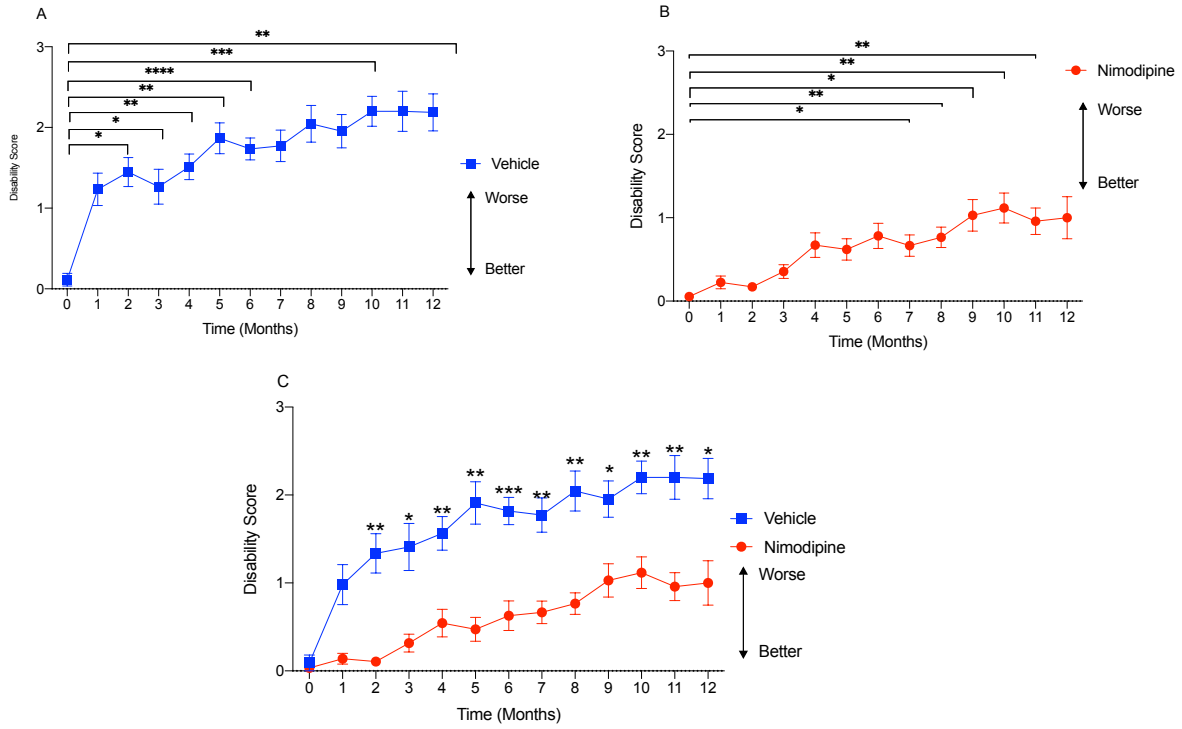

Figure 4-8 Nimodipine chronic tail disability

Tail disability scores while walking on a horizontal surface for animals injected with LPS and administered vehicle (n=11) as controls, **A.** and LPS-injected animals and administered nimodipine (n=18) as treatment group **B.** **C)** Relative tail disability scores of combined control and treatment groups. Results were subject to *Two-way ANOVA*; (*: $P<0.05$) and (**: $P<0.01$), (***: $P<0.001$) and (****: $P<0.0001$). Values are means ± SEM.

Collectively, treatment with nimodipine for the first four days following lesion induction, provides protection against both acute and progressive tail disability (Figure 4-9).

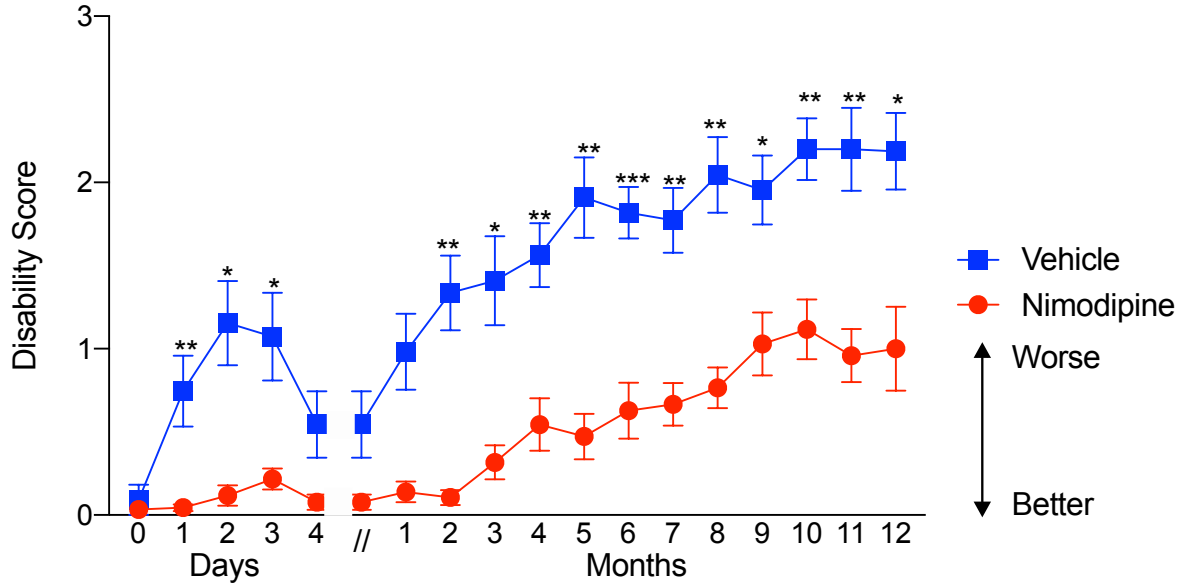

Figure 4-9 Nimodipine acute and chronic tail disability

Tail disability scores while walking on a horizontal surface for animals injected with LPS and administered vehicle (n=11) as controls and nimodipine treatment groups (n=18) in acute and chronic stages. Results were subject to *Two-way ANOVA*; (*: $P<0.05$), (**: $P<0.01$) and (***: $P<0.001$). Animals were trained from one day before surgery, and every month after that. Day 0 corresponds to baseline value recorded before surgery. Values are means ± SEM.

4.3.3 MRI Volume

MRI scans were mainly used to identify the lesion epicentre, in addition to allow the calculation of lesion volume and length, as described previously (4.2.9.3), and they revealed a significant protection from atrophy in the nimodipine-treated group compared with vehicle-treated controls (**: $P<0.01$), (*: $P<0.05$), as shown by Figures 4-10, 4-11 and 4-12.

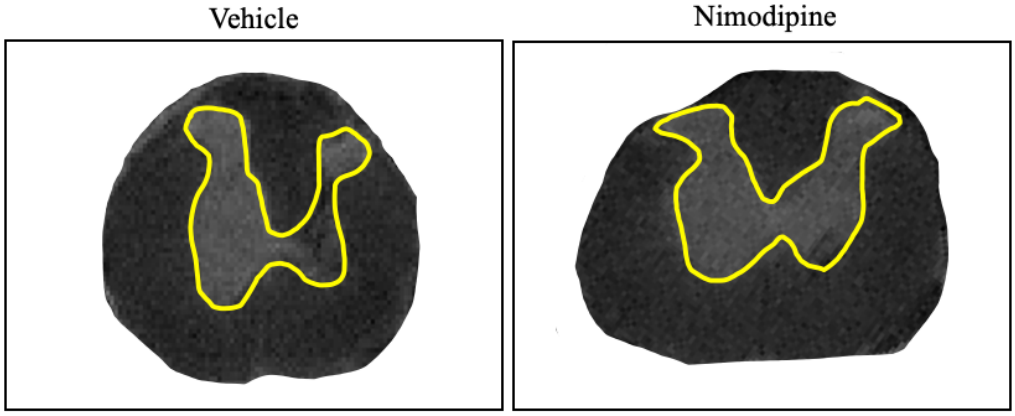

Figure 4-10 MRI images comparing a typical animal with an LPS lesion treated with vehicle and one treated with nimodipine.

Ex-vivo magnetic resonance images of sections from the lesion's epicentre of LPS- injected animals treated with vehicle (control) and nimodipine (30mg/kg), showing that acute treatment with nimodipine decreases the magnitude of grey matter atrophy.

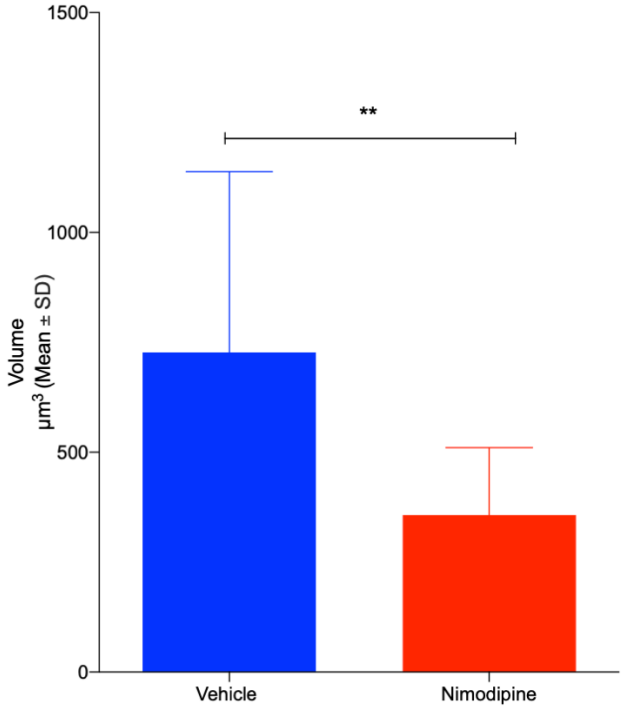

Figure 4-11 Nimodipine treatment atrophy volume

Graph showing the average atrophy volume of vehicle controls (n=11) and nimodipine treatment (n=16). Results were subject to *t-test*; (**: $P<0.01$). Values are means ± S. D.

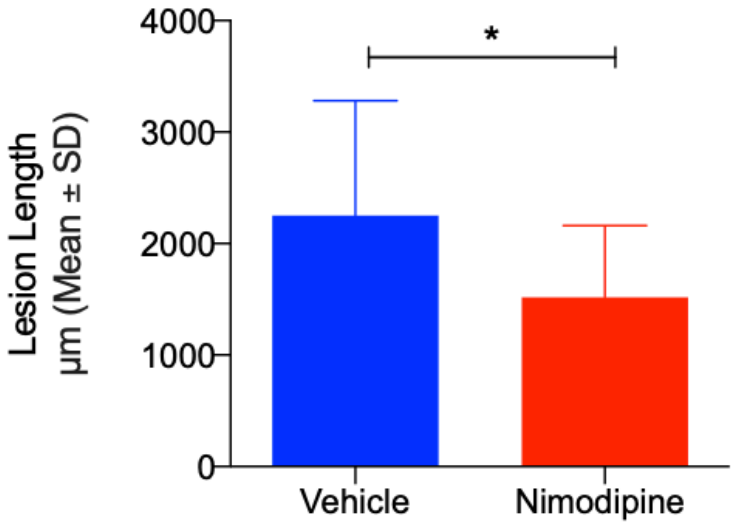

Figure 4-12 Nimodipine treatment lesion length

Graph showing the average lesion length of vehicle controls (n=11) and nimodipine treatment (n=16). Results were subject to *t-test*; (*: $P<0.05$). Values are means ± S. D.

4.3.4 Histology

4.3.4.1 Histological changes associated with nimodipine treatment

Staining with H&E revealed clear signs of chronic atrophy around the site of the injection in all animals, irrespective of the treatment (Figure 4-13 A). However, the percentage of grey matter protection provided by treatment with nimodipine was statistically significant (**: $P<0.01$), as shown in Figure 4-13 B. A preservation of some motor neurons was also evident in ventral grey matter of the injection side, compared with the contralateral ventral grey matter, in animals treated with nimodipine (Figure 4-14 A-B), however, no significant increase in motor neuron number was observed, compared with vehicle-treated controls.

Evidence of demyelination was assessed using LFB staining. Although there appeared to be some myelin pallor, indicative of subtle myelin loss, in the grey matter of the injected side in animals treated with vehicle (Figure 4-14), this was difficult to quantify. However, no such loss of staining was observed in animals treated with nimodipine.

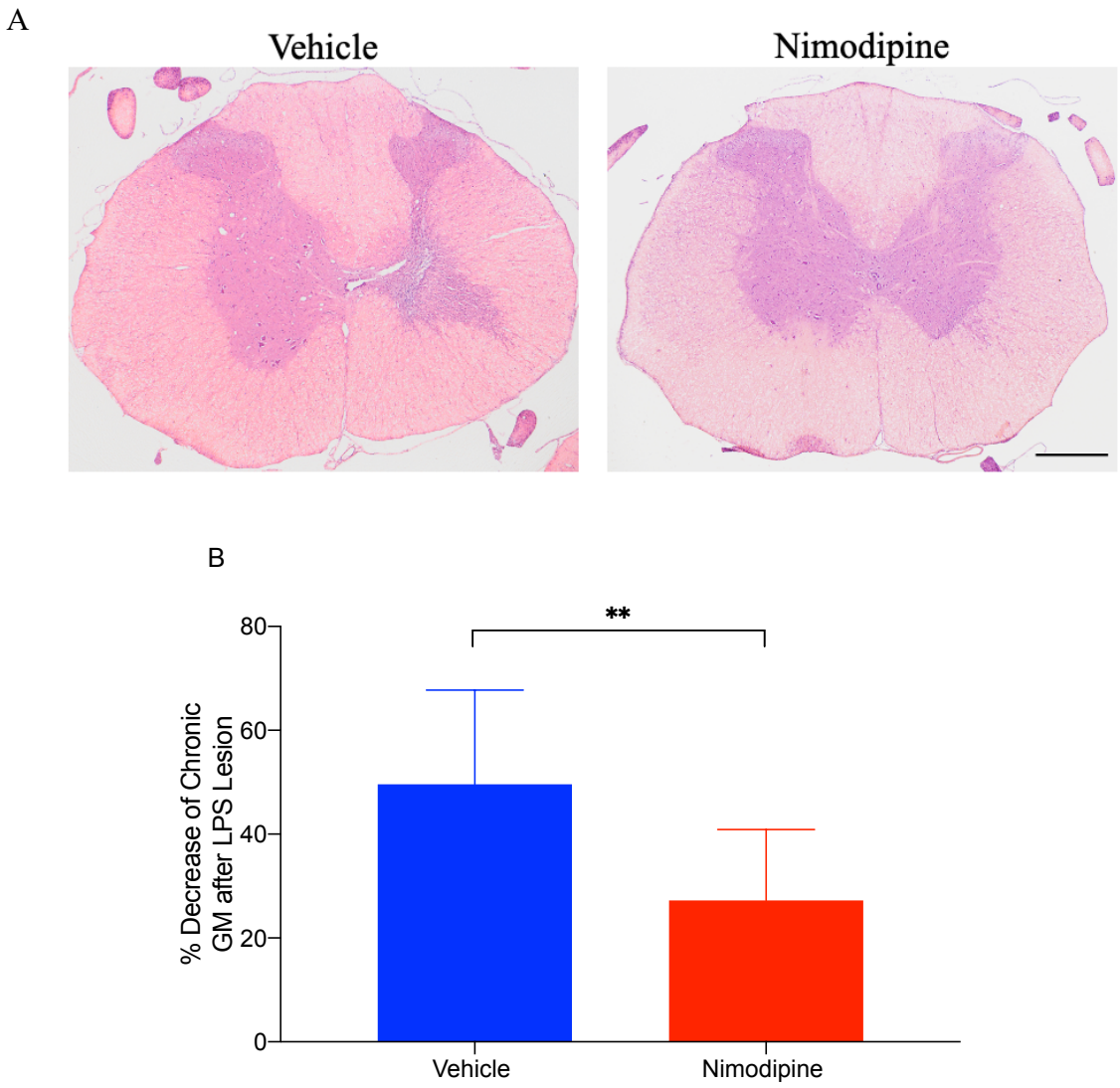

Figure 4-13 Nimodipine treatment grey matter atrophy

A. Images of sections stained with H&E, from the lesion's epicentre of LPS-injected animals treated with vehicle (controls) and nimodipine treatment groups. Scale bar is 500µm. **B.** Graph showing the percentage of decrease in grey matter of vehicle controls (n=8) and nimodipine treatments (n=12). Results were subject to t-test; (**: $P<0.01$). Values are means ± S.D.

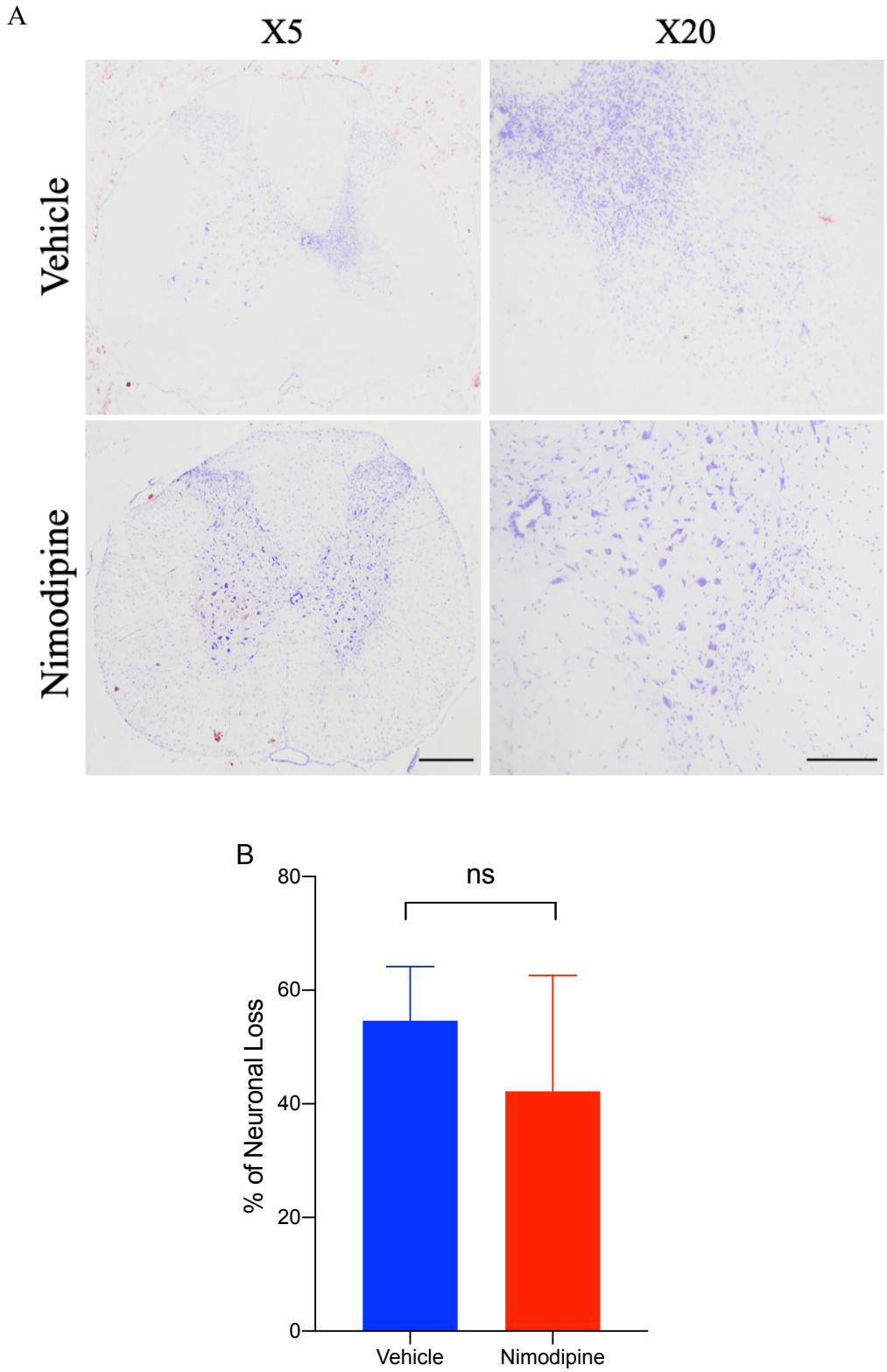

Figure 4-14 Nimodipine treatment CV staining

A. Transverse sections showing chronic lesions in spinal cords stained with CV, comparing the ipsilateral and contralateral ventral horn of vehicle controls, and nimodipine treatment, with the corresponding magnification image of the lesion side only. Scale bar is 500µm (low magnification) and 200µm (higher magnification). **B.** Graph showing percentage of motor neuron loss of animals

injected with LPS and treated with vehicle (controls) (n=6), or nimodipine (n=6). Values are means ± S.D.

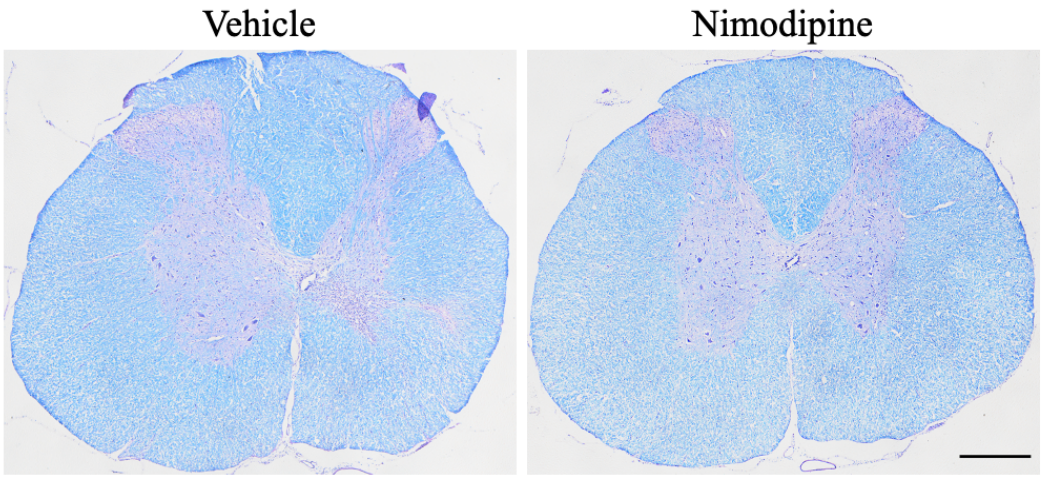

Figure 4-15 Nimodipine chronic LFB staining

Transverse sections showing chronic lesions in spinal cords stained with LFB (myelin), comparing the ipsilateral and contralateral ventral horn of vehicle controls and nimodipine treatment groups at 12 months post LPS injection. Scale bar is 500µm.

4.4 Discussion

The present study shows that acute impaired blood flow is an important modulator of progressive neurological disability and atrophy in our model of slowly progressive MS. Further, improving blood flow acutely, significantly improves long-term disability and atrophy.

4.4.1 The effect of nimodipine in protection from disability and tissue damage

The current study highlights the importance of hypoperfusion in long-term disability and atrophy of the grey matter, and is in line with previous research that has revealed a key role for hypoperfusion and hypoxia in neurological function in EAE (Davies *et al.*, 2013; Desai *et al.*, 2020). Similarly, perfusion-weighted imaging and various tomography studies have demonstrated that there is a decrease in cerebral perfusion, in both the grey and white matter, in MS patients, which occurs independently of the disease course, but plays an integral role during early MS pathology (D'Haeseleer *et al.*, 2011; Hostenbach *et al.*, 2016; Swank *et al.*, 2016). In MS, impaired CBF has been linked to elevated levels of ET-1, but it is mostly produced by endothelial cells, and can be found in some neurons (Hostenbach *et al.*, 2016; Lee *et al.*, 1990; Sluck *et al.*, 1999). ET-1 is likely released by the CNS circulation from reactive astrocytes in MS plaques, leading to long-lasting arteriolar vasoconstriction, and beneficial effects of ET-1 antagonists have been reported (D'Haeseleer *et al.*, 2013). In addition, various animal models have demonstrated the effect of chronic CNS hypoperfusion on increasing mitochondrial dysfunction, as well as the production of free radicals, which causes oxidative stress, culminating in neuronal damage (Aliev *et al.*, 2010). It seems reasonable to propose that in our model, astrocytic ET1 release, due to acute inflammation, constricts spinal blood vessels, resulting in impaired blood flow and hypoxia, associated with mitochondrial dysfunction and disability.

The protective effect of nimodipine has been generally attributed to ameliorating perfusion, due to its activity as a calcium channel blocker (Pisani *et al.*, 1998; Scriabine *et al.*, 1989). However, it has also been suggested that nimodipine might diminish inflammation by inhibiting LPS-mediated microglial activation, or by inducing microglial-specific apoptosis (Li *et al.*, 2009; Schampel *et al.*, 2017). In addition, nimodipine has been shown to attenuate NO production and decrease the expression of TNF- α and COX (Li *et al.*, 2009). These factors can significantly contribute to neurotoxicity and neurodegeneration (Floyd, 1999; Liu *et al.*, 2002; McGuire *et al.*, 2001; Smith *et al.*, 2001; Smith & Lassmann, 2002). During neuroinflammation, activated microglia can have both beneficial and detrimental consequences on the nervous system, such as clearing of debris, as well as the production of proinflammatory factors, such as iNOS and COX, that are implicated in neuronal damage and various neurodegenerative diseases (Huang *et al.*, 2014; Johnson *et al.*, 2016; Lin *et al.*, 2012; Loihl & Murphy, 1998). Previous studies have reported on the effect of nimodipine in inducing anti-inflammatory effects on microglia, by acting at the level of IL-1β accumulation and release, and by protecting microglial cells against Aβ peptide-mediated damage (Sanz *et al.*, 2012).

Furthermore, other studies have highlighted the neuroprotective effect of nimodipine, which acts by reducing the cytotoxicity that comes about as a result of stress conditions, such as oxygen and glucose deprivation, *in vitro* in PC-12 pheochromocytoma cells, and in Schwann, neuronal and astrocytic cells (Bork *et al.*, 2015; Lecht *et al.*, 2012; Leisz *et al.*, 2019; Li *et al.*, 2009). Therefore, it does not seem unreasonable to speculate that, in our studies, nimodipine may act by ameliorating the acute inflammation and subsequent microglial activation, as a result of the LPS injection, and thereby diminishing hypoxia and improving latent hypoperfusion, which consequently significantly reduced the early damage that leads to acute and chronic disability and progressive atrophy.

In neurons, calcium channels and transporters are the main source for calcium entry, and contribute to membrane depolarization following energy failure (Gleichmann & Mattson, 2011). Nimodipine is an L-type calcium channel blocker, with a selectivity for cerebral blood vessels, and that can cross the BBB, thus, it is able to reduce the trans-membranous influx of calcium into the neurons (Bork *et al.*, 2015; Horn *et al.*, 2001; Rowland *et al.*, 2019; Scriabine *et al.*, 1989). Due to this CNS selectivity and BBB permeability, nimodipine is a preferred therapy to limit cellular damage, compared with other calcium channel blockers (Pisani *et al.*, 1998; Rowland *et al.*, 2019). In recent years the plausible cellular neuroprotective or neuroregenerative effects of nimodipine, beside its vasodilation role, have been evaluated. These studies focus on observing cognitive performance, particularly improving learning and spatial memory (Haile *et al.*, 2009; Lecht *et al.*, 2012; LeVere *et al.*, 1989; Levy *et al.*, 1991; Scriabine *et al.*, 1989). These results have associated the beneficial effect of nimodipine with calcium homeostasis, as dysregulated calcium can result in excessive production of free radicals and excitotoxic acids, such as glutamate, and possibly pathologic apoptosis, all which contribute to neuronal damage (Dolga *et al.*, 2011; Haile *et al.*, 2009). Such observations could explain why our results show an improvement in learned behaviour in nimodipine treatment groups, and not controls, such as the upside-down grip test on the right-hindlimb.

In rats, nimodipine has been shown significantly to reduce dysfunction, and to decrease demyelination, caused by hypoxia or hypertension, and also to enhance remyelination in EAE (De Riu *et al.*, 1995; Desai *et al.*, 2020; Schampel *et al.*, 2017). Nimodipine also reduces the degeneration of dopaminergic neurons in a LPS model (Li *et al.*, 2009), where it has been suggested that L-type calcium channel blocking may be a critical step in this neurodegenerative pathway (Horn *et al.*, 2001). Such neuroprotective consequences are most effective during mild stress conditions and are highly dependent on the degree of neurological damage present in the tissue (Bork *et al.*, 2015).

L-type channels are known to display a particularly high sensitivity to hypoxia. In fact, during acute CNS hypoxia, calcium channel blocking, via nimodipine administration, has also been shown to reduce cytotoxic oedema and attenuate cognitive dysfunction (Rowland *et al.*, 2019). However, other calcium channel blockers, such as nifedipine and diltiazem, have failed to provide neuroprotection. We suspect that nimodipine acts in concert, via different mechanisms, to induce the neuroprotection seen in our model.

In MS patients, the relationship between regional CNS cerebral perfusion and lesions has been studied (Aboul-Enein & Lassmann, 2005; D'Haeseleer *et al.*, 2015; D'Haeseleer *et al.*, 2013; Haider *et al.*, 2016; Holland *et al.*, 2012; Martinez Sosa & Smith, 2017; Wuerfel *et al.*, 2004). These studies suggest that lesions tend to accumulate, or persist more, in regions with lower relative perfusion, particularly in the white matter (Holland *et al.*, 2012). Further, changes in perfusion occur prior to lesion formation, in addition to the consequences of gliosis, remyelination and tissue damage (Wuerfel *et al.*, 2004). These results suggest that hypoperfusion plays a direct role in lesion pathogenesis, but while this may be true, the changes in perfusion could be a secondary response to inflammation, hypoxia, mitochondrial dysfunction, and changes in cellular metabolism (Holland *et al.*, 2012; Martinez Sosa & Smith, 2017). In our model of disease, we believe nimodipine may have played a crucial role in the acute stage, in improving perfusion, and decreasing inflammation, transient hypoxia, and therefore protecting from metabolic dysfunction. Furthermore, the protection provided by nimodipine during the most vulnerable stage of disease, continued throughout the entirety of the study, which led to a reduction in atrophy. Therefore, we speculate that improving perfusion, at the beginning stages of disease, by using nimodipine, could modulate acute and chronic CNS repair mechanisms, such that lesions and long-term disability are less severe.

4.4.2 Conclusion

The implementation of a CNS-selective vasodilator, nimodipine, during the acute and most vulnerable stages that lead to chronic atrophy, ultimately resulted in a significant decrease in disability, lesion length and overall atrophy. We speculate that the increase in vasodilation helped to reduce the hypoxic mechanism that we have found to drive slowly progressive neurodegeneration. We believe that nimodipine should be considered for repurposing for neuroprotection in MS.

Chapter 5 General Discussion

MS is a debilitating, chronic inflammatory neurological condition characterized by focal lesions in the white and grey matter, leading to damage of myelin, axons, neurons and synapses (Bø *et al.*, 2000; Bø, Vedeler*, et al.*, 2003b; Compston & Coles, 2008; Dutta, Chang*, et al.*, 2011; Lassmann, 1999; Lassmann *et al.*, 2001; Trapp *et al.*, 2018). Although inflammatory demyelination plays an important role early on in the disease course, neuro/axonal loss is the major determinant of progressive irreversible disability (Chard *et al.*, 2003; Cifelli *et al.*, 2002; Lassmann, 1999, 2005; Lassmann *et al.*, 2007; Lassmann *et al.*, 2012). Of the currently approved therapies, some have shown to reduce the risk of accumulation of new focal lesions, however most have shown to be less efficacious in the progressive phase of the disease, presenting a major unfulfilled clinical need (Le Page *et al.*, 2015; Lorefice *et al.*, 2018). Moreover, the identification of mechanisms of progression, and therapeutic approaches for neuroprotection, have been hampered by a lack of accurate animal models. This thesis introduces a new model of progressive MS characterised by slowly progressive atrophy of the spinal cord grey matter, which is driven by innate immune mechanisms and later accompanied by chronic and progressive disability, gliosis and atrophy. This model presents an opportunity to study the mechanisms responsible for the acute and chronic slow-burning degeneration seen in patients with progressive MS. Acutely, the lesion is characterised by a transient disability, associated with tissue hypoxia and inflammation, all of which resolve after a few days. However, the disability reappears a month later, significantly deteriorating over the next 2 months, progressively worsening over the lifetime of the animal, and is associated with significant grey matter atrophy, chronic inflammation and astrogliosis.

Interestingly, treatment to reverse the acute hypoxia, with either normobaric oxygen or the CNS-selective vasodilator, nimodipine, not only attenuates the acute disability, but also

protects against the accumulation of progressive disability and atrophy. These results shed light on mechanisms of progression in neuroinflammatory disease, and provide a realistic therapeutic approach, namely by targeting CNS blood flow, for neuroprotection in both relapsing and progressive MS.

5.1 The effect of grey matter degeneration in MS

In MS, cortical lesions correlate more precisely with the progression of disability, than damage to the white matter (Fisniku *et al.*, 2008). In fact, the demyelination seen in the cerebellar grey matter is higher than any other brain region, and five times the extent of cortical white matter demyelination (Eshaghi *et al.*, 2018; Gilmore *et al.*, 2009; Moccia *et al.*, 2017). In particular, MS patients present symptoms more closely related to spinal cord damage, in lieu of the brain, such as progressive paraparesis (Thompson *et al.*, 1997; Tsagkas *et al.*, 2018, 2019). The results of this thesis highlight the importance of the role played by the spinal cord grey matter in the development of acute and chronic disability.

Several mechanisms have been implicated to play a role in grey matter neurodegeneration, including mitochondrial failure, meningeal inflammation, hypoxia oxidative stress and iron deposition (Chard *et al.*, 2003; Eshaghi *et al.*, 2018; Klaver *et al.*, 2013; Mahad *et al.*, 2009; Martinez Sosa & Smith, 2017; Pérez-Cerdá *et al.*, 2016; Prins *et al.*, 2015). Despite the classification of different lesion subtypes, and advances in the ability to detect structural abnormalities in the grey matter, key mechanisms of damage remain unclear (Aboul-Enein & Lassmann, 2005; Lassmann, 2005, 2015; Lassmann *et al.*, 2012). Post-mortem studies have revealed that extensive neuronal loss within the grey matter can occur independently of grey or white matter demyelination, suggesting that grey matter atrophy may occur as a result of a non-inflammatory process, or due to local inflammation, or as a consequence of white matter lesions (Bendfeldt *et al.*, 2009; Calabrese *et al.*, 2015; Eshaghi *et al.*, 2018).

5.2 Improving cerebral blood flow as a therapeutic approach for neuroprotection in MS

Current disease-modifying treatments for MS can reduce the frequency of relapses, but, when they occur, they can still be severe. Steroids can shorten the duration of relapses, as they have a strong impact on inflammation, but any benefit regarding disability in the long-term is negligible (Lorefice *et al.*, 2018; Mallucci *et al.*, 2015). We have identified the value of therapeutic normobaric oxygen therapy, and use of a CNS-selective vasodilator, in reducing both acute and chronic disability, and progressive atrophy in a model of progressive MS. These therapies appear to provide protection largely through the most detrimental phase of the early chronic neurological deficit and atrophy formation, which occur during the first three months following lesion induction. These findings further highlight the importance of this early inflammatory event in initiating progressive disability and atrophy.

Neuronal and axonal injury are evident in acute MS lesions, although at this early stage the damage may remain clinically silent, but persisting and accumulating in the background until the reserve capacity for function is surpassed, resulting in the onset of progressive disease (Ferguson *et al.*, 1997; Lassmann *et al.*, 2007; Lassmann & Van Horssen, 2011; Trapp *et al.*, 1998).

Several studies have suggested an important role for hypoxia and mitochondrial dysfunction in causing disability during the acute stages of MS, and that the more prolonged or severe the tissue hypoxia is, the more mitochondrial dysfunction promotes energy deficiency and degeneration (Aboul-Enein & Lassmann, 2005; Chávez *et al.*, 1995; Desai *et al.*, 2016; LaManna, 2007; Lassmann, 2016; Mahad *et al.*, 2008; Martinez Sosa & Smith, 2017; Trapp & Stys, 2009; Yang *et al.*, 2015). We believe that the inflammation-induced hypoxia, as seen in our various animal models of MS, is so severe, that it overwhelms the ability to maintain physiological homeostasis (Davies *et al.*, 2013; Desai *et al.*, 2016). Our results show that

oxygen therapy, in particular 80% oxygen, can restore neurological function in the short term, and protect from degeneration and motor neuron loss in the long term. Further, increasing tissue oxygenation by improving blood flow, also provides significant protection from acute disability, and progressive disability, atrophy and neuronal loss. We suggest that the same pathological mechanisms could ensue in patients with MS, and, therefore, that such a therapeutic approach may be particularly efficacious in patients very early in the disease course, including those not yet showing clinical symptoms, such as patients diagnosed with radiologically isolated syndrome (RIS).

The mechanism through which oxygen and nimodipine provide protection, may involve mitochondrial complex IV of the respiratory chain. It has been noted that complex IV can be targeted and irreversibly compromised by increased levels of NO, as is believed to occur within MS lesions (Smith & Lassmann, 2002). Oxygen therapy can decrease the raised levels of NO (Baratz-Goldstein *et al.*, 2017; Davies *et al.*, 2013; Desai *et al.*, 2016), however, it can also induce vasoconstriction with the attendant reduction in glucose delivery and the removal of metabolic waste products (Demchenko *et al.*, 2005; Lambertsen *et al.*, 1953; Omae *et al.*, 1998). Nimodipine, on the other hand, can not only increase blood flow, but also reduce calcium influx into neurons, and reduce microglial activation, thereby diminishing neurotoxicity and hypoxia (Desai *et al.*, 2020; Li *et al.*, 2009; Pisani *et al.*, 1998; Rowland *et al.*, 2019), and this beneficial profile may account for the more significant protection against long-term atrophy shown by nimodipine in this thesis.

Before considering oxygen as a therapy, it should be stated that increased oxygen exposure could potentially lead to increased oxidative stress, particularly when induced at a higher pressure, such as with hyperbaric oxygen therapy (Cornet *et al.*, 2013; Thom, 2009). Generally, oxidative stress is viewed as a negative effect, however, increased production of ROS, as a result of hyperoxia, has been shown to develop vascular healing, due to the increase

of growth factors that control vascular homeostasis, such as angiopoietin, fibroblast growth factor and VEGF (Thom, 2009). However, oxygen therapy has been readily administered in other conditions where it is considered safe to use, and inexpensive (Baratz-Goldstein *et al.*, 2017; Barrett *et al.*, 2004; Hadanny *et al.*, 2015; Zhang *et al.*, 2005), and, in separate studies in our laboratory, raised oxygen has actually been found to result in a reduction in oxidative damage (unpublished observations).

Nimodipine has been shown to have cerebrovasodilatory and anti-ischaemic effects in humans at 1nM concentration, or even less, as higher concentrations have been reported to block the release of some neurotransmitters and hormones that are necessary for neuronal survival (Scriabine *et al.*, 1989). At present, nimodipine is an approved therapy for the prevention and treatment of neurological deficits in patients with aneurysmal subarachnoid hemorrhage (aSAH) and delayed cerebral ischaemia (DCI) (Carlson *et al.*, 2020). In a 2a clinical trial of aSAH, nimodipine was administered intraventricularly and demonstrated to have significant efficacy whilst retaining a favorable safety profile (Carlson *et al.*, 2020; Hänggi *et al.*, 2017). Future clinical use of nimodipine in MS patients is facilitated by the long history of safe administration in humans, and the fact that oral administration has been shown to alleviate painful tonic crises in four patients suffering from MS (de Sà, 1995). The findings in our study support the value of nimodipine as a preferred therapy for MS.

5.3 The link between hypoperfusion and hypoxia

In early MS, lesions may form anywhere in the CNS, however they have been shown to accumulate in areas of low perfusion. Some lesions disappear due to the resolution of oedema, inflammation, hypoxia and remyelination, while lesions located in areas of low blood perfusion tend to persist, indicating that the vasculature is a major determining factor for lesion progression (Haider *et al.*, 2016; Holland *et al.*, 2012). Early in the disease, inflammation can contribute to CNS hypoperfusion (D'Haeseleer *et al.*, 2013; Dénes *et al.*, 2010; Murray *et al.*,

2014), resulting in hypoxia, and, in consequence, mitochondria generating large amounts of oxygen free radicals, further reducing the oxygen remaining for ATP production (Chandel *et al.*, 1998b; Guzy *et al.*, 2005). At normal concentrations, ROS are part of the normal physiology of the CNS, and can regulate fundamental cell activities, but at high levels, ROS can cause cell injury, decrease antioxidant defenses and ultimately cause cell death (Aliev *et al.*, 2003; Zhu *et al.*, 2007).

The Notch signalling pathway controls important processes involved in endothelial cell proliferation and survival (Borggrefe *et al.*, 2016; Coleman *et al.*, 2007; Dengler *et al.*, 2013; Hashimoto *et al.*, 2015). Under hypoxic conditions, HIF-1α is upregulated in endothelial cells and astrocytes, leading to VEGF-A secretion, and, consequent Notch expression in endothelial cells (Stone *et al.*, 1995). These autocrine interactions cause FIH to be sequestered, preventing the hydroxylation of HIF-1α, thereby enhancing its availability (Borggrefe *et al.*, 2016; Kim *et al.*, 2020). In summary, the HIF-Notch interaction is involved in the process of vascular protection within the CNS, and when the Notch signalling pathway is blocked, no functional vessel perfusion can occur (Kim *et al.*, 2020). HIF and Notch have complex intertwined roles within the CNS. Any hinderance to the dynamics of these pathways can lead to persistent hypoxic-ischaemic environment, which consequently has been proven to lead to neurodegeneration (Hernandez-Gerez *et al.*, 2019; Lassmann, 2016). Exploring the contribution of hypoxia and hypoperfusion-mediated pathways is important for the complete understanding of the factors that drive neurodegeneration, and for insights into plausible therapeutic interventions.

As previously mentioned, under hypoxic conditions, both FIH and PHDs are inactive, resulting in the stabilization of the HIF-α subunit, which can trigger the increased transcription of genes that code for proteins involved in angiogenesis, such as VEGF and erythropoietin (Lee *et al.*, 2007; Rey *et al.*, 2019; Saravani *et al.*, 2019). As an adaptive mechanism, these factors

work to increase oxygen availability to hypoxic regions (Kim *et al.*, 2020; Semenza, 2003). Indeed, capillary blood volume has the capacity to increase by such a degree, that it is a clear evolutionary mechanism in response to glucose and oxygen demand, when the CNS is metabolically deficient (Shockley *et al.*, 1988). VEGF is also expressed by hypoxic astrocytes, resulting in endothelial cell activation, and it is produced by endothelial cells to control angiogenesis (Lee *et al.*, 2007). Microvascular remodeling, as a response to mild hypoxia starts four or five days post low oxygen exposure, and is completed, in adult brain rats, after approximately three weeks (Pichiule *et al.*, 2002; Xu *et al.*, 2006). We venture the possibility that, in our lesion model, these physiological mechanisms come to play, in order to reduce histotoxic hypoxia, however, it may be the case that by the time these systems are fully activated, some inflammation and hypoxia have already caused irreversible tissue damage, which progresses with time. The use of nimodipine, as a vasodilator agent, may act on decreasing hypoxia and therefore disability and chronic atrophy in our model of progressive MS.

5.4 Limitations

This thesis has provided convincing evidence of post-inflammatory atrophy and methods of protection, but the time series of immunohistochemical studies involved relatively few animals at each time point, particularly within the saline control groups, and this did not always allow statistical analysis. Nevertheless, the atrophy observed in the sections used for histological analysis, along with behavioural observations, provides evidence of the time course of inflammation-induced disability and atrophy at the site of injection.

Furthermore, physiological changes related to ageing are inherent in all animals. They can present as build-up of toxin protein aggregates spread through various CNS regions, and have been identified as contributor to ageing and neurodegenerative pathologies (Few, 1966; Moreno-García *et al.*, 2018). The accumulation of lipofuscin (LF) is one of such protein

aggregates, and it has been associated with neuronal loss, glial proliferation and activation, as well as with neurodegenerative diseases (Moreno-García *et al.*, 2018; Reeg *et al.*, 2015). As our lesion progresses over a long period of time, we observed some evidence of LF at the chronic time points during immunohistochemical analysis. LF is an auto-fluorescent lipopigment, and in the CNS, it is especially abundant in nerve cells, forming a pattern of senescence, thereby altering the neuronal cytoskeleton and cellular metabolism (Hebbar *et al.*, 2017; Moreno-García *et al.*, 2018). Therefore, LF can be an important confounding variable with fluorescence immunohistochemistry, especially when labelling the cytoplasm of motor neurons in ageing chronic tissue, but LF is unlikely to have confused the interpretation of neuronal survival in this study because motor neurons were distinguished using CV staining.

5.5 Future directions

The findings in this thesis provide a foundation upon which future research projects should be based. For example, we have found that reducing hypoxia, and increasing perfusion, can significantly improve the progression of disease in a model of MS. It would be of interest to repeat the therapeutic experiments, with final perfusion at the acute time-points, to determine the acute histological effects of treatment in order to identify the exact mechanism(s) of action. It would also be interesting to examine the value of combined oxygen and nimodipine therapy, as these therapies may be additive or even synergistic in their action.

Furthermore, these therapeutic methods may be very useful for young individuals suffering from MS, particularly during clinically isolated syndrome (CIS), RIS or RRMS. However, it is unknown whether such therapeutic approach may be effective in patients with progressive disease forms of the disease. Future research could focus on evaluating the efficacy of delayed chronic administration of oxygen and nimodipine in animals with established

lesions and determine whether such an approach would provide protection from progressive disability and atrophy.

5.6 Concluding remarks

In this thesis we have presented a newly developed model lesion of slowly progressive neurodegeneration and atrophy, closely resembling that of SPMS. The findings have revealed that a lifetime of progressive disability and atrophy can result from just a few days of inflammatory hypoxia during young adulthood. Remarkably, avoidance of the hypoxia by oxygen or nimodipine treatment for just a few days provides lifetime protection from both disability and atrophy. Nimodipine is worthy of consideration for repurposing for the therapy of MS.

BIBLIOGRAPHY

Aboul-Enein, F., & Lassmann, H. (2005). Mitochondrial damage and histotoxic hypoxia: a pathway of tissue injury in inflammatory brain disease? *Acta Neuropathol, 109*(1), 49-55.

Aboul-Enein, F., Rauschka, H., Kornek, B., Stadelmann, C., Stefferl, A., Brück, W., Lucchinetti, C., Schmidbauer, M., Jellinger, K., & Lassmann, H. (2003). Preferential Loss of Myelin-Associated Glycoprotein Reflects Hypoxia-Like White Matter Damage in Stroke and Inflammatory Brain Diseases. *JNEN: Journal of Neuropathology & Experimental Neurology, 62*(1), 25-33.

Acker, H. (2005). The oxygen sensing signal cascade under the influence of reactive oxygen species. *Philosophical Transactions of the Royal Society B: Biological Sciences, 360*(1464), 2201-2210.

Adamczyk, B., & Adamczyk-Sowa, M. (2016). New Insights into the Role of Oxidative Stress Mechanisms in the Pathophysiology and Treatment of Multiple Sclerosis. *Oxidative Medicine and Cellular Longevity, 2016*.

Adams, C. W. (1988). Perivascular iron deposition and other vascular damage in multiple sclerosis. *Journal of Neurology, Neurosurgery & Psychiatry, 51*(2), 260-265.

Aliev, G., Obrenovich, M. E., Smith, M. A., & Perry, G. (2003). Hypoperfusion, Mitochondria Failure, Oxidative Stress, and Alzheimer Disease. *Journal of biomedicine & biotechnology, 2003*(3), 162-163.

Aliev, G., Palacios, H. H., Gasimov, E., Obrenovich, M. E., Morales, L., Leszek, J., Bragin, V., Solís Herrera, A., & Gokhman, D. (2010). Oxidative Stress Induced Mitochondrial Failure and Vascular Hypoperfusion as a Key Initiator for the Development of Alzheimer Disease. *Pharmaceuticals (Basel, Switzerland), 3*(1), 158-187.

Anand, R. J., Gribar, S. C., Li, J., Kohler, J. W., Branca, M. F., Dubowski, T., Sodhi, C. P., & Hackam, D. J. (2007). Hypoxia causes an increase in phagocytosis by macrophages in a HIF-1α-dependent manner. *Journal of leukocyte biology, 82*(5), 1257-1265.

Angelova, P. R., Kasymov, V., Christie, I., Sheikhbahaei, S., Turovsky, E., Marina, N., Korsak, A., Zwicker, J., Teschemacher, A. G., Ackland, G. L., Funk, G. D., Kasparov, S., Abramov, A. Y., & Gourine, A. V. (2015). Functional oxygen sensitivity of astrocytes. *The Journal of neuroscience, 35*(29), 10460-10473.

Arteel, G., Thurman, R., Yates, J., & Raleigh, J. (1995). Evidence that hypoxia markers detect oxygen gradients in liver: pimonidazole and retrograde perfusion of rat liver. *British Journal of Cancer, 72*(4), 889.

Arteel, G., Thurman, R. G., & Raleigh, J. A. (1998). Reductive metabolism of the hypoxia marker pimonidazole is regulated by oxygen tension independent of the pyridine nucleotide redox state. *European Journal of Biochemistry, 253*(3), 743-750.

Aviles-Reyes, R. X., Angelo, M. F., Villarreal, A., Rios, H., Lazarowski, A., & Ramos, A. J. (2010). Intermittent hypoxia during sleep induces reactive gliosis and limited neuronal death in rats: implications for sleep apnea. *Journal of neurochemistry, 112*(4), 854-869.

Backes, W., & Nijenhuis, R. (2014). Mapping the Vasculature of the Spinal Cord. In (pp. 258-264).

Baratz-Goldstein, R., Toussia-Cohen, S., Elpaz, A., Rubovitch, V., & Pick, C. G. (2017). Immediate and delayed hyperbaric oxygen therapy as a neuroprotective treatment for traumatic brain injury in mice. *Molecular and cellular neurosciences, 83*, 74-82.

Barnett, M. H., & Prineas, J. W. (2004). Relapsing and remitting multiple sclerosis: Pathology of the newly forming lesion. *Annals of Neurology, 55*(4), 458-468.

Barrett, K. F., Masel, B., Patterson, J., Scheibel, R. S., Corson, K. P., & Mader, J. T. (2004). Regional CBF in chronic stable TBI treated with hyperbaric oxygen. *Undersea & hyperbaric medicine, 31*(4), 395-406.

Bear, M. F. (2001). *Neuroscience : exploring the brain / Mark F. Bear, Barry W. Connors, Michael A. Paradiso* (2nd ed. ed.). Baltimore, Md.: Baltimore, Md. : Lippincott Williams & Wilkins.

Beckman, J., & Koppenol, W. (1996). Nitric oxide, superoxide, and peroxynitrite: The good, the bad, and the ugly. *American Journal Of Physiology-Cell Physiology, 271*(5), C1424-C1437.

Bendfeldt, K., Kuster, P., Traud, S., Egger, H., Winklhofer, S., Mueller-Lenke, N., Naegelin, Y., Gass, A., Kappos, L., Matthews, P. M., Nichols, T. E., Radue, E.-W., & Borgwardt, S. J. (2009). Association of regional gray matter volume loss and progression of white matter lesions in multiple sclerosis — A longitudinal voxel-based morphometry study. *NeuroImage (Orlando, Fla.), 45*(1), 60-67.

Benedict, R. H. B., Ramasamy, D., Munschauer, F., Weinstock-Guttman, B., & Zivadinov, R. (2009). Memory impairment in multiple sclerosis: correlation with deep grey matter and mesial temporal atrophy. *J Neurol Neurosurg Psychiatry, 80*(2), 201.

Bennett, D. J., Gorassini, M., Fouad, K., Sanelli, L., Han, Y., & Cheng, J. (1999). Spasticity in rats with sacral spinal cord injury. *Journal of neurotrauma, 16*(1), 69.

Bernard, C. C. A., Johns, T. G., Slavin, A., Ichikawa, M., Ewing, C., Liu, J., & Bettadapura, J. (1997). Myelin oligodendrocyte glycoprotein: a novel candidate autoantigen in multiple sclerosis. *J Mol Med, 75*(2), 77-88.

Biber, K., Neumann, H., Inoue, K., & Boddeke, H. W. G. M. (2007). Neuronal 'On' and 'Off' signals control microglia. *Trends in Neurosciences, 30*(11), 596-602.

Bidmon, H.-J., Kato, K., Schleicher, A., Witte, O. W., & Zilles, K. (1998). Transient Increase of Manganese–Superoxide Dismutase in Remote Brain Areas After Focal Photothrombotic Cortical Lesion. *Stroke (1970), 29*(1), 203-211.

Bitsch, W., Schuchardt, W., Bunkowski, W., Brück, W., & Kuhlmann, W. (2000). Acute axonal injury in multiple sclerosis. Correlation with demyelination and inflammation. *Brain, 123*(6), 1174-1183.

Bø, L., Nyland, H., Trapp, B. D., & Mork, S. (2000). Cortical demyelination in multiple sclerosis. *Journal of Neuropathology and Experimental Neurology, 59*(5), 431-431.

Bø, L., Vedeler, C. A., Nyland, H., Trapp, B. D., & Mørk, S. J. (2003a). Intracortical multiple sclerosis lesions are not associated with increased lymphocyte infiltration. *Multiple Sclerosis, 9*(4), 323-331.

Bø, L., Vedeler, C. A., Nyland, H., Trapp, B. D., & Mørk, S. J. (2003b). Subpial demyelination in the cerebral cortex of multiple sclerosis patients. *Journal of Neuropathology and Experimental Neurology, 62*(7), 723-732.

Bonetti, B., & Raine, C. S. (1997). Multiple sclerosis: Oligodendrocytes display cell death–related molecules in situ but do not undergo apoptosis. *Annals of Neurology, 42*(1), 74-84.

Borggrefe, T., Lauth, M., Zwijsen, A., Huylebroeck, D., Oswald, F., & Giaimo, B. D. (2016). The Notch intracellular domain integrates signals from Wnt, Hedgehog, TGFβ/BMP and hypoxia pathways. *Biochimica et biophysica acta. Molecular cell research, 1863*(2), 303-313.

Bork, K., Wurm, F., Haller, H., Strauss, C., Scheller, C., Gnanapragassam, V. S., & Horstkorte, R. (2015). Neuroprotective and neuroregenerative effects of nimodipine in a model system of neuronal differentiation and neurite outgrowth. *Molecules (Basel, Switzerland), 20*(1), 1003-1013.

Brink, P. B., Veerhuis, C. W. R., Breij, D. E., Van Der Valk, D. P., Dijkstra, D. C., & Bö, D. L. (2005). The Pathology of Multiple Sclerosis Is Location-Dependent: No Significant Complement Activation Is Detected in Purely Cortical Lesions. *JNEN: Journal of Neuropathology & Experimental Neurology, 64*(2), 147-155.

Brück, W., Porada, P., Poser, S., Rieckmann, P., Hanefeld, F., Kretzschmarch, H. A., & Lassmann, H. (1995). Monocyte/macrophage differentiation in early multiple sclerosis lesions. *Annals of Neurology, 38*(5), 788-796.

Calabrese, M., De Stefano, N., Atzori, M., Bernardi, V., Mattisi, I., Barachino, L., Morra, A., Rinaldi, L., Romualdi, C., Perini, P., Battistin, L., & Gallo, P. (2007). Detection of Cortical Inflammatory Lesions by Double Inversion Recovery Magnetic Resonance Imaging in Patients With Multiple Sclerosis. *Archives of neurology (Chicago), 64*(10), 1416-1422.

Calabrese, M., Magliozzi, R., Ciccarelli, O., Geurts, J. J. G., Reynolds, R., & Martin, R. (2015). Exploring the origins of grey matter damage in multiple sclerosis. *Nature reviews. Neuroscience, 16*(3), 147-158.

Calabrese, M., Romualdi, C., Poretto, V., Favaretto, A., Morra, A., Rinaldi, F., Perini, P., & Gallo, P. (2013). The changing clinical course of multiple sclerosis: A matter of gray matter. *Annals of Neurology, 74*(1), 76-83.

Carlson, P. A., Hänggi, D., Macdonald, R., L. , & Shuttleworth, C., W. (2020). Nimodipine Reappraised: An Old Drug With a Future. *Current Neuropharmacology, 18*(1), 65-82.

Castellazzi, G., Debernard, L., Melzer, T. R., Dalrymple-Alford, J. C., D'Angelo, E., Miller, D. H., Wheeler-Kingshott, C. A. M., & Mason, D. F. (2018). Functional connectivity alternations reveal complex mechanisms based on clinical and radiological status in mild relapsing remitting multiple sclerosis. *Frontiers in Neurology , 9 , Article 690. (2018)*.

Castellazzi, M., Lamberti, G., Resi, M. V., Baldi, E., Caniatti, L. M., Galante, G., Perri, P., & Pugliatti, M. (2019). Increased Levels of Endothelin-1 in Cerebrospinal Fluid Are a Marker of Poor Visual Recovery after Optic Neuritis in Multiple Sclerosis Patients. *Disease markers, 2019*, 1-5.

Cavallari, P., & Pettersson, L. (1989). Tonic suppression of reflex transmission in low spinal cats. *Exp Brain Res, 77*(1), 201-212.

Chandel, N. S., Maltepe, E., Goldwasser, E., Mathieu, C. E., Simon, M. C., & Schumacker, P. T. (1998a). Mitochondrial reactive oxygen species trigger hypoxia-induced

transcription. *Proceedings of the National Academy of Sciences of the United States of America, 95*(20), 11715.

Chandel, N. S., Maltepe, E., Goldwasser, E., Mathieu, C. E., Simon, M. C., & Schumacker, P. T. (1998b). Mitochondrial reactive oxygen species trigger hypoxia-induced transcription. *Proceedings of the National Academy of Sciences - PNAS, 95*(20), 11715-11720.

Chard, D., Griffin, C. M., Rashid, W., Davies, G., Altmann, D., Kapoor, R., Barker, G., Thompson, A., & Miller, D. (2003). Progressive grey matter atrophy in clinically early relapsing-remitting multiple sclerosis. *Journal Of Neurology Neurosurgery And Psychiatry, 74*(10), 1456-1456.

Chávez, J. C., Pichiule, P., Boero, J., & Arregui, A. (1995). Reduced mitochondrial respiration in mouse cerebral cortex during chronic hypoxia. *Neuroscience Letters, 193*(3), 169-172.

Chen, J., Zhang, F., Zhao, L., Cheng, C., Zhong, R., Dong, C., & Le, W. (2020). Hyperbaric oxygen ameliorates cognitive impairment in patients with Alzheimer's disease and amnestic mild cognitive impairment. *Alzheimer's & dementia : translational research & clinical interventions, 6*(1), e12030-e12030.

Chen, T.-C., Yeh, C.-Y., Lin, C.-W., Yang, C.-M., Yang, C.-H., Lin, I. H., Chen, P.-Y., Cheng, J.-Y., & Hu, F.-R. (2017). Vascular hypoperfusion in acute optic neuritis is a potentially new neurovascular model for demyelinating diseases. *PLoS ONE, 12*(9), e0184927-e0184927.

Ciarlone, G. E., Hinojo, C. M., Stavitzski, N. M., & Dean, J. B. (2019). CNS function and dysfunction during exposure to hyperbaric oxygen in operational and clinical settings. *Redox biology, 27*, 101159-101159.

Cifelli, A., Arridge, M., Jezzard, P., Esiri, M. M., Palace, J., & Matthews, P. M. (2002). Thalamic neurodegeneration in multiple sclerosis. *Annals of Neurology, 52*(5), 650-653.

Coleman, M. L., Michael, A. M., Kirsty, S. H., Charlotte, C., Jasmin, M., Mariola, E., Kristina, M. C., Matthew, E. C., David, E. L., Benedikt, M. K., Neil, J. O., Peter, J. R., & Christopher, J. S. (2007). Asparaginyl Hydroxylation of the Notch Ankyrin Repeat Domain by Factor Inhibiting Hypoxia-inducible Factor. *Journal of Biological Chemistry, 282*(33), 24027-24038.

Coles, A., Cox, A., Page, E., Jones, J., Trip, S., Deans, J., Seaman, S., Miller, D., Hale, G., Waldmann, H., & Compston, D. (2006). The window of therapeutic opportunity in multiple sclerosis. *J Neurol, 253*(1), 98-108.

Compston, A., & Coles, A. (2008). Multiple sclerosis. *The Lancet, 372*(9648), 1502-1517.

Confavreux, C., & Vukusic, S. (2006). Natural history of multiple sclerosis: a unifying concept. *Brain, 129*(3), 606-616.

Cornet, A. D., Kooter, A. J., Peters, M. J., & Smulders, Y. M. (2013). The potential harm of oxygen therapy in medical emergencies. *Critical care (London, England), 17*(2), 313-313.

Correale, J. (2014). The role of microglial activation in disease progression. *Multiple Sclerosis Journal, 20*(10), 1288-1295.

Correale, J., Gaitán, M. I., Ysrraelit, M. C., & Fiol, M. P. (2016). Progressive multiple sclerosis: from pathogenic mechanisms to treatment. *Brain (London, England : 1878), 140*(3), aww258-546.

Correale, J., Marrodan, M., & Ysrraelit, M. C. (2019). Mechanisms of Neurodegeneration and Axonal Dysfunction in Progressive Multiple Sclerosis. *Biomedicines, 7*(1).

D'Haeseleer, M., Cambron, M., Vanopdenbosch, L., & De Keyser, J. (2011). Vascular aspects of multiple sclerosis. *Lancet Neurology, 10*(7), 657-666.

D'Haeseleer, M., Hostenbach, S., Peeters, I., El Sankari, S., Nagels, G., De Keyser, J., & D'Hooghe, M. B. (2015). Cerebral hypoperfusion: a new pathophysiologic concept in multiple sclerosis? *Journal of cerebral blood flow and metabolism, 35*(9), 1406-1410.

D'Haeseleer, M., Angelo, E., Roel, B., Yves, F., Melissa, C., Anne-Marie, V., Christian, V., Johan, D., & Jacques De, K. (2013). Cerebral hypoperfusion in multiple sclerosis is reversible and mediated by endothelin-1. *Proceedings of the National Academy of Sciences - PNAS, 110*(14), 5654-5658.

Dal Canto, M. C. (1982). Uncoupled relationship between demyelination and primary infection of myelinating cells in Theiler's virus encephalomyelitis. *Infection and immunity, 35*(3), 1133.

Dal Canto, M. C., Kim, B. S., Miller, S. D., & Melvold, R. W. (1996). Theiler's murine encephalomyelitis virus (TMEV)-induced demyelination: A model for human multiple sclerosis. *Methods: A Companion to Methods in Enzymology, 10*(3), 453-461.

Damoiseaux, J. G., Döpp, E. A., Calame, W., Chao, D., MacPherson, G. G., & Dijkstra, C. D. (1994). Rat macrophage lysosomal membrane antigen recognized by monoclonal antibody ED1. *Immunology, 83*(1), 140-147.

Dave, K. R., Prado, R., Busto, R., Raval, A. P., Bradley, W. G., Torbati, D., & Pérez-pinzón, M. A. (2003). Hyperbaric oxygen therapy protects against mitochondrial dysfunction and delays onset of motor neuron disease in wobbler mice. *Neuroscience, 120*(1), 113-120.

Davies, A. L., Desai, R. A., Bloomfield, P. S., McIntosh, P. R., Chapple, K. J., Linington, C., Fairless, R., Diem, R., Kasti, M., Murphy, M. P., & Smith, K. J. (2013). Neurological deficits caused by tissue hypoxia in neuroinflammatory disease. *Annals of Neurology, 74*(6), 815-825.

De Groot, C., Bergers, E., Kamphorst, W., Ravid, R., Polman, C., Barkhof, F., & van Der Valk, P. (2001). Post-mortem MRI-guided sampling of multiple sclerosis brain lesions - Increased yield of active demyelinating and (p)reactive lesions. *Brain, 124*, 1635-1645.

De Riu, P. L., Demontis, M. P., Anania, V., Caria, M. A., Mameli, O., Becciu, A., & Tolu, E. (1995). Brain electrobiogenesis protection induced by nimodipine and MK-801 during acute hypoxia in hypertensive rats. *Pharmacological research, 31*(3), 169-173.

de Sà, J. (1995). Nimodipine can be useful in the treatment of paroxysmal signs in multiple sclerosis. *Journal of Neuroimmunology, 56*, 61-61.

de Vries, H. E., Witte, M., Hondius, D., Rozemuller, A. J. M., Drukarch, B., Hoozemans, J., & van Horssen, J. (2008). Nrf2-induced antioxidant protection: A promising target to counteract ROS-mediated damage in neurodegenerative disease? *Free radical biology & medicine, 45*(10), 1375-1383.

Demchenko, I. T., Luchakov, Y. I., Moskvin, A. N., Gutsaeva, D. R., Allen, B. W., Thalmann, E. D., & Piantadosi, C. A. (2005). Cerebral blood flow and brain oxygenation in rats breathing oxygen under pressure. *Journal of cerebral blood flow and metabolism, 25*(10), 1288-1300.

Dénes, Á., Humphreys, N., Lane, T. E., Grencis, R., & Rothwell, N. (2010). Chronic systemic infection exacerbates ischemic brain damage via a CCL5 (regulated on activation, normal T-cell expressed and secreted)-mediated proinflammatory response in mice. *The Journal of neuroscience, 30*(30), 10086-10095.

Dengler, V. L., Galbraith, M. D., & Espinosa, J. M. (2013). Transcriptional regulation by hypoxia inducible factors. *Critical reviews in biochemistry and molecular biology, 49*(1), 1-15.

Desai, R. A., Davies, A. L., Del Rossi, N., Tachrount, M., Dyson, A., Gustavson, B., Kaynezhad, P., Mackenzie, L., van der Putten, M. A., McElroy, D., Schiza, D., Linington, C., Singer, M., Harvey, A. R., Tachtsidis, I., Golay, X., & Smith, K. J. (2020). Nimodipine reduces dysfunction and demyelination in models of multiple sclerosis. *Annals of Neurology , 88 (1) pp. 123-136. (2020)*.

Desai, R. A., Davies, A. L., Tachrount, M., Kasti, M., Laulund, F., Golay, X., & Smith, K. J. (2016). Cause and prevention of demyelination in a model multiple sclerosis lesion. *Annals of Neurology, 79*(4), 591-604.

Di Meo, S., Reed, T. T., Venditti, P., & Victor, V. M. (2016). Role of ROS and RNS Sources in Physiological and Pathological Conditions. *Oxidative Medicine and Cellular Longevity, 2016*, 1-44.

Diaz, E., & Morales, H. (2016). Spinal Cord Anatomy and Clinical Syndromes. *Seminars in Ultrasound, CT, and MRI, 37*(5), 360-371.

Dimauro, S., & Schon, E. A. (2003). Mitochondrial respiratory-chain diseases. *The New England Journal of Medicine, 348*(26), 2656.

Ding, J., Zhou, D., Liu, C., Pan, L., Ya, J., Ding, Y., Ji, X., & Meng, R. (2019). Normobaric oxygen: A novel approach for treating chronic cerebral circulation insufficiency. *Clinical interventions in aging, 14*, 565-570.

Dolga, A. M., Terpolilli, N., Kepura, F., Nijholt, I. M., Knaus, H. G., D'Orsi, B., Prehn, J. H. M., Eisel, U. L. M., Plant, T., Plesnila, N., & Culmsee, C. (2011). KCa2 channels activation prevents [Ca2+]i deregulation and reduces neuronal death following glutamate toxicity and cerebral ischemia. *Cell death & disease, 2*(4), e147-e147.

Dong, W., Qi, Z., Liang, J., Shi, W., Zhao, Y., Luo, Y., Ji, X., & Liu, K. J. (2015). Reduction of zinc accumulation in mitochondria contributes to decreased cerebral ischemic injury by normobaric hyperoxia treatment in an experimental stroke model. *Experimental neurology, 272*, 181-189.

Dore-Duffy, P., & La Manna, J. (2007). Physiologic angiodynamics in the brain. *Antioxidants & Redox Signaling, 9*(9), 1363-1371.

Duan, S., Shao, G., Yu, L., & Ren, C. (2015). Angiogenesis contributes to the neuroprotection induced by hyperbaric oxygen preconditioning against focal cerebral ischemia in rats. *International journal of neuroscience, 125*(8), 625-634.

Duschek, S., & Schandry, R. (2007). Reduced brain perfusion and cognitive performance due to constitutional hypotension. *Clin Auton Res, 17*(2), 69-76.

Dutta, R., Chang, A., Doud, M. K., Kidd, G. J., Ribaudo, M. V., Young, E. A., Fox, R. J., Staugaitis, S. M., & Trapp, B. D. (2011). Demyelination causes synaptic alterations in hippocampi from multiple sclerosis patients. *Annals of Neurology, 69*(3), 445-454.

Dutta, R., & Trapp, B. D. (2011). Mechanisms of neuronal dysfunction and degeneration in multiple sclerosis. *Progress in neurobiology, 93*(1), 1-12.

Dutta, R., & Trapp, B. D. (2014). Relapsing and progressive forms of multiple sclerosis: insights from pathology. *Current Opinion in Neurology, 27*(3), 271-278.

Eddleston, M., De La Torre, J. C., Oldstone, M. B. A., Loskutoff, D. J., Edgington, T. S., & Mackman, N. (1993). Astrocytes are the primary source of tissue factor in the murine central nervous system: A role for astrocytes in cerebral hemostasis. *Journal of Clinical Investigation, 92*(1), 349-358.

Elvidge, G. P., Glenny, L., Appelhoff, R. J., Ratcliffe, P. J., Ragoussis, J., & Gleadle, J. M. (2006). Concordant regulation of gene expression by hypoxia and 2-oxoglutarate-dependent dioxygenase inhibition: The role of HIF-1α, HIF-2α, and other pathways. *Journal of Biological Chemistry, 281*(22), 15215-15226.

Eng, L. F., & Ghirnikar, R. S. (1994). GFAP and Astrogliosis. *Brain pathology (Zurich, Switzerland), 4*(3), 229-237.

Eshaghi, A., Marinescu, R. V., Young, A. L., Firth, N. C., Prados, F., Jorge Cardoso, M., Tur, C., De Angelis, F., Cawley, N., Brownlee, W. J., De Stefano, N., Laura Stromillo, M., Battaglini, M., Ruggieri, S., Gasperini, C., Filippi, M., Rocca, M. A., Rovira, A., Sastre-Garriga, J., Geurts, J. J. G., Vrenken, H., Wottschel, V., Leurs, C. E., Uitdehaag, B., Pirpamer, L., Enzinger, C., Ourselin, S., Gandini Wheeler-Kingshott, C. A., Chard, D., Thompson, A. J., Barkhof, F., Alexander, D. C., & Ciccarelli, O. (2018). Progression of regional grey matter atrophy in multiple sclerosis. *Brain (London, England : 1878), 141*(6), 1665-1677.

Felts, P. A., Woolston, A.-M., Fernando, H. B., Asquith, S., Gregson, N. A., Mizzi, O. J., & Smith, K. J. (2005). Inflammation and primary demyelination induced by the intraspinal injection of lipopolysaccharide. *Brain, 128*(7), 1649-1666.

Ferguson, B., Matyszak, M., Esiri, M. M., & Perry, V. (1997). Axonal damage in acute multiple sclerosis lesions. *Brain, 120*, 393-399.

Few, A. B. (1966). The occurrence of lipofuscin pigment as related to aging in the lumbar spinal cord, dorsal root ganglia and paravertebral ganglia of the dog and pig. In: ProQuest Dissertations Publishing.

Fischer, M. T., Sharma, R., Lim, J. L., Haider, L., Frischer, J. M., Drexhage, J., Mahad, D., Bradl, M., van Horssen, J., & Lassmann, H. (2012). NADPH oxidase expression in active multiple sclerosis lesions in relation to oxidative tissue damage and mitochondrial injury. *Brain (London, England : 1878), 135*(3), 886-899.

Fischer, M. T., Wimmer, I., Höftberger, R., Gerlach, S., Haider, L., Zrzavy, T., Hametner, S., Mahad, D., Binder, C. J., Krumbholz, M., Bauer, J., Bradl, M., & Lassmann, H. (2013). Disease-specific molecular events in cortical multiple sclerosis lesions. *Brain (London, England : 1878), 136*(6), 1799-1815.

Fisniku, L. K., Chard, D. T., Jackson, J. S., Anderson, V. M., Altmann, D. R., Miszkiel, K. A., Thompson, A. J., & Miller, D. H. (2008). Gray matter atrophy is related to long-term disability in multiple sclerosis. *Annals of Neurology, 64*(3), 247-254.

Floyd, R. A. (1999). Neuroinflammatory processes are important in neurodegenerative diseases: an hypothesis to explain the increased formation of reactive oxygen and nitrogen species as major factors involved in neurodegenerative disease development. *Free radical biology & medicine, 26*(9), 1346-1355.

Forslin, Y., Bergendal, Å., Hashim, F., Martola, J., Shams, S., Wiberg, M. K., Fredrikson, S., & Granberg, T. (2018). Detection of Leukocortical Lesions in Multiple Sclerosis and Their Association with Physical and Cognitive Impairment: A Comparison of Conventional and Synthetic Phase-Sensitive Inversion Recovery MRI. *AJNR. American journal of neuroradiology, 39*(11), 1995.

Frischer, J. M., Bramow, S., Dal-Bianco, A., Lucchinetti, C. F., Rauschka, H., Schmidbauer, M., Laursen, H., Sorensen, P. S., & Lassmann, H. (2009). The relation between inflammation and neurodegeneration in multiple sclerosis brains. *Brain (London, England : 1878), 132*(5), 1175-1189.

Geurts, J. G. J., Bö, D. L., Roosendaal, P. S., Hazes, P. T., Daniëls, P. R., Barkhof, P. F., Witter, P. M., Huitinga, P. I., & Van Der Valk, P. P. (2007). Extensive Hippocampal Demyelination in Multiple Sclerosis. *Journal of Neuropathology and Experimental Neurology, 66*(9), 819-827.

Gilmore, C. P., Donaldson, I., Bö, L., Owens, T., Lowe, J., & Evangelou, N. (2009). Regional variations in the extent and pattern of grey matter demyelination in multiple sclerosis: a comparison between the cerebral cortex, cerebellar cortex, deep grey matter nuclei and the spinal cord. *J Neurol Neurosurg Psychiatry, 80*(2), 182.

Gleichmann, M., & Mattson, M. P. (2011). Neuronal Calcium Homeostasis and Dysregulation. *Antioxidants & Redox Signaling, 14*(7), 1261-1273.

Gonsette, R. E. (2008). Neurodegeneration in multiple sclerosis: The role of oxidative stress and excitotoxicity. *Journal Of The Neurological Sciences, 274*(1-2), 48-53.

González-Andrade, J. F., & Jose, A. (2010). Disease-modifying therapies in relapsing-remitting multiple sclerosis. *Neuropsychiatric disease and treatment, 6*(1), 365-373.

Graumann, U., Reynolds, R., Steck, A. J., & Schaeren-Wiemers, N. (2006). Molecular Changes in Normal Appearing White Matter in Multiple Sclerosis are Characteristic of Neuroprotective Mechanisms Against Hypoxic Insult. *Brain pathology (Zurich, Switzerland), 13*(4), 554-573.

Greijer, A. E., & van Der Wall, E. (2004). The role of hypoxia inducible factor 1 (HIF-1) in hypoxia induced apoptosis. *J Clin Pathol, 57*(10), 1009.

Grossman, M. L., Basbaum, A. I., & Fields, H. L. (1982). Afferent and efferent connections of the rat tail flick reflex (a model used to analyze pain control mechanisms). *Journal of comparative neurology (1911), 206*(1), 9-16.

Guan, S.-Y., Leng, R.-X., Tao, J.-H., Li, X.-P., Ye, D.-Q., Olsen, N., Zheng, S. G., & Pan, H.-F. (2017). Hypoxia-inducible factor-1α: a promising therapeutic target for autoimmune diseases. In (Vol. 21, pp. 715-723).

Guertin, P. A. (2013). Central pattern generator for locomotion: anatomical, physiological, and pathophysiological considerations. *Frontiers In Neurology, 3*.

Guzy, R. D., Hoyos, B., Robin, E., Chen, H., Liu, L., Mansfield, K. D., Simon, M. C., Hammerling, U., & Schumacker, P. T. (2005). Mitochondrial complex III is required for hypoxia-induced ROS production and cellular oxygen sensing. *Cell metabolism, 1*(6), 401-408.

Hadanny, A., Golan, H., Fishlev, G., Bechor, Y., Volkov, O., Suzin, G., Ben-Jacob, E., & Efrati, S. (2015). Hyperbaric oxygen can induce neuroplasticity and improve cognitive functions of patients suffering from anoxic brain damage. *Restorative neurology and neuroscience, 33*(4), 471-486.

Haider, L., Zrzavy, T., Hametner, S., Höftberger, R., Bagnato, F., Grabner, G., Trattnig, S., Pfeifenbring, S., Brück, W., & Lassmann, H. (2016). The topograpy of demyelination and neurodegeneration in the multiple sclerosis brain. *Brain (London, England : 1878), 139*(3), 807-815.

Haile, M., Limson, F., Gingrich, K., Li, Y.-S., Quartermain, D., Blanck, T., & Bekker, A. (2009). Nimodipine prevents transient cognitive dysfunction after moderate hypoxia in adult mice. *Journal of neurosurgical anesthesiology, 21*(2), 140-144.

Hamby, M. E., Hewett, J. A., & Hewett, S. J. (2006). TGF-β1 potentiates astrocytic nitric oxide production by expanding the population of astrocytes that express NOS-2. *Glia, 54*(6), 566-577.

Hänggi, D., Etminan, N., Aldrich, F., Steiger, H. J., Mayer, S. A., Diringer, M. N., Hoh, B. L., Mocco, J., Faleck, H. J., & Macdonald, R. L. (2017). Randomized, Open-Label, Phase 1/2a Study to Determine the Maximum Tolerated Dose of Intraventricular Sustained Release Nimodipine for Subarachnoid Hemorrhage (NEWTON [Nimodipine Microparticles to Enhance Recovery While Reducing Toxicity After Subarachnoid Hemorrhage]). *Stroke (1970), 48*(1), 145-151.

Harrison, J. K., Yan, J., Shizong, C., Yiyang, X., Dominique, M., Robert, K. M., Wolfgang, J. S., Mina, N. S., Soumya, A., Darren, A. T., Paolo, B., Kevin, B. B., & Lili, F. (1998). Role for neuronally derived fractalkine in mediating interactions between neurons and CX3CR1-expressing microglia. *Proceedings of the National Academy of Sciences of the United States of America, 95*(18), 10896.

Hashimoto, T., & Shibasaki, F. (2015). Hypoxia-Inducible Factor as an Angiogenic Master Switch. *Frontiers in pediatrics, 3*, 33-33.

Haws, C. W., Gourley, J. K., & Heistad, D. D. (1983). Effects of nimodipine on cerebral blood flow. *Journal of Pharmacology and Experimental Therapeutics, 225*(1), 24-28.

Hebbar, S., Khandelwal, A., Jayashree, R., Hindle, S. J., Chiang, Y. N., Yew, J. Y., Sweeney, S. T., & Schwudke, D. (2017). Lipid metabolic perturbation is an early-onset phenotype in adult spinster mutants: A Drosophila model for lysosomal storage disorders. *Molecular biology of the cell, 28*(26), 3728-3740.

Hernandez-Gerez, E., Fleming, I. N., & Parson, S. H. (2019). A role for spinal cord hypoxia in neurodegeneration. *Cell death & disease, 10*(11), 861-868.

Hochmeister, J. S., Grundtner, E. R., Bauer, E. J., Engelhardt, E. B., Lyck, E. R., Gordon, E. G., Korosec, E. T., Kutzelnigg, E. A., Berger, E. J., Bradl, E. M., Bittner, E. R., & Lassmann, E. H. (2006). Dysferlin Is a New Marker for Leaky Brain Blood Vessels in Multiple Sclerosis. *Journal of Neuropathology and Experimental Neurology, 65*(9), 855-865.

Holland, C. M., Charil, A., Csapo, I., Liptak, Z., Ichise, M., Khoury, S. J., Bakshi, R., Weiner, H. L., & Guttmann, C. R. G. (2012). The Relationship between Normal Cerebral Perfusion Patterns and White Matter Lesion Distribution in 1,249 Patients with Multiple Sclerosis. *Journal of neuroimaging, 22*(2), 129-136.

Horn, J., de Haan, R. J., Vermeulen, M., Luiten, P. G., & Limburg, M. (2001). Nimodipine in animal model experiments of focal cerebral ischemia: a systematic review. *Stroke (1970), 32*(10), 2433-2438.

Hostenbach, S., D'Haeseleer, M., Kooijman, R., & De Keyser, J. (2016). The pathophysiological role of astrocytic endothelin-1. *Progress in neurobiology, 144*, 88-102.

Huang, B.-R., Chang, P.-C., Yeh, W.-L., Lee, C.-H., Tsai, C.-F., Lin, C., Lin, H.-Y., Liu, Y.-S., Wu, C. Y.-J., Ko, P.-Y., Huang, S.-S., Hsu, H.-C., & Lu, D.-Y. (2014). Anti-Neuroinflammatory Effects of the Calcium Channel Blocker Nicardipine on Microglial Cells: Implications for Neuroprotection. *PLoS ONE, 9*(3), e91167-e91167.

Hulst, H. E., Schoonheim, M. M., Roosendaal, S. D., Popescu, V., Schweren, L. J. S., Van Der Werf, Y. D., Visser, L. H., Polman, C. H., Barkhof, F., & Geurts, J. J. G. (2012). Functional adaptive changes within the hippocampal memory system of patients with multiple sclerosis. *Human Brain Mapping, 33*(10), 2268-2280.

Ingram, G., Loveless, S., Howell, O. W., Hakobyan, S., Dancey, B., Harris, C. L., Robertson, N. P., Neal, J. W., & Morgan, B. P. (2014). Complement activation in multiple sclerosis plaques: an immunohistochemical analysis. *Acta neuropathologica communications, 2*(1), 53-53.

Jin, Y. H., Kang, H. S., Hou, W., Meng, L., & Kim, B. S. (2015). The level of viral infection of antigen-presenting cells correlates with the level of development of Theiler's murine encephalomyelitis virus-induced demyelinating disease. *Journal of virology, 89*(3), 1867.

Johns, T. G., Kerlero de Rosbo, N., Menon, K. K., Abo, S., Gonzales, M. F., & Bernard, C. C. (1995). Myelin oligodendrocyte glycoprotein induces a demyelinating encephalomyelitis resembling multiple sclerosis. *Journal of immunology (Baltimore, Md. : 1950), 154*(10), 5536.

Johnson, T. W., Wu, Y., Nathoo, N., Rogers, J. A., Wee Yong, V., Dunn, J. F., & Baud, O. (2016). Gray Matter Hypoxia in the Brain of the Experimental Autoimmune Encephalomyelitis Model of Multiple Sclerosis. *PLoS ONE, 11*(12).

Karsten, B., Almut, G., & Holger, K. E. (2013). Hypoxia and inflammation are two sides of the same coin. *Proceedings of the National Academy of Sciences - PNAS, 110*(46), 18351-18352.

Katz Sand, I. (2015). Classification, diagnosis, and differential diagnosis of multiple sclerosis. *Current Opinion in Neurology, 28*(3), 193-205.

Kidd, D., Barkhof, F., McConnell, R., Algra, P., Allen, I. V., & Revesz, T. (1999). Cortical lesions in multiple sclerosis. *Brain, 122*, 17-26.

Kim, G. W., Kondo, T., Noshita, N., & Chan, P. H. (2002). Manganese superoxide dismutase deficiency exacerbates cerebral infarction after focal cerebral ischemia/reperfusion in mice: Implications for the production and role of superoxide radicals. *Stroke (1970), 33*(3), 809-815.

Kim, S., Lee, M., & Choi, Y. K. (2020). The Role of a Neurovascular Signaling Pathway Involving Hypoxia-Inducible Factor and Notch in the Function of the Central Nervous System. *Biomolecules & therapeutics, 28*(1), 45-57.

Klaver, R., De Vries, H. E., Schenk, G. J., & Geurts, J. J. G. (2013). Grey matter damage in multiple sclerosis: A pathology perspective. *Prion, 7*(1), 66-75.

Koch, M. W., Ramsaransing, G. S. M., Arutjunyan, A. V., Stepanov, M., Teelken, A., Heersema, D. J., & Keyser, J. (2005). Oxidative stress in serum and peripheral blood leukocytes in patients with different disease courses of multiple sclerosis. *J Neurol, 253*(4), 483-487.

Koch-Henriksen, N., Brønnum-Hansen, H., & Stenager, E. (1998). Underlying cause of death in Danish patients with multiple sclerosis: results from the Danish Multiple Sclerosis Registry. *Journal of neurology, neurosurgery and psychiatry, 65*(1), 56-59.

Kooi, E.-J., Geurts, J. G. J., Van Horssen, J. G. J., Bø, J. G. L., & Van Der Valk, J. G. P. (2009). Meningeal Inflammation is not Associated With Cortical Demyelination in Chronic Multiple Sclerosis. *Journal of Neuropathology and Experimental Neurology, 68*(9), 1021-1028.

Kooi, E.-J., Strijbis, J. G. E., Van Der Valk, J. G. P., & Geurts, J. G. J. (2012). Heterogeneity of cortical lesions in multiple sclerosis: Clinical and pathologic implications. *Neurology, 79*(13), 1369-1376.

Kornek, B., & Lassmann, H. (2003). Neuropathology of multiple sclerosis—new concepts. *Brain Research Bulletin, 61*(3), 321-326.

Krapf, H., Morrissey, S., Zenker, O., Zwingers, T., Gonsette, R., & Hartung, H. (1999). Mitoxantrone in progressive multiple sclerosis: MRI results of the European Phase III trial. *Neurology, 52*(6), A495-A495.

Kupersmith, M. J., Alban, T., Zeiffer, B., & Lefton, D. (2002). Contrast-enhanced MRI in acute optic neuritis: relationship to visual performance. *Brain (London, England : 1878), 125*(4), 812-822.

Kutzelnigg, A., Faber-Rod, J. C., Bauer, J., Lucchinetti, C. F., Sorensen, P. S., Laursen, H., Stadelmann, C., Brück, W., Rauschka, H., Schmidbauer, M., & Lassmann, H. (2007). Widespread Demyelination in the Cerebellar Cortex in Multiple Sclerosis. *Brain Pathology, 17*(1), 38-44.

Kutzelnigg, A., Lucchinetti, C. F., Stadelmann, C., Brck, W., Rauschka, H., Bergmann, M., Schmidbauer, M., Parisi, J. E., & Lassmann, H. (2005). Cortical demyelination and diffuse white matter injury in multiple sclerosis. *Brain, 128*(11), 2705-2712.

La Mantia, L., Di Pietrantonj, C., Rovaris, M., Rigon, G., Frau, S., Berardo, F., Gandini, A., Longobardi, A., Weinstock-Guttman, B., & Vaona, A. (2016). Interferons-beta versus glatiramer acetate for relapsing-remitting multiple sclerosis. *Cochrane database of systematic reviews, 11*(11), CD009333-CD009333.

LaManna, J. C. (2007). Hypoxia in the central nervous system. *Essays in Biochemistry, 43*, 139-151.

LaManna, J. C., Chavez, J., & Pichiule, P. (2004). Structural and functional adaptation to hypoxia in the rat brain. *Journal Of Experimental Biology, 207*(18), 3163-3169.

Lambertsen, C. J., Dough, R. H., Cooper, D. Y., Emmel, G. L., Loeschcke, H. H., & Schmidt, C. F. (1953). Oxygen toxicity; effects in man of oxygen inhalation at 1 and 3.5 atmospheres upon blood gas transport, cerebral circulation and cerebral metabolism. *Journal of applied physiology (1948), 5*(9), 471-486.

Lassmann, H. (1999). The pathology of multiple sclerosis. *Journal Of The Neurological Sciences, 238*, S13-S13.

Lassmann, H. (2005). Inflammation in neurodegenerative diseases: An overview from a pathological standpoint. *European Journal of Neurology, 12*, 308-309.

Lassmann, H. (2015). Spinal cord pathology in multiple sclerosis. *The Lancet Neurology, 14*(4), 348-349.

Lassmann, H. (2016). Demyelination and neurodegeneration in multiple sclerosis: The role of hypoxia. *Annals of Neurology, 79*(4), 520-521.

Lassmann, H., & Bradl, M. (2017). Multiple sclerosis: experimental models and reality. *Acta Neuropathol, 133*(2), 223-244.

Lassmann, H., Brück, W., & Lucchinetti, C. (2001). Heterogeneity of multiple sclerosis pathogenesis: implications for diagnosis and therapy. *Trends in Molecular Medicine, 7*(3), 115-121.

Lassmann, H., Brück, W., & Lucchinetti, C. F. (2007). The Immunopathology of Multiple Sclerosis: An Overview. *Brain Pathology, 17*(2), 210-218.

Lassmann, H., Jack Van, H., & Don, M. (2012). Progressive multiple sclerosis: pathology and pathogenesis. *Nature Reviews Neurology, 8*(11), 647.

Lassmann, H., & Van Horssen, J. (2011). The molecular basis of neurodegeneration in multiple sclerosis. In (Vol. 585, pp. 3715-3723).

Lawson, L. J., Perry, V. H., & Gordon, S. (1992). Turnover of resident microglia in the normal adult mouse brain. *Neuroscience, 48*(2), 405-415.

Le Page, E., Veillard, D., Laplaud, D. A., Hamonic, S., Wardi, R., Lebrun, C., Zagnoli, F., Wiertlewski, S., Deburghgraeve, V., Coustans, M., & Edan, G. (2015). Oral versus intravenous high-dose methylprednisolone for treatment of relapses in patients with multiple sclerosis (COPOUSEP): a randomised, controlled, double-blind, non-inferiority trial. *The Lancet (British edition), 386*(9997), 974-981.

Lecht, S., Rotfeld, E., Arien-Zakay, H., Tabakman, R., Matzner, H., Yaka, R., Lelkes, P. I., & Lazarovici, P. (2012). Neuroprotective effects of nimodipine and nifedipine in the NGF-differentiated PC12 cells exposed to oxygen-glucose deprivation or trophic withdrawal. *International journal of developmental neuroscience, 30*(6), 465-469.

Lee, M., Lee, M. E., De la Monte, S. M., De La Monte, S. M., Ng, S.-C., Ng, M. E., Bloch, K. D., Bloch, K. D., Quertermous, T., & Quertermous, T. (1990). Expression of the potent vasoconstrictor endothelin in the human central nervous system. *The Journal of clinical investigation, 86*(1), 141-147.

Lee, S., Chen, T. T., Barber, C. L., Jordan, M. C., Murdock, J., Desai, S., Ferrara, N., Nagy, A., Roos, K. P., & Iruela-Arispe, M. L. (2007). Autocrine VEGF Signaling Is Required for Vascular Homeostasis. *Cell (Cambridge), 130*(4), 691-703.

Leech, S., Kirk, J., Plumb, J., & McQuaid, S. (2007). Persistent endothelial abnormalities and blood–brain barrier leak in primary and secondary progressive multiple sclerosis. *Neuropathology and Applied Neurobiology, 33*(1), 86-98.

Leenders, K. L., Perani, D., Lammertsma, A. A., Heather, J. D., Buckingham, P., Healy, M. J. R., Jones, T., Gibbs, J. M., Wise, R. J. S., Hatazawa, J., Herold, S., Beaney, R. P., Brooks, D. J., Spinks, T., Rhodes, C., & Frackowiak, R. S. J. (1990). Cerebral blood flow, blood volume and oxygen utilization: Normal values and effect of age. *Brain (London, England : 1878), 113*(1), 27-47.

Leisz, S., Simmermacher, S., Prell, J., Strauss, C., & Scheller, C. (2019). Nimodipine-Dependent Protection of Schwann Cells, Astrocytes and Neuronal Cells from Osmotic,

Oxidative and Heat Stress Is Associated with the Activation of AKT and CREB. *International journal of molecular sciences, 20*(18), 4578.

LeVere, T. E., Brugler, T., Sandin, M., & Gray-Silva, S. (1989). Recovery of Function After Brain Damage: Facilitation by the Calcium Entry Blocker Nimodipine. *Behavioral neuroscience, 103*(3), 561-565.

Levy, A., Kong, R. M., Stillman, M. J., Shukitt-Hale, B., Kadar, T., Rauch, T. M., & Lieberman, H. R. (1991). Nimodipine improves spatial working memory and elevates hippocampal acetylcholine in young rats. *Pharmacology, biochemistry and behavior, 39*(3), 781-786.

Li, Y., Hu, X., Liu, Y., Bao, Y., & An, L. (2009). Nimodipine protects dopaminergic neurons against inflammation-mediated degeneration through inhibition of microglial activation. *Neuropharmacology, 56*(3), 580-589.

Lin, C., Wu, C. J., Wei, I. H., Tsai, M. H., Chang, N. W., Yang, T. T., & Kuo, Y. M. (2012). Chronic treadmill running protects hippocampal neurons from hypobaric hypoxia-induced apoptosis in rats. *Neuroscience, 231*, 216-224.

Lipscombe, D., Helton, T. D., & Xu, W. (2004). L-Type Calcium Channels: The Low Down. *Journal of Neurophysiology, 92*(5), 2633-2641.

Liu, B. I. N., Gao, H. M., Wang, J. Y., Jeohn, G. H., Cooper, C. L., & Hong, J. S. (2002). Role of Nitric Oxide in Inflammation-Mediated Neurodegeneration. *Annals of the New York Academy of Sciences, 962*(1), 318-331.

Loihl, A. K., & Murphy, S. (1998). Expression of nitric oxide synthase-2 in glia associated with CNS pathology. *Progress in brain research, 118*, 253-267.

Lorefice, L., Fenu, G., Fois, M., Frau, J., Coghe, G., Marrosu, M. G., & Cocco, E. (2018). Pulse steroid therapy in multiple sclerosis and mood changes: An exploratory prospective study. *Multiple sclerosis and related disorders, 20*, 104-108.

Lovas, G., Szilagyi, N., Majtenyi, K., Palkovits, M., & Komoly, S. (2000). Axonal changes in chronic demyelinated cervical spinal cord plaques. *Brain, 123*, 308-317.

Love, S. (2006). Demyelinating diseases. *J Clin Pathol, 59*(11), 1151.

Lucas, C. V., Bensch, K. G., & Eng, L. F. (1980). In vitro polymerization of glial fibrillary acidic (GFA) protein extracted from multiple sclerosis (MS) brain. *Neurochemical research, 5*(3), 247-255.

Lucchinetti, C. F., Brück, W., Parisi, J., Scheithauer, B., Rodriguez, M., & Lassmann, H. (2000). Heterogeneity of multiple sclerosis lesions: Implications for the pathogenesis of demyelination. *Annals of Neurology, 47*(6), 707-717.

Lucchinetti, C. F., Popescu, B. F. G., Bunyan, R. F., Moll, N. M., Roemer, S. F., Lassmann, H., Brück, W., Parisi, J. E., Scheithauer, B. W., Giannini, C., Weigand, S. D., Mandrekar, J., & Ransohoff, R. M. (2011). Inflammatory Cortical Demyelination in Early Multiple Sclerosis. *The New England Journal of Medicine, 365*(23), 2188-2197.

Mahad, D., Trapp, B. D., & Lassmann, H. (2015). Pathological mechanisms in progressive multiple sclerosis. *Lancet Neurology, 14*(2), 183-193.

Mahad, D., Ziabreva, I., Campbell, G., Lax, N., White, K., Hanson, P. S., Lassmann, H., & Turnbull, D. M. (2009). Mitochondrial changes within axons in multiple sclerosis. *Brain, 132*(5), 1161-1174.

Mahad, D., Ziabreva, I., Lassmann, H., & Turnbull, D. (2008). Mitochondrial defects in acute multiple sclerosis lesions. *Brain, 131*(7), 1722-1735.

Mallucci, G., Peruzzotti-Jametti, L., Bernstock, J. D., & Pluchino, S. (2015). The role of immune cells, glia and neurons in white and gray matter pathology in multiple sclerosis. *Progress in neurobiology, 127-128*, 1-22.

Marik, C., Felts, P. A., Bauer, J., Lassmann, H., & Smith, K. J. (2007). Lesion genesis in a subset of patients with multiple sclerosis: a role for innate immunity? *Brain, 130*(11), 2800-2815.

Marina, N., Turovsky, E., Christie, I. N., Hosford, P. S., Hadjihambi, A., Korsak, A., Ang, R., Mastitskaya, S., Sheikhbahaei, S., Theparambil, S. M., & Gourine, A. V. (2017). Brain metabolic sensing and metabolic signaling at the level of an astrocyte. *Glia (2017) (In press).*

Martinez Sosa, S., & Smith, K. J. (2017). Understanding a role for hypoxia in lesion formation and location in the deep and periventricular white matter in small vessel disease and multiple sclerosis. *Clinical Science , 131 (20) pp. 2503-2524. (2017)*.

Martirosyan, N. L., Feuerstein, J. E. S., Theodore, N., Cavalcanti, D. D., Spetzler, R. F., & Preul, M. C. (2011). Blood supply and vascular reactivity of the spinal cord under normal and pathological conditions: A review. *Journal of neurosurgery. Spine, 15*(3), 238-251.

Matute, C., Sanchez-Gomez, M. V., Martinez-Millan, L., & Miledi, R. (1997). Glutamate receptor-mediated toxicity in optic nerve oligodendrocytes. *Proceedings of the National Academy of Sciences - PNAS, 94*(16), 8830-8835.

Mayer, P. L., & Kier, E. L. (1991). The controversy of the periventricular white matter circulation: a review of the anatomic literature. *American journal of neuroradiology : AJNR, 12*(2), 223-228.

McDonald, W. I., Miller, D. H., & Barnes, D. (1992). The pathological evolution of multiple sclerosis. *Neuropathology and Applied Neurobiology, 18*(4), 319-334.

McGuire, S. O., Ling, Z. D., Lipton, J. W., Sortwell, C. E., Collier, T. J., & Carvey, P. M. (2001). Tumor Necrosis Factor α Is Toxic to Embryonic Mesencephalic Dopamine Neurons. *Experimental neurology, 169*(2), 219-230.

McMahon, J. M., McQuaid, S., Reynolds, R., & FitzGerald, U. F. (2012). Increased expression of ER stress- and hypoxia-associated molecules in grey matter lesions in multiple sclerosis. *Multiple Sclerosis Journal, 18*(10), 1437-1447.

Meng, R., Ding, Y., Asmaro, K., Brogan, D., Meng, L., Sui, M., Shi, J., Duan, Y., Sun, Z., Yu, Y., Jia, J., & Ji, X. (2015). Ischemic Conditioning Is Safe and Effective for Octo- and Nonagenarians in Stroke Prevention and Treatment. *Neurotherapeutics, 12*(3), 667-677.

Metz, G. A., & Whishaw, I. Q. (2002). Cortical and subcortical lesions impair skilled walking in the ladder rung walking test: a new task to evaluate fore- and hindlimb stepping, placing, and co-ordination. *J Neurosci Methods, 115*(2), 169-179.

Michel-Monigadon, D., Brachet, P., Neveu, I., & Naveilhan, P. (2011). Immunoregulatory properties of neural stem cells. *Immunotherapy, 3*(4s), 39-41.

Michiels, C. (2004). Physiological and Pathological Responses to Hypoxia. *The American Journal of Pathology, 164*(6), 1875-1882.

Mikkelsen, H. B., Huizinga, J. D., Larsen, J. O., & Kirkeby, S. (2017). Ionized calcium-binding adaptor molecule 1 positive macrophages and HO-1 up-regulation in intestinal muscularis resident macrophages. *Anatomical record (Hoboken, N.J. : 2007), 300*(6), 1114-1122.

Miller, E., Walczak, A., Saluk, J., Ponczek, M. B., & Majsterek, I. (2012). Oxidative modification of patient's plasma proteins and its role in pathogenesis of multiple sclerosis. *Clinical Biochemistry, 45*(1-2), 26-30.

Miller, R. H., & Raff, M. C. (1984). Fibrous and protoplasmic astrocytes are biochemically and developmentally distinct. *The Journal of neuroscience, 4*(2), 585-592.

Mink, J. W., Blumenschine, R. J., & Adams, D. B. (1981). Ratio of central nervous system to body metabolism in vertebrates: its constancy and functional basis. *American journal of physiology. Regulatory, integrative and comparative physiology, 241*(3), 203-R212.

Mizuno, T., Kawanokuchi, J., Numata, K., & Suzumura, A. (2003). Production and neuroprotective functions of fractalkine in the central nervous system. *Brain Research, 979*(1-2), 65-70.

Moccia, M., Quarantelli, M., Lanzillo, R., Cocozza, S., Carotenuto, A., Carotenuto, B., Alfano, B., Prinster, A., Triassi, M., Nardone, A., Palladino, R., Brunetti, A., & Brescia Morra, V. (2017). Grey:white matter ratio at diagnosis and the risk of 10-year multiple sclerosis progression. *European Journal of Neurology, 24*(1), 195-204.

Molina-Holgado, E., Vela, J., Arevalo-Martin, A., & Guaza, C. (2001). LPS/IFN-gamma cytotoxicity in oligodendroglial cells: role of nitric oxide and protection by the anti-inflammatory cytokine IL-10. *European Journal Of Neuroscience, 13*(3), 493-502.

Möller, J. R., Yanagisawa, K., Brady, R. O., Tourtellotte, W. W., & Quarles, R. H. (1987). Myelin-associated glycoprotein in multiple sclerosis lesions: A quantitative and qualitative analysis. *Annals of Neurology, 22*(4), 469-474.

Moody, D. M., Bell, M. A., & Challa, V. R. (1990). Features of the cerebral vascular pattern that predict vulnerability to perfusion or oxygenation deficiency: an anatomic study. *AJNR. American journal of neuroradiology, 11*(3), 431.

Moreno-García, A., Kun, A., Calero, O., Medina, M., & Calero, M. (2018). An Overview of the Role of Lipofuscin in Age-Related Neurodegeneration. *Frontiers in neuroscience, 12*, 464-464.

Murray, K. N., Girard, S., Holmes, W. M., Parkes, L. M., Williams, S. R., Parry-Jones, A. R., & Allan, S. M. (2014). Systemic inflammation impairs tissue reperfusion through endothelin-dependent mechanisms in cerebral ischemia. *Stroke (1970), 45*(11), 3412-3419.

Nash, B., Ioannidou, K., & Barnett, S. C. (2011). Astrocyte phenotypes and their relationship to myelination. *J Anat, 219*(1), 44-52.

Nataf, S., Guillen, M., & Pays, L. (2019). TGFB1-Mediated Gliosis in Multiple Sclerosis Spinal Cords Is Favored by the Regionalized Expression of HOXA5 and the Age-

Dependent Decline in Androgen Receptor Ligands. *International journal of molecular sciences, 20*(23), 5934.

Negre-Salvayre, A., Coatrieux, C., Ingueneau, C., & Salvayre, R. (2008). Advanced lipid peroxidation end products in oxidative damage to proteins. Potential role in diseases and therapeutic prospects for the inhibitors. *British Journal of Pharmacology, 153*(1), 6-20.

Neubauer, R., Gottlieb, S., & Kagan, R. (1990). Enhancing "idling" neurons. *The Lancet (British edition), 335*(8688), 542-542.

Neumann, H., Schmidt, H., Cavalié, A., Jenne, D., & Wekerle, H. (1997). Major histocompatibility complex (MHC) class I gene expression in single neurons of the central nervous system: differential regulation by interferon (IFN)-gamma and tumor necrosis factor (TNF)-alpha. *The Journal of experimental medicine, 185*(2), 305.

Newcombe, J., Li, H., & Cuzner, M. L. (1994). Low density lipoprotein uptake by macrophages in multiple sclerosis plaques: implications for pathogenesis. *Neuropathology and Applied Neurobiology, 20*(2), 152-162.

Nikić, I., Doron, M., Catherine, S., Mary, B., Mario, K., Florence, M. B., Wolfgang, B., Derron, B., Thomas, M., & Martin, K. (2011). A reversible form of axon damage in experimental autoimmune encephalomyelitis and multiple sclerosis. *Nature Medicine, 17*(4), 495.

Noseworthy, J. H., Lucchinetti, C., Rodriguez, M., & Weinshenker, B. G. (2000). Multiple sclerosis. *N Engl J Med, 343*(13), 938-952.

Novy, J., Carruzzo, A., Maeder, P., & Bogousslavsky, J. (2006). Spinal Cord Ischemia: Clinical and Imaging Patterns, Pathogenesis, and Outcomes in 27 Patients. *Archives of neurology (Chicago), 63*(8), 1113-1120.

Omae, T., Ibayashi, S., Kusuda, K., Nakamura, H., Yagi, H., & Fujishima, M. (1998). Effects of high atmospheric pressure and oxygen on middle cerebral blood flow velocity in humans measured by transcranial Doppler. *Stroke (1970), 29*(1), 94-97.

Pache, M., Kaiser, H. J., Akhalbedashvili, N., Lienert, C., Dubler, B., Kappos, L., & Flammer, J. (2003). Extraocular Blood Flow and Endothelin-1 Plasma Levels in Patients with Multiple Sclerosis. *European Neurology, 49*(3), 164-168.

Parabucki, A. B., Božić, I. D., Bjelobaba, I. M., Lavrnja, I. C., Brkić, P. D., Jovanović, T. S., Savić, D. Z., Stojiljković, M. B., & Peković, S. M. (2012). Hyperbaric oxygenation alters temporal expression pattern of superoxide dismutase 2 after cortical stab injury in rats. *Croatian medical journal, 53*(6), 586-597.

Patestas, M. A. (2006). *A textbook of neuroanatomy / Maria A. Patestas, Leslie P. Gartner*. Malden, MA: Malden, MA : Blackwell Pub.

Pérez-Cerdá, F., Sánchez-Gómez, M. V., & Matute, C. (2016). The link of inflammation and neurodegeneration in progressive multiple sclerosis. *Multiple sclerosis and demyelinating disorders, 1*(1), 1.

Peterson, J. W., Bö, L., Mörk, S., Chang, A., & Trapp, B. D. (2001). Transected neurites, apoptotic neurons, and reduced inflammation in cortical multiple sclerosis lesions. *Annals of Neurology, 50*(3), 389-400.

Petzold, A., Eikelenboom, M., Gveric, D., Keir, G., Chapman, M., Lazeron, R., Cuzner, M., Polman, C., Uitdehaag, B., Thompson, E., & Giovannoni, G. (2002). Markers for different glial cell responses in multiple sclerosis: clinical and pathological correlations. *Brain, 125*, 1462-1473.

Phaniendra, A., Jestadi, D., & Periyasamy, L. (2015). Free Radicals: Properties, Sources, Targets, and Their Implication in Various Diseases. *Ind J Clin Biochem, 30*(1), 11-26.

Pichiule, P., & LaManna, J., C. (2002). Angiopoietin-2 and rat brain capillary remodeling during adaptation and deadaptation to prolonged mild hypoxia. *Journal of Applied Physiology, 93*(3), 1131-1139.

Pirko, F. I., Lucchinetti, F. C., Sriram, F. S., & Bakshi, F. R. (2007). Gray matter involvement in multiple sclerosis. *Neurology, 68*(9), 634-642.

Pisani, A., Calabresi, P., Tozzi, A., D'Angelo, V., & Bernardi, G. (1998). L-type Ca2+ channel blockers attenuate electrical changes and Ca2+ rise induced by oxygen/glucose deprivation in cortical neurons. *Stroke (1970), 29*(1), 196-202.

Plantone, D., De Angelis, F., Doshi, A., & Chataway, J. (2016). Secondary Progressive Multiple Sclerosis: Definition and Measurement. *Cns Drugs, 30*(6), 517-526.

Prineas, J. W., Kwon, E. E., Cho, E. S., Sharer, L. R., Barnett, M. H., Oleszak, E. L., Hoffman, B., & Morgan, B. P. (2001). Immunopathology of secondary-progressive multiple sclerosis. *Annals of Neurology, 50*(5), 646-657.

Prins, M., Schul, E., Geurts, J., Der Valk, P., Drukarch, B., & Dam, A. M. (2015). Pathological differences between white and grey matter multiple sclerosis lesions. *Annals of the New York Academy of Sciences, 13511*(1), 99-113.

Qi, X., Lewin, A. S., Sun, L., Hauswirth, W. W., & Guy, J. (2006). Mitochondrial Protein Nitration Primes Neurodegeneration in Experimental Autoimmune Encephalomyelitis. *The Journal of biological chemistry, 281*(42), 31950-31962.

Rademakers, S., Lok, J., van Der Kogel, A., Bussink, J., & Kaanders, J. (2011). Metabolic markers in relation to hypoxia; staining patterns and colocalization of pimonidazole, HIF-1 alpha, CAIX, LDH-5, GLUT-1, MCT1 and MCT4. *Bmc Cancer, 11*(1).

Raleigh, J. A., Calkins-Adams, D. P., Rinker, L. H., Ballenger, C. A., Weissler, M. C., Fowler, W. C., Novotny, D. B., & Varia, M. A. (1998). Hypoxia and vascular endothelial growth factor expression in human squamous cell carcinomas using pimonidazole as a hypoxia marker. *Cancer research, 58*(17), 3765.

Rao, M. S., Leo, J. G., Bernardin, J. L., & Unverzagt, J. F. (1991). Cognitive dysfunction in multiple sclerosis.: I. Frequency, patterns, and prediction. *Neurology, 41*(5), 685-691.

Redford, E. J., Kapoor, R., & Smith, K. J. (1997). Nitric oxide donors reversibly block axonal conduction: demyelinated axons are especially susceptible. *Brain (London, England : 1878), 120 (Pt 12)*(12), 2149-2157.

Reeg, S., & Grune, T. (2015). Protein Oxidation in Aging: Does It Play a Role in Aging Progression? *Antioxidants & Redox Signaling, 23*(3), 239-255.

Reimer, M. M., Sorensen, I., Kuscha, V., Frank, R. E., Liu, C., Becker, C. G., & Becker, T. (2008). Motor Neuron Regeneration in Adult Zebrafish. *Journal of Neuroscience, 28*(34), 8510-8516.

Rey, F., Balsari, A., Giallongo, T., Ottolenghi, S., Di Giulio, A. M., Samaja, M., & Carelli, S. (2019). Erythropoietin as a Neuroprotective Molecule: An Overview of Its Therapeutic Potential in Neurodegenerative Diseases. *ASN neuro, 11*, 175909141987142-1759091419871420.

Ridet, J. L., Privat, A., Malhotra, S. K., & Gage, F. H. (1997). Reactive astrocytes: cellular and molecular cues to biological function. *Trends in neurosciences (Regular ed.), 20*(12), 570-577.

Robinson, A. P., Harp, C. T., Noronha, A., & Miller, S. D. (2014). The experimental autoimmune encephalomyelitis (EAE) model of MS. utility for understanding disease pathophysiology and treatment. *Handbook of clinical neurology, 122*, 173-189.

Rosbo, N. K., Honegger, P., Lassmann, H., & Matthieu, J. M. (1990). Demyelination Induced in Aggregating Brain Cell Cultures by a Monoclonal Antibody Against

Myelin/Oligodendrocyte Glycoprotein. *Journal of neurochemistry, 55*(2), 583-587.

Rosenberg, S., Kaplan, S., & Rosario, E. (2015). The Effect of Hyperbaric Oxygen Therapy on Functional Impairments Caused by Ischemic Stroke. *Archives of physical medicine and rehabilitation, 96*(10), e46-e47.

Rossignol, D. A., Rossignol, L. W., Jill, S. J., Melnyk, S., & Mumper, E. (2007). The effects of hyperbaric oxygen therapy on oxidative stress, inflammation, and symptoms in children with autism: An open-label pilot study. *BMC pediatrics, 7*(1), 36-36.

Rowland, M. J., Ezra, M., Winkler, A., Garry, P., Lamb, C., Kelly, M., Okell, T. W., Westbrook, J., Wise, R. G., Douaud, G., & Pattinson, K. T. S. (2019). Calcium channel blockade with nimodipine reverses MRI evidence of cerebral oedema following acute hypoxia. *Journal of cerebral blood flow and metabolism, 39*(2), 285-301.

Sadeghian, M., Mastrolia, V., Haddad, A. R., Mosley, A., Mullali, G., Schiza, D., Sajic, M., Hargreaves, I., Heales, S., Duchen, M. R., & Smith, K. J. (2016). Mitochondrial dysfunction is an important cause of neurological deficits in an inflammatory model of multiple sclerosis. *Scientific Reports , 6 , Article 33249. (2016)*.

Sanz, J. M., Chiozzi, P., Colaianna, M., Zotti, M., Ferrari, D., Trabace, L., Zuliani, G., & Di Virgilio, F. (2012). Nimodipine inhibits IL-1β release stimulated by amyloid β from microglia: Nimodipine and IL-1β. *British Journal of Pharmacology, 167*(8), 1702-1711.

Saravani, M., Rokni, M., Mehrbani, M., Amirkhosravi, A., Faramarz, S., Fatemi, I., Tarzi, M. E., & Nematollahi, M. (2019). The evaluation of VEGF and HIF-1 alpha gene polymorphisms and multiple sclerosis susceptibility. *Journal Of Gene Medicine, 21*(12).

Schampel, A., Volovitch, O., Koeniger, T., Scholz, C.-J., Jörg, S., Linker, R. A., Wischmeyer, E., Wunsch, M., Hell, J. W., Ergün, S., & Kuerten, S. (2017). Nimodipine fosters remyelination in a mouse model of multiple sclerosis and induces microglia-specific apoptosis. *Proceedings of the National Academy of Sciences - PNAS, 114*(16), E3295-E3304.

Schmierer, K., McDowell, A., Petrova, N., Carassiti, D., Thomas, D. L., & Miquel, M. E. (2018). Quantifying multiple sclerosis pathology in post mortem spinal cord using MRI. *Neuroimage , 182 pp. 251-258. (2018)*.

Schuh, C., Wimmer, I., Hametner, S., Haider, L., Van Dam, A., Liblau, R., Smith, K., Probert, L., Binder, C. J., Bauer, J., Bradl, M., Mahad, D., & Lassmann, H. (2014). Oxidative

tissue injury in multiple sclerosis is only partly reflected in experimental disease models. *Acta Neuropathologica, 128*(2), 247-266.

Scriabine, A., Schuurman, T., & Traber, J. (1989). Pharmacological basis for the use of nimodipine in central nervous system disorders. *The FASEB journal, 3*(7), 1799-1806.

Semenza, G. L. (2002). Signal transduction to hypoxia-inducible factor 1. *Biochemical Pharmacology, 64*(5-6), 993-998.

Semenza, G. L. (2003). Targeting HIF-1 for cancer therapy. *Nature reviews. Cancer, 3*(10), 721-732.

Semenza, G. L. (2007). Hypoxia-inducible factor 1 (HIF-1) pathway. *Science's STKE : signal transduction knowledge environment, 2007*(407), cm8.

Semenza, G. L. (2010). Defining the role of hypoxia-inducible factor 1 in cancer biology and therapeutics. *Oncogene, 29*(5), 625.

Sharma, R., Fischer, M.-T., Bauer, J., Felts, P., Smith, K., Misu, T., Fujihara, K., Bradl, M., & Lassmann, H. (2010). Inflammation induced by innate immunity in the central nervous system leads to primary astrocyte dysfunction followed by demyelination. *Acta Neuropathol, 120*(2), 223-236.

Sharp, R. F., & Bernaudin, M. (2004). HIF1 and oxygen sensing in the brain. *Nature Reviews Neuroscience, 5*(6), 437.

Shi, Q., Liu, X., Wang, N., Zheng, X., Fu, J., & Zheng, J. (2016). Nitric oxide from brain microvascular endothelial cells may initiate the compensatory response to mild hypoxia of astrocytes in a hypoxia-inducible factor-1α dependent manner. *American journal of translational research, 8*(11), 4735-4749.

Shockley, R. P., & LaManna, J. C. (1988). Determination of rat cerebral cortical blood volume changes by capillary mean transit time analysis during hypoxia, hypercapnia and hyperventilation. *Brain Research, 454*(1), 170-178.

Sitia, S., Tomasoni, L., Atzeni, F., Ambrosio, G., Cordiano, C., Catapano, A., Tramontana, S., Perticone, F., Naccarato, P., Camici, P., Picano, E., Cortigiani, L., Bevilacqua, M., Milazzo, L., Cusi, D., Barlassina, C., Sarzi-Puttini, P., & Turiel, M. (2010). From endothelial dysfunction to atherosclerosis. *Autoimmunity reviews, 9*(12), 830-834.

Sluck, J. M., Lin, R. C. S., Katolik, L. I., Jeng, A. Y., & Lehmann, J. C. (1999). Endothelin converting enzyme-1-, endothelin-1-, and endothelin-3-like immunoreactivity in the rat brain. *Neuroscience, 91*(4), 1483-1497.

Smith, H. L., & Mallucci, G. R. (2016). The unfolded protein response: mechanisms and therapy of neurodegeneration. *Brain (London, England : 1878), 139*(8), 2113-2121.

Smith, K. J., Kapoor, R., Hall, S. M., & Davies, M. (2001). Electrically active axons degenerate when exposed to nitric oxide. *Annals of Neurology, 49*(4), 470-476.

Smith, K. J., & Lassmann, H. (2002). The role of nitric oxide in multiple sclerosis. *Lancet Neurology, 1*(4), 232-241.

Smith, K. J., McDonald, I., Miller, D., & Lassmann, H. (2005). Chapter 13 - The pathophysiology of multiple sclerosis. In (pp. 601-659).

Smith, K. J., & McDonald, W. I. (1999). The pathophysiology of multiple sclerosis: the mechanisms underlying the production of symptoms and the natural history of the disease. *Philosophical transactions. Biological sciences, 354*(1390), 1649-1673.

Smolders, J., Remmerswaal, E. B. M., Schuurman, K. G., Melief, J., van Eden, C. G., van Lier, R. A. W., Huitinga, I., & Hamann, J. (2013). Characteristics of differentiated CD8 + and CD4 + T cells present in the human brain. *Acta Neuropathologica, 126*(4), 1-11.

Sofroniew, M. V. (2016). Reactive Astrocytes in Neural Repair and Protection. *The Neuroscientist (Baltimore, Md.), 11*(5), 400-407.

Sofroniew, M. V., & Vinters, H. V. (2009). Astrocytes: biology and pathology. *Acta Neuropathol, 119*(1), 7-35.

Stavrou, S., Feng, Z., Lemon, S. M., & Roos, R. P. (2010). Different Strains of Theiler's Murine Encephalomyelitis Virus Antagonize Different Sites in the Type I Interferon Pathway. *The Journal of Virology, 84*(18), 9181.

Stifani, N. (2014). Motor neurons and the generation of spinal motor neuron diversity. *Frontiers in cellular neuroscience, 8*, 293-293.

Stone, J., Itin, A., Alon, T., Pe'er, J., Gnessin, H., Chan-Ling, T., & Keshet, E. (1995). Development of retinal vasculature is mediated by hypoxia-induced vascular endothelial growth factor (VEGF) expression by neuroglia. *The Journal of neuroscience, 15*(7), 4738-4747.

Swank, R. L., Roth, J. G., & Woody, D. C. (2016). Cerebral Blood Flow and Red Cell Delivery in Normal Subjects and in Multiple Sclerosis. *Neurological research (New York), 5*(1), 37-59.

Tao, J.-H., Barbi, J., & Pan, F. (2015). Hypoxia-inducible factors in T lymphocyte differentiation and function. A Review in the Theme: Cellular Responses to Hypoxia. *American Journal of Physiology, 309*(9), C580.

Taylor, C. T. (2008). Interdependent roles for hypoxia inducible factor and nuclear factor-κB in hypoxic inflammation. *The Journal of physiology, 586*(17), 4055-4059.

Thom, S. R. (2009). Oxidative stress is fundamental to hyperbaric oxygen therapy. *Journal of Applied Physiology, 106*(3), 988-995.

Thompson, A., Polman, C., Miller, D., & McDonald, W. (1997). Primary progressive multiple sclerosis. *Brain, 120*(6), 1085-1096.

Toosy, A. T., Mason, D. F., & Miller, D. H. (2014). Optic neuritis. *Lancet Neurology, 13*(1), 83-99.

Trapp, B. D., Peterson, J., Ransohoff, R. M., Rudick, R., Mork, S., & Bo, L. (1998). Axonal transection in the lesions of multiple sclerosis. *New England Journal Of Medicine, 338*(5), 278-285.

Trapp, B. D., & Stys, P. K. (2009). Virtual hypoxia and chronic necrosis of demyelinated axons in multiple sclerosis. *Lancet Neurology, 8*(3), 280-291.

Trapp, B. D., Vignos, M., Dudman, J., Chang, A., Fisher, E., Staugaitis, S. M., Battapady, H., Mork, S., Ontaneda, D., Jones, S. E., Fox, R. J., Chen, J., Nakamura, K., & Rudick, R. A. (2018). Cortical neuronal densities and cerebral white matter demyelination in multiple sclerosis: a retrospective study. *Lancet Neurology, 17*(10), 870-884.

Traugott, U., Reinherz, E. L., & Raine, C. S. (1983). Multiple sclerosis: Distribution of T cells, T cell subsets and Ia-positive macrophages in lesions of different ages. *Journal of Neuroimmunology, 4*(3), 201-221.

Tsagkas, C., Magon, S., Gaetano, L., Pezold, S., Naegelin, Y., Amann, M., Stippich, C., Cattin, P., Wuerfel, J., Bieri, O., Sprenger, T., Kappos, L., & Parmar, K. (2018). Spinal cord volume loss: A marker of disease progression in multiple sclerosis. *Neurology, 91*(4), e349-e358.

Tsagkas, C., Magon, S., Gaetano, L., Pezold, S., Naegelin, Y., Amann, M., Stippich, C., Cattin, P., Wuerfel, J., Bieri, O., Sprenger, T., Kappos, L., & Parmar, K. (2019). Preferential spinal cord volume loss in primary progressive multiple sclerosis. *Multiple Sclerosis Journal, 25*(7), 947-957.

Tsunoda, I., & Fujinami, R. (2010). Neuropathogenesis of Theiler's Murine Encephalomyelitis Virus Infection, An Animal Model for Multiple Sclerosis. *Journal of Neuroimmune Pharmacology, 5*(3), 355-369.

Tsunoda, I., Libbey, J. E., & Fujinami, R. S. (2007). TGF-β1 suppresses T cell infiltration and VP2 puff B mutation enhances apoptosis in acute polioencephalitis induced by Theiler's virus. *Journal of Neuroimmunology, 190*(1), 80-89.

Van Der Valk, P., & De Groot, C. J. A. (2000). Staging of multiple sclerosis (MS) lesions: pathology of the time frame of MS. In (Vol. 26, pp. 2-10). Oxford, UK.

van Horssen, J., Singh, S., van Der Pol, S., Kipp, M., Lim, J., Peferoen, L., Gerritsen, W., Kooi, E.-J., Witte, M., Geurts, J., de Vries, H., Peferoen-Baert, R., van Den Elsen, P., van Der Valk, P., & Amor, S. (2012). Clusters of activated microglia in normal-appearing white matter show signs of innate immune activation. *Journal of Neuroinflammation, 9*, 156.

van Laarhoven, H. W. M., Kaanders, J. H. A. M., Lok, J., Peeters, W. J. M., Rijken, P. F. J. W., Wiering, B., Ruers, T. J. M., Punt, C. J. A., Heerschap, A., & van Der Kogel, A. J. (2006). Hypoxia in relation to vasculature and proliferation in liver metastases in patients with colorectal cancer. *International Journal of Radiation Oncology, Biology, Physics, 64*(2), 473-482.

Versijpt, J., Debruyne, J. C., Van Laere, K. J., De Vos, F., Keppens, J., Strijckmans, K., Achten, E., Slegers, G., Dierckx, R. A., Korf, J., & De Reuck, J. L. (2005). Microglial imaging with positron emission tomography and atrophy measurements with magnetic resonance imaging in multiple sclerosis: a correlative study. *Multiple Sclerosis, 11*(2), 127-134.

Voskuhl, R. R., Peterson, R. S., Song, B., Ao, Y., Morales, L. B. J., Tiwari-Woodruff, S., & Sofroniew, M. V. (2009). Reactive Astrocytes Form Scar-Like Perivascular Barriers to Leukocytes during Adaptive Immune Inflammation of the CNS. *The Journal of neuroscience, 29*(37), 11511-11522.

Walton, M. I., Bleehen, N. M., & Workman, P. (1985). The reversible N-oxidation of the nitroimidazole radiosensitizer Ro 03-8799. *Biochemical Pharmacology, 34*(21), 3939-3940.

Wang, G. L., Jiang, B. H., Rue, E. A., & Semenza, G. L. (1995). Hypoxia-inducible factor 1 is a basic-helix-loop-helix-PAS heterodimer regulated by cellular O2 tension. *Proceedings of the National Academy of Sciences of the United States of America, 92*(12), 5510.

Waxman, S. G. (1982). Membranes, myelin, and the pathophysiology of multiple sclerosis. *The New England Journal of Medicine, 306*(25), 1529.

Waxman, S. G. (2001). Acquired channelopathies in nerve injury and MS. *Neurology, 56*(12), 1621-1627.

Wuerfel, J., Bellmann-Strobl, J., Brunecker, P., Aktas, O., McFarland, H., Villringer, A., & Zipp, F. (2004). Changes in cerebral perfusion precede plaque formation in multiple sclerosis: a longitudinal perfusion MRI study. *Brain, 127*(1), 111-119.

Wynford-Thomas, R., Jacob, A., & Tomassini, V. (2018). Neurological update: MOG antibody disease. *J Neurol, 266*(5), 1280-1286.

Xu, K., & LaManna, J., C. (2006). Chronic hypoxia and the cerebral circulation. *Journal of Applied Physiology, 100*(2), 725-730.

Xu, S., Denton, C. P., Dashwood, M. R., Abraham, D. J., & Black, C. M. (1998). Endothelin-1 Regulation of Intercellular Adhesion Molecule-1 Expression in Normal and Sclerodermal Fibroblasts. *Journal of cardiovascular pharmacology, 31 Suppl 1*(1), S545-S547.

Yang, R., & Dunn, J. F. (2015). Reduced cortical microvascular oxygenation in multiple sclerosis: a blinded, case-controlled study using a novel quantitative near-infrared spectroscopy method. *Scientific reports, 5*(1), 16477-16477.

Yu, A. C. H., Lee, Y. L., & Eng, L. F. (1993). Astrogliosis in culture: I. The model and the effect of antisense oligonucleotides on glial fibrillary acidic protein synthesis. *Journal of neuroscience research, 34*(3), 295-303.

Zalc, B. (2018). One hundred and fifty years ago Charcot reported multiple sclerosis as a new neurological disease. *Brain, 141*(12), 3482-3488.

Zamvil, S. S., & Steinman, L. (2003). Diverse Targets for Intervention during Inflammatory and Neurodegenerative Phases of Multiple Sclerosis. *Neuron, 38*(5), 685-688.

Zhang, J. H., Lo, T., Mychaskiw, G., & Colohan, A. (2005). Mechanisms of hyperbaric oxygen and neuroprotection in stroke. *Pathophysiology (Amsterdam), 12*(1), 63-77.

Zhang, Z. A., Nonaka, H., & Hatori, T. (1997). The microvasculature of the spinal cord in the human adult. *Neuropathology, 17*(1), 32-42.

Zhu, X., Smith, M. A., Honda, K., Aliev, G., Moreira, P. I., Nunomura, A., Casadesus, G., Harris, P. L. R., Siedlak, S. L., & Perry, G. (2007). Vascular oxidative stress in Alzheimer disease. *Journal Of The Neurological Sciences, 257*(1), 240-246.

Zouki, C., Baron, C., Fournier, A., & Filep, J. G. (1999). Endothelin-1 enhances neutrophil adhesion to human coronary artery endothelial cells: Role of ET(A) receptors and platelet-activating factor. *British Journal of Pharmacology, 127*(4), 969-979.